

Mass Spectrometry-Based Interaction Study of the STIM1 and VASP Proteins

(Massenspektrometrie-basierte Interaktionsstudie der Proteine STIM1 und VASP)

Dissertation

**zur Erlangung des naturwissenschaftlichen Doktorgrades
des Fachbereichs Chemie der
Technischen Universität Dortmund**

vorgelegt von
Thomas Premsler
aus Dresden

Dortmund, Juni 2012

Eingereicht am: 18.06.2012

an der TU Dortmund, Fachbereich Chemie

1. Gutachter: Prof. Dr. Albert Sickmann
2. Gutachter: Prof. Dr. Jan Hengstler
der Dissertation

1. Prüfer: Prof. Dr. Albert Sickmann

2. Prüfer: Prof. Dr. Jan Hengstler

3. Prüfer: Prof. Dr. Claus Czeslik

Wiss. Mitarbeiter: Dr. Gabriele Trötscher-Kaus

des Promotionskolloquiums

Tag des Promotionskolloquiums: 05.10.2012

Doktorurkunde ausgehändigt am: _____

Table of contents

I List of abbreviations	6
II Amino acids: Residue mass and structure	10
III Genetic code	13
IV Summary	14
V Zusammenfassung	16
1 Introduction	18
1.1 Blood platelets and hemostasis	18
1.1.1 Platelet morphology	19
1.1.2 Platelet inhibition	20
1.1.3 Platelet activation	22
1.2 Platelet shape change and the Ena/ VASP protein family	24
1.2.1 VASP domain structure	25
1.2.2 VASP-mediated remodelling of the actin-cytoskeleton	27
1.2.3 VASP phosphorylation	29
1.3 Calcium signaling in late platelet response	29
1.3.1 The calcium sensor STIM1	30
1.3.2 STIM1-ORAI1 interaction and CRAC entry	32
1.4 Protein interaction studies	33
1.4.1 Co-immunoprecipitation of protein complexes	34
1.4.2 Affinity purification of individual proteins and protein complexes	35
1.4.3 Pull down assays	36
1.4.4 Size exclusion chromatography in protein purification	37
1.5 Protein identification by mass spectrometry	37
1.5.1 Preparing protein samples for MS analysis	38
1.5.1.1 Cell lysis	38
1.5.1.2 Separation of protein samples by gel electrophoresis	40
1.5.1.3 Protein digestion and denaturation	40
1.5.1.4 Separation of proteome samples by liquid chromatography	41
1.5.2 Mass spectrometric analysis	42
1.5.2.1 Electrospray ionization and LC-ESI-MS	43
1.5.2.2 Quadrupoles and ion traps	45
1.5.2.3 Interpretation of mass spectrometric datasets	47
2 Objective	49
3 Materials and Methods	50
3.1 Table 3.1: Chemicals, media and enzymes	50
3.2 Table 3.2: Kits	52
3.3 Table 3.3: Additional material	52

3.4 Table 3.4: Instruments	52
3.5 Software and databases	53
3.6 Cellular material	53
3.6.1 Table 3.5: <i>Escherichia coli</i> strains (<i>E.coli</i>)	53
3.6.2 HEK293 cells	54
3.6.3 Platelet purification	54
3.7 Vector constructs	55
3.7.1 Generation of VASP deletion constructs	56
3.7.1.1 VASP mutagenesis primers	56
3.7.1.2 VASP deletion PCR	57
3.7.1.3 Agarose gel electrophoresis	57
3.7.1.4 PCR cloning in StrataClone SoloPack competent <i>E.coli</i>	57
3.7.1.5 Colony picking and plasmid preparation	58
3.7.1.6 BamHI/ EcoRI restriction digest	58
3.7.1.7 Ligation and transformation in <i>E.coli</i> DH5 α	59
3.7.1.8 VASP constructs - plasmid preparation and controls	59
3.8 Protein expression	60
3.8.1 Transformation of VASP-AAA, VASP-DDE and STIM1Ctail in <i>E.coli</i>	60
3.8.2 Protein expression in <i>E.coli</i>	60
3.8.3 Transfection of VASP deletion constructs in HEK293 cells	61
3.9 Cell lysis, protein purification and interactome screening	62
3.9.1 Lysis of human platelets	62
3.9.2 IMAC purification of His ₆ -tagged bait proteins	62
3.9.3 Size exclusion chromatography of purified His ₆ -tagged proteins	64
3.9.4 Immobilization of purified recombinant proteins	64
3.9.5 Interactome screening of native platelet lysates	65
3.10 Protein analysis	65
3.10.1 Protein quantification by BCA assay	65
3.10.2 1D-SDS-PAGE	65
3.10.3 Western blotting	66
3.10.4 Immunodetection	66
3.10.5 Colloidal Coomassie staining of 1D-SDS-PAGE gels	67
3.10.6 Silver staining of 1D-SDS-PAGE gels	67
3.10.7 IP and Co-IP	68
3.10.8 Calpain in-solution digestion	69
3.10.9 In-gel digestion and peptide extraction	69
3.10.10 Nano-LC-ESI-MS/MS	70
3.10.10.1 Instrumentation and nano-HPLC	70
3.10.10.2 MS and MS/MS acquisition	71
3.10.10.3 MS data evaluation	71

4 Results	73
4.1 Recombinant protein expression in <i>E.coli</i>	73
4.2 Purification of STIM1Ctail, VASP-AAA and VASP-DDE protein from <i>E.coli</i>	74
4.3 Generation of mutant VASP-DNA constructs for eukaryotic transfection	77
4.4 Validation of VASP-vector assembly	79
4.5 Transfection of VASP deletion constructs in HEK293 cells	80
4.6 Purification of recombinant proteins from HEK293 cells	82
4.7 Generation of STIM1Ctail affinity column and platelet interactome screening	88
4.8 Identification of differential proteins by nano-LC-ESI-MS/MS analysis	89
4.9 Interactome screening by STIM1-specific Co-IP in native platelet lysates	92
4.10 Validation of specific STIM1-CLP36 interaction in resting murine platelets	96
4.11 GPIb-CLP36 interaction in resting platelets	98
4.12 Calpain effect on CLP36 stability	100
5 Discussion	102
5.1 Overview: Screening the VASP and STIM1 interactome in resting platelets	102
5.2 Analysis of the VASP interactome in platelets	103
5.2.1 Expression of human VASP fusion proteins in <i>E.coli</i>	103
5.2.2 Expression of human VASP fusion proteins in HEK293	105
5.2.3 Concluding remarks on the VASP-specific interactome study	108
5.3 Analysis of the STIM1 interactome in platelets	109
5.3.1 Remarks on the identified STIM1 interactome	109
5.3.2 STIM1 interaction with PDZ and LIM domain protein family member CLP36	114
5.3.3 GPIb-CLP36 interaction	117
5.3.4 Ca ²⁺ -dependent degradation of CLP36 by calpain	120
5.3.5 Negative regulation of GPVI signaling by CLP36	122
5.3.6 Concluding remarks on the STIM1-specific interactome study	125
6 Literature	128
7 Appendix	144
7.1 Vector maps	144
7.2 Applied full-length nt-sequences	147
7.3 Applied full-length aa-sequences	151
7.4 Sequencing data	154
7.5 Data of the <i>in vitro</i> calpain in-solution digestion assay	162
7.6 Persönliche Daten	164
7.6.1 Lebenslauf	164
7.6.2 Veröffentlichungen	165
7.6.3 Vorträge	165
7.6.4 Posterpräsentationen	165
8 Danksagung	166
9 Eidesstattliche Erklärung	168

I List of abbreviations

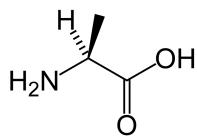
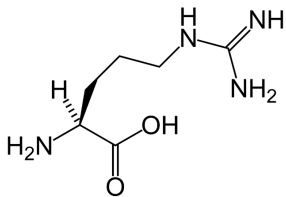
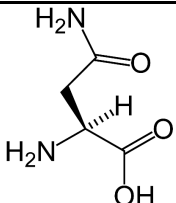
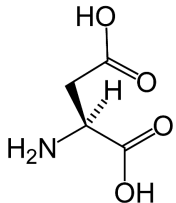
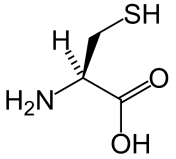
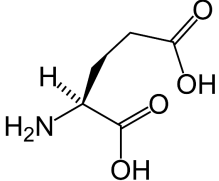
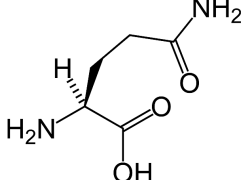
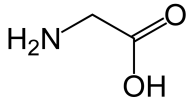
Δ	deletion, difference
1-DE	one-dimensional gel electrophoresis
2-DE	two-dimensional gel electrophoresis
Å	Ångström
aa	amino acid
ABP	actin-binding protein
AC	adenylate cyclase
Acc.Nr.	UniProtKB/ Swiss-Prot accession number
Amp	ampicillin
BCA	bicinchoninic acid
bp	base pair
BSA	bovine serum albumin
$[Ca^{2+}]_i$	intracellular calcium concentration
CaM	calmodulin
CC	coiled-coil motif
c_E	final concentration
CH	calponin homology domain
CHAPS	3-[(3-cholamidopropyl)dimethylammonio]-1-propanesulfonate
CHL	chloramphenicol
CID	collision-induced dissociation
(Co-)IP	(co-)immunoprecipitation
CRAC	calcium release-activated calcium channel
CRP	C-reactive protein
Ctrl	control (affinity column)
CV	column volume, bed volume
Da	Dalton = 1 amu (atomic mass unit)
DAG	diacylglycerol
DMEM	Dulbecco's modified Eagle's medium
DMSO	dimethyl sulfoxide
(D)PBS	(Dulbecco's) phosphate buffered saline
DTS	dense tubular system
DTT	dithiothreitol
EDTA	ethylenedinitrilo-tetraacetic acid disodium dihydrate
ER	endoplasmic reticulum
ESI	electrospray ionization
EVH	Ena/ VASP homology domain
FA	formic acid
FAB	F-actin binding region

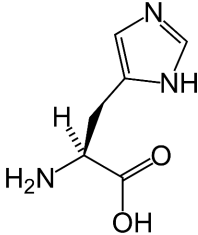
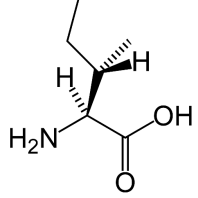
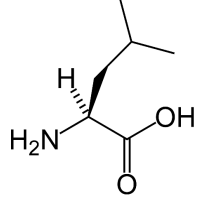
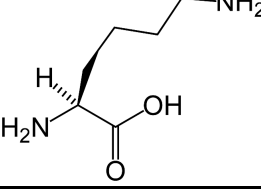
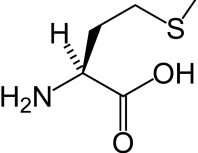
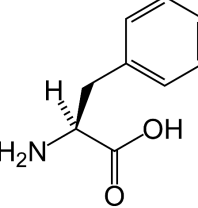
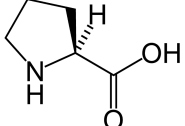
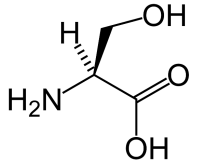
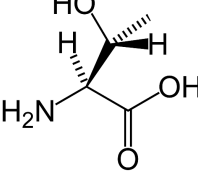
FCS	fetal calf serum
FDR	false discovery rate
FPLC	fast protein liquid chromatography
FTICR	Fourier-transform ion cyclotron resonance
GAB	G-actin binding region
GP	glycoprotein
GPCR	G-protein-coupled receptor
GST	glutathione-S-transferase
HA	hemagglutinin
HEK293	immortalized human embryonic kidney cells
HEPES	N-2-hydroxyethylpiperazine-N-2-ethanesulfonic acid
hIP	STIM1-specific Co-IP in human platelets
HPLC	high-performance liquid chromatography
HRP	horseradish peroxidase
IAA	iodoacetamide
ID	identification
IEC	ion exchange chromatography
IEF	isoelectric focussing
Ig(G)	immunoglobulin (G)
IMAC	immobilized metal ion affinity chromatography
IP ₃	inositol 1,4,5-trisphosphate
IPTG	isopropyl β -D-1-thiogalactopyranoside
LB medium	lysogeny broth medium
LC	liquid chromatography
LC-ESI-MS	online-coupled LC- and ESI-MS systems
LCR	low complexity region
LIM	Lin-11, Isl-1 and Mec-3 motif
m	mass
M	mol per litre
MA	mass analyzer
mAB	monoclonal antibody
MALDI	matrix-assisted laser desorption/ ionization
MBP	maltose binding protein
MCS	multiple cloning site
MDLC	multidimensional liquid chromatography
MeCN	acetonitrile
MEM	Eagle's minimum essential medium
MES	2-N-morpholino ethanesulfonic acid
mgf	Mascot generic format
mIP	STIM1-specific Co-IP in platelets of STIM1 ^{+/+} mice

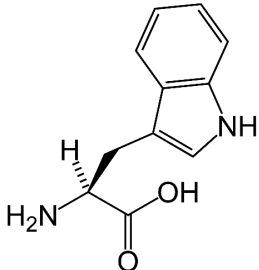
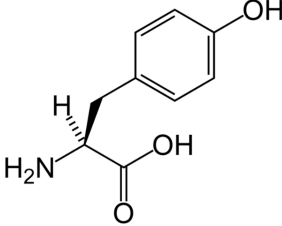
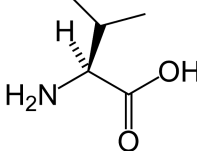
MLC (K)/ (P)	myosin light chain (kinase)/ (phosphatase)
MS	mass spectrometry, mass spectrometer
MS/MS	tandem mass spectrometry
MudPIT	multidimensional protein identification technology
MW	molecular weight
m/z	mass-to-charge ratio
Neo	neomycin
NP-40	Nonidet P40 substitute
nt	nucleotide
pAB	polyclonal antibody
PAGE	polyacrylamide gel electrophoresis
PB	protein band
PCR	polymerase chain reaction
PDE	phosphodiesterase
PDZ	postsynaptic density 95, discs large and zonula occludens-1 motif
Pen	penicillin
pI	isoelectric point
PIP ₂	phosphatidylinositol 4,5-bisphosphate
PKA	protein kinase A, cAMP-dependent protein kinase
PKC	Ser/ Thr protein kinase C
PKG	protein kinase G, cGMP-dependent protein kinase
PM	plasma membrane
PMF	peptide mass fingerprinting
PRP	platelet-rich plasma
PRR	proline-rich region
pSer, pS	phospho-serine
pThr, pT	phospho-threonine
PTM	post-translational modification
pTyr, pY	phospho-tyrosine
PVDF	polyvinylidene difluoride
RP	reversed-phase, reversed-phase chromatography
RT	retention time
(RT-)PCR	(reverse transcription) polymerase chain reaction
SAM	sterile α -motif
SC	STIM1Ctail affinity column
SDS	sodium dodecylsulfate
SEC	size exclusion chromatography
SERCA	sarcoplasmic/ endoplasmic reticulum Ca ²⁺ ATPase
sGC	soluble guanylyl cyclase
SOCE	store-operated calcium entry

STIM1	stromal interaction molecule 1
Strep	streptomycin
TD	tetramerization domain
TFA	trifluoroacetic acid
TM	transmembrane domain
TOF	time-of-flight
Tris	tris(hydroxymethyl)aminomethane
U	units
VASP	vasodilator-stimulated phosphoprotein
v/v	volume per volume
vWF	von Willebrand factor
wt	wildtype
w/v	weight per volume
X-gal	bromo-chloro-indolyl-galacto-pyranoside
z	charge

II Amino acids: Residue mass and structure

Name	Symbol	Structure	Monoisotopic mass (-H ₂ O) [Da]
Alanine	Ala, A		71.03711
Arginine	Arg, R		156.10111
Asparagine	Asn, N		114.04293
Aspartic acid	Asp, D		115.02694
Cysteine	Cys, C		103.00919
Glutamic acid	Glu, E		129.04259
Glutamine	Gln, Q		128.05858
Glycine	Gly, G		57.02146

Histidine	His, H		137.05891
Isoleucine	Ile, I		113.08406
Leucine	Leu, L		113.08406
Lysine	Lys, K		128.09496
Methionine	Met, M		131.04049
Phenylalanine	Phe, F		147.06841
Proline	Pro, P		97.05276
Serine	Ser, S		87.03203
Threonine	Thr, T		101.04768

Tryptophan	Trp, W	 <p>The structure shows the side chain of tryptophan, which is an indol-3-ylmethyl group. The alpha-carbon is bonded to an amino group (H₂N), a hydrogen atom (H), and a carboxyl group (COOH). The beta-carbon is bonded to the indol-3-ylmethyl group.</p>	186.07931
Tyrosine	Tyr, Y	 <p>The structure shows the side chain of tyrosine, which is a 4-hydroxybenzyl group. The alpha-carbon is bonded to an amino group (H₂N), a hydrogen atom (H), and a carboxyl group (COOH). The beta-carbon is bonded to the 4-hydroxybenzyl group.</p>	163.06333
Valine	Val, V	 <p>The structure shows the side chain of valine, which is an isopropyl group. The alpha-carbon is bonded to an amino group (H₂N), a hydrogen atom (H), and a carboxyl group (COOH). The beta-carbon is bonded to two methyl groups and a hydrogen atom.</p>	99.06841

III Genetic code

	U	C	A	G	
U	Phe Phe Leu Leu	Ser Ser Ser Ser	Tyr Tyr Stop Stop	Cys Cys Stop Trp	U C A G
C	Leu Leu Leu Leu	Pro Pro Pro Pro	His His Gln Gln	Arg Arg Arg Arg	U C A G
A	Ile Ile Ile Met	Thr Thr Thr Thr	Asn Asn Lys Lys	Ser Ser Arg Arg	U C A G
G	Val Val Val Val	Ala Ala Ala Ala	Asp Asp Glu Glu	Gly Gly Gly Gly	U C A G

IV Summary

The vasodilator-stimulated phosphoprotein VASP and the stromal interaction molecule STIM1 are regarded as being amongst the key players functioning in the processes upon platelet activation. Thereby, VASP, due to its actin filament-remodelling activity, is closely related to platelet adhesion and shape change. The Ca^{2+} -sensing molecule STIM1, on the other hand, has been linked to CRAC entry in the course of platelet Ca^{2+} -signaling, which consequently results in enhanced granular secretion, recruitment of further platelets and subsequent aggregation at the site of vessel injury. To further understand the precise mechanisms regulating the specific effects of these two components, we here addressed both the VASP- and STIM1 interactome in resting platelets by applying a differential pull down-based proteomics strategy. In detail, His₆-tagged DNA-vector constructs of (a) phosphomimetic mutants of human VASP; and (b) of the cytosolic part of human STIM1 were heterologously expressed and IMAC purified. The resulting fusion proteins were intended for subsequent immobilization on Affi-Gel 10 resin to generate VASP- and STIM1-specific affinity supports. These affinity columns should consequently serve for specific interactome screenings on native lysates of resting human platelets.

Following this strategy, however, synthesis and isolation of the intended VASP fusion proteins turned out to be challenging: Initially, prokaryotic translation in *E.coli* was partially inhibited, most probably as a consequence of the codon bias problem inherent to prokaryotic vs eukaryotic protein expression. This issue was finally addressed by changing to an alternate, eukaryotic expression system (i.e. stably transfected HEK293 cells). Nevertheless, the resulting protein yields were still too low to enable sufficient subsequent enrichment. In this context, the applied IMAC approach may have also been further limited by partial inaccessibility of the targeted C-terminal His₆- tags, presumably caused by structural folding of the C-termini of the designed protein constructs. The generated stable cell lines may hence be well suitable to address the phospho-specific VASP interactome in the HEK293 model system (e.g. in Co-IP-based approaches); however, they were not adequate in the context of a platelet-related study as intended here. Therefore, this part of our analysis was finally rejected.

In contrast, when applying the same strategy to unravel the STIM1-specific interactome of resting platelets, a total of 87 non-redundant, platelet-related proteins were detected successfully. These components were classified in four functional complexes: (a) the actin-myosin complex; (b) the adhesion complex, including the (c) GPIb-IX-V subcomplex; and (d) the signaling-related complex. Of these, one of the most promising candidates - i.e. PDLIM family member CLP36, which was related to three of the four functional complexes - was chosen for a more detailed analysis (*in vitro* and *in vivo*). Deriving from these studies, α -actinin-bound CLP36 seems to stabilize STIM1 anchoring to the F-actin cytoskeleton, hence preventing uncontrolled STIM1-mediated CRAC entry and consequent intravascular platelet activation and aggregation. There is furthermore evidence that, upon platelet induction, this interaction is finally reversed by limited proteolysis via the Ca^{2+} -dependent endoprotease calpain. Since CLP36 was also found to act as a negative regulator of GPVI-ITAM signaling, as indicated by functional platelet characterization in $\text{Clp36}^{\Delta\text{LIM}}$ mice, this cytoskeleton adaptor protein presumably plays multiple roles in the context of platelet inhibition. Further research on this protein candidate may thus help to improve our knowledge of intravascular thrombus formation and of the pathological mechanisms contributing to manifestation of acute ischemic diseases.

V Zusammenfassung

Das Vasodilatator-stimulierte Phosphoprotein VASP und das Stromal-Interaktionsmolekül STIM1 zählen zu den zentralen Komponenten, die an den im Verlauf der Thrombozytenaktivierung auftretenden Prozessen beteiligt sind. Aufgrund seiner Aktinfilament-remodellierenden Aktivität wird VASP hierbei in engen Zusammenhang mit der Adhäsion und Gestaltänderung aktivierter Thrombozyten gebracht. Der Ca^{2+} -Sensor STIM1 hingegen ist in den, über CRAC-Kanäle medierten, Ca^{2+} -Flux im Zuge des thrombozytären Ca^{2+} -Signalings eingebunden, was letztlich zur verstärkten granulären Sekretion, der Rekrutierung weiterer Thrombozyten und schließlich zur Aggregation im Bereich der Gefäßläsion führt. Um tieferen Einblick in die hinter diesen jeweilig spezifischen Funktionen stehenden regulatorischen Mechanismen zu erhalten, wurde im Rahmen der vorliegenden Studie eine Analyse des VASP- und des STIM1-Interaktoms in ruhenden Thrombozyten vorgenommen. Dies geschah unter Anwendung eines Pulldown-basierten, differentiellen proteomischen Ansatzes. So wurden His₆-getaggte DNA-Vektorstrukture von (a) phospho-mimetischen humanen VASP-Mutanten; und (b) der zytosolischen Domänen von humanem STIM1 heterolog exprimiert und mittels IMAC aufgereinigt. Die so gewonnenen Fusionsproteine sollten anschließend, nach Immobilisierung an einer Affi-Gel 10 Matrix zur Generierung von VASP- bzw. STIM1-spezifischen Affinitätsmatrices, für spezifische Interaktomsscreenings in nativen Lysaten ruhender humaner Thrombozyten genutzt werden.

Im Zuge dieser Vorgehensweise erwies sich die Synthese und Aufreinigung der VASP Fusionsproteine allerdings als schwierig: So ließ sich zunächst nur eine schwache Translation in *E.coli* feststellen, was vermutlich auf die bei prokaryotischer Expression von eukaryotischem Genmaterial häufig auftretende 'Codon Bias-Problematik' zurückzuführen war. Durch den Wechsel in ein eukaryotisches Expressionssystem (stabil transfizierte HEK293 Zellen) konnten diese Limitierungen schließlich umgangen werden. Die Expressionslevel der synthetisierten VASP Fusionsproteine fielen allerdings auch hier letztlich viel zu gering aus, um anschließend eine ausreichend hohe Anreicherung zu gewährleisten. In diesem Zusammenhang muss auch vermutet werden, dass die IMAC-Aufreinigung der Proteinkonstrukte eventuell durch partielle strukturelle Unzugänglichkeit der

C-terminalen His₆-Affinitätstags als Folge C-terminaler Proteinfaltungen zusätzlich beeinträchtigt worden sein könnte. Die generierten stabilen Zelllinien mögen somit zwar durchaus dafür geeignet sein, eine phospho-spezifische VASP Interaktionsstudie im HEK293 Modellsystem vorzunehmen (z.B. über einen Co-IP-basierten Ansatz). Für die hier beabsichtigte Untersuchung humaner Thrombozyten erwiesen sie sich jedoch letztlich als unzulänglich. Aus diesem Grund muss dieser Teil der vorliegenden Studie vorerst als gescheitert angesehen werden. Im Falle der Analyse des thrombozytären Interaktoms von humanem STIM1 konnten hingegen mittels der beschriebenen Strategie insgesamt 87 nicht-redundante thrombozytäre Proteine erfolgreich detektiert werden. Diese Komponenten waren vier funktionellen Komplexen zuzuordnen: (a) dem Aktin-Myosin Komplex; (b) dem Adhäsionskomplex, einschließlich des (c) GPIb-IX-V Subkomplexes; und (d) dem Signaling-assoziierten Komplex. Einer der in diesem Zusammenhang vielversprechendsten Kandidaten - das zur PDLIM Familie gehörende Protein CLP36, welches funktionelle Assoziation zu drei der vier angesprochenen Komplexe zeigt - wurde schließlich einer detaillierteren Analyse (*in vitro* und *in vivo*) unterzogen. Auf Basis dieser Untersuchungen lässt sich schlussfolgern, dass α -Aktinin-gebundenes CLP36 vermutlich die Verankerung von STIM1 am F-Aktin Zytoskelett stabilisiert, und somit unkontrolliertem STIM1/ CRAC-vermitteltem Ca²⁺-Einstrom und der damit einhergehenden intravaskulären Thrombozytenaktivierung und -aggregation entgegenwirkt. Desweiteren bestehen Hinweise darauf, dass diese Interaktion in aktivierten Thrombozyten durch limitierte Proteolyse, vermittelt durch die Ca²⁺-abhängige Endoprotease Calpain, aufgehoben wird. Da CLP36 außerdem als Negativregulator im Zuge des GPVI-ITAM Signalings zu fungieren scheint - was hier anhand thrombozytärer Funktionsanalysen in Clp36 ^{Δ LIM} Mäusen belegt werden konnte - kommt diesem zytoskelettalen Adapterprotein vermutlich eine umfassendere Rolle im Kontext der Thrombozyteninhibierung zu. Weitere eingehendere Untersuchung dieses Kandidaten kann somit möglicherweise dazu beitragen, unser Wissen bezüglich der intravaskulären Thrombusbildung, sowie der pathologischen Mechanismen, die letztlich zur Ausbildung akuter ischämischer Erkrankungen führen, zu erweitern.

1 Introduction

1.1 Blood platelets and hemostasis

Blood plays an indispensable, multifaceted role, for instance in metabolic, oxygen or hormone transport, immune defence and temperature regulation. It is composed of cells of mesenchymal origin (blood cells) and carrier fluid (blood plasma). Plasma is a clear solution (90% water) and accounts for up to 56% of the total blood volume [1]. It contains amongst others sugars, lipids, vitamins, electrolytes, carrier proteins, hormones, enzymes, blood clotting factors, and antibodies. Blood cells, on the other hand, comprise erythrocytes ($4-5 \times 10^{12}/\text{L}$ blood), leukocytes (part of the immune system, $4-11 \times 10^9/\text{L}$ blood), and platelets ($2-3 \times 10^{11}/\text{L}$ blood) [2]. Blood platelets are small, anucleated discoid-shaped cellular particles (diameter 2-4 μm) originating from constriction of precursor megakaryocytes in the bone marrow [3]. In the intact vasculature, they circulate in the blood in a quiescent state for approximately seven days until they are degraded in the spleen and the liver. They play an essential role in hemostasis, i.e. the arrest of hemorrhage upon tissue trauma [4, 5]: Accordingly, vascular lesion first leads to rapid platelet adhesion to the zone of injury, followed by platelet activation. Upon subsequent recruitment and aggregation of further platelets, a thrombus is finally formed which loosely occludes the disrupted area. This 'primary' or 'cellular' hemostasis is accompanied by a series of enzymatic reactions which stabilize the thrombus via generation of a strong fibrin fiber mesh (secondary hemostasis, or humoral coagulation cascade) [6]. Simultaneously, platelet surface molecules and factors released from the platelets' intracellular granules (e.g. integrins and P-selectin) induce processes like immune response and tissue regeneration [7-11].

Many of the mediators related to physiological hemostasis are not only involved in platelet-related pathological events (such as atherosclerosis, coronary and peripheral artery disease, or cerebrovascular disease) [4, 12], but also in tumor angiogenesis, tumor progression and malignancy [13, 14]. Therefore, a comprehensive knowledge of the underlying regulatory mechanisms and signaling pathways is of high medical interest and offers yet unexplored possibilities to develop anti-atherosclerotic and anti-angiogenic agents.

1.1.1 Platelet morphology

Upon activation, platelets extend their surface to efficiently occlude the lesion, changing their shape from discoid to a flattened, star-shaped one by formation of lamellipodia and filopodia. For this purpose, the plasma membrane (PM) of resting platelets contains numerous invaginations (i.e. the open canalicular system) serving both as membrane sources and guidance systems for secretory granules during the platelet activation process.

Apart from typical cellular organelles, such as mitochondria, Golgi apparatus and lysosomes, the platelet cytoplasm contains the already mentioned secretory granules and the dense tubular system (DTS) which functions as an essential Ca^{2+} -reservoir (see Figure 1.1 A). Platelet granules are generally subdivided into alpha, delta ('dense') and lambda granules. Alpha granules contain proteins involved in clot formation, including platelet factor 4, von Willebrand factor (vWF), fibrinogen, fibronectin, and coagulation factors V and XIII, as well as growth factors (PDGF, IGF-1, and TGF- β) and carrier proteins (multimerin-1) [15]. In addition, various glycoproteins (GP) known to increase platelet adhesion to the region of vascular lesion are also embedded in the alpha granule membrane, such as integrin $\alpha_{\text{IIb}}\beta_3$, P-selectin or GPIb-IX-V. The content of delta granules is composed of small, soluble molecules (ADP, ATP, pyrophosphate, serotonin, histamine and Ca^{2+}) which further contribute to platelet adhesion as well as to vasoconstriction and regulation of inflammation [16]. Lambda granules finally resemble lysosomes whose hydrolytic enzymes mediate clot resorption once the lesion has been repaired.

One further morphological characteristic is given by the dense platelet cytoskeleton. The cytoplasm is traversed by a complex, rigid actin fiber mesh and a ring-shaped microtubuli-based structure located close to the PM region [17]. Several protein interactions, such as filamin - GPIb-IX-V, directly anchor the cytoskeleton to the PM. Moreover, the intracellular side of the PM is stabilized by a strong spectrin-based supporting structure [18, 19].

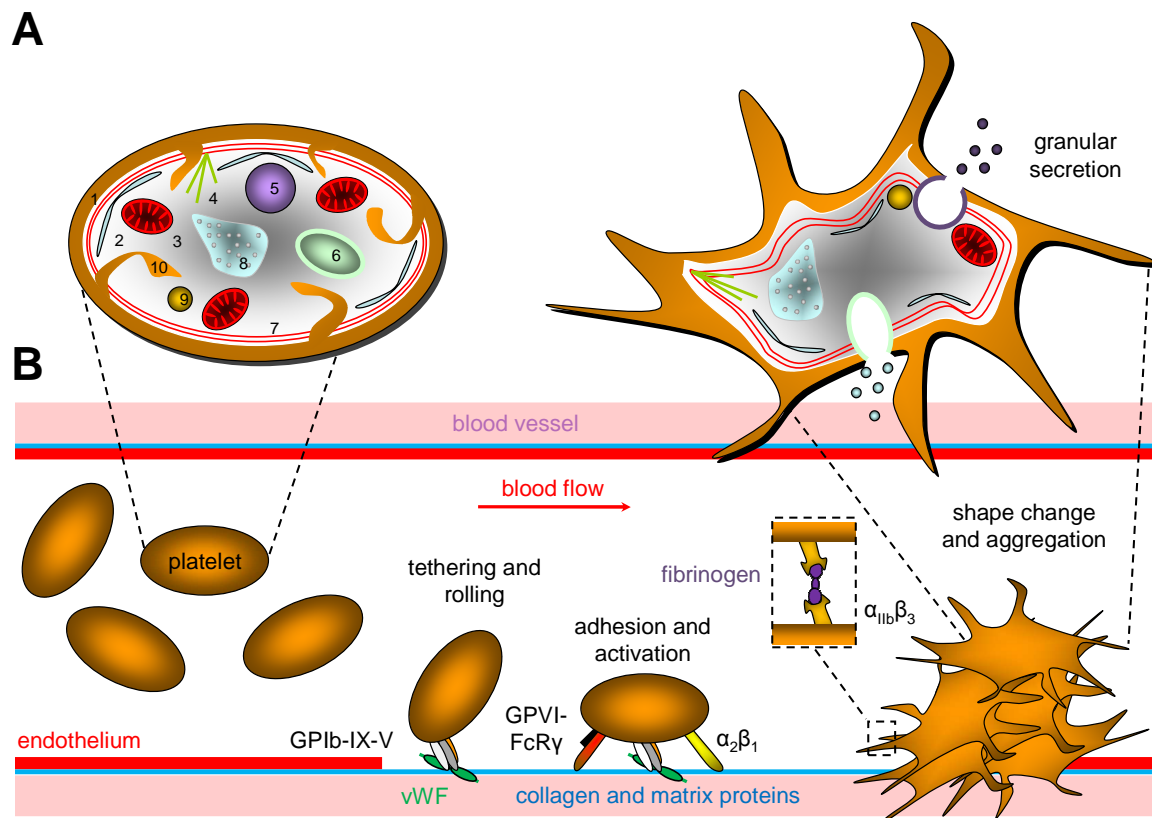


Figure 1.1: (A) Platelet morphology: (1) plasma membrane, (2) dense tubular system, (3) mitochondrion, (4) actin fibers, (5) dense granule, (6) alpha granule, (7) ring-shaped microtubuli structure, (8) glycogen store, (9) lysosome, (10) invagination. (B) Platelet recruitment following vessel injury. Initially, platelets loosely adhere to exposed collagen-bound vWF via the platelet surface receptor GPIb-IX-V ('rolling'). Subsequent firm adhesion to subendothelial matrix proteins is mediated by platelet GPVI-Fc receptor gamma chain (FcR γ) and integrin $\alpha_2\beta_1$. Upon granular secretion, further platelets are recruited and activated, which finally results in thrombus formation based on $\alpha_{IIb}\beta_3$ -fibrinogen interaction.

1.1.2 Platelet inhibition

To prevent uncontrolled intravascular thrombus formation under physiological conditions, platelet activity is tightly controlled by adequate inhibitory mechanisms. Accordingly, platelet antagonists such as vasodilators, prostacyclins (e.g. PGI₂) and prostaglandins (e.g. PGE₁), inhibit activation, adhesion and aggregation of resting platelets by enhancing the intracellular concentration of the cyclic nucleotides cAMP and cGMP [20]. Regarding cAMP formation, this commonly implies modulation of G-protein-coupled receptors (GPCRs), a group of transmembrane receptors known for fast and amplified transduction of external stimuli via constitutively associated heterotrimeric G-proteins and firmly controlled subsequent signaling cascades [21].

As a detailed example, both PGE₁ and PGI₂ bind to prostaglandin G_{as}-coupled receptors which subsequently activate the adenylate cyclase (AC) [22]. Once stimulated, the AC catalyzes cAMP synthesis (Figure 1.2). Intracellular levels of cGMP, on the other hand, are predominantly increased by induction of the intracellular soluble guanylyl cyclase (sGC), e.g. as a consequence of endothelial release of the vasodilator nitric oxide (NO) [23]. In this context, NO (also 'endothelium-derived relaxing factor' EDRF) furthermore inhibits phosphodiesterase (PDE) function and thus prevents cyclic nucleotide degradation [24].

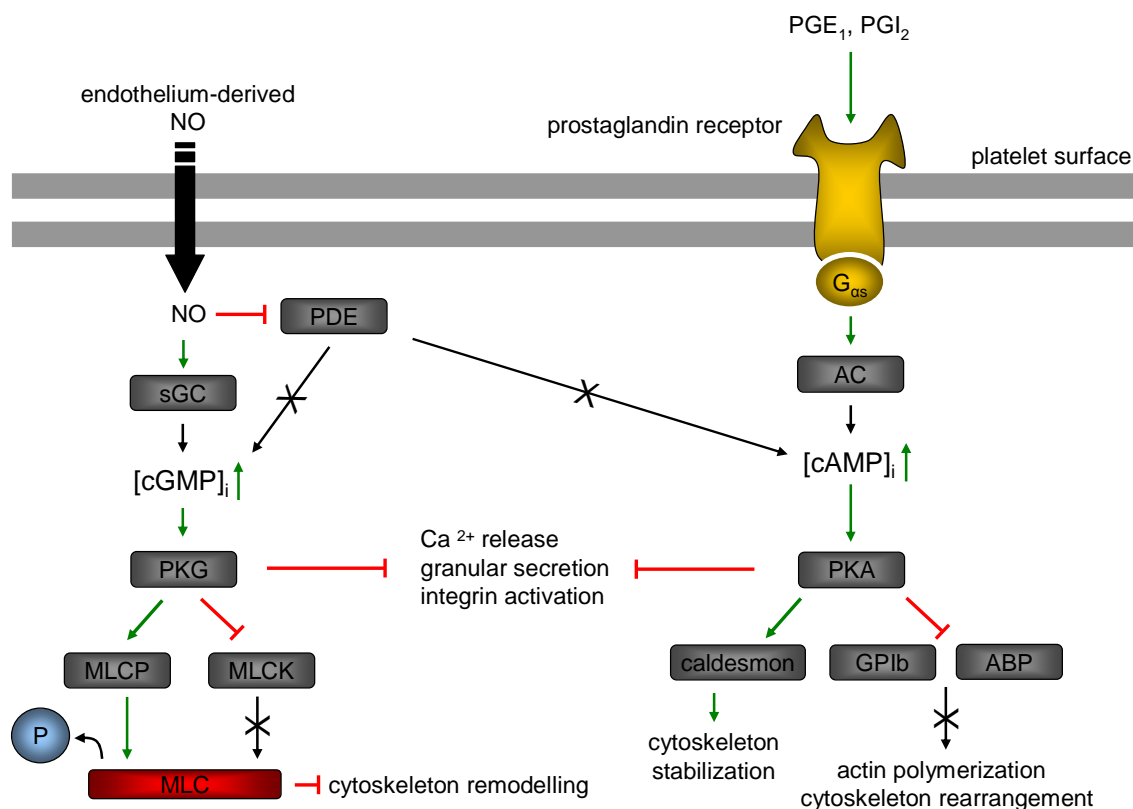


Figure 1.2: Platelet inhibitory pathways, based on Schwarz et al. [20]. Green arrows indicate activation, red lines inhibition. Black arrows mark subsequent signaling cascades and effects, with crossed-out ones symbolizing signal prevention.

Generally, cyclic nucleotide-mediated platelet inhibition is executed by the cAMP- and cGMP-dependent protein kinases PKA and PKG [20, 25]. Though the precise mechanisms still have to be fully resolved, both kinases are regarded as particularly counteracting cytoskeleton remodelling processes occurring upon platelet activation, as for instance during platelet shape change. In detail, several PKA phosphorylation

substrates have been related to the maintenance of the cortical actin cytoskeleton: Accordingly, phosphorylation of GPIb inhibits collagen-induced actin polymerization [26], phospho-caldesmon stabilizes actin filament structures [27] and phosphorylation of actin binding proteins (ABP) prevents actin cytoskeleton rearrangement [28]. PKG-mediated phosphorylation events, on the other hand, have been shown to both activate the myosin light chain phosphatase (MLCP) and inhibit the myosin light chain kinase (MLCK). This promotes dephosphorylation of myosin light chains (MLC), thus preserving intracellular actomyosin relaxation and consequently stabilizing resting platelets' morphology [29]. Apart from the described processes, PKA-/ PKG-dependent platelet inhibition moreover comprises repression of (a) Ca^{2+} -release from intracellular stores; (b) integrin activation; and (c) granule secretion [20].

1.1.3 Platelet activation

The complex biochemical mechanisms regulating platelet activity imply modulation of activating and inhibitory downstream signaling pathways, cytoskeleton reorganization and platelet shape change, receptor translocation to the platelet surface, as well as relocation and secretion of intracellular secretory granules. Initially, circulating platelets adhere to sites of vessel injury by a series of interactions between platelet tyrosine kinase-dependent adhesion receptors (PTKs) and either exposed subendothelial collagen or collagen-bound vWF. This is for instance illustrated by the contacts of platelet GPIb-IX-V with vWF, which permits platelet rolling on the subendothelial matrix [30] (see Figure 1.1 B). Subsequent firm platelet adhesion requires participation of two structurally distinct platelet-collagen receptors, the immune receptor homologue GPVI and integrin $\alpha_2\beta_1$ [31, 32]. In this context, the GPVI-collagen interaction represents the main activating signal. In the further process, GPVI and platelet Fc receptor gamma chain (FcR γ) form a functional complex which, upon Src phosphorylation, induces phospholipase C γ 2 (PLC γ 2) and phosphatidylinositol-3-kinase (PI3K)/ Akt signaling - and thus intracellular synthesis of second messenger molecules IP $_3$ and diacylglycerol (DAG) [33, 34]. IP $_3$ mediates cytosolic Ca^{2+} -release from intracellular stores [21]. With regard to both cellular hemostasis and the subsequent coagulation cascade, Ca^{2+} -availability plays a pivotal role: In platelets, for instance, Ca^{2+} binds to calmodulin (CaM) which in turn stimulates MLCK. Consequently, MLCK-mediated phosphorylation of myosin light chains initiates cytoskeleton shape change and thus platelet spreading [35]. For

further details on platelet Ca^{2+} -signaling see also 1.3. DAG, on the other hand, stimulates granular secretion of e.g. PDGF, serotonin, fibrinogen and ADP via activation of Ser/ Thr protein kinase C (PKC). Moreover, it induces translocation of granular membrane glycoproteins (such as fibrinogen receptor integrin $\alpha_{\text{IIb}}\beta_3$) to the platelet surface [36].

Once released to the blood flow, the components of the platelet secretome - mainly thrombin, thromboxane A_2 (TxA_2) and ADP - stimulate the second step of cellular hemostasis, i.e. recruitment of further platelets to the site of injury. In this context, direct platelet-to-platelet contact is based on coordinated adhesion of GPIb-IX-V to vWF and activated integrin $\alpha_{\text{IIb}}\beta_3$ to fibrinogen, respectively. As in platelet inhibition, several soluble agonists act via GPCRs and the associated signaling cascades comprising protein kinases, phospholipases and Ras-family members [21]. Basically, the essential steps during agonist-induced platelet activation resemble those of collagen-based ones: increase of intracellular Ca^{2+} -concentration $[\text{Ca}^{2+}]_i$, PKC activation and, finally, remodelling of the actin cytoskeleton. This is achieved by the complex interplay of different heterotrimeric G-protein subunits. As an example, binding of thrombin, TxA_2 or ADP to G_{α_q} and $G_{\alpha_{12/13}}$ family members subsequently induces phospholipase $C\beta$ (PLC β) as well as the Rho/ ROCK signaling pathway (for details see Figure 1.3) [37-39]. Simultaneously, down-regulation of inhibitory mechanisms takes place: Accordingly, G_{α_i} stimulation by ADP and/ or thrombin inhibits the AC and hence reduces cytosolic cAMP levels [20]. The related $G_{\beta\gamma}$ -subunits, however, also activate PLC and PI3K and thus further enhance thrombus growing [37]. Thrombus stabilization is finally achieved both by induction of the coagulation cascade and by platelet receptor desensitization, which is presumably mediated via outside-in signaling [40]. In this context, functional implication of integrins and receptor kinases as well as release of growth arrest specific proteins from platelet alpha granules is discussed; yet the precise mechanisms still have to be elucidated [41, 42].

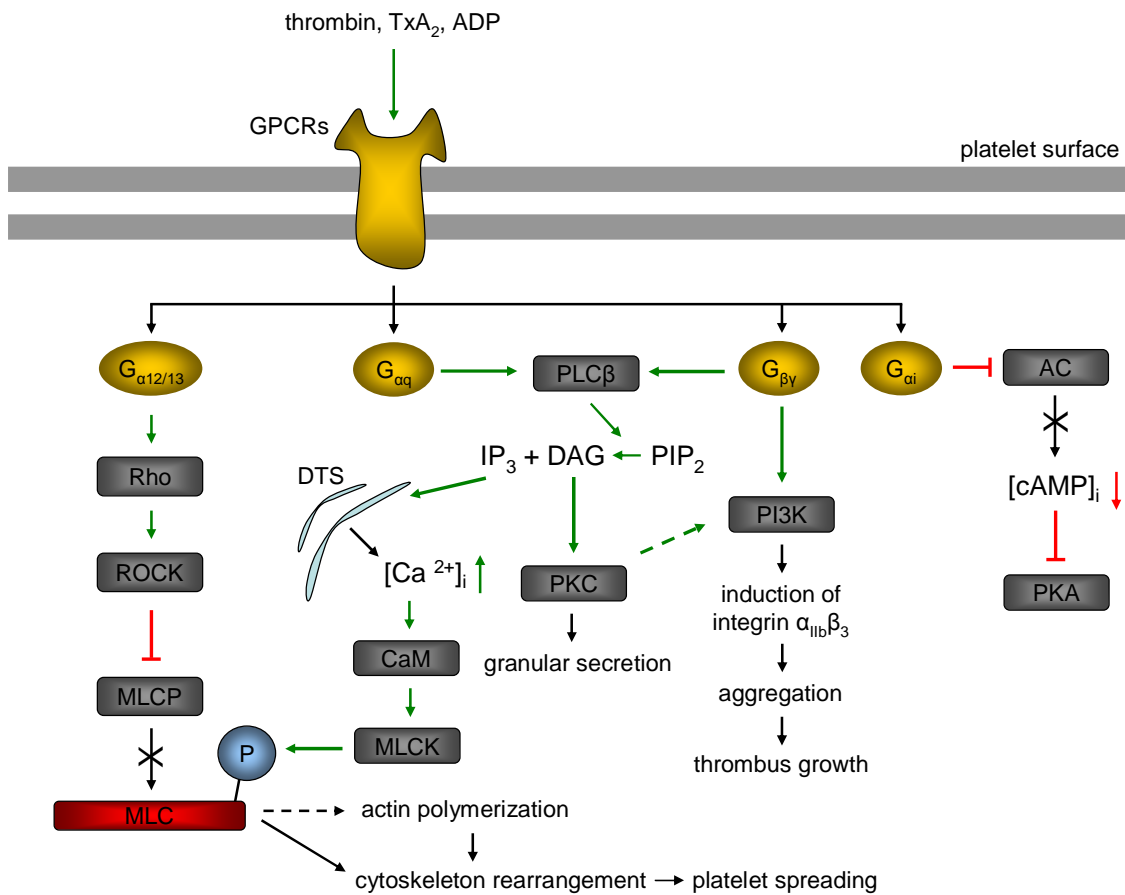


Figure 1.3: GPCR-mediated platelet activation by binding of thrombin, TxA₂ and ADP (based on [20, 37-39]). Green arrows indicate activation, red lines inhibition. Black arrows mark subsequent signaling cascades and effects, with crossed-out ones symbolizing signal prevention.

1.2 Platelet shape change and the Ena/ VASP protein family

Platelet shape change upon activation is predominantly based on reorganization of the actin cytoskeleton. Having approximately two million copies per cell, actin monomers represent the most abundant protein in platelets [43]. Since in eukaryotic cells the main source of polymerization-competent globular actin (G-actin) is provided by profilin-actin complexes (also profilactin) [44-46], both lamellipodia and filopodia formation depend on the ability to recruit, process and incorporate profilactin onto the barbed ends of elongating actin filaments (F-actin). In this context, the role of profilin in filament assembly is manifold [47-49]: (a) profilin catalyzes the ADP-to-ATP exchange for G-actin, thus restoring the pool of ATP-actin monomers obligatory for polymerization; (b) profilin-bound G-actins exclusively elongate at filament barbed ends and not at pointed ends; and (c) profilin exhibits high affinity to proline-rich

regions present in several filament elongation factors, such as the Arp2/3 complex activator WASP, formins and proteins of the so-called Ena/ VASP family.

The latter ones are involved in multiple actin-mediated processes related to cell motility and adhesion, as well as in cytoskeleton-PM anchoring to provide cellular shape stability and mediate tissue permeability [50]. Ena/ VASP proteins are consequently associated with actin bundles, stress fibers, focal adhesions (i.e. cell-matrix interaction), cell-cell contacts, or to highly dynamic membrane structures such as leading edges of neuronal growth cones [51]. In addition, they colocalize with unipolar actin filaments of lamellipodia and particularly filopodial tips. Apart from the founding member VASP ('vasodilator-stimulated phosphoprotein'), this protein family comprises *Drosophila* Ena ('enabled'), the mammalian and the avian Ena orthologs (Mena and Avena, respectively) and the Ena-VASP-like protein (Evl) [50-52].

VASP itself is expressed in various cell types and tissues (e.g. epithelia and endothelia); however, it reveals highest levels in platelets where it is closely connected to inhibitory pathways [53]. Subsequent to platelet antagonist (e.g. NO and PGI₂) induced increase of intracellular cAMP- and cGMP-concentration, VASP-function in filament elongation is inhibited by PKA- and PKG-mediated phosphorylation [54, 55]. This model is further strengthened by studies on VASP-deficient mice exhibiting impaired cyclic nucleotide mediated inhibition and hence enhanced collagen and thrombin induced platelet activation [56]. Although the detailed role of VASP in platelets is not yet fully understood, its participation in dynamic cytoskeletal processes and its response to platelet antagonists renders it an essential key player in regulating platelet shape change upon activation and thus justifies further focus on this family of filament elongation factors.

1.2.1 VASP domain structure

Ena/ VASP family members share a common domain organization consisting of highly conserved N-terminal and C-terminal regions, i.e. Ena/ VASP homology domains EVH1 and EVH2, separated by more variable low complexity regions (LCR) and proline-rich regions (PRR, see also Figure 1.4 A) [57]. In the following, a detailed functional description of the Ena/ VASP structural domains will be provided using human VASP (39.8 kDa, 380 aa) as an example. Accordingly, the N-terminal EVH1-domain (in VASP aa 2-113) mediates Ena/ VASP translocation to focal adhesions, lamellipodia and filopodia, and binds to ligands containing an FP₄ consensus

sequence (E/DFPPPPXD/E, i.e. a polyproline II helix) [58]. These motifs are found in a variety of scaffolding and focal adhesion proteins, such as zyxin, vinculin, migfilin, paladin or α -actinin (Figure 1.4 B) [51].

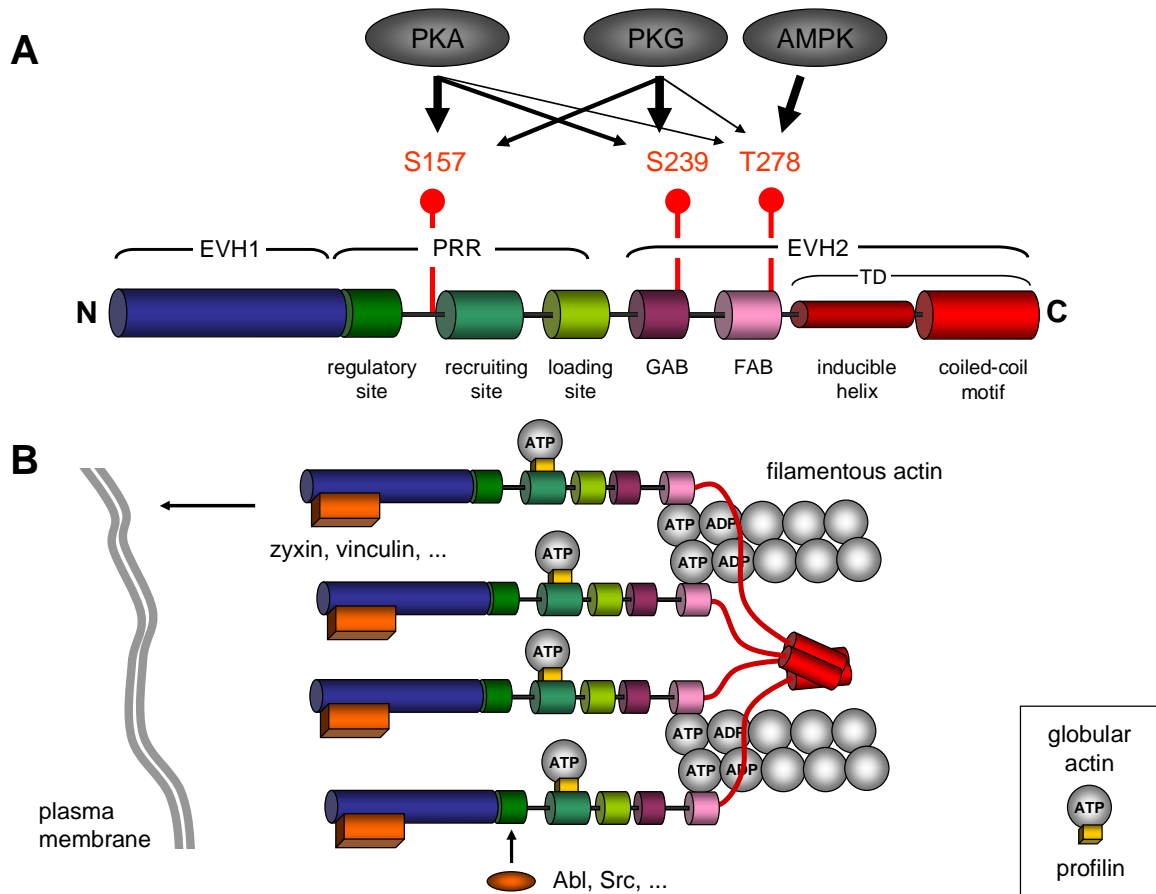


Figure 1.4: (A) VASP domain structure: (1) N-terminal EVH1 domain (aa 2-113), (2) central PRR-domain (aa 118-216) consisting of regulatory-, recruiting- and loading poly-Pro-sites, (3) C-terminal EVH2 domain (aa 225-377) composed of the GAB- and FAB-region, followed by the VASP-TD domain. VASP phosphorylation sites S157, S239 and T278, which are differentially phosphorylated by PKA, PKG and AMPK (with thicker arrows indicating higher site preference), are highlighted in red. (B) VASP tetramer recruitment to sites of filament assembly, based on Ferron et al. [61]. VASP-EVH1 domains mediate subcellular localization via interaction with scaffolding proteins which are directly or indirectly connected to the plasma membrane. The recruiting poly-Pro-sites sequester multiple profilin-actin complexes thus increasing local G-actin concentration.

The C-terminal EVH2 domain (aa 225-377) consists of three conserved blocks [59]: (a) a thymosin-like motif essential in G-actin binding (also called GAB-region, aa 225-245); (b) an F-actin attachment site (FAB-region, aa 259-278); (c) and a coiled-coil motif (CC) containing a C-terminal tetramerization domain (TD, aa 343-377) which

mediates both VASP homo- and hetero-oligomerization with other Ena/ VASP family members in a bouquet-like structure [59, 60] (Figure 1.4 B).

Finally, according to Ferron et al. [61], the central PRR-domain of VASP (aa 118-216) can be subdivided into three distinct groups (Figure 1.4 A): The first group of proline residues (aa 118-135) is predicted to bind to various signaling and scaffolding proteins, such as Abl, Src, Nck, Crk and cortactin [61-63]. Being presumably involved in VASP regulation, Ferron et al. define it as 'regulatory poly-Pro-site' [61]. The second group of proline residues (aa 160-194) comprises three canonical profilin-recognition sequences (GP₅-motifs) and is thus able to bind multiple profilactin complexes [64]. Hence, it has been described as 'recruiting poly-Pro-site'. The third group of highly conserved proline residues (aa 195-216) apparently transfers profilactin from the PRR- to the EVH2-domain, therefore being depicted as 'loading poly-Pro-site'. Both the loading poly-Pro-site and the GAB-region exhibit higher affinities to profilin-actin complexes than to profilin or G-actin alone [61, 65].

1.2.2 VASP-mediated remodelling of the actin-cytoskeleton

Actin-cytoskeleton remodelling as well as generation of long, unbranched and crosslinked bundles of F-actin filaments e.g. during filopodia formation is assumed to result from three cooperative Ena/ VASP-related molecular mechanisms: (a) prevention of CapZ-capping of barbed ends of F-actins [66]; (b) inhibition of Arp2/3-mediated actin filament branching [67]; and (c) recruitment of profilin-actin complexes at sites of actin reorganization, which furthermore appears to enhance the anti-capping effect [64, 68]. In this context, based on the energetics and structural conditions for the interaction of profilactin and VASP, Ferron et al. [61] proposed the following model of VASP-mediated processive G-actin polymerization during filament elongation (see Figure 1.5):

Accordingly, VASP tetramers are first recruited to the sites of actin-filament assembly (e.g. at the PM) by interaction of the EVH1-domain with scaffolding proteins (zyxin, vinculin, etc.) [69-71]. Here, activity of the recruiting poly-Pro-site increases the local concentration of profilactin complexes - and hence of polymerizable G-actin-monomers. Subsequently, the loading poly-Pro-site directs the transition of attached profilin-actin complexes from the recruiting poly-Pro-site to the VASP EVH2-GAB-domain, where the G-actin monomer subunits are finally added at the barbed end of the EVH2-FAB-tethered growing filament. Simultaneously, this transfer of G-actin

triggers profilin dissociation and processive stepping of the involved subunits of the VASP tetramer. Actin-mediated hydrolysis of ATP is generally regarded as the driving force behind the suggested mechanism; however, nucleotide-independent conformational changes due to the G- to F-actin transition are also discussed in this context [61].

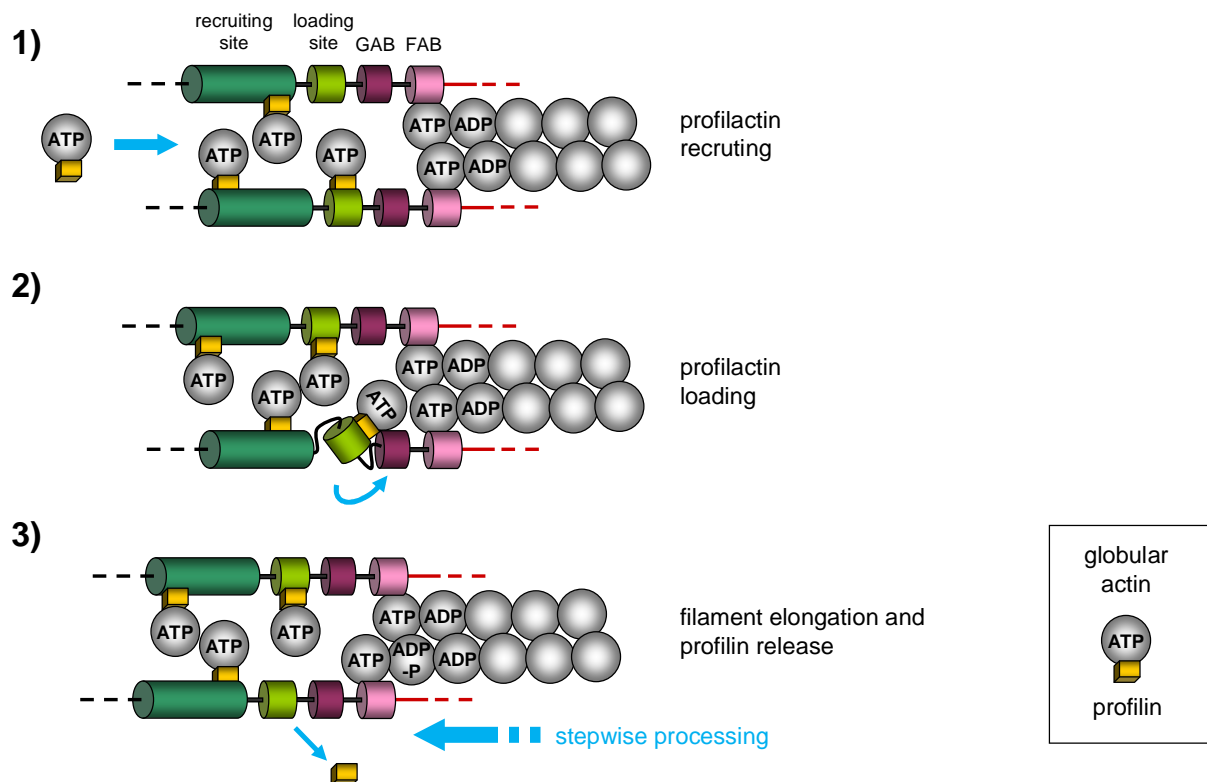


Figure 1.5: VASP-mediated filament elongation, based on Ferron et al. [61]. Blue arrows indicate central steps of the elongation mechanism: (1) interaction of profilin-actin complexes with VASP recruiting- and loading poly-Pro-sites, (2) transfer of profilactin from the loading poly-Pro-site onto the GAB-region, and (3) addition of the G-actin subunit at the barbed end of the growing F-actin filament and simultaneous profilin release.

Even though VASP tetramerization, via the CC-domains, appears to be required for efficient filament elongation, its detailed mechanistic function is still controversial. For instance, it remains speculative whether each VASP subunit supports elongation of one filament or two subunits per filament are involved. Nevertheless, regarding actin bundle formation, functional tetramers may be more efficient, in particular with respective VASP subunits acting cooperatively, both within and between neighbouring tetramers. In addition, both tetramerization and tethering via the EVH1-

domain may stabilize VASP binding to particular filaments during the processive stepping procedure, as it sequentially enables individual VASP subunits to release and advance while the remaining ones still sustain contact [61].

1.2.3 VASP phosphorylation

Since Ena/ VASP proteins are known substrates of serine/ threonine kinases, differential phosphorylation is regarded crucial for: (a) subcellular trafficking of Ena/ VASP tetramers to the PM and to growing F-actin filaments; (b) regulation of profilactin recruitment and processing; and (c) dynamic specification of protein-protein interactions, e.g. with Abl, Src or Crk [54, 72].

VASP itself harbours three known phosphorylation sites - S157, S239, T278 - with S157 being preferentially phosphorylated by PKA, S239 by PKG and T278 by AMP-activated protein kinase AMPK [54, 73-75] (see also Figure 1.4 A). In detail, VASP phosphorylation at S157, which is located between the regulatory- and the recruiting poly-Pro-site, has been reported to inhibit binding of certain SH3-domain-containing proteins (e.g. Abl) to the PRR-domain [74]. On the other hand, phosphorylation of S239 and T278, which are located at the C-terminal ends of the EVH2-GAB- (S239) and -FAB-region (T278), has been implicated in modulation of actin assembling properties. Despite the importance of Ena/ VASP-mediated signaling dynamics, detailed molecular mechanisms, analyses of spatial and temporal phosphorylation patterns and protein-protein interactions involved *in vivo* have remained elusive. Moreover, also the presence and relevance of possible additional yet-unknown VASP phosphorylation sites, as for instance recently indicated by Zahedi et al. for VASP S238 and T249 [76], has to be illuminated.

1.3 Calcium signaling in late platelet response

Although platelet activation can be induced by various agonists and receptors, the majority of downstream signaling pathways culminate in one central step: the elevation of intracellular Ca^{2+} -levels [77]. Cytosolic Ca^{2+} is a key signaling messenger in virtually all cells and regulates a wide variety of cellular functions from gene transcription to apoptosis. Accordingly, in platelets changing $[\text{Ca}^{2+}]_i$ is related to both primary and secondary hemostasis events, such as platelet shape change and degranulation, inside-out activation of integrin $\alpha_{IIb}\beta_3$, further aggregation, thrombus stabilization and, finally, induction of immune response [77-79].

Generally, cytosolic Ca^{2+} -levels can be altered by two distinct mechanisms: Ca^{2+} -depletion from intracellular stores and Ca^{2+} -influx from the extracellular space. As mentioned in 1.1.1, the major intracellular Ca^{2+} -pool in platelets is provided by the DTS [80, 81], where a high Ca^{2+} -concentration is actively maintained via sarcoplasmic/ endoplasmic reticulum Ca^{2+} -ATPases (SERCAs) [82, 83]. Upon platelet activation and subsequent PLC-mediated production of IP_3 , Ca^{2+} -release into the cytosol is operated through IP_3 receptor channels (IP_3 -R) localized within the DTS membrane [21, 84]. This fast initial mechanism has been well established for several years and seems to be sufficient to trigger the basic events of primary hemostasis without any significant delay [85]. Besides IP_3 , also cyclic ADP ribose, nicotinic acid adenine dinucleotide phosphate (NADDP) and Ca^{2+} itself have been reported to cause Ca^{2+} -store release.

Ca^{2+} -depletion from intracellular stores is usually transient; however, many cellular functions and store refilling require persistently elevated $[\text{Ca}^{2+}]_i$ levels based on influx of extracellular Ca^{2+} , which is tightly regulated by numerous Ca^{2+} -selective ion channels located within the PM [86, 87]. This amplification of an initial Ca^{2+} -signal commonly occurs in response to agonist-induced store depletion itself, hence being also referred to as store-operated calcium entry (SOCE) [85]. In particular later platelet responses leading to thrombus stabilization and/ or secondary hemostasis can be related to SOCE-dependent Ca^{2+} -signaling. Nevertheless, the complex SOCE-related molecular coupling processes, which take up to 15 sec [88], still remain obscure. The best characterized type of SOCE has initially been reported in lymphocytes and mast cells and is based on Ca^{2+} -release-activated Ca^{2+} -channels (CRAC) in the PM [89]. In this context, more recent studies identified the Ca^{2+} -sensitive 'stromal interaction molecules' [90-92] and members of the PM protein family ORAI [93, 94] as key players of the molecular CRAC entry machinery.

1.3.1 The calcium sensor STIM1

Stromal interaction molecules (STIMs) are single pass, type I transmembrane Ca^{2+} -sensitive proteins located in the ER or PM. Mammals express two isoforms (STIM1 and STIM2), with only a small fraction of STIM1 being targeted to the PM [95, 96]. In 2007, Grosse et al. were the first to link the STIM1 isoform (in human 77.5 kDa, 685 aa) to SOCE signaling via a CRAC mechanism in platelets, where the protein is located within the DTS membrane [97]. In general, the lumen-oriented N-terminal

segment of STIM1 encodes a Ca^{2+} -binding EF-hand domain (aa 63-98), and a sterile α -motif (SAM, aa 132-200, i.e. a putative protein interaction module mediating homo- and hetero-oligomerization) prior to the 21 residue transmembrane segment (aa 214-234). The cytosolic C-terminal region contains two CC-motifs (aa 248-388) and finally, at the C-terminal end, a Pro/ Ser- and a Lys-rich region (aa 600-629 and aa 672-685, respectively) [95, 98] (see also Figure 1.6). The primary sequence-based domains are highly conserved between homologues and across species [99]. Moreover, the 3D-structure of the EF-SAM motif, which forms a distinct compact entity, exposes a unique feature: The luminal STIM1 segment contains a second, non-canonical EF-hand motif not involved in Ca^{2+} -binding, but having stabilizing function instead [95]. At neutral pH, the tertiary distribution of EF-SAM residues exhibits a negatively charged surface; however, there is also a small patch of basic residues present within the SAM domain of the protein [98]. Thereby, the negative potential may be responsible for electrostatic guidance of Ca^{2+} to the binding loop of the canonical EF-hand motif, whereas the positive SAM portion might support additional biomolecular interactions, e.g. with membrane lipids.

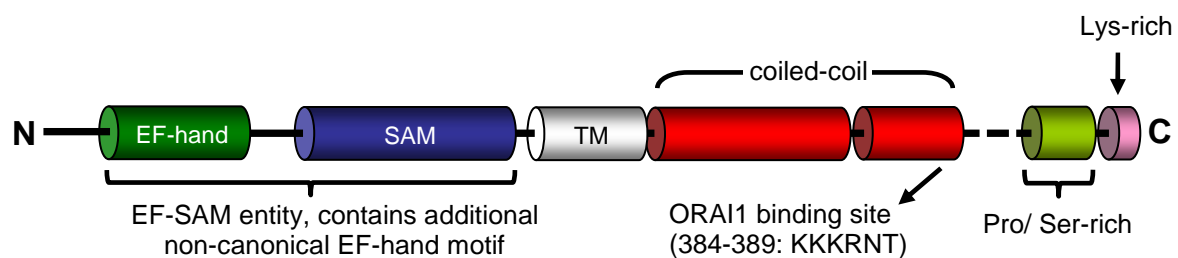


Figure 1.6: Human STIM1 domain structure: (1) N-terminal Ca^{2+} -binding EF-hand domain (aa 63-98), (2) SAM motif (aa 132-200), (3) transmembrane domain (TM, aa 214-234), (4) two CC-motifs (aa 248-388), (5) C-terminal Pro/ Ser- (aa 600-629) and Lys-rich regions (aa 672-685). The EF-SAM region forms a distinct entity and harbours an additional non-canonical EF-hand motif [95]. The predicted ORAI1 binding site is located at the end of the second CC-domain, i.e. aa 384-389.

Based on recent data, CRAC activation and initiation occurs as a multi-step, STIM1-mediated process: Under resting conditions, the STIM1 EF-hand domain is Ca^{2+} -loaded and the protein exists as a stable, globular monomer located in the ER/ DTS. Upon activation-induced store depletion, STIM1 Ca^{2+} -binding is immediately abrogated [91, 92] and the EF-SAM entity is significantly destabilized, resulting in STIM1 transitioning from holo- Ca^{2+} -loaded monomers to higher-order apo- Ca^{2+} -

depleted homotypic dimers/ oligomers in a partial unfolding-coupled process [95, 98]. This preliminary monomer-to-oligomer transition is reversible, as binding of Ca^{2+} restores the compact monomeric EF-SAM folding. Once oligomerized, homotypic STIM1 complexes translocate from a disperse DTS distribution to distinct clusters of DTS-PM junctions [95].

1.3.2 STIM1-ORAI1 interaction and CRAC entry

The true identity of the mentioned CRAC channels has also remained elusive until very recently. As initially indicated by studies on leukocytes, primary megakaryocytes and platelets of respective knock-out mice, the ORAI1 protein was finally described as the long-sought CRAC channel moiety in platelets [94, 100, 101]. Proteins of the ORAI family (ORAI1, ORAI2 and ORAI3; 28-33 kDa) contain four transmembrane segments - with both the N- and the C-terminal end facing the cytosol - and reveal high levels of glycosylation [102, 103]. They are assumed to function as homotetramers [104, 105].

ORAI1 tetramers are teardrop shaped and estimated to form the CRAC channel pore [94, 101, 106]. Accordingly, subsequent to Ca^{2+} -store depletion, ORAI1 is recruited to the same DTS-PM junctions as STIM1 dimers, creating sites of direct STIM1-ORAI1 heterotypic interaction ('punctae') [107-109] (Figure 1.7; predicted ORAI1 binding site in STIM1: aa 384-389). The minimal CRAC complex hence presumably consists of one STIM1 dimer and the ORAI1 tetramer channel pore [110, 111]. Following STIM1-ORAI1 coupling, the newly assembled CRAC channel is finally activated and the consequent influx of Ca^{2+} persistently enhances $[\text{Ca}^{2+}]_i$ for further intracellular signaling events and Ca^{2+} -store refilling. Still, numerous questions remain unanswered regarding the proposed STIM1-mediated CRAC initiation mechanism: From a structural point of view, how does partial unfolding of STIM1 by Ca^{2+} -depletion lead to EF-SAM oligomerization? How does this oligomerization promote homotypic interactions of cytoplasmic STIM1 domains, resulting in translocation of the protein complex to DTS-PM junctions? Moreover and more importantly, how does oligomerized STIM1 couple to and induce ORAI1-composed Ca^{2+} -channels? Does the STIM1-ORAI1 interaction occur directly or are there additional factors involved? Last but not least, is the discussed model also relevant in platelets *in vivo*?

One possibility to particularly address the latter issues, and thus further enhance our understanding of the molecular machinery regulating CRAC entry, might be given by

elucidating the protein-protein interactions of the cytosolic STIM1 domains in platelets.

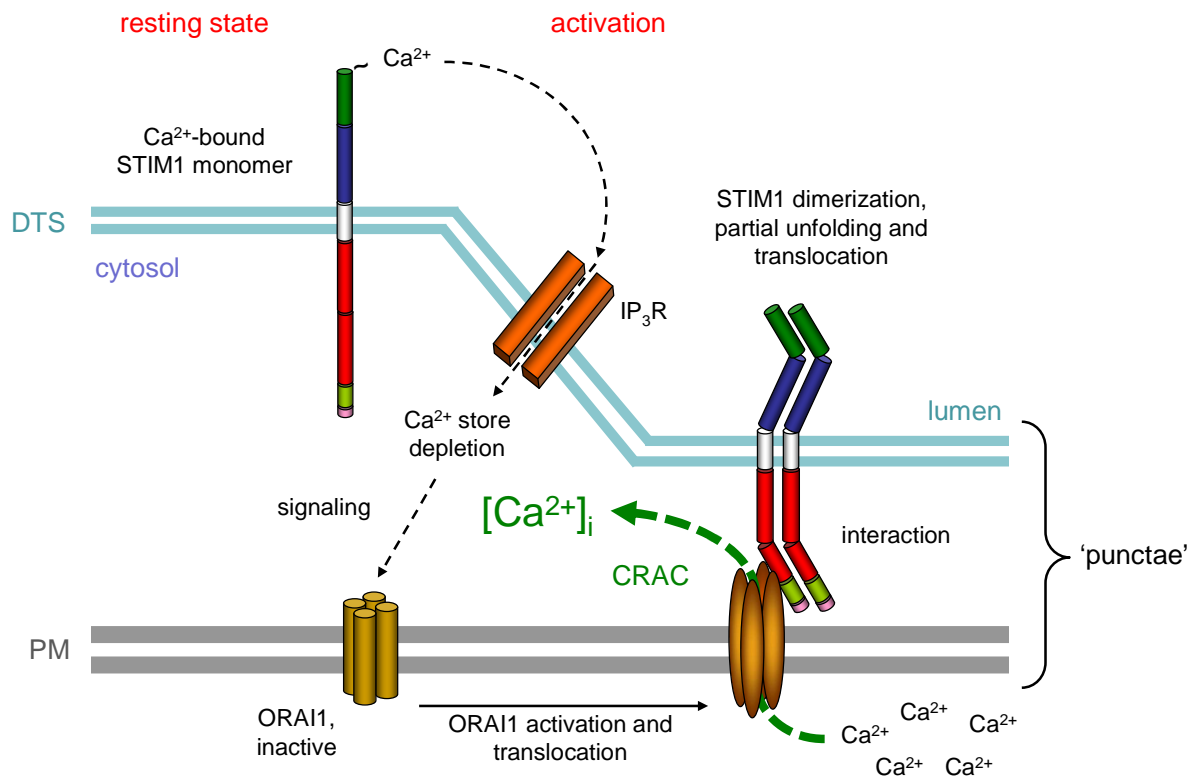


Figure 1.7: Scheme of STIM1-ORAI1 mediated CRAC entry in platelets, based on Stathopoulos et al. [95]. Under resting conditions, DTS-localized STIM1 monomers are Ca²⁺-loaded and maintain a well-folded luminal EF-SAM region. Activation-induced store release deprives Ca²⁺ from the STIM1 EF-hand domain, with EF-SAM entities undergoing partial unfolding-coupled oligomerization. The resulting STIM1 dimers translocate to the PM to interact with activated ORAI1 tetramers thus forming the CRAC channel pore for prolonged Ca²⁺-influx.

1.4 Protein interaction studies

Protein-protein interactions are the basis of many processes in living cells and regulate the majority of biological functions, e.g. during signal transduction, protein activation/ inactivation as well as structural maintenance, biosynthesis and transport of nutrients and metabolites. Such interactions might occur persistently in form of protein complexes or transiently as for instance during protein modification. Nowadays, a multitude of techniques and strategies is available to investigate this decisive issue of systems biology, with each individual one having distinct advantages and disadvantages with regard to sensitivity and specificity. Thus, the

following sections provide a brief excerpt of those biochemical methods selected for the purpose of this recent study.

1.4.1 Co-immunoprecipitation of protein complexes

Immunoprecipitation (IP) of intact protein complexes (i.e. antigen and associated ligands) is called co-immunoprecipitation (Co-IP) and considered to be the gold standard for protein-protein interaction assays [112, 113]. By targeting a protein believed to participate in a larger protein complex with a specific antibody in a Co-IP approach, the entire protein complex can be co-isolated as well, thus enabling subsequent identification of further suspected constituents. Prerequisites are maintenance of native experimental conditions and stable binding between the complex members [114]. Being solely capable of verifying interactions between suspected interaction partners, this method strongly depends on the availability of suitable antibodies (both for the IP and for subsequent ID via Western blotting) and did originally not provide screening approaches. However, implementation of protein mass spectrometry (MS) (see 1.5.2) instead of Western blotting partially overcomes the latter limitation since it allows a non-targeted analysis of the whole immunoprecipitate.

IP and Co-IP experiments can be performed both directly and indirectly. During a direct approach, the respective antibodies are first immobilized on a solid support, such as agarose or sepharose resins [115, 116]. The resulting antibody-bead complexes are subsequently added to the sample mixture and the targeted proteins are selectively captured via specific antibody-antigen interaction. When performing an indirect (Co-)IP approach, free antibodies are directly incubated with the sample protein mixture [113]. Once associated, antibody-target protein complexes are finally precipitated by adding a solid support coated with the bacterial surface proteins A or G which bind the Fc-regions of most IgG species and subclasses. Random orientation of the coupled antibodies on the resin, as it frequently occurs in direct (Co-)IP approaches, is *a priori* prevented [117]. Thus providing a higher degree of antibody mobility, this method is particularly useful in case of low target protein concentration as well as low antibody-epitope affinity.

Despite the applied (Co-)IP method, the major technical obstacle is the availability of target protein-specific antibodies - which might be circumvented with the aid of protein tags. If the protein of interest is expressed recombinantly, additional

oligopeptide sequences can be appended to its native aa-sequence, usually at the N- or C- terminal end [118]. These 'fusion tags' assist during protein identification as well as artificial modification and purification. With respect to Co-IPs, several types of protein tags are feasible: (a) epitope tags, e.g. the hemagglutinin tag (HA) and the V5-tag; (b) affinity tags, such as the glutathione-S-transferase tag (GST) and poly-histidine tags (His-tag) (see also 1.4.2); and (c) chromatography tags as for instance the polyanionic FLAG-tag [119, 120]. For each of these oligopeptides, high-affinity antibodies can be efficiently generated and used to exclusively target any recombinant protein carrying the respective tag. However, tag addition as well as expression in producer cell lines might affect native protein function and interaction behaviour to some extent. This has to be considered when evaluating the biological relevance of the obtained data. For this reason, protein tags are often specifically designed to enable their subsequent removal by chemical agents or by specific proteolysis [120]. Moreover, for further verification of Co-IP data, a counter-IP can be performed - meaning a targeted Co-IP of questionable protein interaction partners followed by specific screening of the obtained interactome for the original protein of interest. True interactions are likely to Co-IP in either way.

1.4.2 Affinity purification of individual proteins and protein complexes

Affinity chromatography generally enables isolation and concentration of a specific subset of molecules based on highly specific and reversible interactions, such as receptor/ ligand- or antigen/ antibody-binding. This method is widely applicable, however, it is most commonly used for the purification of either modified (e.g. glycosylated) or recombinant proteins carrying an affinity tag [121-124]. Depending on the stringency of chromatographic conditions, targeted proteins can be isolated together with associated components. Hence affinity chromatography approaches are also suitable for protein complex and interaction studies.

The stationary phase typically consists of an agarose gel matrix adequately modified with the corresponding ligand onto which the initial sample solution (usually crude cell/ tissue lysates or blood serum) is directly applied in a batch or a column setup [122]. During the affinity purification process, the targeted proteins are trapped on the stationary phase by exploiting the predefined interaction properties. Non-bound sample molecules either pass the matrix directly without significant retardation or are

removed by subsequent washing of the resin. The trapped proteins are finally recovered from the immobilized ligand by specific elution.

For large scale protein purification, fusion tag-targeted approaches are commonly preferred. As tag-ligand chemistry is usually well-characterized, tagged fusion proteins are easy to manipulate and can often be isolated from crude sample mixtures in a single-step affinity purification approach based on an immobilized version of their specific ligands. Such protein tags include the maltose binding protein (MBP-tag), the GST-tag, as well as the His-tag which will be described in more detail in the following [125-127]. Accordingly, His-tags are short sequences of four (His₄-tag) to nine (polyHis-tag) histidine residues and are among the most common fusion tags [125]. As histidines have high affinity for metal ions by forming specific coordinated complexes, His-tagged proteins can be trapped on a matrix containing immobilized (e.g. via chelators) metal ions, such as cobalt, nickel or copper. The respective technique is consequently described as 'immobilized metal ion affinity chromatography' (IMAC) [128, 129]. Subsequent elution strategies include change of pH (as protonated His residues dissociate from the IMAC resin) as well as addition of either metal chelating agents (e.g. EDTA) or competitive molecules such as imidazole.

1.4.3 Pull down assays

Regarding the study of putative protein interactions, all techniques described so far follow the same principle: A protein of interest is isolated based on specific affinities and additional interacting components are co-purified simultaneously - yet indirectly. Pull down assays, however, offer an alternative affinity purification technique where random proteins (meaning without further modification or specification) themselves may be used as a 'stationary phase' to directly screen for their individual interactome [130, 131]. Accordingly, the protein of interest (i.e. 'the bait') is first purified and subsequently immobilized on a solid-phase material. The thus generated 'bait support' is then incubated with the sample mixture and used for a targeted 'pull down' of putative bait-interaction partners (i.e. 'the prey'). In this context, activated solid-phase supports, such as Affi-Gel 10 (BioRad) or SulfoLink (Pierce), allow for direct covalent immobilization of almost any bait molecule to beaded agarose or sepharose. The most convenient conjugation chemistries applied are those directed towards primary amines (-NH₂) and sulfhydryl groups (-SH) of cysteine residues. For this

purpose, a terminal cysteine residue is frequently added at either the N- or the C-terminus of synthetically produced bait peptides. Additional functional groups targeted for covalent linking are hydroxyls, carboxylic acids and carbohydrate moieties [115, 116]. To preserve proper structural folding, incubation of both bait and prey material has to be performed under native conditions throughout the whole procedure. For this reason, the application of this technique is moreover commonly limited to analysis of non-membrane bait proteins.

1.4.4 Size exclusion chromatography in protein purification

In size exclusion chromatography (SEC), dissolved analytes are separated by their molecular hydrodynamic volume or size, respectively [132]. Being considered a low resolution chromatography, this technique is routinely applied under low pressure conditions for the final ‘polishing’ and desalting of crude protein purifications. The underlying principle is that analytes of different sizes will pass with different retention times through a chemically inert stationary phase consisting of porous particles of a defined pore size. During the procedure, small-sized molecules penetrate into the pores of the stationary phase and thus traverse a larger volume (i.e. the respective pore volume plus the interparticle volume) than comparatively larger sample components. As a consequence, high-molecular-weight analytes elute prior to low-molecular-weight material. Equally sized molecules, however, theoretically elute together. Generally, the so-called exclusion limit defines the upper end of separation, i.e. when sample components are too large to traverse the stationary phase and thus elute in the void volume [132, 133]. The permeation limit, on the other hand, describes the other extreme: All analytes below this molecular weight value penetrate the entire pore volume and finally elute in one single fraction. As the mobile phase is usually the same solvent used to dissolve the sample, even individual biological activities of e.g. purified proteins can be maintained [132, 133].

1.5 Protein identification by mass spectrometry

In the post-genomics era, large-scale proteomic and functional studies aim at a global view on the total protein content expressed by a cell type, tissue or organism. However, the proteome of a given biological system is highly dynamic and multifaceted. Therefore, besides protein identification, such approaches also have to

consider post-translational modifications (PTMs), alternative splice- and isoforms of proteins, quantitative aspects and protein-protein interactions [134].

Generally, proteomic workflows comprise adequate sample preparation (including cell lysis), specific enrichment or purification strategies (as proteome datasets are often biased towards high abundant proteins), followed by protein separation and fractionation often based on techniques like gel electrophoresis or (multidimensional) liquid chromatography. Protein/ peptide sequencing, identification and characterization (including e.g. PTM annotation) is finally performed via mass spectrometric measurements and subsequent computational data analysis using distinct search algorithms (most commonly Mascot [135]), databases (e.g. UniProtKB/ Swiss-Prot at www.ebi.ac.uk/uniprot) and further bioinformatic tools. Continual progress in sample preparation and separation as well as in sensitivity, scanspeed and resolution of mass spectrometers has enhanced the potential of this strategy decisively. For instance, both PTMs as well as (semi-)quantitative tasks are nowadays efficiently addressable. MS-based proteomics consequently holds the key to a refined knowledge in fundamental systems biology – including cellular mechanisms related to platelet regulation and function [136]. Hence the following sections will outline proteomic workflows in general and provide an insight into those MS methods used in the context of this work.

1.5.1 Preparing protein samples for MS analysis

1.5.1.1 Cell lysis

Sample preparation for proteomic research encompasses as a first step protein extraction from respective biological material (e.g. by cell disruption), followed by specific protein enrichment and removal of interfering or contaminating lysate components. For cell lysis, one distinguishes between mechanical (also 'physical') and non-mechanical cell disruption strategies [137].

Regarding mechanical cell lysis, high-pressure- (also 'high shear'-) homogenization as well as sonication have been applied within the current study. High-shear mechanical processors are often referred to as the method of choice for large-scale approaches and have proven to be especially suitable for bacteria and mycelia [137]. In a French press, the cell suspension is e.g. pressed through a narrow valve or channel, which consequently disrupts cell membranes by strong liquid shear and highly focused turbulences at the entrance orifice, as well as by the sudden pressure

drop to atmospheric value as soon as the lysate passes the exit orifice [137, 138]. Sonication (also 'ultrasonic treatment' or 'sonoporation') on the other hand, which is best suited for volumes less than 100 mL, utilizes pulsed, high frequency sound waves to lyse cells with less resistant cell walls, such as certain bacteria and fungi as well as animal cells and tissue in laboratory scale [138]. The resulting pressure waves confer mechanical energy to the liquid, leading to streaming and the formation and sudden collapse of low-pressure vapor cavities (i.e. cavitation process). As a consequence, intensive shock waves spread out through the suspension with sufficient energy to cause agitation and disruption of cellular barriers by shearing and breaking of covalent bonds. However, one general negative side effect of any physical cell disruption technique is given by the accompanying harsh conditions, in particular sample heating. Hence to avoid unintended protein denaturation and aggregation, the whole equipment has to be constantly cooled and repetition cycles should be kept at a minimum.

In contrast, non-mechanical lysis of cell walls and plasma membranes provides a mild and efficient alternative. Such strategies include enzymatic digestion of bacterial, yeast or plant cell walls by glycanases and proteases [139], plasmolysis by osmotic shock in hypotonic buffers, as well as chemical permeabilization of the plasma membrane phospholipid bilayer by organic solvents (e.g. chloroform, benzene, ether, methanol and toluene) or chaotropic agents (such as urea and guanidine) [140, 141], as well as by detergents (for instance digitonin, Nonidet P-40, and Triton X-100) [137, 142]. Depending on the type of detergent, cell lysis might occur (a) denaturing when using strong solubilizing ionic agents; or (b) non-denaturing in case of non-ionic and zwitterionic compounds. The latter ones, such as Triton X-100 or CHAPS, are consequently preferred when studying native protein interactions and functions [142].

Subsequent to cell disruption, sample complexity has to be further reduced prior to MS analysis. Final enrichment and purification of the protein fraction of interest can be performed in a targeted approach as described in 1.4.1 - 1.4.3, as well as by either overall protein precipitation or specific sample separation - with gel electrophoresis and liquid chromatography being widely applied techniques in this context.

1.5.1.2 Separation of protein samples by gel electrophoresis

Electrophoresis, i.e. ion migration in an electric field, is a frequently applied technique for the separation of complex mixtures, including protein samples. In gel electrophoresis, this process occurs e.g. within a polyacrylamide or agarose gel matrix; molecular segregation hence depends on both electrophoretic mobility of the analyte ions and gel filtration effects specified by the size of the gel pores, which results in retardation of larger molecules in relation to smaller ones.

In polyacrylamide gel electrophoresis (PAGE) - a technique commonly applied for protein separation - gels are generated by co-polymerizing acrylamide monomers via crosslinking reagents such as N,N'-methylenebisacrylamide [143]. Prior to PAGE, protein samples have to be efficiently solubilized. In addition, by forming complexes with the anionic detergent sodium dodecylsulfate (SDS), proteins are denatured (see also 1.5.1.1) and their endogenous net charges are negatively masked [143, 144]. Hence, upon application of an electric field, the protein mixture starts migrating towards the anode and the individual components are separated into series of discrete bands following the order of their molecular masses (1D-SDS-PAGE). To increase sample resolution, two orthogonal separation modes, such as isoelectric focussing (IEF) and SDS-PAGE, can be combined (i.e. two-dimensional gel electrophoresis, 2-DE) [145, 146]. Subsequent to 1-DE and 2-DE, separated proteins can be detected via gel staining (e.g. Coomassie blue- and silver staining) [147] or Western blotting, and distinct proteins of interest can furthermore be excised, proteolytically processed and extracted for MS-based characterization.

1.5.1.3 Protein digestion and denaturation

Due to their large molecular weight (MW), intact proteins are difficult to analyze by means of mass spectrometry and thus are commonly cleaved into peptide fragments prior to MS analysis. Such cleavage can be performed either in-gel or in-solution via usage of proteolytic enzymes which specifically recognize and hydrolyse peptide bonds between distinct amino acids. One of the most frequently applied proteases in proteome studies is the highly effective serine protease trypsin [148]. It cleaves peptide bonds C-terminally of arginine and lysine residues (except these amino acids are followed by proline [149]) and thus creates fragments of approximately 10-17 aa with defined C-terminal ends. Trypsin digestion is regularly performed over night at 37°C in a protease-to-protein ratio of 1:20 - 1:100. However, since complex protein

structures (caused by intra- and intermolecular ion bonds, hydrogen bridges, hydrophobic interactions and disulfide bonds) often disturb proteolytic cleavage, initial denaturation is mandatory. For instance chaotropes (commonly urea or thiourea) help to undo hydrogen bridges. Detergents, on the other hand, are used in particular when hydrophobic proteins are to be solubilized as they prevent protein precipitation by conferring a hydrophilic character [142, 144]. Regarding disulfide bonds, a common derivatisation procedure is given by dithiothreitol (DTT)-mediated chemical reduction. In order to avoid reorganization of the resulting free cysteines, these sidechains are subsequently irreversibly modified by alkylation, e.g. via iodoacetic acid or iodoacetamide (IAA) [150].

1.5.1.4 Separation of proteome samples by liquid chromatography

Liquid chromatography (LC) offers the possibility of sample fractionation and concentration as well as removal of contaminations, such as salts, buffers and detergents. In principle, dissolved analytes (i.e. in a mobile phase) are applied to a stationary phase where they are retained based on their individual affinities towards the respective matrix material [151]. Unbound or unspecific remnants and contaminations are subsequently removed and the trapped molecules are finally released by suitable elution profiles.

Nowadays, high-performance LC (HPLC, also high-pressure LC) - an automated, fast and very sensitive high-throughput LC setup - is regularly used in proteomic studies [152]. Here, the analytes are automatically applied to the HPLC system, e.g. via an autosampler. For the generation of solvent gradients particularly necessary for continuous analyte elution, at least a binary solvent system is regularly implied in proteomic HPLC setups. In proteome research, HPLC approaches typically utilize a precolumn concentration setup for fast sample loading and desalting [153], coupled to the main separation column. Since reduction of the inner diameter of the separation column results in enhanced sensitivity [152], optimal HPLC separation is commonly achieved with small columns densely packed with 2-5 μm particle size resins. Following the column unit, an UV-detector enables constant monitoring of the chromatographic separation. Accordingly, the UV-absorbance of peptide bonds is regularly determined at 214 nm, the one of aromatic side chains of Phe, Tyr or Trp residues at 254 and 280 nm, respectively [154].

Of the numerous chromatographic procedures, two have to be particularly mentioned with regard to protein mass spectrometry: ion exchange chromatography (IEC) and reversed-phase chromatography (RP). The competitive interaction of charged molecules presents the basic principle of IEC. Here, the stationary phase contains ionic functional groups which selectively interact with analyte counter ions [155, 156]. In contrast to IEC, which is often applied for pre-fractionation, RP enables separation of organic substances according to their hydrophobicity [152, 157]. The RP stationary phase is commonly substituted with long chains of alkyl residues, thus providing an organic, non-polar matrix. Depending on the hydrophobic characteristics of the analyte, C1 up to C30 RP materials are used (commonly C4 or C8 for hydrophobic proteins and C18 for peptides) [158]. For improved separation, the mobile phase is composed of an aqueous buffer solution (including low amounts of ion pair reagents such as formic acid or trifluoroacetic acid) and an organic modifier. Due to low viscosity, low chemical reactivity, absence of UV-absorbance above 200 nm and a medium polarity enabling both miscibility with water and solubility of ionic as well as non-polar compounds, acetonitrile (MeCN) is most frequently applied in this context [156]. During the chromatographic procedure, polar sample components elute first from the column while non-polar molecules (e.g. peptides) are stronger retained as a result of hydrophobic interactions with the stationary phase. The bound analytes are finally eluted by gradually increasing the organic content of the mobile phase, with non-polar molecules consequently having longer retention times (RTs) than more polar ones.

Nowadays, RP accounts for the majority of LC, in particular in proteome research where it enables efficient separation of complex protein and peptide mixtures and simultaneously provides suitable conditions for subsequent MS analysis [152]. In recent years, multidimensional LC-MS (MDLC-MS) is increasingly emerging, with MudPIT (i.e. multidimensional protein identification technology) being one of the most prominent techniques in this context [159, 160]. Such approaches enable separation and identification of highly complex peptide mixtures.

1.5.2 Mass spectrometric analysis

Mass spectrometers are composed of three functional units: Firstly, the ion source where charged analyte ions are generated, desolvated and transferred into the mass analyzer. In proteomics, which requires gentle and reliable ionization of large

biomolecules, either electrospray ionization (ESI) [161, 162] or matrix-assisted laser desorption/ ionization (MALDI) [163, 164] are generally applied. The resulting analyte ions are subsequently stored, separated or further fragmented in the mass analyzer unit. Such MS analyzers include quadrupole systems (e.g. triple-quadrupoles, see 1.5.2.2), electric ion traps, as well as time-of-flight- (TOF), Fourier-transform ion cyclotron resonance- (FTICR, also FTMS) and Orbitrap instruments [165-167]. Hybrid instruments, such as linear ion traps (Qtrap, LTQ), LTQ-Orbitraps or quadrupole-TOF analyzers (QTOF), combine certain advantages [168, 169]. Finally, the MS detector unit traces the current induced by analyte ions and continuously records respective ion signal intensities. Since the amount of ions delivered by the mass analyzer is usually relatively small, some types of electron multipliers are applied for further signal amplification by secondary electron emission [170, 171]. Deriving from the analyzer-detector interplay, the total of ion signal intensities is displayed as a function of m/z (m : mass, z : charge) throughout the whole scanning period - hence generating a typical mass spectrum. Nowadays, there are multiple instrumental MS setups commercially available, with each single one having individual specificities and distinct fields of application. The following sections, however, will only focus on MS units which have been of particular relevance in the context of this work.

1.5.2.1 Electrospray ionization and LC-ESI-MS

Electrospray means the dispersion of a liquid into many small, charged droplets within an electrostatic field [172]. During ESI, peptide ions are desolvated - i.e. transferred from solution into gas phase - at atmospheric pressure. In detail, the sample solution is injected to the MS ion source, e.g. via a fused silica capillary held at a voltage of several kV depending on the source design (Figure 1.8). Upon entering the electrostatic field, charged droplets are generated and continuously reduced in volume by constant solvent evaporation [173]. When reaching the Rayleigh limit, the charge accumulation on the droplet's surface culminates in so-called Coulomb explosions, leading to formation of microdroplets. According to both the 'charged residue model' (established by Dole et al., 1968) [174] and the 'single ion in droplet theory' by Friedrich Röllgen et al. (1989) [175], numerous subsequent Coulomb explosions finally produce droplets having a radius of approximately one nanometer and containing only a single analyte ion. Upon collision with nitrogen molecules infused at the interface between the source region and the mass analyzer,

these distinct analyte ions are finally completely desolvated. Another theory, the 'ion evaporation model', has been established by Iribane and Thomson in 1976 [176]. Accordingly, the Coulomb explosions generate bigger microdroplets (radius approximately eight nanometers) containing several molecule ions and thus being highly charged. At these conditions, free molecule ions are constantly emitted into the gas phase. Although the amount of charges decreases during this process, the ion emission still persists since the microdroplet volume is simultaneously reduced by continuous solvent evaporation - until the analyte ions, both singly and multiply charged, are completely desolvated.

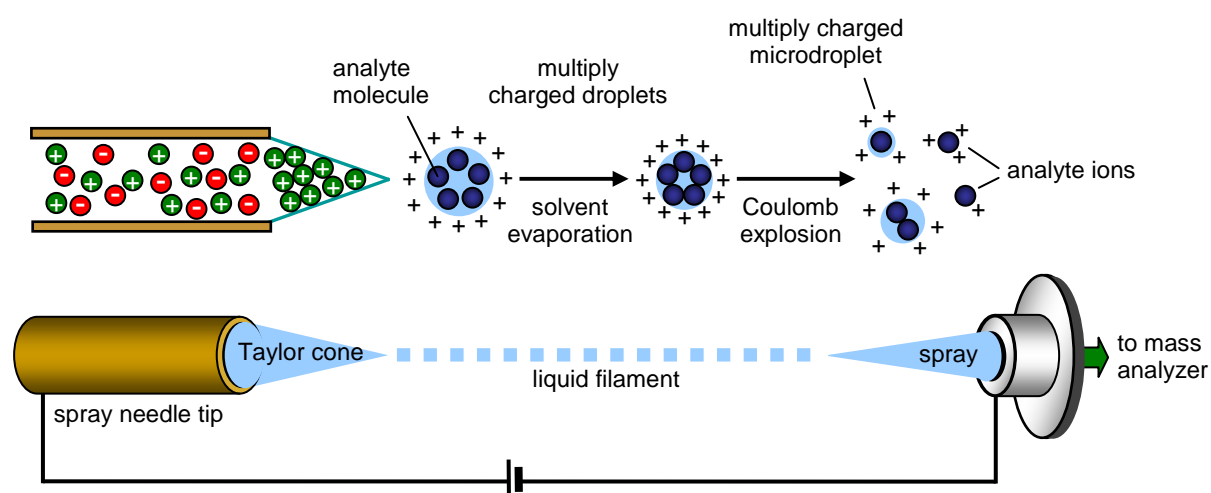


Figure 1.8: ESI ionization. Upon application of an electric field, charged sample droplets are generated and accelerated towards the mass analyzer interface. During this process, constant solvent evaporation culminates in Coulomb explosions and thus in generation of first multiply charged microdroplets and finally in completely desolvated analyte ions.

In either case, for adequate sample desolvatisation organic liquids (ethanol, MeCN, etc.) proved to be advantageous since the correspondingly high vapor pressure accelerates solvent evaporation during the ESI process [177]. Moreover, peptide protonation (as required for MS measurement in positive ion mode) is promoted by addition of weak organic acids, commonly formic acid (FA) at a concentration of 0.01-0.2%. Additional components like salts, detergents or strong ion-pairing agents such as trifluoroacetic acid (TFA) [178], however, may disturb ESI-MS either by affecting the ionization process (e.g. prevention of free analyte formation due to detergent-peptide interactions) or by subsequently contributing to strong ion signals themselves. As a consequence, when using appropriate conditions HPLC-based

sample purification/ separation and ESI-MS can efficiently be combined in an online LC-ESI-MS setup [179]. In this context, to maintain stable ionization, the applied voltage and the flow rate, as well as sample conductivity and liquid surface tension have to be balanced adequately. The challenge is to improve both the ESI ionization process and the sensitivity of detection by using small separation columns and low flow rates (i.e. nano-LC) [152]. Hence, columns having an inner diameter of 75-100 μm are most frequently utilized in proteomic applications nowadays.

1.5.2.2 Quadrupoles and ion traps

From the MS ion source, peptide ions are directed towards the mass analyzer for m/z determination. Typical ESI mass analyzer used in the context of this work were quadrupoles and ion trap instruments. Quadrupoles are composed of four parallel metal electrodes (circular or hyperbolic rods) to which an electric field - i.e. a superimposition of a constant and an alternating current - is applied. In detail, opposite electrodes are in-phase and have the same polarity; juxtapositioned electrodes possess reversed polarity and a phase difference of 180° [180]. Once injected, the analyte ions are guided to traverse these oscillating quadrupole fields. Thereby, depending on the applied voltages, exclusively ions of a defined m/z ratio travel on stable trajectories and will reach the detector unit. All other ions are either deflected or absorbed upon collision with the electrodes. This allows for selected scanning of a whole range of ions of particular m/z values. Modern quadrupoles are thus able to address m/z values up to 4,000 with a mass resolution between 500 and 5,000 [180]. Often linear arrangements of three quadrupoles Q_1 - Q_3 (i.e. triple-quadrupole instrument) are applied (Figure 1.9).

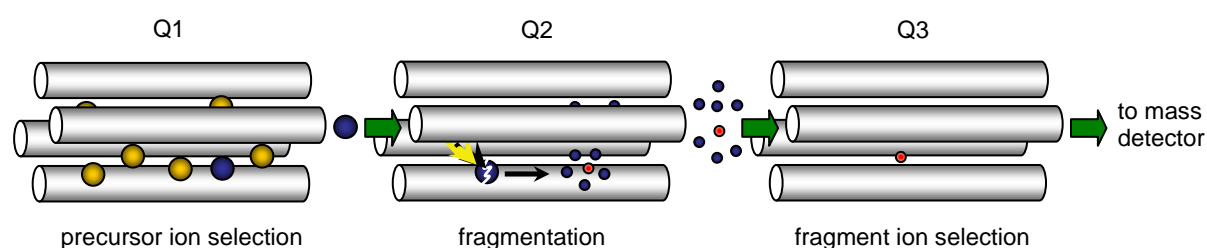


Figure 1.9: Triple-quadrupole instrument. Q_1 and Q_3 function as mass filters for precursor- and fragment ion selection, respectively. Q_2 acts as collision cell for CID fragmentation of selected precursor ions.

In this context, Q_1 and Q_3 commonly function as mass filters and Q_2 acts as collision cell where precursor ions selected in Q_1 are fragmented by colliding with intra-systemic nitrogen, helium or argon gas molecules ('collision-induced dissociation', CID) [181]. Thus generated fragment ions are then transferred to Q_3 and are either completely or selectively conveyed to the MS detector unit (tandem MS, MS^2 or MS/MS). In contrast to MS survey scans (m/z ratios of all precursor ions) MS/MS fragmentation of isolated precursor ions consequently delivers profound sequence information.

Whereas quadrupole systems selectively filter for ions of certain m/z values, ion traps have specifically been developed to accumulate and store ions of a defined mass range prior to successive m/z determination. Classical electric ion traps consist of a circular electrode ('ring electrode'), to which a radio frequency voltage is applied, and two endcap electrodes held at ground (or auxiliary) potential [182] (Figure 1.10). Analyte ions are injected and finally ejected via small orifices located in the center of each endcap. Functionally, electric ion traps are based on the same principles as quadrupoles; however, in contrast to quadrupoles, upon application of an adequate alternating current a three-dimensional quadrupolar field is generated inside the trap [183]. As soon as analyte ions enter the trap, they are first decelerated by collision with helium gas ('collisional cooling') and finally caught in the center of the ion trap. Here, they are maintained on stable trajectories and successively ejected towards the detector with the aid of multipolar electric fields. Modern electric ion traps provide mass resolutions up to 20,000 and cover m/z values of up to 6,000 [184]. Apart from 3D electric ion traps, linear ion traps are increasingly utilized in proteomic research - either as stand-alone device or in hybrid instruments. Here, analyte ions are maintained in a trapping field generated by a set of quadrupole rods [185, 186]. Similar to triple-quadrupole systems, ion traps also enable distinct peptide fragmentation: The selected precursor ions are first isolated (ions of diverging m/z values are ejected from the trap) and subsequently excited by increasing the applied voltages. This finally culminates in controlled collision with helium gas molecules and thus in CID fragmentation. Once generated fragments can either be ejected for detection (MS^2) or selectively subjected to further fragmentation cycles (i.e. $MS^3 - MS^n$) to gain supplemental structural information.

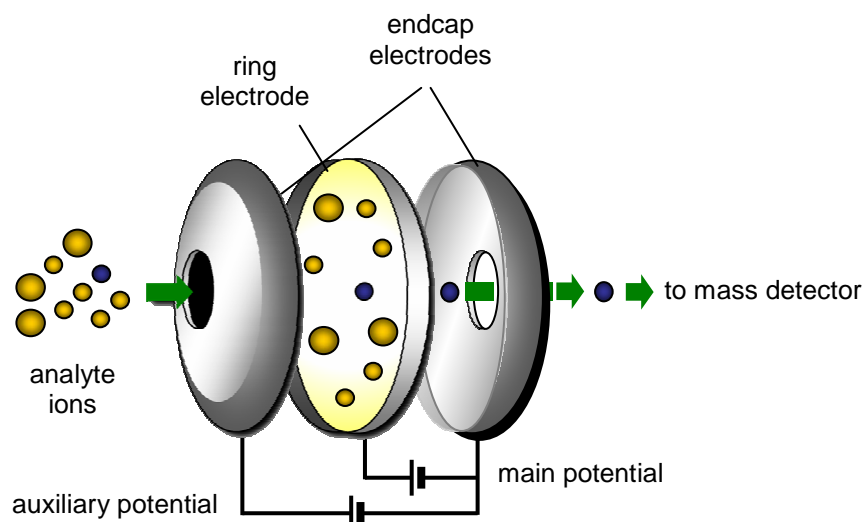


Figure 1.10: Electric ion trap, consisting of a ring- and two endcap electrodes. Analyte ions entering the system through a small orifice are stored, fragmented and selectively ejected towards the MS detector via modulation of three-dimensional quadrupolar electric fields generated inside the He-filled trap.

1.5.2.3 Interpretation of mass spectrometric datasets

During the MS/MS fragmentation process, peptides predominantly dissociate at the peptide bonds, which generates both charged and neutral fragments. In case of the charge remaining at the N-terminal fragment side, the respective ions are called a-, b- and c-ions (following the Roepstorff-Fohlmann-Biemann nomenclature) [187, 188]; if it remains at the C-terminal side, they are called x-, y-, z-ions. Once assigned to the [a,b,c]- or [x,y,z]-series, the primary aa-sequence of the original molecule can theoretically be concluded based on the individual molecular masses of all successive fragments of a distinct precursor peptide (i.e. de-novo sequencing) [189]. In addition, as mentioned in 1.5.2.2, MSⁿ approaches also provide specific supplemental information e.g. on PTMs.

The generated data might be analyzed manually; however, usage of advanced proteomic informatics tools vastly reduces the time required for large datasets derived from LC-ESI-MS/MS experiments. Using search algorithms like Mascot [135], SEQUEST [190], OMSSA [191], Phenyx [192] or X!Tandem [193], experimental MS spectra are automatically compared to *in silico* predicted ones provided by adequate proteomic databases. Databases frequently applied in this context are the International Protein Index (IPI, www.ebi.ac.uk) or the UniProtKB/ Swiss-Prot

(www.ebi.ac.uk/uniprot) database. Potentially matching sequences are subsequently summarized in identification lists [194, 195]. This process regularly implies profound statistical validation including determination of thresholds or evaluation of false discovery rates (FDR) [196-198]. The likelihood of matching peptides being random hits is calculated and displayed as scores (e.g. high Mascot scores relate to 'true' hits); respective cut-off scores have to be defined depending on the applied algorithm. In addition, search parameter settings commonly specify: (a) the applied protease; (b) the number of allowed missed cleavage sites; (c) modifications (e.g. carbamidomethylation, methionine oxidation and phosphorylation sites); (d) MS and MS/MS mass tolerances; as well as (e) charge and expected fragment ion series. The total amount of identified peptides is finally assembled to proteins which are subsequently ranked based on their individual overall identification score. Most often, consistent protein annotation relies on assignment of at least two distinct peptides, thereby excluding so-called 'one-hit wonders'. Determination of isoforms moreover requires reliable identification of at least one unique peptide for the putative isoform. However, for final protein characterization - including PTM annotation as well as structural and quantitative evaluations - and adequate integration in complex biological interaction networks (i.e. systems biology), more sophisticated computational strategies are required. Valuable protein-specific information is provided by online databases such as UniProtKB/ Swiss-Prot (e.g. on protein domain structure, putative modification sites, isoforms, homologies and reported function), as well as by sequence- and structural alignment tools as for instance SMART (<http://smart.embl-heidelberg.de>), PFAM (<http://pfam.sanger.ac.uk>) or the RCSB protein database (www.rcsb.org/pdb/home/home.do). Finally, bioinformatics tools like STRING 8.3 (<http://string-db.org>) also include data derived from other -omics approaches (i.e. genomics, transcriptomics, metabolomics, lipidomics), thus helping to deduce a scheme of known and predicted interaction pathways related to the identified protein.

2 Objective

Following platelet recruitment to sites of vessel injury, elevation of intracellular Ca^{2+} -levels and platelet shape change provide the basis for later-occurring events of cellular hemostasis. Therefore, numerous studies have focused on gaining insight into related signaling pathways and the underlying protein-protein interactions. The actin filament-remodelling protein VASP and the Ca^{2+} -sensing molecule STIM1 are regarded as being amongst the key players involved during this stage of platelet response. Although these two proteins have clearly been linked to cytoskeleton shape change and platelet CRAC entry, their precise regulatory and functional mechanisms are still far from being fully understood. Therefore, it is the overall aim of this work to specifically address the VASP and STIM1 interactome in resting platelets.

First, inspired by Benz et al. [199], a differential proteomics strategy should be developed to analyze protein binding of VASP in a phosphorylation-dependent manner. For this purpose, affinity-tagged phospho-mimetic mutants of human VASP will be overexpressed, purified and immobilized on an affinity support. The resulting bait matrices should consequently serve to perform differential phospho-specific interactome studies in native platelet lysates of human origin. In parallel, the interactome of STIM1 will be examined in a similar pull down-based approach: Here, affinity-tagged truncated STIM1 constructs (cytosolic portion) should be used as bait and native lysates of resting human platelets as prey material.

Differential analysis and component identification of all interactome samples will finally be achieved by 1D-SDS-PAGE and subsequent nano-LC-ESI-MS/MS. Putative protein interaction partners will moreover be specifically confirmed by independent methods, such as Co-IP and Western blotting. In this context, particular interest focuses on hitherto unknown VASP- and STIM1 binding partners as these candidates may help to deduce signaling pathways possibly involved in platelet activation and shape change - and thus in the regulation of thrombotic events.

3 Materials and Methods

3.1 Table 3.1: Chemicals, media and enzymes

Reagent	Manufacturer
Acetic acid	Merck KGaA, Darmstadt, Germany
Acetonitrile, ULC/ MS	Merck KGaA, Darmstadt, Germany
N-Acetyl- β -D-glucosamine	Sigma-Aldrich Chemie GmbH, Steinheim, Germany
Affi-Gel 10	BioRad Lab GmbH, München, Germany
Agarose	Sigma-Aldrich Chemie GmbH, Steinheim, Germany
Ammonium bicarbonate	Merck KGaA, Darmstadt, Germany
Ammonium sulfate	Merck KGaA, Darmstadt, Germany
Ampicillin	Sigma-Aldrich Chemie GmbH, Steinheim, Germany
Bacto agar	Becton Dickinson GmbH, Heidelberg, Germany
Bacto tryptone	Becton Dickinson GmbH, Heidelberg, Germany
Bacto yeast extract	Becton Dickinson GmbH, Heidelberg, Germany
BamHI restriction enzyme	New England BioLabs GmbH, Frankfurt, Germany
Benzonase endonuclease	Merck KGaA, Darmstadt, Germany
Boric acid	Sigma-Aldrich Chemie GmbH, Steinheim, Germany
Bovine serum albumin	Sigma-Aldrich Chemie GmbH, Steinheim, Germany
Bromo-chloro-indolyl-galacto-pyranoside	Sigma-Aldrich Chemie GmbH, Steinheim, Germany
Bromophenol blue sodium salt	Merck KGaA, Darmstadt, Germany
Calcium chloride	Merck KGaA, Darmstadt, Germany
Calpain-1 (μ -calpain), human	Merck KGaA, Darmstadt, Germany
Calpain-2 (m-calpain), rat	Merck KGaA, Darmstadt, Germany
Chloramphenicol	Applichem GmbH, Darmstadt, Germany
3-[(3-Cholamidopropyl)dimethylammonio]-1-propane-sulfonate	Merck KGaA, Darmstadt, Germany
Citric acid	Merck KGaA, Darmstadt, Germany
Cloned <i>Pfu</i> DNA polymerase AD	Agilent Technologies Dtl. GmbH, Böblingen, Germany
Cloned <i>Pfu</i> reaction buffer AD (10x)	Agilent Technologies Dtl. GmbH, Böblingen, Germany
CLP36 protein (PDLIM1), human	Abnova Corporation, Jhongli City, Taiwan
Complete Mini Protease Inhibitor	Roche Diagnostics, Mannheim, Germany
Complete Mini Protease Inhibitor, EDTA-free	Roche Diagnostics, Mannheim, Germany
Complete Protease Inhibitor	Roche Diagnostics, Mannheim, Germany
Coomassie G-250	Merck KGaA, Darmstadt, Germany
Dimethyl sulfoxide	Applichem GmbH, Darmstadt, Germany
Dithiothreitol	Merck KGaA, Darmstadt, Germany
DNA Ladder (123 bp)	Sigma-Aldrich Chemie GmbH, Steinheim, Germany
DNA Loading Buffer	MBI Fermentas GmbH, St. Leon-Rot, Germany
dNTP-Mix	MBI Fermentas GmbH, St. Leon-Rot, Germany
Dulbecco's modified Eagle's medium	PAA Laboratories GmbH, Cölbe, Germany
Dulbecco's phosphate buffered saline	PAA Laboratories GmbH, Cölbe, Germany
Eagle's minimum essential medium	PAA Laboratories GmbH, Cölbe, Germany
EcoRI restriction enzyme	New England BioLabs GmbH, Frankfurt, Germany
Ethanol (96%) (v/v)	Carl Roth GmbH, Karlsruhe, Germany
Ethanol (for DNA preparation)	Sigma-Aldrich Chemie GmbH, Steinheim, Germany
Ethanolamine	Merck KGaA, Darmstadt, Germany
Ethylenedinitrilo-tetraacetic acid disodium dihydrate	Merck KGaA, Darmstadt, Germany
ExGen 500 <i>in vitro</i> transfection reagent	MBI Fermentas GmbH, St. Leon-Rot, Germany
Fetal calf serum	PAA Laboratories GmbH, Cölbe, Germany
Formaldehyde solution (37%) (v/v)	Carl Roth GmbH, Karlsruhe, Germany
Formic acid, ULC/ MS	Merck KGaA, Darmstadt, Germany
GelRed Nucleic Acid Gel Stain	VWR International GmbH, Nürnberg, Germany
GeneRuler 1kb DNA Ladder	MBI Fermentas GmbH, St. Leon-Rot, Germany
Geneticin (G418)	Applichem GmbH, Darmstadt, Germany
D-Glucose	Merck KGaA, Darmstadt, Germany
L-Glutamine	Invitrogen GmbH, Karlsruhe, Germany
Glycerol (87%) (v/v)	Merck KGaA, Darmstadt, Germany
Glycine	Applichem GmbH, Darmstadt, Germany
Hexamminecobalt (III) chloride	Sigma-Aldrich Chemie GmbH, Steinheim, Germany
Hydrochloric acid (37%) (v/v)	Merck KGaA, Darmstadt, Germany

N-2-Hydroxyethylpiperazine-N-2-ethanesulfonic acid	Applichem GmbH, Darmstadt, Germany
Igepal CA-630	Sigma, Deisenhofen, Germany
Imidazole	Merck KGaA, Darmstadt, Germany
Iodoacetamide	Merck KGaA, Darmstadt, Germany
Isopropyl β -D-1-thiogalactopyranoside	MBI Fermentas GmbH, St. Leon-Rot, Germany
L-Lysine hydrochloride	Merck KGaA, Darmstadt, Germany
Magnesium chloride, anhydrous	Sigma-Aldrich Chemie GmbH, Steinheim, Germany
Manganese chloride	Merck KGaA, Darmstadt, Germany
Mark 12 MW Standard	Invitrogen GmbH, Karlsruhe, Germany
β -Mercaptoethanol	Biomol GmbH, Hamburg, Germany
Methanol, Rotipuran	Carl Roth GmbH, Karlsruhe, Germany
Monosodium phosphate	Merck KGaA, Darmstadt, Germany
2-N-Morpholino ethanesulfonic acid	Carl Roth GmbH, Karlsruhe, Germany
NEB BSA solution	New England BioLabs GmbH, Frankfurt, Germany
NEBuffer 3 (10x)	New England BioLabs GmbH, Frankfurt, Germany
Ni-NTA agarose	Qiagen GmbH, Hilden, Germany
Nicotinamide	Sigma-Aldrich Chemie GmbH, Steinheim, Germany
Nonfat dried milk powder	Applichem GmbH, Darmstadt, Germany
Nonidet P40 substitute	Fluka GmbH, Steinheim, Germany
NuPAGE LDS Sample Buffer (4x)	Invitrogen GmbH, Karlsruhe, Germany
NuPAGE MOPS SDS Running Buffer (20x)	Invitrogen GmbH, Karlsruhe, Germany
NuPAGE Transfer Buffer (20x)	Invitrogen GmbH, Karlsruhe, Germany
Ortho-phosphoric acid (89%) (v/v)	VWR International GmbH, Nürnberg, Germany
Overnight Express Instant TB Medium	Merck KGaA, Darmstadt, Germany
PageRuler Prestained Protein Ladder	MBI Fermentas GmbH, St. Leon-Rot, Germany
Penicillin	PAA Laboratories GmbH, Cölbe, Germany
PhosSTOP Phosphatase Inhibitor	Roche Diagnostics, Mannheim, Germany
Ponceau S	Merck KGaA, Darmstadt, Germany
Potassium chloride	Merck KGaA, Darmstadt, Germany
Potassium dihydrogen phosphate	Merck KGaA, Darmstadt, Germany
Potassium hydroxide	Merck KGaA, Darmstadt, Germany
2-Propanol	Merck KGaA, Darmstadt, Germany
Quick Ligation Reaction Buffer	New England BioLabs GmbH, Frankfurt, Germany
Rubidium chloride	Merck KGaA, Darmstadt, Germany
See Blue Plus2 Prestained Protein Standard	Invitrogen GmbH, Karlsruhe, Germany
Silver nitrate	Carl Roth GmbH, Karlsruhe, Germany
Sodium acetate	Merck KGaA, Darmstadt, Germany
Sodium azide	Merck KGaA, Darmstadt, Germany
Sodium carbonate, anhydrous	Applichem GmbH, Darmstadt, Germany
Sodium chloride	Merck KGaA, Darmstadt, Germany
Sodium citrate	Merck KGaA, Darmstadt, Germany
Sodium dihydrogen phosphate monohydrate	Merck KGaA, Darmstadt, Germany
Sodium dodecylsulfate	Applichem GmbH, Darmstadt, Germany
Sodium hydrogen carbonate	Merck KGaA, Darmstadt, Germany
di-Sodium hydrogen phosphate dihydrate	Merck KGaA, Darmstadt, Germany
Sodium hydroxide	VWR International GmbH, Nürnberg, Germany
Sodium thiosulfate pentahydrate	Merck KGaA, Darmstadt, Germany
Streptomycin	PAA Laboratories GmbH, Cölbe, Germany
Taq-Polymerase	MBI Fermentas GmbH, St. Leon-Rot, Germany
Trifluoroacetic acid, ULC/ MS	Merck KGaA, Darmstadt, Germany
Tris-hydroxymethyl-aminomethane, base	Applichem GmbH, Darmstadt, Germany
Triton X-100	Roche Diagnostics GmbH, Mannheim, Germany
Trypsin Gold, modified, seq. grade	Promega GmbH, Mannheim, Germany
Tween 20	Sigma-Aldrich, Steinheim, Germany
Urea	Applichem GmbH, Darmstadt, Germany

3.2 Table 3.2: Kits

Kit	Manufacturer
BCA Protein Assay Kit	Thermo Fisher Scientific, Bonn, Germany
β -Gal Staining Kit	Invitrogen GmbH, Karlsruhe, Germany
GenomeLab DTCS Quick Start Kit	Beckman Coulter GmbH, Krefeld, Germany
MinElute Gel Extraction Kit	Qiagen GmbH, Hilden, Germany
Ni-NTA Spin Kit	Qiagen GmbH, Hilden, Germany
NucleoBond Xtra Maxi EF Kit	Macherey-Nagel, Düren, Germany
NucleoSpin Plasmid Kit	Macherey-Nagel, Düren, Germany
QIAquick PCR Purification Kit	Qiagen GmbH, Hilden, Germany
Quick Ligation Kit	New England BioLabs GmbH, Frankfurt, Germany
StrataClone PCR Cloning Kit	Stratagene GmbH, Heidelberg, Germany

3.3 Table 3.3: Additional material

Chromatography	C18 trapping column: inner diameter 100 μ m, length 2 cm, packed in-house with Synergi Hydro RP, particle size 4 μ m, pore size 80 Å, Phenomenex, Aschaffenburg, Germany
	Econo Chromatography Column (2.5 x 20 cm), BioRad Lab GmbH, München, Germany
	Gravity flow column (5/ 10/ 20 mL), Qiagen GmbH, Hilden, Germany
	RP main column: inner diameter 75 μ m, length 30 cm, packed in-house with Synergi Hydro RP, particle size 2 μ m, pore size 80 Å, Phenomenex, Aschaffenburg, Germany
	Superdex HiLoad 26/ 60 FPLC separation column (200 pep grade), Amersham Biosciences, Freiburg, Germany
Reaction tubes and Vessels	15/ 50 mL Falcon tubes, Becton Dickinson GmbH, Heidelberg, Germany
	0.2 mL Multiply PCR microtube strips, Sarstedt AG & Co, Nümbrecht, Germany
	12 cm Petri plates, Sarstedt AG & Co, Nümbrecht, Germany
	6-well Petri plates, Sarstedt AG & Co, Nümbrecht, Germany
	0.5 mL Protein LoBind tubes, Eppendorf AG, Hamburg, Germany
	0.5/ 1.5/ 2 mL Reaction tubes, Eppendorf AG, Hamburg, Germany
SDS-PAGE and Western blot	25/ 75 cm ² Tissue culture flasks, Sarstedt AG & Co, Nümbrecht, Germany
	CL-X Posure Film, Thermo Fisher Scientific, Bonn, Germany
	Hybond-ECL Nitrocellulose Membranes, Amersham Biosciences, Freiburg, Germany
	Immobilon-PSQ PVDF Transfer Membrane, Millipore GmbH, Schwalbach, Germany
	NuPAGE precast Bis-Tris gels (10/ 12/ 4-12%), Invitrogen GmbH, Karlsruhe, Germany
	SuperSignal West Pico Chemiluminescence Substrate, Thermo Fisher Scientific, Bonn, Germany
XCell II Blot Modul, Invitrogen GmbH, Karlsruhe, Germany	
XCell SureLock Mini Cell, Invitrogen GmbH, Karlsruhe, Germany	

3.4 Table 3.4: Instruments

Cell lysis	SLM Aminco French Pressure Cell Press, Heinemann, Schwäbisch Gmünd, Germany
	Sonopuls UW 2070, Bandelin Electronic GmbH & Co KG, Berlin, Germany
	Sonorex RK 52 ultrasonic bath, Bandelin Electronic GmbH & Co KG, Berlin, Germany
Centrifuges	Allegra 21R centrifuge, F2402H rotor, Beckman Coulter GmbH, Krefeld, Germany
	Avanti J-20XP, Beckman Coulter GmbH, Krefeld, Germany
	Centrifuge 5415R, Eppendorf AG, Hamburg, Germany
	Centrifuge 5804R, Eppendorf AG, Hamburg, Germany
	Centrifuge 5810R, A-4-62 and A-4-81 rotor, Eppendorf AG, Hamburg, Germany
	Multifuge 3S-R, Heraeus, Kendro Lab Products, Osterode, Germany
	Optima Ultracentrifuge, TLA 100.4 rotor, Beckman Coulter GmbH, Krefeld, Germany
	Speed Vac Plus SC 110A, Thermo Savant LabSystems, Egelsbach, Germany
	Speed Vac SPD 111V, Thermo Savant LabSystems, Egelsbach, Germany
	Speed Vac SPD131DDA (Thermo Fisher Scientific, Dreieich, Germany)
	Ultracentrifuge L7, SW41 rotor, Beckman Coulter GmbH, Krefeld, Germany
Chromatography	ÄKTA FPLC System, Amersham Biosciences, Freiburg, Germany
	Famos, Switchos, Ultimate nano-HPLC system, Dionex, Idstein, Germany
	Fraction Collector 2110, BioRad Lab GmbH, München, Germany
	Ultimate 3000 HPLC System, Dionex, Idstein, Germany
Incubation	Certomat, B. Braun Melsungen AG, Melsungen, Germany
	CO ₂ incubator MCO 18AIC(UV), SANYO Sales & Marketing Europe GmbH, München, Germany

	Grant-bio rotor PTR-30, Grant Instruments Ltd., Shepreth, England
	IKA HS 260 basic shaker, IKA Werke GmbH & Co. KG, Staufen, Germany
	Thermomixer comfort, Eppendorf AG, Hamburg, Germany
Mass spectrometers	LTQ-FT Ultra, Thermo Fisher Scientific, Dreieich, Germany
	LTQ XL, Thermo Fisher Scientific, Dreieich, Germany
	QStar Elite, Applied Biosystems, Darmstadt, Germany
	Qtrap 4000, Applied Biosystems, Darmstadt, Germany
PCR, cloning and DNA sequencing	Gel chamber class II 40-1214, PEQLAB Biotechnologie GmbH, Erlangen, Germany
	Genetic Analysis System CEQ 8000, Beckman Coulter GmbH, Krefeld, Germany
	Spectrophotometer UV-1601, Shimadzu Deutschland GmbH, Duisburg, Germany
	Thermocycler T1, Biometra GmbH, Göttingen, Germany
	Transilluminator TFX-35M UV, Gibco BRL Life Technologies, Eggenstein, Germany
	Video camera (Hama objective M49 IV), INTAS Science Imaging Instruments GmbH, Göttingen, Germany
Scanner	Power Look 2100 XL, Umax Systems GmbH, Willich, Germany
SDS-PAGE and Western blot	Electrophoresis Power Supply EPS 1001, Amersham GE Healthcare, Freiburg, Germany
	Electrophoresis Power Supply EPS 3501 XL, Amersham GE Healthcare, Freiburg, Germany
	Fusion FX7 CCD Imaging System, Vilbert Lourmat Deutschland GmbH, Eberhardzell, Germany
	PowerPac 3000 power supply, BioRad Lab GmbH, München, Germany
	PowerPac Basic power supply, BioRad Lab GmbH, München, Germany
	Processor X-OMAT 1000, Eastman Kodak Company, Rochester, NY, USA

3.5 Software and databases

Analyst 1.4 (MDS AB Sciex)

Analyst QS 2.0 (MDS AB Sciex)

CEQ 8000 software, version 9.0 (Beckman Coulter Inc.)

Chromeleon 6.8.SR8 (Dionex Softron)

Fusion software, version 15.12 (Vilbert Lourmat GmbH)

GATC Viewer 1.00 (GATC Biotech AG)

Mascot Daemon 2.2.0.2, server version 2.2.0.4 (Matrix Sciences Ltd.)

Silverfast Ai6.0.2r.36 scanning software (Lasersoft Imaging AG)

Xcalibur 2.1.0 build 1139 (Thermo Fisher Scientific)

3.6 Cellular material

3.6.1 Table 3.5: *Escherichia coli* strains (*E.coli*)

<i>E.coli</i> strain	Characteristics
<i>E.coli</i> BL21	<ul style="list-style-type: none"> - IPTG-inducible T7 RNA polymerase gene - Suitable for high-level expression of non-toxic genes - Tetracycline and CHL resistance
<i>E.coli</i> BL21-CodonPlus-RP	<ul style="list-style-type: none"> - Similar to <i>E.coli</i> BL21 - Addresses codon bias problem of GC-rich genomes by expressing tRNAs for AGA, AGG and CCC
<i>E.coli</i> DH5 α	<ul style="list-style-type: none"> - Reduced endogenous nuclease activity due to RecA- and endonuclease I deficiency - Applied for molecular cloning and plasmid DNA production
<i>E.coli</i> Rosetta	<ul style="list-style-type: none"> - IPTG-inducible T7 RNA polymerase gene - Suitable for high-level expression of non-toxic genes - Mutated lac permease gene (<i>lacZY</i>) for uniform IPTG entry and regulatable induction levels - Addresses codon bias problem by expressing tRNAs for AGG, AGA, AUA, CUA, CCC, GGA on CHL resistance factor

Except for *E.coli* BL21-CodonPlus-RP (Stratagene GmbH, Heidelberg, Germany), all *E.coli* strains were kindly provided by Prof. Dr. Thomas Renné (Department of Molecular Medicine and Surgery, Karolinska Institute, Stockholm, Sweden) and Prof. Dr. Ulrich Walter (Institute of Clinical Biochemistry and Pathobiochemistry, Center of Inner Medicine, Würzburg, Germany). They were stored at -80°C in glycerol stocks until further usage.

3.6.2 HEK293 cells

HEK293 cells were kindly provided by Dr. Raffael Kettler (Leibniz-Institute for Analytical Sciences - ISAS - e.V., Dortmund, Germany) and were cultivated in tissue culture flasks in HEK293 complete medium at 37°C and 5% CO₂. Having grown to a confluence of 80-90% (determined microscopically) within 5-7 days of incubation, cells were washed twice with DPBS and harvested by stringently rinsing the flasks with DPBS. Upon centrifugation at 200 x g at 4°C for 7 min, the resulting cell pellets were (a) either processed further; or (b) stored at -80°C for subsequent treatment, or (c) passaged at a ratio of 1:10 for continued cell culture and spreading. Cell culture medium was exchanged twice a week. For long-time preservation, harvested cell pellets of confluent 25 cm² tissue culture flasks were suspended in HEK293 cryomedium (800 µL per pellet) and stored at -196°C.

HEK293 complete medium

DMEM, 1% (v/v) MEM, 10% (v/v) FCS, 1% (v/v) Pen/ Strep

HEK293 cryomedium

HEK293 complete medium, 36% (v/v) FCS, 9% (v/v) DMSO

3.6.3 Platelet purification

A total of 200 mL human blood from healthy donors was collected in 50 mL tubes (each containing 10 mL of anti-coagulation buffer) and centrifuged for 20 min at 300 x g at 20°C. The upper phase (i.e. platelet-rich plasma, PRP) was subsequently cleared from remaining leukocytes and erythrocytes by two additional 20 min centrifugation steps (20°C) at 300 and 400 x g, respectively. Upon discard of the final supernatant, residual plasma proteins were removed from the obtained platelet pellet by resuspending twice with 20 mL washing buffer, followed by 20 min centrifugation at 400 x g (20°C). Finally, the resulting platelet pellet was aliquoted à 100 µL, flash

frozen in liquid nitrogen and stored at -80°C until further use. The same protocol was applied for platelet enrichment out of 500 mL fresh, leukocyte-depleted apheresis concentrates from healthy donors which were kindly provided by the Department of Transfusion Medicine, University of Würzburg, Germany.

In addition, all purified mouse platelets (C57Bl6-Sv129 mixed background) used in this study were kindly provided by Dr. Attila Braun (Rudolf-Virchow-Center, Würzburg, Germany).

Anti-coagulation buffer, pH 6.5

100 mM sodium citrate, 7 mM citric acid, 140 mM glucose, 15 mM EDTA

Tyrode's buffer (10x)

1.45 M NaCl, 50 mM KCl, 10 mM MgCl_2

Washing buffer, pH 6.4

50 mL anti-coagulation buffer, 50 mL Tyrode's buffer (10x), 400 mL water

3.7 Vector constructs

Table 3.6: Original vectors

Original vector	Characteristics
<i>pcDNA3.1/V5-HisA</i> (Invitrogen GmbH, Karlsruhe, Germany)	- 5,500 bp, MCS nt 902-999 - CMV-, SV40- and T7 promoter - Amp resistance, Neo resistance - C-terminal V5-tag, C-terminal His ₆ -tag
<i>pcDNA3.1/V5-His lacZ</i> (Invitrogen GmbH, Karlsruhe, Germany)	- See <i>pcDNA3.1/V5-HisA</i> - 8,500 bp - Control vector, encodes β -galactosidase - Calculated MW of fusion protein 121 kDa
<i>pGEX 6p1</i> (GE Healthcare, München, Germany)	- 4,900 bp, MCS nt 945-981 - IPTG-inducible, Tac promoter - Amp resistance - N-terminal GST-tag
<i>pQE-30</i> (Qiagen GmbH, Hilden, Germany)	- 3,500 bp, MCS nt 145-192 - IPTG-inducible, T5 promoter - Amp resistance - N-terminal His ₆ -tag

Table 3.7: Recombinant vector constructs

Recombinant vector construct	Insert characteristics
STIM1Ctail (in <i>pGEX 6p1</i>)	- STIM1 cytoplasmic region (aa 484-685) - Insertion sites BamHI, XhoI - N-terminal GST-tag, C-terminal His ₆ -tag - Calculated MW of fusion protein 49 kDa
VASP-AAA ('non-phospho VASP') (in <i>pQE-30</i>)	- Human full length VASP, site-directed mutagenesis of S157A, S239A and T278A - Insertion sites BamHI, Sal I - N-terminal His ₆ -tag - Calculated MW of fusion protein 41 kDa

VASP-DDE ('phospho-VASP') (in <i>pQE-30</i>)	- Human full length VASP, site-directed mutagenesis of S157D, S239D and T278E - Insertion sites BamHI, Sal I - N-terminal His ₆ -tag - Calculated MW of fusion protein 41 kDa
VASP-DDEΔFABΔTD, VASP-AAAΔFABΔTD (in <i>pcDNA3.1/V5-HisA</i>)	- VASP-DDE/ -AAA, deletion of VASP-FAB and -TD domains (Δaa 259-380) - Insertion sites BamHI, EcoRI - C-terminal V5-tag, C-terminal His ₆ -tag - Calculated MW of fusion proteins 29 kDa
VASP-DDEΔTD, VASP-AAAΔTD (in <i>pcDNA3.1/V5-HisA</i>)	- VASP-DDE/ -AAA, deletion of VASP-TD domain (Δaa 343-380) - Insertion sites BamHI, EcoRI - C-terminal V5-tag, C-terminal His ₆ -tag - Calculated MW of fusion proteins 38 kDa

The phosphomimetic human VASP constructs 'VASP-AAA' and 'VASP-DDE' were kindly provided by Prof. Dr. Thomas Renné (Department of Molecular Medicine and Surgery, Karolinska Institute, Stockholm, Sweden); the STIM1 expression construct 'STIM1Ctail' by Prof. Dr. Bernhard Nieswandt and Dr. Attila Braun (Rudolf-Virchow-Center, Würzburg, Germany). Prof. Dr. Thomas Renné also provided an MBP fusion tag vector as positive *E.coli* transformation- and expression control (MW of fusion protein ~ 40 kDa). VASP deletion constructs 'VASP-AAAΔTD', 'VASP-DDEΔTD', 'VASP-AAAΔFABΔTD' and 'VASP-DDEΔFABΔTD' were generated as described in 3.7.1. For detailed vector maps, as well as full length nt- and aa-sequences, see 7.1-7.3.

3.7.1 Generation of VASP deletion constructs

3.7.1.1 VASP mutagenesis primers

For deletion of VASP subdomains, the following oligonucleotides were chosen as PCR primers (Table 3.8):

Primer	nt sequence (5'-to-3')	Details
VASP-Fwd	AGTGGATCCATGAGC GAGACGGTCATCTG	- VASP forward primer (29 nt) - Melting temperature 69.5°C - Confers <u>BamHI</u> restriction site to the 5'-end of the VASP sequence
VASP-Rev I	TCGAGGTCACCTAAT GAGCCTTAAGCTG	- VASP reverse primer (27 nt) - Melting temperature 65.0°C - Deletes VASP-TD domain (nt 1027-1143) - Confers <u>EcoRI</u> -restriction site to the 3'-end of the VASP-sequence
VASP-Rev II	CTCTCACCAGCTT CGCTTAAGCTG	- VASP reverse primer (24 nt) - Melting temperature 64.4°C - Deletes VASP-TD and -FAB domains (nt 775-1143) - Confers <u>EcoRI</u> -restriction site to the 3'-end of the VASP-sequence

3.7.1.2 VASP deletion PCR

Using the VASP *pQE-30* vector constructs ‘VASP-AAA/ -DDE’ as DNA templates, VASP deletion PCRs were prepared in 0.2 mL PCR reaction tubes and performed in a T1 Thermocycler as outlined in the following (Table 3.9):

Component	Stock	In 25 μ L reaction volume	Temp.	Time
DNA template	0.1 μ g/ μ L	500 ng	96°C	2 min
<i>Pfu</i> DNA polymerase	2.5 U/ μ L	1.25 U	96°C	30 sec
Primer	100 pmol/ μ L	5 pmol per primer*	64°C	30 sec
<i>Pfu</i> reaction buffer	10x	2.5 μ L	72°C	2 min
dNTP-Mix	10 mM	0.5 μ L	72°C	20 min
DMSO	-	5% (v/v)	12°C	∞

* a) for deletion of VASP-TD domain: VASP-Fwd + VASP-Rev I
 b) for deletion of VASP-FAB and -TD domains: VASP-Fwd + VASP-Rev II

The resulting VASP-PCR products were separated by agarose gel electrophoresis, purified using the QIAquick PCR Purification Kit according to the manufacturer’s instructions and stored at -20°C.

3.7.1.3 Agarose gel electrophoresis

1% (w/v) agarose was dissolved in 100 mL TBE buffer by heating. Having cooled down to 50-60°C, the gel solution was supplemented with 4 μ L GelRed Nucleic Acid Gel Stain and poured into a gel chamber. For analysis, 2-5 μ L DNA samples were mixed 2:1 with DNA Loading Buffer, loaded into the gel slots and subjected to a voltage of 109 V for 45 min. DNA bands were finally visualized by exposing the gel to UV light on a TFX-35M UV transilluminator and pictures were taken with an INTAS video camera system.

10x TBE buffer

0.89 M Tris base, 0.89 M boric acid, 20 mM EDTA

3.7.1.4 PCR cloning in StrataClone SoloPack competent *E.coli*

For enhanced amplification prior to enzymatic restriction, a StrataClone PCR Cloning Kit was used according to the manufacturer’s instructions. Purified VASP-PCR products were first incubated with 1 U Taq-Polymerase and 0.5 μ L of the 10 mM dNTP-Mix at 72°C for 10 min to allow for generation of poly-A sticky ends, then cooled down to 4°C and subsequently integrated into a *pSC-A-amp/kan* vector (4.3 kb). Finally, 2 μ L of the recombinant vector constructs were transformed

into 50 μL StrataClone SoloPack competent *E.coli* cells. Transformed cells were seeded on 12 cm LB-Amp agar Petri plates (pre-treated by plating of 40 μL 2% (w/v) X-gal solution for subsequent blue-white screening) and incubated overnight at 37°C.

LB-Amp agar solution (1L)

15 g Bacto agar, 10 g Bacto tryptone, 5 g Bacto yeast extract, 5 g NaCl, 100 mg Amp

3.7.1.5 Colony picking and plasmid preparation

Insert-positive clones were picked and proliferated in LB-Amp medium (2 mL for subsequent miniprep and 200 mL for maxiprep) overnight at 37°C and 200 rpm. The next day, plasmid preparation was performed using a NucleoSpin Plasmid Kit for miniprep and a NucleoBond Xtra Maxi EF Kit for maxiprep. DNA concentrations were evaluated by measuring the OD₂₆₀ via an UV-1601 spectrophotometer.

LB-Amp medium (1L)

10 g Bacto tryptone, 5 g Bacto yeast extract, 5 g NaCl, 100 mg Amp

3.7.1.6 BamHI/ EcoRI restriction digest

BamHI/ EcoRI restriction digest of (a) purified *pSC-A-amp/kan* vectors containing the VASP-inserts ('source'); and (b) of the *pcDNA3.1/V5-HisA* vector ('target') was performed at 37°C overnight (Table 3.10).

Component	Stock	In 30 μL reaction volume
DNA template	Source: 2-3 $\mu\text{g}/\mu\text{L}$ Target: 4 $\mu\text{g}/\mu\text{L}$	4-6 μg 6 μg
BamHI	20 U/ μL	10 U
EcoRI	20 U/ μL	10 U
BSA solution	100 $\mu\text{g}/\text{mL}$	33 ng
NEBuffer 3	10x	3 μL

The whole reaction volume was subsequently separated by agarose gel electrophoresis and further purified using the QIAquick PCR Purification Kit for the VASP-inserts and the MinElute Gel Extraction Kit for linearized *pcDNA3.1/V5-HisA* vector according to the manufacturer's instructions. Purified DNA samples were quantified by OD₂₆₀ measurement and stored at -20°C.

3.7.1.7 Ligation and transformation in *E.coli* DH5 α

Integration and ligation of the isolated VASP-inserts into linearized *pcDNA3.1/V5-HisA* vector was performed according to the Quick Ligation Kit protocol (Table 3.11).

Component	Stock	In 20 μ L reaction volume
Digested vector	2-3 μ g/ μ L	~ 3 μ g (1 μ L)
Digested insert	2-3 μ g/ μ L	~ 9-12 μ g (4.5 μ L)
Quick Ligation Reaction Buffer		10 μ L

The whole reaction volume was subsequently transformed into 50 μ L competent *E.coli* DH5 α . In detail, the transformation reaction was first cooled on ice for 30 min, heat-shocked at 42°C for 45 sec, again chilled on ice for 2 min and finally incubated in 800 μ L SOC medium at 37°C for 1 hour. Upon reducing the total volume to 100 μ L in a Speed Vac Plus SC 110A (1,000 rpm for 5 min), transformed cells were seeded on 12 cm LB-Amp agar Petri plates overnight at 37°C.

SOC medium (1L), pH 7.0

20 g Bacto tryptone, 5 g Bacto yeast extract, 0.5 g NaCl, 2.5 mL 1 M KCl, 20 mL 1 M glucose

3.7.1.8 VASP constructs - plasmid preparation and controls

Colony picking of insert-positive clones and maxiprep plasmid preparations were performed as described in 3.7.1.5. Isolated recombinant plasmids were stored at -80°C. Correctness of vector recombination was validated (a) by VASP control PCRs using VASP primers VASP-Fwd/ -Rev I or -Rev II as described in 3.7.1.2; (b) by BamHI/ EcoRI control digests (see 3.7.1.6); and (c) by nucleotide sequencing.

In detail, VASP construct minipreps were sequenced using the GenomeLab DTCS Quick Start Kit ('Q-Kit'). Accordingly, 50-100 fmol of DNA template (i.e. 1 μ L of a 50- μ L plasmid miniprep in 5 μ L water) was first denatured at 96°C for 2 min and then briefly chilled on ice. Upon addition of 3 μ L Q-Kit solution and 5 pmol sequencing primer (either T7-Fwd or BGH-Rev, see below), the sequencing reaction was executed in a T1 Thermocycler under the following conditions (Table 3.12):

Primer	nt sequence (5'-to-3')	Details	Temp.	Time
T7-Fwd	TAATACGACT CACTATAGGG	- Forward sequencing primer - Melting temperature 48.0°C - Stock: 5 pmol/ μ L	98°C	40 sec
			96°C	20 sec
BGH-Rev	TAGAAGGCA CAGTCGAGG	- Reverse sequencing primer - Melting temperature 54.8°C - Stock: 5 pmol/ μ L	50°C	20 sec
			65°C	2 min
			12°C	∞
			30 cycles	

The reaction was finally stopped by addition of 15 μL stop solution. To remove salt and free ddNTPs, the DNA was subsequently precipitated with 60 μL absolute ethanol (-20°C) and centrifuged at maximum speed in an Allegra 21R centrifuge (rotor F2402H) at 4°C for 5 min. The obtained DNA pellet was washed with 180 μL 70% (v/v) ethanol (25°C), followed by 5 min centrifugation as before. The resulting pellet was dried for 30 min at 25°C in the dark, dissolved in 35 μL Q-Kit sample loading solution and either stored at -20°C or directly analyzed in a CEQ 8000 Genetic Analysis System using the CEQ 8000 software. In addition, final full-length sequencing of VASP construct maxipreps was provided by GATC Biotech (Konstanz, Germany); the delivered nucleotide sequences were analyzed via the GATC Viewer software.

Stop solution (per 10 μL sequencing reaction)

2 μL 100 mM EDTA (pH 8.0), 2 μL 3 M sodium acetate (pH 5.2), 1 μL glycogen solution (stock: 20 $\mu\text{g}/\mu\text{L}$, provided by the Q-Kit), 10 μL water

3.8 Protein expression

3.8.1 Transformation of VASP-AAA, VASP-DDE and STIM1Ctail in *E.coli*

For rapid transformation, 50 μL of competent *E.coli* BL21 were seeded on 12 cm LB-Amp agar Petri plates pre-treated by plating of 34 $\mu\text{g}/\text{mL}$ CHL and incubated overnight at 37°C . The next day, colonies were picked and suspended in 200 μL transformation buffer. Upon addition of 1 μg plasmid DNA, the reaction was first chilled on ice for 10 min and then heat-shocked for 90 sec at 42°C . Finally, the whole transformation reaction was seeded on 12 cm LB-Amp-CHL agar Petri plates and incubated overnight at 37°C . In addition, for an enhanced protein expression, VASP-AAA and VASP-DDE were also transformed in *E.coli* Rosetta or BL21-CodonPlus-RP according to the manufacturer's instructions.

Transformation buffer, pH 6.3

10 mM MES-KOH, 100 mM RbCl, 45 mM MnCl_2 , 10 mM CaCl_2 , 3 mM hexaminecobalt (III) chloride

3.8.2 Protein expression in *E.coli*

Insert-positive clones were picked and incubated in 3 mL/ 10 mL/ 100 mL LB-Amp-CHL medium at 37°C and 220 rpm overnight. The next day, these 'pre-cultures' were added to a total volume of 50 mL/ 250 mL/ 500 mL LB-Amp-CHL medium for further

proliferation and cultivated at 37°C and 220 rpm until bacterial concentration reached an OD₆₀₀ of 0.4-0.6 (log-phase). Then the reaction was briefly chilled on ice and protein expression was induced by addition of IPTG at a final concentration of 1 mM. Bacterial cultivation was subsequently continued at 220 rpm for 16-24 hours. In this context, different incubation conditions (16°C, 25°C, 30°C and 37°C at 130-220 rpm) as well as media (LB-Amp/ 2% (v/v) ethanol, Superbroth medium, Overnight Express Instant TB Medium) were tested regarding their potential of significantly improving protein expression. Finally, these 'expression cultures' were centrifuged at 7,000 x g (4°C) for 10 min and bacterial cell pellets (up to 20 g/ 500 mL expression culture) were stored at -80°C. Generally, protein expression was controlled by 1D-SDS-PAGE and Western blotting.

LB-Amp-CHL medium (1L)

10 g Bacto tryptone, 5 g Bacto yeast extract, 5 g NaCl, 100 mg Amp, 34 mg CHL

Superbroth medium (1L)

35 g Bacto tryptone, 20 g Bacto yeast extract, 5 g NaCl

3.8.3 Transfection of VASP deletion constructs in HEK293 cells

HEK293 cells were cultivated in 6-well plates in HEK293 complete medium at 37°C and 5% CO₂ up to a confluence of 60-70% (determined microscopically). 3 µg of plasmid DNA (i.e. VASP-AAAΔFAB, VASP-DDEΔFAB, VASP-AAAΔFABΔTD and VASP-DDEΔFABΔTD) were diluted in 200 µl 150 mM NaCl (sterile), mixed with 9.87 µl ExGen 500 *in vitro* transfection reagent and incubated at room temperature for 10 min. For evaluation of transfection efficiency, *pcDNA3.1/V5-HisA lacZ* was used as a positive control. Upon exchanging the cell culture medium with 2 mL of fresh HEK293 complete medium per well, the individual transfection reactions were finally added to the cells and incubation was started at 37°C and 5% CO₂.

In case of transient expression, incubation was stopped after 48 hours; cells were harvested and stored at -80°C. For stable protein expression, the culture medium was exchanged with 2 mL G418-selection medium 24 hours after transfection and cell culture was continued for 4-6 weeks. During this procedure and depending on cell density, insert-positive cells were extended first in 25 cm² and then in 75 cm² tissue culture flasks. Recombinant protein expression was regularly controlled by Western blotting and in case of *pcDNA3.1/V5-HisA lacZ* expression additionally by

β -gal staining using the Invitrogen β -Gal Staining Kit according to the manufacturer's instructions. Once established, stable recombinant HEK293 cell lines were confluent grown in 75 cm² tissue culture flasks and finally harvested and stored at -80°C until further usage. In addition, for long-time preservation harvested cell pellets of confluent 25 cm² tissue culture flasks were suspended in HEK293 cryomedium supplemented with 500 μ g/ mL G418 (800 μ L per pellet) and stored at -196°C.

G418-selection medium

DMEM, 1% (v/v) MEM, 10% (v/v) FCS, 1% (v/v) Pen/ Strep, 500 μ g/ mL G418

3.9 Cell lysis, protein purification and interactome screening

3.9.1 Lysis of human platelets

Platelet pellet aliquots (volume: 100 μ L) were suspended in chilled native platelet lysis buffer (1 mL per aliquot) and the suspension was lysed by 10 intervals of sonication in a Sonorex RK 52 ultrasonic bath (5 sec at 70% maximum power rate). Each interval was followed by 3 sec of vortexing and chilling on ice. The resulting lysate was cleared from remaining cellular debris by 30 min ultracentrifugation at 20,000 x g (4°C). The protein content of the supernatant was subsequently quantified by BCA assay. Following lysis, samples were either directly processed or immediately stored at -80°C.

Native platelet lysis buffer (2x), pH 7.4

100 mM Tris-HCl, 2 mM EDTA, 2% (v/v) Triton X-100

Prior to use, 1x lysis buffer was completed with protease- and phosphatase inhibitors (Complete Mini Protease- and PhosSTOP Phosphatase Inhibitor, Roche, according to the manufacturer's instructions).

3.9.2 IMAC purification of His₆-tagged bait proteins

Harvested pellets of recombinant *E.coli* or HEK293 cells were completely resuspended in chilled lysis buffer at a final concentration of 0.2 g/ mL. Subsequent cell lysis was performed depending on the amount of starting material: Sample volumes up to 25 mL (i.e. 5 g) were lysed by 5 intervals of sonication using a Sonopuls UW 2070 ultrasonicator. Each interval (10 sec at 75% maximum power rate) was followed by chilling on ice. Larger sample amounts were disrupted twice in a French press at 1 kbar and 4°C. The lysate was ultracentrifuged at 28,000 x g (4°C) for 30 min and the resulting supernatant was incubated with Ni-NTA agarose (0.5 mL per 1 g starting material, pre-equilibrated with lysis buffer) in a gravity flow

column by head-over-tail rotation (4 hours at 4°C). Following incubation, the matrix was washed with 4 column volumes (CV) lysis buffer and 5 CV washing buffer. Bound proteins were finally eluted with 5 CV elution buffer and either processed further or stored at -80°C.

Lysis buffer, pH 7.9

20 mM Tris-HCl, 500 mM NaCl, 5 mM imidazole

Prior to use, lysis buffer was completed with protease- and phosphatase inhibitors (Complete Mini Protease Inhibitor EDTA-free and PhosSTOP Phosphatase Inhibitor, Roche, according to the manufacturer's instructions).

Washing buffer, pH 7.9

20 mM Tris-HCl, 500 mM NaCl, 25 mM imidazole

Elution buffer, pH 7.9

20 mM Tris-HCl, 500 mM NaCl, 400 mM imidazole

Alternatively, in case of recombinant HEK293 cells, purification of His₆-tagged proteins was also performed using Qiagen Ni-NTA spin columns. Accordingly, cell pellets of three biological replicates (i.e. 5×10^6 cells or three confluent 75 cm² tissue culture flasks) were pooled and processed based on the Ni-NTA Spin Kit protocol for protein purification either under native or denaturing conditions. In brief, cells were lysed by incubation in 700 µL of the respective Ni-NTA lysis buffer for 15-30 min on ice and endogenous DNA was digested by addition of Benzonase endonuclease (3 U/ mL culture volume). Cellular debris was removed by centrifugation at 12,000 x g for 30 min (4°C) and up to 600 µL of the lysate supernatant were consequently incubated on the Ni-NTA spin column (pre-equilibrated with Ni-NTA lysis buffer). The flow through was collected by 5-min centrifugation at 270 x g (4°C) and the column was washed twice with 600 µL Ni-NTA washing buffer. Bound proteins were finally eluted twice with 200-300 µL Ni-NTA elution buffer via centrifugation at 890 x g for 2 min and stored at -80°C. In either case, the IMAC-based purification procedure was monitored by 1D-SDS-PAGE and Western blotting.

Native Ni-NTA lysis buffer, pH 8.0

50 mM NaH₂PO₄, 300 mM NaCl, 10 mM imidazole, 1% (v/v) NP-40

Prior to use, lysis buffer was completed with protease- and phosphatase inhibitors (Complete Mini Protease Inhibitor EDTA-free and PhosSTOP Phosphatase Inhibitor, Roche, according to the manufacturer's instructions).

Denaturing Ni-NTA lysis buffer, pH 8.0

7 M urea, 100 mM NaH₂PO₄, 10 mM Tris-HCl

Prior to use, lysis buffer was completed with protease- and phosphatase inhibitors (Complete Mini Protease Inhibitor EDTA-free and PhosSTOP Phosphatase Inhibitor, Roche, according to the manufacturer's instructions).

Native Ni-NTA washing buffer, pH 8.0

50 mM NaH₂PO₄, 300 mM NaCl, 20 mM imidazole

Denaturing Ni-NTA washing buffer, pH 6.3

8 M urea, 100 mM NaH₂PO₄, 10 mM Tris-HCl

Native Ni-NTA elution buffer, pH 8.0

50 mM NaH₂PO₄, 300 mM NaCl, 500 mM imidazole

Denaturing Ni-NTA elution buffer, pH 4.5

8 M urea, 100 mM NaH₂PO₄, 10 mM Tris-HCl

3.9.3 Size exclusion chromatography of purified His₆-tagged proteins

IMAC elution fractions were pooled and loaded on a Superdex HiLoad 26/ 60 separation column (pre-equilibrated with FPLC buffer at 4°C). SEC was subsequently performed in FPLC buffer on an ÄKTA FPLC system at 4°C and at a constant flow rate of 1.5 mL/ min for 4 hours. Fractions were collected every 2 min (i.e. 3 mL volume per fraction) and stored at 4°C. Finally, the separation column was washed and re-equilibrated with FPLC-buffer. The whole procedure was constantly monitored via the ÄKTA UV detector unit at 280 nm.

FPLC buffer, pH 7.9 (degassed)

20 mM Tris-HCl, 500 mM NaCl

3.9.4 Immobilization of purified recombinant proteins

Protein coupling to Affi-Gel 10 was performed under aqueous conditions according to the manufacturer's instructions. For each sample, an Affi-Gel 10 slurry volume of 1 mL was transferred to a fritted Econo Chromatography Column and washed with 3 CV deionized water (4°C) at gravity flow. Upon addition of the protein solution (at least 0.5 mL per mL gel) binding was performed at 4°C for 4 hours. The column was subsequently washed with 1 CV PBS (pH 7.4) and remaining free active esters were blocked by incubating in 1 M ethanolamine-HCl solution (pH 8.0, at least 0.1 mL per mL gel) at 4°C for 1h. Finally, the resulting affinity matrix was washed with 3 CV of

ice-cold deionized water and stored in an aqueous solution of 0.2% (w/v) sodium azide (pH 7.4) at 4°C.

3.9.5 Interactome screening of native platelet lysates

The generated affinity columns were washed twice in ice-cold deionized water and then pre-equilibrated in 10 CV ice-cold PBS (pH 7.4) at 4°C. Native platelet lysates were added (at least 10 mg per mL affinity support), the remaining column volume was filled with native platelet lysis buffer and incubation was performed by head-over-tail rotation overnight at 4°C. The next day, the supernatant was discarded by gravity flow, the bead material was washed with 10 CV PBS and bound proteins were eluted by applying a pH-gradient of 10 mM glycine/ HCl pH 6.0, pH 5.0, pH 4.0, pH 3.0 and pH 2.0. For each pH-step, an elution volume of 3 CV was used. Immediately after elution, pH-values were adjusted to pH 7.0 by addition of an appropriate volume of 1M Tris-buffer, and the total volume of the individual pH-fractions was reduced to 1 mL in a SPD 111V Speed Vac (35°C). The resulting five elution samples were either processed further or stored at -80°C.

3.10 Protein analysis

3.10.1 Protein quantification by BCA assay

Samples were diluted 1:10, 1:25 and 1:50 in water and quantified in triplets using the BCA Protein Assay Kit according to the manufacturer's instructions.

3.10.2 1D-SDS-PAGE

For 1D-SDS-PAGE, NuPAGE precast Bis-Tris gels (gel size 80 mm x 80 mm), XCell SureLock Mini Cell electrophoresis chambers and NuPAGE MOPS SDS Running Buffer (1x, pH 7.7) were used. Appropriate sample amounts were resolved in 1x NuPAGE LDS Sample Buffer, denatured at 85°C for 15 min (300 rpm) and applied to the sample wells. For subsequent molecular mass evaluation, 3 µL of Mark 12 MW Standard or See Blue Plus2 Pre-Stained Protein Standard (in case of subsequent Western blotting) were chosen. Electrophoresis was performed at 4°C first at 50 V for 15 min, followed by 200 V for approximately 50 min using a PowerPac power supply.

3.10.3 Western blotting

Electroblotting of PAGE-separated protein samples on nitrocellulose or PVDF membranes was performed using an XCell II Blot Modul according to the manufacturer's instructions. Blotting membranes, pads and Whatman papers were pre-soaked with transfer buffer for 5 min. PVDF membranes were activated by incubation in ethanol for 2 min. Blotting was performed at a constant voltage of 30 V per membrane for 1 hour and subsequently controlled by briefly incubating the membranes in 5% (w/v) aqueous Ponceau S solution. For subsequent immunodetection, membranes were repeatedly washed with TBS-T buffer to remove remaining Ponceau S, and finally incubated in 50 mL blocking solution for at least 1 hour at room temperature.

Transfer buffer (1L)

50 mL NuPAGE Transfer Buffer (20x), 100 mL methanol

TBS-T buffer, pH 7.4

10 mM Tris-HCl, 150 mM NaCl, 0.05% (v/v) Tween 20

Blocking solution (see also Table 3.13)

5% (w/v) BSA- or 5% (w/v) dried milk powder in TBS-T buffer

3.10.4 Immunodetection

Blocked blotting membranes were washed with TBS-T buffer (1 x 15 min, 2 x 5 min) and incubated with the primary antibody solution at room temperature for at least 1.5 hours (see Table 3.13). After briefly rinsing with ultrapure water (twice), washing with TBS-T buffer was repeated as above, followed by incubation with the secondary antibody solution at room temperature for at least 1 hour. Unbound components were subsequently removed by washing as above and HRP-detection was performed using the SuperSignal West Pico Chemiluminescence Substrate. Accordingly, blotting membranes were rinsed with 2 mL detection solution (peroxide A : luminal B = 1:1) for 1 min and exposed to CL-X Posure films for 30 sec, 2 min and 10 min. Films were developed using an X-OMAT 1000 Processor. Alternatively, a Fusion FX7 CCD Imaging System was applied for digital Western blot development and analysis.

Table 3.13: Primary antibodies

IgG	Source	Dilution	In
mAB anti-CLP36 (PDLIM1) (Abcam, Cambridge, UK)	Rabbit	1:1,000	TBS-T/ 5% BSA (w/v)
mAB anti-GPIIb (13G12) (Emfret, Eibelstadt, Germany)	Rat	1:1,000	TBS-T/ 5% BSA (w/v)
mAB anti-His ₄ -tag (Qiagen GmbH, Hilden, Germany)	Mouse	1:2,000	TBS-T/ 5% dried milk powder (w/v)
mAB anti-His ₅ -tag (Qiagen GmbH, Hilden, Germany)	Mouse	1:2,000	TBS-T/ 5% dried milk powder (w/v)
mAB anti-His ₆ -tag (Roche Diagnostics, Mannheim, Germany)	Mouse	1:6,000	TBS-T/ 5% BSA (w/v)
mAB anti-His(C-term)-tag (Invitrogen GmbH, Karlsruhe, Germany)	Mouse	1:5,000	TBS-T/ 5% BSA (w/v)
mAB anti-STIM1 (5A2) (Abnova, Taipei, Taiwan)	Mouse	1:1,000	TBS-T/ 5% BSA (w/v)
mAB anti-V5-tag (Invitrogen GmbH, Karlsruhe, Germany)	Mouse	1:5,000	TBS-T/ 5% dried milk powder (w/v)
mAB anti-VASP IE273*	Mouse	1:1,000	TBS-T/ 5% dried milk powder (w/v)

* purified from hybridoma cells provided by Prof. Dr. Thomas Renné (Department of Molecular Medicine and Surgery, Karolinska Institute, Stockholm, Sweden)

Secondary antibodies (all from Sigma-Aldrich Chemie GmbH, Steinheim, Germany)

pAB anti-mouse HRP-conjugated (1:8,000 in TBS-T)

pAB anti-rabbit HRP-conjugated (1:8,000 in TBS-T)

pAB anti-rat HRP-conjugated (1:8,000 in TBS-T)

3.10.5 Colloidal Coomassie staining of 1D-SDS-PAGE gels

Immediately after electrophoresis, NuPAGE precast Bis-Tris gels were incubated in 100 mL Coomassie solution at room temperature at 60 rpm overnight. After extensive washing in ultrapure water, stained gels were scanned using a Power Look 2100 XL. Protein spots of interest were excised and stored in 0.5 mL Protein LoBind tubes at -80°C for subsequent analysis by protein mass spectrometry.

Coomassie solution

34% (v/v) methanol, 2% (v/v) ortho-phosphoric acid, 17% (w/v) ammonium sulfate, 0.066% (w/v) Coomassie G-250

3.10.6 Silver staining of 1D-SDS-PAGE gels

Immediately after electrophoresis, NuPAGE precast Bis-Tris gels were silver-stained according to a modified protocol (Table 3.14) based on Blum et al. [200].

Step	Duration	Components (in 100 mL ultrapure water)
Fixation	At least 1 h	40% (v/v) ethanol, 10% (v/v) acetic acid
Sensitization	1 min	0.02% (w/v) sodium thiosulfate pentahydrate
Staining	20 min (4°C)	0.1% (w/v) AgNO ₃
Development	Up to 10 min	3% (w/v) sodium carbonate, 0.05% (v/v) formaldehyde
Stop	30 min	0.05 M EDTA

Stained gels were scanned and protein spots were excised and stored in 0.5 mL Protein LoBind tubes at -80°C for subsequent analysis by protein mass spectrometry.

3.10.7 IP and Co-IP

All IP samples were kindly provided by Dr. Attila Braun (Rudolf-Virchow-Center, Würzburg, Germany). In detail, purified resting platelets (approximately 0.5×10^9) of (a) human origin; or (b) of either wildtype ('STIM1^{+/+}') or STIM1^{-/-} mice (both C57Bl6-Sv129 mixed background) were solubilized in 1 mL IP buffer and lysed at room temperature for 10 min. Cell debris was subsequently removed by centrifugation at 14,000 rpm for 10 min. To reduce unspecific antibody binding, samples were initially incubated with 25 μ L protein G sepharose (previously equilibrated in IP buffer) for 30 min at 4°C under rotation. Upon centrifugation at 2,500 rpm for 5 min (4°C), the supernatants were separated from the protein G sepharose pellet and transferred into a fresh Eppendorf tube. Then the platelet samples were first probed with 10 μ g of the required IP-antibody (see Table 3.15) for 1 hour at 4°C, followed by an overnight incubation with 25 μ L equilibrated protein G sepharose at 4°C under rotation.

Table 3.15: IP-antibodies

IgG	Source	Dilution	Manufacturer
pAB anti-CLP36	Mouse	1:500	BD Biosciences, Heidelberg, Germany
pAB anti-GPIb (15E2)	Rat	1:1,000	Emfret, Eibelstadt, Germany
pAB anti-STIM1	Rabbit	1:8,000	Cell Signaling, Frankfurt, Germany

The next day, antibody-antigen complexes were washed three times with IP buffer (followed by centrifugation at 2,500 rpm at 4°C for 5 min), resolved in 60 μ L 2x SDS sample buffer and denatured at 95°C for 5 min. Upon removal of remaining protein G sepharose by centrifugation at 12,000 rpm at room temperature for 5 min, the IP-supernatants were finally analyzed by 1D-SDS-PAGE and subsequent silver staining and/ or immunoblotting against STIM1, CLP36 or GPIb proteins (3.10.3 and 3.10.4).

IP buffer

15 mM Tris-HCl (pH 8.0), 155 mM NaCl, 1 mM EDTA, 1% (v/v) Igepal, 0.005 % (w/v) sodium azide. Prior to use, IP buffer was completed with protease inhibitors (Complete Mini Protease Inhibitor, Roche, according to the manufacturer's instructions).

SDS sample buffer (2x)

10% (v/v) 1.25 M Tris (pH 6.8), 10% (v/v) β -mercaptoethanol, 20 % (v/v) glycerol, 4% (w/v) SDS, 0.02% (w/v) bromophenol blue sodium salt

3.10.8 Calpain in-solution digestion

Calpain in-solution digestion was performed based on a modified protocol of Lakey et al. [201]. Accordingly, 30 pmol of human CLP36 protein (PDLIM1, purchased from Abnova) were resolved in a total volume of 100 μ L calpain activating solution. For proteolytic cleavage, 3 U calpain-1 and 4.5 U calpain-2 were added and samples were incubated at 25°C for up to 90 min. The reaction was stopped by heating at 95°C for 10 min, thus inactivating calpain. In case of additional tryptic in-solution digestion, samples were subsequently diluted 1:1 with 20 mM Tris-HCl (pH 7.2) to reduce the content of β -mercaptoethanol and then incubated with Trypsin Gold solution (12.5 ng/ μ L in freshly prepared 50 mM NH_4HCO_3) at a ratio of 50:1 (i.e. sample protein : trypsin) for 1 hour at 37°C. In parallel, for evaluation of distinct tryptic cleavage patterns, 5 pmol of human CLP36 protein were tryptically digested under equal conditions yet without prior calpain treatment. All proteolytic reactions were monitored by 1D-SDS-PAGE and finally, upon carbamidomethylation as described in 3.10.9, analyzed for calpain and/ or trypsin cleavage sites by protein mass spectrometry.

Calpain activating solution, pH 7.2

0.1 M NaCl, 20 mM Tris-HCl, 2 mM MgCl_2 , 10 mM β -mercaptoethanol, 5 mM CaCl_2

3.10.9 In-gel digestion and peptide extraction

Excised protein spots (see 3.10.5 and 3.10.6) were repeatedly washed in 50 mM NH_4HCO_3 (pH 7.8) and 25 mM NH_4HCO_3 / 50% (v/v) MeCN at 37°C for 10 min. Prior to protein digestion, carbamidomethylation of the sample was performed. Accordingly, disulfide bonds were reduced by incubating in 10 mM DTT (in 50 mM NH_4HCO_3) at 56°C for 30 min, followed by alkylation of the resulting free cysteines using 30 mM IAA (in 50 mM NH_4HCO_3) at 25°C for 30 min in the dark. The reaction was stopped by addition of 10 mM DTT (in 50 mM NH_4HCO_3). After this procedure, the sample was washed as above and completely dried in a SPD 111V Speed Vac at 35°C. 10 μ L Trypsin Gold solution (12.5 ng/ μ L in freshly prepared 50 mM NH_4HCO_3) were added to the dried gel spots and excess liquid was removed after a 10-min period at 4°C. Tryptic digestion was then performed at 37°C overnight. Peptides were extracted twice with 10 μ L 5% (v/v) FA (37°C, 15 min) and finally with 10 μ L 5% (v/v) FA/ 50% (v/v) MeCN (37°C, 15 min). The three fractions were pooled, reduced to a

total volume of 15 μL using a SPD 111V Speed Vac at 35°C and stored at -80°C until being further analyzed by nano-LC-ESI-MS. Protein digestion was controlled by comparative 1D-SDS-PAGE of sample aliquots before and after digestion and subsequent silver staining.

3.10.10 Nano-LC-ESI-MS/MS

3.10.10.1 Instrumentation and nano-HPLC

For protein identification, three different nano-LC-ESI-MS systems were applied: (a) a QStar Elite; (b) a Qtrap 4000; or (c) an LTQ XL mass analyzer. For analysis of calpain-digested samples, an LTQ-FT Ultra was used. Both QStar and Qtrap instruments were online coupled to a Famos™, Switchos™, Ultimate™ nano-HPLC system; the LTQ XL and the LTQ-FT Ultra were coupled to an Ultimate 3000 system. Since there were hardly any differences in nano-LC separation parameters of the four MS systems, the procedure can generally be described as follows: Tryptic sample peptides were reconstituted in 15 μL 0.1% (v/v) TFA and loaded onto a self-packed C18 trapping column (Synergi Hydro RP, inner diameter 100 μm , length 2 cm, particle size 4 μm , pore size 80 Å) for further desalting and preconcentration in the nano-HPLC system (flow rate 7 $\mu\text{L}/\text{min}$ 0.1% (v/v) TFA, prolonged loading time of 25 min). Peptide separation was then performed at 60°C on a self-packed reversed-phase main column (Synergi Hydro RP, inner diameter 75 μm , length 30 cm, particle size 2 μm , pore size 80 Å) by applying a 40-min binary gradient (alternatively 80-min) of solvent A and B ranging from 5 to 50% solvent B at a flow rate of 270 nL/min. Separated peptides were directly eluted into the online ESI ion source for subsequent MS (and MS/MS) acquisition, columns were washed at 95% solvent B for 5 min and finally re-equilibrated at 5% solvent B for 15 min.

Solvent A

0.1% (v/v) FA

for QStar 0.2% (v/v) FA

Solvent B

0.1% (v/v) FA/ 84% (v/v) MeCN

for QStar 0.2% (v/v) FA/ 84% (v/v) MeCN

3.10.10.2 MS and MS/MS acquisition

MS data acquisition was comparable for all four mass spectrometers; a summary of parameters is provided in Table 3.16. Generally, full MS survey scans from 350 to 2,000 m/z were acquired and the three most intense peaks were subjected to CID MS/MS. To increase the dynamic range of the analysis, a dynamic exclusion of 20 sec was taken into account thus avoiding repeated fragmentation of previously analyzed precursor ions. Automatic MS/MS accumulation was set to highest quality and a maximum accumulation time of 2 sec. Mass spectra were recorded using adequate MS operating software (Table 3.16).

Table 3.16: MS acquisition parameters used in this study

Acquisition Parameter	Mass spectrometer			
	QStar Elite	LTQ XL	Qtrap 4000	LTQ-FT Ultra
Ionisation voltage	2.2 kV	1.7 kV	2.3 kV	1.4 kV (Nano Mate, Advion)
MS survey scan, max. accumulation time	380-1,500 m/z, 0.5 sec	400-2,000 m/z, 1.2 sec	380-1,500 m/z, 1.0 (or 0.5*) sec	350-2,000 m/z, 1.0 sec
CID MS/MS scans, max. accumulation time	110-1,500 m/z, 2 sec	Default, 0.5 sec	115-1,500 m/z, 0.5 sec	Default, 0.5 sec
Operating software	Analyst QS 2.0	Xcalibur 2.1.0	Analyst 1.4	Xcalibur 2.1.0

* in enhanced resolution mode

3.10.10.3 MS data evaluation

Generally, upon conversion of LC-MS raw data into Mascot generic format (mgf), database searching was performed using the Mascot™ search algorithm for MS/MS spectra (Mascot Daemon 2.2.02 software platform and Mascot server version 2.2.04). The procedure was comparable for all four mass spectrometers; individual specifications are summarized in Table 3.17. In the following, evaluation of QStar Elite MS data files, which were the first to be generated in the course of this study, is exemplarily described in more detail:

Accordingly, QStar Elite MS data files were transformed into mgf-format using the Analyst QS software version 2.0 with the mascot.dll plug-in 1.6b7. Spectra with less than 10 signals were omitted, precursor mass tolerance for grouping was set to 0.05 Da, and the maximum number of cycles between groups was set to 3. Signals below 0.1% base peak intensities were removed. Mascot searches were subsequently performed as outlined in Table 3.17. All peptide MS/MS spectra with a minimum Mascot score of 34 (p-value of 0.05) were taken into consideration for further interpretation and were additionally validated manually. This procedure included evaluation of (a) the signal-to-noise ratio; (b) the adequate annotation of prominent signals; and (c) the sequence coverage, in particular of b- and y-ions. To

consider an identified protein a ‘true hit’, at least two peptides had to be validated positively.

Table 3.17: Mascot search parameters used in this study

Mascot search Parameter	Mass spectrometer			
	QStar Elite	LTQ XL	Qtrap 4000	LTQ-FT Ultra
mgf-conversion plug-in	Analyst QS 2.0, mascot.dll 1.6b7	Xcalibur 2.0, extract_msn	Analyst 1.4, Mascot.dll 1.6b5	Xcalibur 2.0, extract_msn
Taxonomy	<i>Homo sapiens/ Mus musculus</i>	<i>Homo sapiens</i>	<i>Homo sapiens</i>	<i>Homo sapiens</i>
Database	UniProtKB/ Swiss-Prot*	UniProtKB/ Swiss-Prot*	UniProtKB/ Swiss-Prot*	UniProtKB/ Swiss-Prot*
Enzyme	Trypsin	Trypsin	Trypsin	Trypsin/ semiTrypsin/ None
Missed cleavage sites	2	2	2	0
Fixed modification	Carbamidom. (C)	Carbamidom. (C)	Carbamidom. (C)	Carbamidom. (C)
Variable modification	Oxidation (M) Phosph. (STY)	Oxidation (M) Phosph. (STY)	Oxidation (M) Phosph. (STY)	Oxidation (M) Phosph. (STY)
Peptide tolerance	± 0.2 Da	± 1.5 Da	± 0.4 Da	± 4 ppm
Peptide charge	2 ⁺ and 3 ⁺	2 ⁺ and 3 ⁺	2 ⁺ and 3 ⁺	2 ⁺ and 3 ⁺
MS/MS tolerance	± 0.5 Da	± 1.5 Da	± 0.4 Da	± 0.4 Da
Instrument	ESI-QUAD-TOF	ESI-Trap	ESI-4-SECTOR	ESI-FTICR

* www.uniprot.org, 11/2009: 512,994 sequences

4 Results

4.1 Recombinant protein expression in *E.coli*

The intended pull down-based approach was started by recombinant expression of modified VASP and STIM1 bait proteins. Upon purification and immobilization on an Affi-Gel 10 affinity support, these should consequently be utilized to selectively screen for specific interaction partners in resting human platelets. Further differential analysis and protein identification of all interactome samples should finally be performed by 1D-SDS-PAGE and subsequent nano-LC-ESI-MS/MS.

Therefore, recombinant vector constructs STIM1Ctail (in *pGEX 6p1*), VASP-AAA and VASP-DDE (both in *pQE-30*) were transformed into Ca²⁺-competent *E.coli* BL21 (see 3.8.1) and plated on LB-Amp-CHL agar plates for overnight selection. For an enhanced protein expression in case of VASP-constructs, *E.coli* Rosetta or BL21-CodonPlus-RP were also applied. Insert positive clones were subsequently used for large scale protein expression in 500 mL of bacterial growth medium. In this context, several cell culture protocols have been compared regarding expression efficiency and reproducibility (see 3.8.2), with 21 hours expression in LB-Amp medium/ 2% (v/v) ethanol at 16°C proving to be the most reliable one. As a control, 100 µL bacterial suspension were taken prior to IPTG induction and at multiple time points during the 21-hours culture and analyzed for accumulation of recombinant proteins by 1D-SDS-PAGE and - in case of phospho-mimetic VASP constructs - by VASP-specific Western blotting.

Accordingly, upon 1D-SDS-PAGE and subsequent Coomassie staining, successful expression of STIM1Ctail fusion protein was indicated by presence of a dominant band at 50 kDa (MW STIM1Ctail: 49 kDa) (Figure 4.1 A left). In contrast, such clear evidence was not observable for cells transformed with the VASP-AAA and -DDE constructs (expected MW: 40-50 kDa), even though simultaneous expression of an MBP-fusion tag vector as positive control proved adequacy of the applied transformation and incubation conditions (Figure 4.1 A right, protein band at 40 kDa). Instead, multiple additional protein bands were detected in an MW range of 40 to 50 kDa in both VASP-derived samples. Whether these bands marked truncated forms of the intended fusion proteins, e.g. due to incorrect biosynthesis, will be discussed in more detail in 5.2.1.

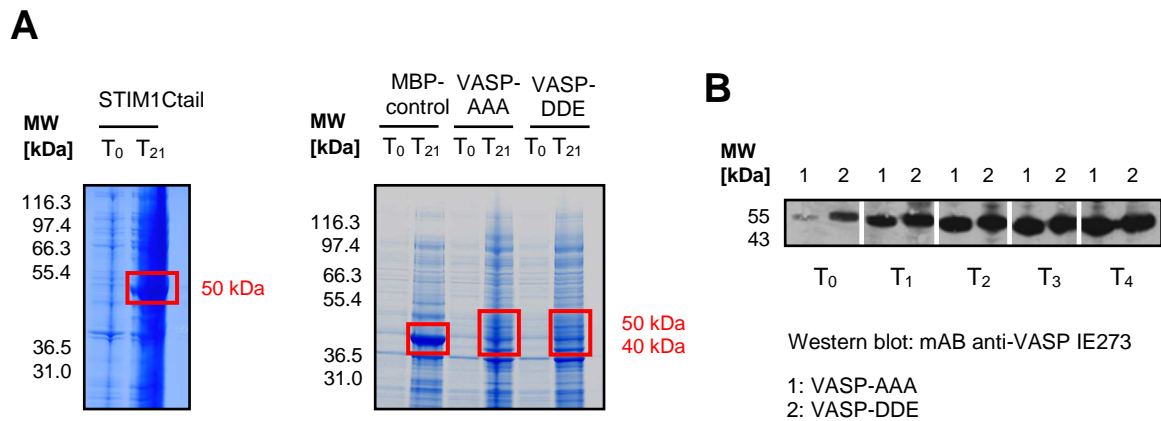


Figure 4.1: Recombinant protein expression of STIM1Ctail, VASP-AAA and VASP-DDE constructs in *E.coli* BL21 (STIM1Ctail) and Rosetta (VASP-constructs). Bacterial culture was performed in LB-Amp medium supplemented with 2% (v/v) ethanol at 16°C. An MBP-fusion tag vector was transformed and expressed as a positive control. (A) 1D-SDS-PAGE and subsequent Coomassie staining of 5 μ L bacterial suspension (left: 10% Bis-Tris gel; right: 4-12% Bis-Tris gel). (B) Monitoring of VASP-AAA and -DDE protein expression by VASP-specific Western blotting. T₀: before IPTG induction; T₁₋₂₁: 1-21 hours after induction.

Following 1D-SDS-PAGE, VASP-specific Western blotting was also performed on VASP-AAA- and VASP-DDE-transformed bacterial samples before (T₀) and after IPTG induction (after 1, 2, 3 and 4 hours of incubation; i.e. T₁₋₄). Here, protein signals detected at approximately 50 kDa finally indicated adequate bacterial expression of these two fusion proteins as well. Moreover, a constant enhancement of signal intensities over time reflected the increasing amounts of newly generated recombinant VASP proteins as a consequence of both bacterial proliferation and *de novo* protein expression (Figure 4.1 B). However, the absence of any prominent VASP-AAA and -DDE protein band in Coomassie-stained SDS-gels - in particular upon comparison to those of STIM1Ctail and the MBP-positive control - led to the conclusion that the overall expression levels of these two protein constructs were considerably low. Thus further protein enrichment was required.

4.2 Purification of STIM1Ctail, VASP-AAA and VASP-DDE protein from *E.coli*

For enrichment of His₆-tagged proteins, IMAC purification was performed. First, bacterial cell pellets (up to 20 g resulting from 500 mL expression culture) were lysed using a French press. Upon ultracentrifugation, recombinant His₆-tagged STIM1Ctail, VASP-AAA and VASP-DDE proteins were isolated from the resulting supernatants

using Ni-NTA agarose IMAC (for details see 3.9.2). For monitoring, the pure lysate supernatant ('input') and the column flow through, as well as the first and the last wash- and selected elution fractions were analyzed by 1D-SDS-PAGE.

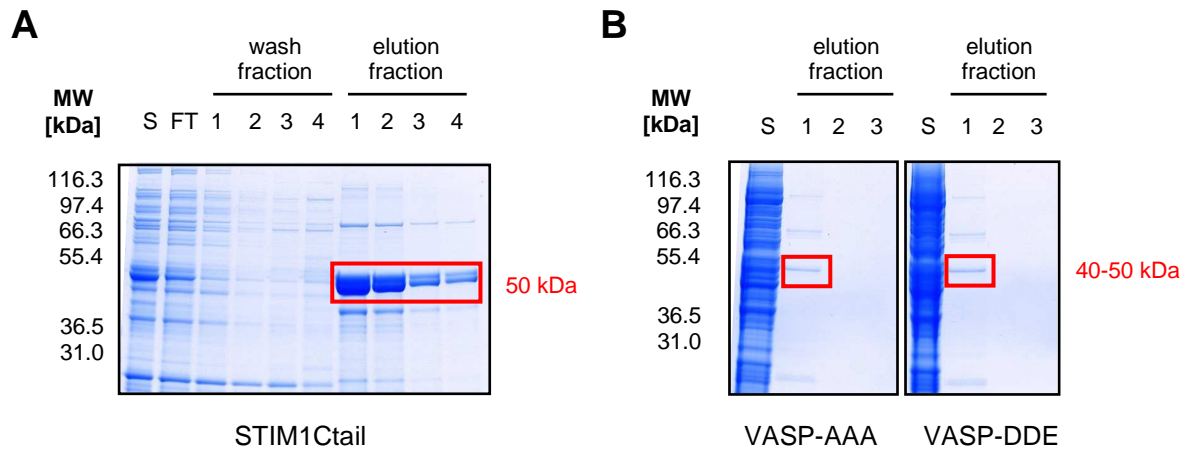


Figure 4.2: IMAC purification of recombinant STIM1Ctail (A), VASP-AAA and VASP-DDE (B) via Ni-NTA agarose; control by 1D-SDS-PAGE (10% Bis-Tris gels, Coomassie staining). S: lysate supernatant (5 μ L); FT: column flow through (5 μ L); 1-4: individual wash- and elution fractions (20 μ L). Washing was repeatedly performed with lysis buffer (1, 2) and washing buffer (3, 4).

As depicted in Figure 4.2 A, IMAC purification of STIM1Ctail samples particularly enriched a 50 kDa protein subset (elution fractions) and reduced unspecific protein background (compare wash fraction 1 with fraction 2 and 4, respectively). The majority of lysate proteins, however, passed the column without significant retardation (see input compared to flow through samples). For further purification and removal of contaminating particulate material (e.g. remnants of Ni-NTA agarose), the STIM1Ctail elution fractions were pooled and SEC was performed (see 3.9.3). During the 4-hours separation procedure, a total of 120 2-min elution fractions were collected and stored at 4°C. The resultant UV₂₈₀ chromatogram (Figure 4.3 A) displayed two distinct peaks: a comparatively small, early-eluting one at fraction 31-33 and a dominant one at fractions 38-40 which was accompanied by prolonged tailing (fractions 44 and 45). These eight fractions plus fractions 48 and 49, which also included a minor peak of the chromatogram, were consequently analyzed by 1D-SDS-PAGE. In accordance with the UV₂₈₀ chromatogram, the majority of proteins eluted in SEC fractions 38-40, including a dominant protein subset of an estimated molecular mass of 50 kDa (Figure 4.3 B).

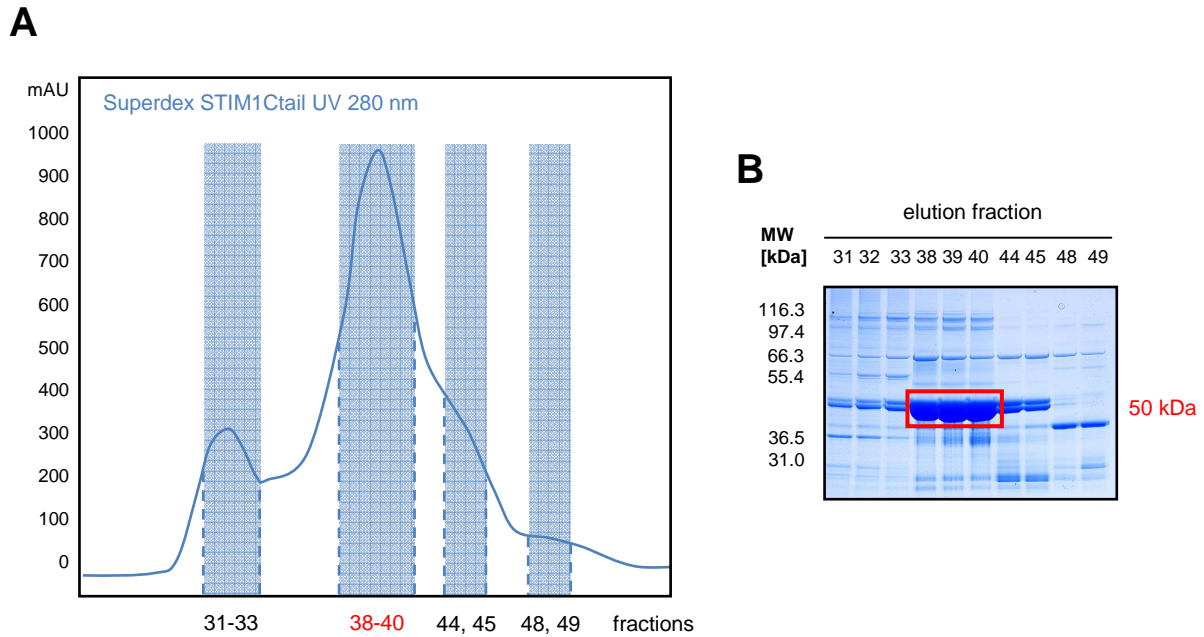


Figure 4.3: SEC of STIM1Ctail IMAC samples using a Superdex HiLoad 26/ 60 separation column and an ÄKTA FPLC system. The 4-hours procedure was constantly monitored via the ÄKTA UV detector unit and a total of 120 2-min elution fractions were collected. (A) UV₂₈₀ chromatogram. Elution windows containing distinct peaks and/ or tailing are marked in blue and (B) were analyzed by 1D-SDS-PAGE (4-12% Bis-Tris gel, sample volume: 20 µL, Coomassie staining).

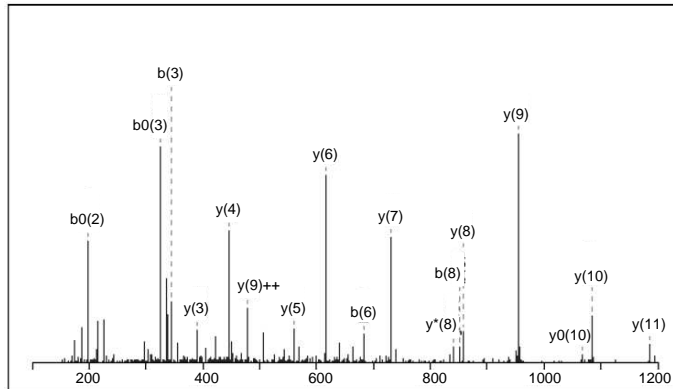
Following in-gel trypsinisation and subsequent MS measurement on a QStar Elite mass analyzer, these prominent 50 kDa protein bands were related to the STIM1Ctail protein construct, i.e. STIM1 aa 484-685 (Figure 4.4, display of an identified STIM1Ctail fragment ion: STIM1 aa 503-514).

In contrast to STIM1Ctail, a parallel approach focussing on purification of recombinant VASP-AAA and -DDE constructs did not yield significant protein enrichment. Accordingly, following 1D-SDS-PAGE of VASP-derived IMAC samples, Coomassie-stained protein bands were comparatively weak (Figure 4.2 B, at 40-50 kDa) and did not contain any detectable VASP-related sequences when analyzed by nano-LC-ESI-MS/MS. Moreover, the presence of further equidistant protein bands in both VASP-AAA and -DDE samples (see Figure 4.2 B, at approximately 60 and 100 kDa) led to the hypothesis that the signals detected here were more likely to originate from unspecific binding of protein multimers to the bead matrix than from specifically enriched VASP constructs. Hence, it had to be deduced that, at least in our hands, protein expression in *E.coli* was insufficient for both generation (see 4.1) and consequent isolation of these two specific fusion proteins. As this might have

been due to limitations inherent to the prokaryotic *E.coli* expression system (for details see 5.2.1), an alternative strategy using HEK293 cells for eukaryotic biosynthesis of recombinant VASP-AAA and -DDE was consequently developed.

MS/MS Fragmentation of L^TEPQLGLGSQR

Found in Stromal interaction molecule 1 precursor (aa 503-514)



Monoisotopic mass of neutral peptide: 1297.6990
 Fixed modification: carbamidomethylation
 Ions score: 76 (expect: 1.6e-006)
 Matches: 17/118 fragment ions (25 most intense peaks)

Figure 4.4: Identification of purified STIM1Ctail by MS/MS analysis on a QStar Elite mass analyzer following in-gel trypsinisation of Coomassie-stained control gels.

4.3 Generation of mutant VASP-DNA constructs for eukaryotic transfection

For synthesis of recombinant VASP fusion proteins in HEK293 cells, the original VASP-AAA and -DDE DNA-constructs had to be further modified (for details see 5.2.2) and cloned into the eukaryotic expression vector *pcDNA3.1/V5-HisA*. Hence, for both VASP-AAA and VASP-DDE, two different constructs were developed: one solely lacking the VASP tetramerization domain (Δ TD; nt 1,027-1,143) and a second one additionally lacking the VASP FAB-region (Δ FAB Δ TD; nt 775-1,143). Accordingly, using the original VASP *pQE-30* vector constructs VASP-AAA and VASP-DDE as DNA-templates, *Pfu*-PCRs were performed to generate the four truncated VASP-inserts 'VASP-AAA Δ TD' and 'VASP-DDE Δ TD' (nt 1-1,026), as well as 'VASP-AAA Δ FAB Δ TD' and 'VASP-DDE Δ FAB Δ TD' (nt 1-774) (for details see 3.7.1.2). In this context, to enable subsequent insertion into the *pcDNA3.1/V5-HisA* MCS, all VASP deletion primers were specifically designed to convey an additional BamHI restriction site to the 5'- and an EcoRI restriction site to the 3'-end of each VASP insert. The resulting PCR products were verified based on molecular mass evaluation by agarose gel electrophoresis (illustrated in Figure 4.5). Upon purification, PCR products were amplified in StrataClone SoloPack competent *E.coli* cells, typically yielding an average DNA concentration of 2-3 μ g/ μ L (see 3.7.1.4 and

3.7.1.5). In parallel, the *pcDNA3.1/V5-HisA* target vector was also amplified and purified in a maxiprep approach (DNA concentration: 3-5 µg/ µL).

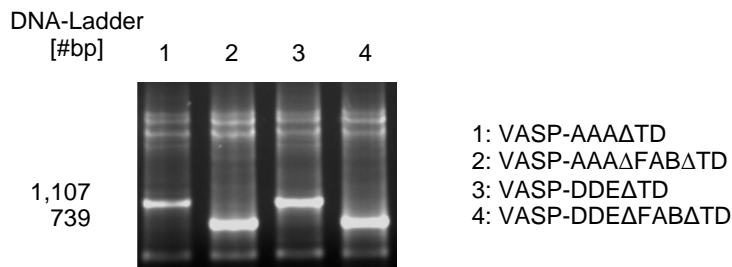


Figure 4.5: Electrophoretic control of VASP-deletion PCR products (1% agarose gel, GelRed staining). In each case a sample volume of 2 µL was applied. Bp-values were estimated via the 123 bp DNA Ladder (for VASPΔTD ~1,000-1,100 bp, for VASPΔFABΔTD ~700-800 bp) and are in good correlation with the calculated ones (for VASPΔTD 1,027 bp, for VASPΔFABΔTD 775 bp).

For generation of compatible 5'- and 3'-sticky ends, which is obligatory for targeted insert-vector recombination, overnight BamHI/ EcoRI restriction digests were performed on the four VASP-*pSC-A-amp/kan* vector constructs ('VASP insert release'), as well as on the *pcDNA3.1/V5-HisA* target vector (appropriate opening of the MCS). Digest efficiencies were monitored by gel electrophoresis (Figure 4.6), samples were purified and quantified by OD₂₆₀ measurement (DNA concentration: 2-3 µg/ µL).

Finally, VASP-inserts were integrated into the linearized *pcDNA3.1/V5-HisA* target vector (insert-to-vector ratio 4:1) and ligation reactions were performed as described in 3.7.1.7. Resulting recombinant VASP vector constructs were amplified in *E.coli* DH5α and isolated in a maxiprep approach, thereby yielding the following concentrations (see also Figure 4.7 A): VASP-AAAΔTD (6,527 bp) 4.9 µg/ µL, VASP-AAAΔFABΔTD (6,275 bp) 5.4 µg/ µL, VASP-DDEΔTD (6,527 bp) 3.9 µg/ µL and VASP-DDEΔFABΔTD (6,275 bp) 3.4 µg/ µL.

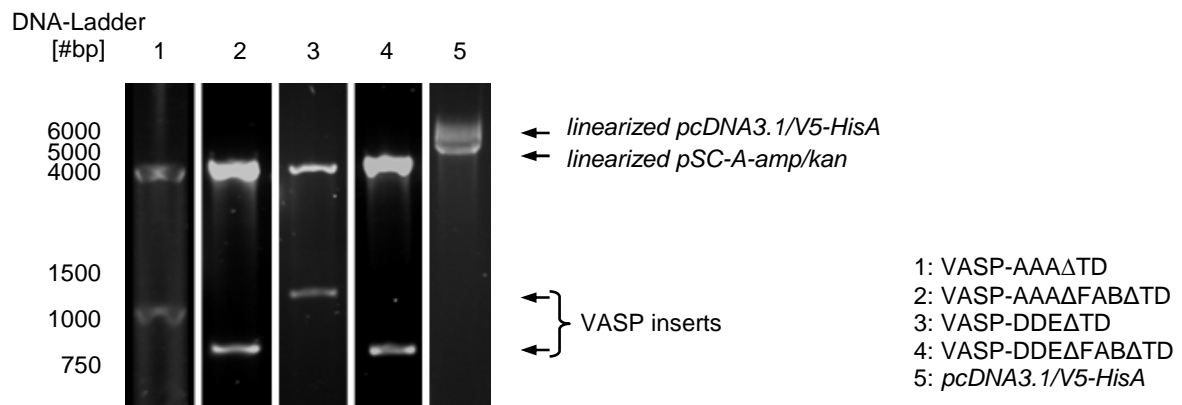


Figure 4.6: Electrophoretic control of BamHI/ EcoRI restriction digests of (a) VASP-*pSC-A-amp/kan* vector constructs; and (b) of *pcDNA3.1/V5-HisA* target vector. In each case a sample volume of 2 μ L was applied on a 1% agarose gel (GelRed staining). Bp-values were estimated via the GeneRuler 1kb DNA Ladder. Large DNA fragments correspond to linearized *pcDNA3.1/V5-HisA* (5.5 kb) or *pSC-A-amp/kan* vector (4.3 kb), shorter ones to released VASP inserts VASP Δ TD (~1,000-1,100 bp) and VASP Δ FAB Δ TD (~700-800 bp), respectively.

4.4 Validation of VASP-vector assembly

Correct VASP-vector recombination was validated by several strategies: First, control PCRs using VASP deletion primers VASP-Fwd/ -RevI (for VASP Δ TD) or VASP-Fwd/ -RevII (for VASP Δ FAB Δ TD) were performed on all four VASP constructs. As depicted in Figure 4.7 B, estimated molecular masses of resulting PCR products corresponded to those calculated for the intended VASP inserts: 1,000-1,100 bp for VASP Δ TD (calculated 1027 bp) and 700-800 bp for VASP Δ FAB Δ TD (775 bp). This finding was moreover confirmed by BamHI/ EcoRI control digests, where - besides linearized *pcDNA3.1/V5-HisA* target vector at 5.5 kb - DNA fragments of similar sizes could be identified (see Figure 4.7 C).

Finally, DNA sequencing reactions were performed on each vector construct. First, precise in-frame integration of VASP inserts in the MCS of *pcDNA3.1/V5-HisA* was evaluated by analyzing the close sequence proximity of the individual 5'- and 3'-insertion sites. This has been executed in-house by sequencing PCRs using the GenomeLab DTCS Quick Start Kit and either PCR primer T7-Fwd (binds 5' of BamHI restriction site) or BGH-Rev (3' of EcoRI). Generally, both the BamHI- and the EcoRI ligation junctions proved to be correct in all four VASP-constructs - thus confirming accurate reading frames - and were moreover followed by the intended DNA sequences. In detail, downstream of the BamHI restriction site, the first 324-340 bp of

VASP (including the start codon) could be identified in case of T7-Fwd sequences. BGH-Rev sequencing data covered only the last 44 (for VASP- Δ FAB Δ TD) to 273 (for VASP- Δ TD) bp of VASP; however, since these sequences included the VASP stop codon upstream of the EcoRI restriction site, they were still sufficient to verify adequate VASP-vector assembly. Ultimate full-length DNA sequencing was finally provided by GATC Biotech (Konstanz, Germany) and confirmed the previous sequencing results. In addition, the V5- and His₆-coding sequences could be detected in-frame, and premature termination sites as well as any other point mutation or nt-sequence aberration could be excluded for all four VASP-vector constructs. For a detailed view on the respective sequencing data, please refer to 7.4.

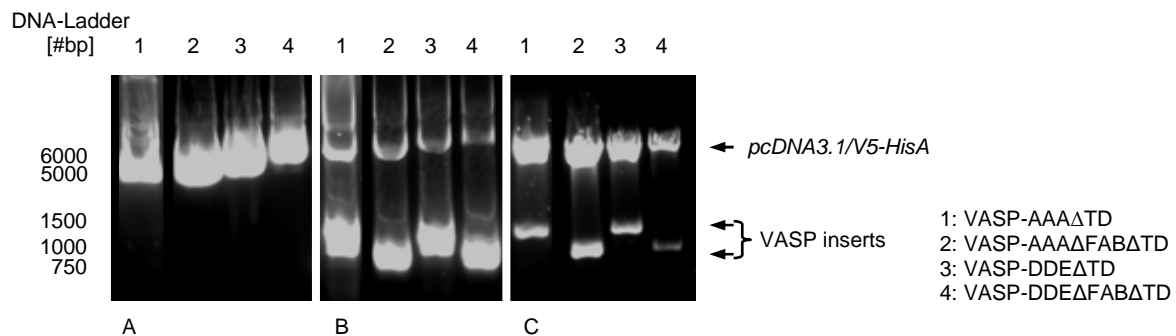


Figure 4.7: Electrophoretic control of VASP-*pcDNA3.1/V5-HisA* vector constructs. (A) Purified plasmid maxipreps, (B) control PCR (primer combinations: VASP-Fwd/ -RevI for VASP Δ TD and VASP-Fwd/ -RevII for VASP Δ FAB Δ TD), (C) BamHI/ EcoRI restriction digest. In each case a sample volume of 2 μ L was applied on a 1% agarose gel (GelRed staining). Bp-values were estimated via the GeneRuler 1kb DNA Ladder. Large DNA fragments correspond to either (A) intact VASP-vector constructs (~6.5 kb) or (C) linearized *pcDNA3.1/V5-HisA* vector (5.5 kb). Shorter sequences (B, C) indicate released VASP inserts VASP Δ TD (~1,000-1,100 bp) and VASP Δ FAB Δ TD (~700-800 bp), respectively.

4.5 Transfection of VASP deletion constructs in HEK293 cells

For stable, long-term expression of recombinant proteins, the VASP-vector constructs were transfected in eukaryotic HEK293 cells following the ExGen 500 transfection manual. Since the *pcDNA3.1*-based vector also confers resistance to neomycin, stably-transfected cells having integrated the vector plasmid in the genome were selected and extended in neomycin (G418) selection medium. As

confirmed microscopically in comparison to non-transfected HEK293 (wildtype, HEK-wt), transfection neither affected cell morphology, nor cell division rate (Figure 4.8). In parallel, a fifth HEK293 cell line stably expressing the vector construct *pcDNA3.1/V5-HisA lacZ* was generated to serve both as (a) an indicator for transfection efficiency by β -gal staining; and (b) as a positive control during evaluation of subsequent protein purification procedures (including 1D-SDS-PAGE and Western blotting against the V5- and His₆-tagged protein products). Thereby, transfection efficiencies were estimated by determining the ratio between transfected (i.e. β -gal stained) HEK-lacZ cells and the total cellular amount. As exemplarily shown in Figure 4.9 A, ExGen 500 transfection efficiency could generally be considered as high and typically amounted up to 80-90%.

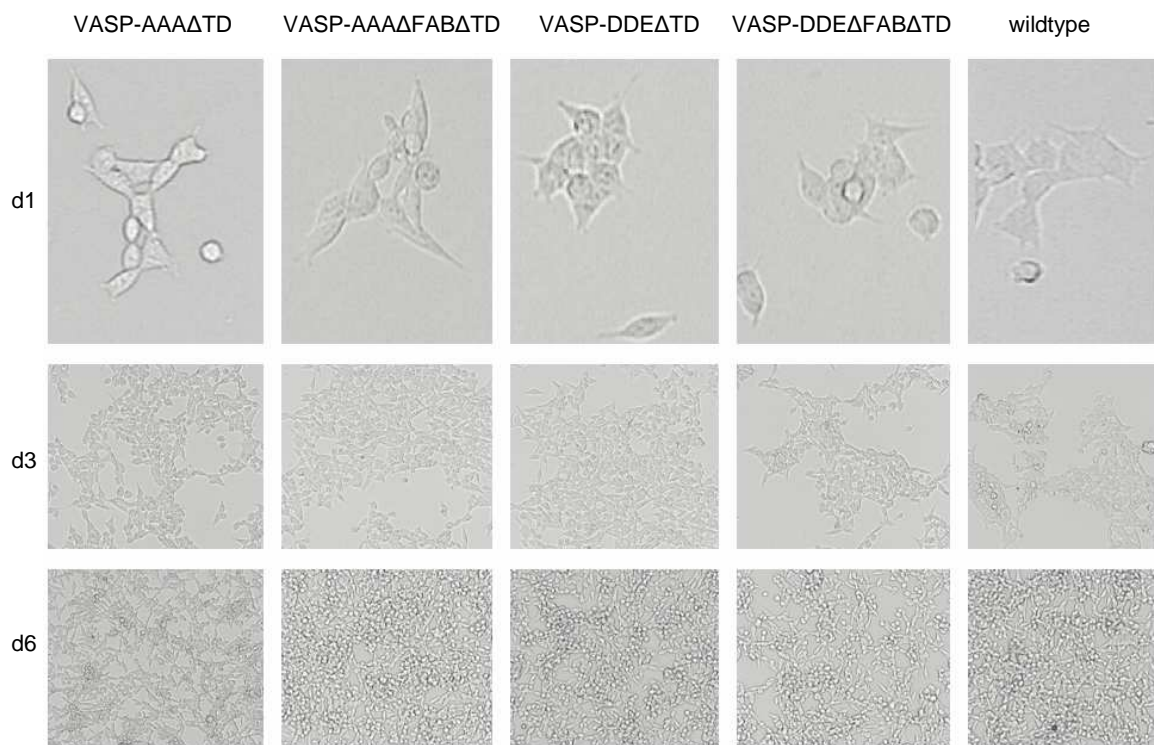


Figure 4.8: Stably-transfected HEK293 vs HEK293 wildtype. Cells were monitored for 1-6 days (d1-d6) after transfection. For evaluation of cell morphology, cell adhesion as well as protrusion formation was taken into consideration. As displayed in the d1-series, morphological differences between the cell lines were negligible. Regarding the cell division rate, half-confluence was generally achieved after three days (d3) and total confluence after 6 days (d6) of incubation.

To verify adequate protein expression, V5-specific Western blotting was subsequently performed on all five stable HEK293 cell lines. Accordingly, the intended recombinant fusion proteins were clearly detectable, with individual MW-

values (estimated via the See Blue Plus2 Pre-Stained Protein Standard) being in good correlation with the calculated ones (for VASP Δ TD 38 kDa, for VASP Δ FAB Δ TD 29 kDa and for lacZ fusion protein 121 kDa, see Figure 4.9 B). Thus, for purification of appropriate protein amounts sufficient for subsequent generation of Affi-Gel-based affinity supports, extended cell cultures were performed and harvested cells were stored until further usage.

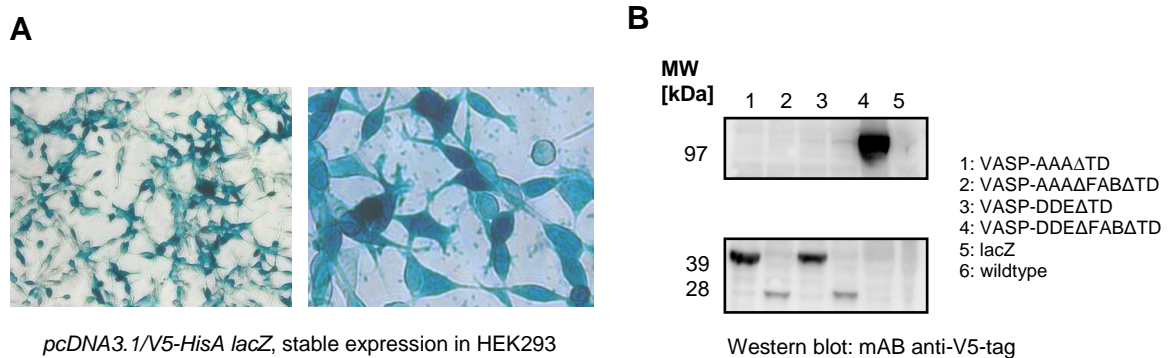


Figure 4.9: Protein expression of stable HEK cell lines. (A) β -gal staining of HEK293 cells stably expressing the V5-His₆-tagged lacZ fusion protein (HEK-lacZ) confirmed high transfection efficiency of the applied ExGen 500 transfection protocol. *Left*: overview; *right*: zoomed-in image. (B) V5-specific Western blotting of native lysates of HEK-VASP-AAA Δ TD, -VASP-AAA Δ FAB Δ TD, -VASP-DDE Δ TD, -VASP-DDE Δ FAB Δ TD and -lacZ in comparison to non-transfected HEK-wt (4-12% Bis-Tris gel, sample amounts 50 μ g).

4.6 Purification of recombinant proteins from HEK293 cells

For initial evaluation of IMAC-based protein purification from the stable HEK293 cell lines, HEK-lacZ positive controls were processed first and compared to equally-treated HEK-wt. In detail, cells from five confluent 75 cm² tissue culture flasks of either HEK-lacZ or HEK-wt (i.e. approximately 8 x 10⁶ cells) were pooled, lysed by sonication and submitted to Ni-NTA agarose IMAC as described in 3.9.2 (section 1). Analogous to 4.2, purification efficiency was finally monitored by analyzing the crude cell lysate, the lysate supernatant upon ultracentrifugation ('input'), as well as the column flow through and selected wash- and elution fractions by 1D-SDS-PAGE. As depicted in Figure 4.10, comparison of protein purification patterns did not reveal distinct differences between HEK-lacZ and HEK-wt samples, neither in the input nor in any of the eluted fractions. Moreover, though the individual input protein profiles markedly differed from the corresponding elution fractions ('output') - thus indicating

adequate purification - significant enrichment of the 121 kDa lacZ fusion protein could not be observed. Since this finding was in contrast to the Western blot data displayed in Figure 4.9 B, the Ni-NTA purification procedure was further modified by altering (a) the binding; (b) the washing; and (c) the elution conditions. First, to improve ligand binding, incubation time was varied from one hour up to an overnight incubation at 4°C. In addition, since exceeding imidazole concentrations may interfere with weak His₆-Ni-NTA interactions, the respective content was altered from 5 to 1 mM in the lysis buffer and from 25 to 10 mM in the washing buffer. Alternatively, imidazole-free purification protocols have also been examined, which included recombinant protein elution either by shifting the buffer pH below a value of 4.0 (where His₆-tags are protonated and consequently dissociate from Ni²⁺ bead material) or by adding Ni²⁺-chelating agents to the elution buffer system (e.g. 200 mM EDTA).

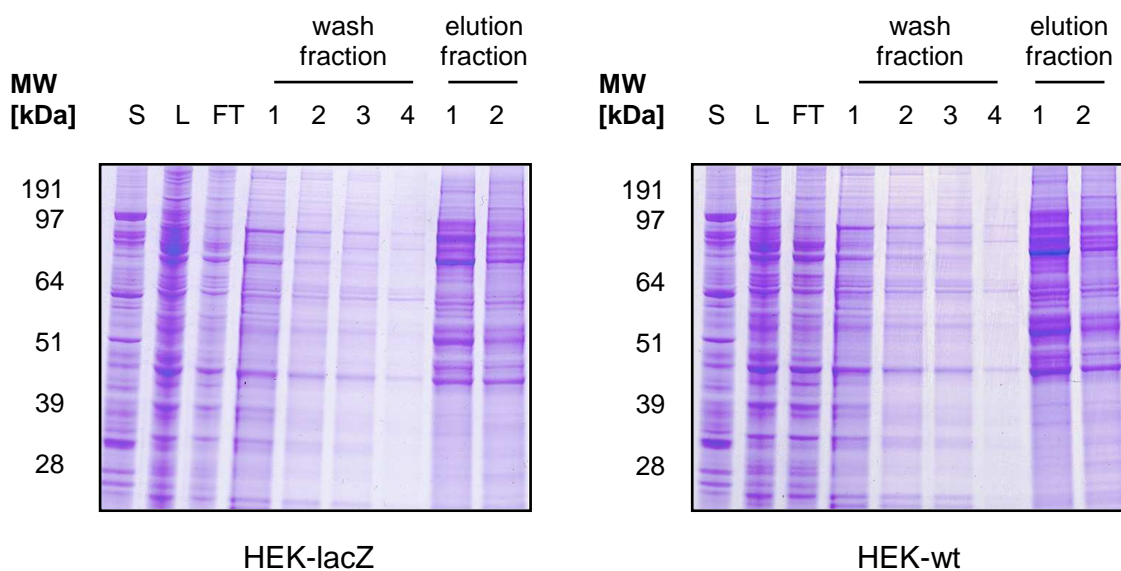


Figure 4.10: IMAC purification of recombinant lacZ protein from HEK-lacZ via Ni-NTA agarose in comparison to equally treated non-transfected HEK-wt. Control by 1D-SDS-PAGE (4-12% Bis-Tris gels) and subsequent Coomassie staining. S: lysate supernatant (5 μ L); L: crude cell lysate (5 μ L); FT: column flow through (5 μ L); 1-4: individual wash- and elution fractions (20 μ L). Washing was repeatedly performed with lysis buffer (1, 2) and washing buffer (3, 4).

However, neither of these strategies subsequently resulted in an improved enrichment of the anticipated 121 kDa lacZ fusion protein in the elution fractions. The respective 1D-SDS control gels closely resembled those exemplarily given in Figure 4.10. Hence, the Ni-NTA agarose-based approach was regarded as insufficient for

protein purification from the generated stable HEK293 cell lines and alternative strategies were consequently taken into consideration.

The most promising one was provided by the Qiagen Ni-NTA Spin Kit, which has been reported to enable reliable purification of His₆-tagged fusion proteins from a variety of biological sources (including HEK293 cells) even under low expression conditions. Following the manufacturer's instructions, three confluent grown 75 cm² tissue culture flasks of each of the recombinant HEK293 cell lines (i.e. approximately 5 x 10⁶ cells) were pooled and processed under native conditions (described in 3.9.2, section 2). The resulting elution fractions were subsequently controlled for qualitative and quantitative fusion protein enrichment via V5-specific Western blotting and differential 1D-SDS-PAGE. According to the anti-V5 Western blot data, all five recombinant proteins were present in the eluted fractions (Figure 4.11 A), with individual signal intensities being comparable to those displayed in Figure 4.9 B. This finding, however, could not be confirmed when analyzing analogous Coomassie-stained control gels: Here, in comparison to equally treated HEK-wt, neither differential protein purification patterns nor specific enrichment of proteins of the expected molecular masses could be observed for IMAC purified VASP (VASP Δ TD 38 kDa, VASP Δ FAB Δ TD 29 kDa) and lacZ samples (121 kDa) (see Figure 4.11 B).

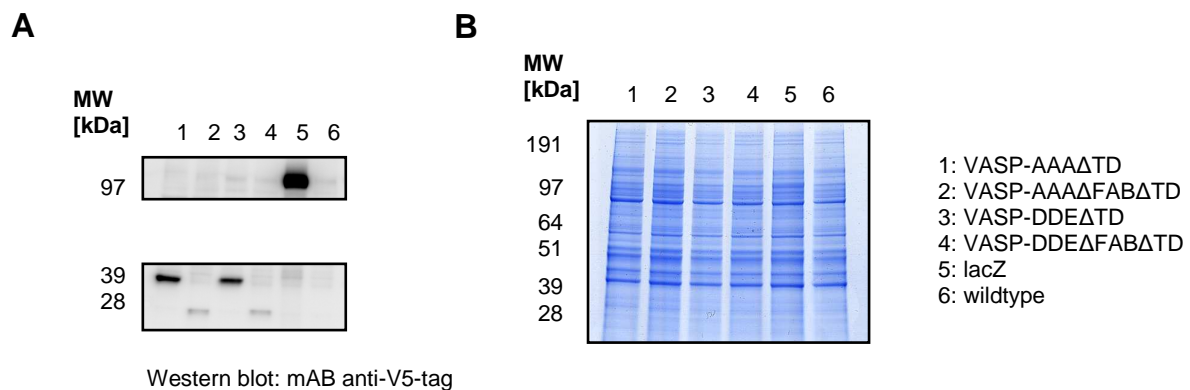


Figure 4.11: IMAC purification of recombinant VASP-AAA Δ TD, VASP-AAA Δ FAB Δ TD, VASP-DDE Δ TD, VASP-DDE Δ FAB Δ TD and lacZ proteins from stable HEK293 cell lines using the Qiagen Ni-NTA Spin Kit (native approach). Analysis of combined eluted fractions; equally-treated HEK-wt samples were taken as a negative control. Control by (A) V5-specific Western blotting and (B) 1D-SDS-PAGE and subsequent Coomassie staining. In each case 4-12% Bis-Tris gels and sample amounts of 50 μ g were applied.

To consequently enhance recombinant protein binding to the Ni-NTA spin column, stringency of the method was successively reduced by lowering the imidazole concentrations of the lysis buffer (10 to 1 mM) as well as of the washing buffer (20 to 10 mM). This has been performed in accordance with the manufacturer's instructions. However, as indicated by 1D-SDS-PAGE analysis subsequent to IMAC purification of adequate HEK293 samples, none of these modifications positively affected enrichment of VASP or lacZ fusion proteins.

Having so far intensively yet unsuccessfully worked on an optimization of the IMAC conditions, it finally had to be excluded that the observed difficulties in recombinant protein enrichment were inherent to the fusion protein constructs themselves. As reported in 4.4, full length DNA sequencing proved correctness of all four VASP vector constructs, including the C-terminal V5- and His₆-encoding sequences (the *pcDNA3.1/V5-HisA lacZ* vector provided by Invitrogen has not additionally been controlled by DNA sequencing). Moreover, V5-specific Western blotting in stably transfected HEK293 cell lines verified expression of C-terminally V5-tagged fusion proteins, with individual molecular masses reflecting those of the intended recombinant proteins (Figure 4.9 B, Figure 4.11 A). Thus, deriving from all these previous findings, primary sequence aberrations were unlikely to be present in the expressed products. In this context, however, VASP-specific Western blotting could not be performed since the available primary antibodies also recognized endogenous VASP of HEK293, hence resulting in superposition of signals (tested with mAB anti-VASP IE273, data not shown).

To furthermore evaluate the structural accessibility of the C-terminal His₆-tag, IMAC purification via the Qiagen Ni-NTA Spin Kit was also executed under denaturing conditions, which would consequently expose so-far partially hidden protein sequences (see 3.9.2, section 2). The resulting sample fractions (i.e. crude cell lysates, lysate supernatants upon ultracentrifugation, column flow through, as well as wash- and elution fractions) were differentially analyzed by 1D-SDS-PAGE and compared to those deriving from native protocols (see 3.9.2). As an example, Coomassie-stained control gels of purified lacZ samples are presented in Figure 4.12 in comparison to equally treated HEK-wt negative controls. Gel data of purified VASP fusion proteins resembled those of lacZ and are thus not explicitly shown. Protein purification patterns noticeably varied in samples isolated under denaturing conditions vs natively purified ones. However, a detailed differential analysis of lacZ

vs corresponding wildtype fractions did not reveal any significant differences both upon native and denaturing purification. Moreover, in either case distinct enrichment of the 121 kDa lacZ fusion protein could not be confirmed in the eluted fractions. The majority of protein bands visualized on the gels may thus above all originate from unspecific interaction of endogenous HEK293 proteins with the affinity support, which would consequently mask signals deriving from comparably lower abundant His₆-tagged target proteins and associated complex components.

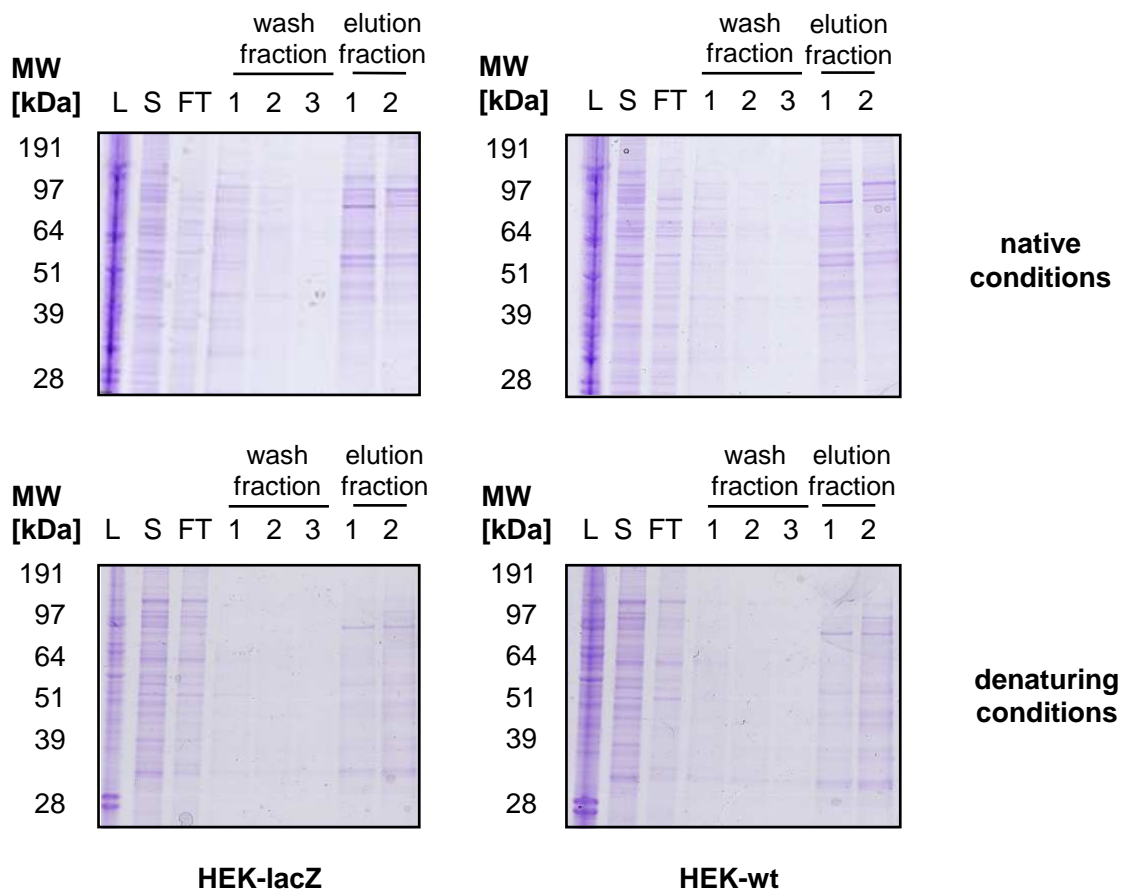


Figure 4.12: IMAC enrichment of recombinant lacZ protein from HEK-lacZ via Qiagen Ni-NTA Spin Kit vs equally treated HEK-wt. Comparison of native and denaturing protein purification conditions. Control by 1D-SDS-PAGE (4-12% Bis-Tris gels) and subsequent Coomassie staining. L: crude cell lysate (5 μ L); S: lysate supernatant ('input', 5 μ L); FT: column flow through (5 μ L); 1-3: individual wash- and elution fractions (20 μ L).

The fact, that application of this IMAC strategy did not lead to considerable enrichment of both lacZ (i.e. the *per se* standard control for correct fusion protein expression) and recombinant VASP protein constructs even under denaturing

conditions, raised the question as to whether the C-terminal His₆-tag conferred by the *pcDNA3.1/V5-HisA* vector was generally accessible to the Ni-NTA support. This theory was furthermore strengthened by polyHis-specific Western blotting of crude HEK293 cell lysates: Even though four different monoclonal anti-His-tag antibodies were tested during the course of several experiments (i.e. anti-His₄-tag, anti-His₅-tag, anti-His₆-tag and anti-His[C-term]-tag; see 3.10.4), no clear evidence could be provided for the presence of adequately tagged proteins neither in the four stable VASP-HEK293 cell lines nor in the lacZ positive control line (exemplarily shown in Figure 4.13). This finding was in contrast to the previously gained anti-V5 Western blotting data that were generated in a similar approach and proved accurate full-length expression of the intended fusion proteins (e.g. Figure 4.9 B). Therefore, the C-terminal His₆-tag itself had to be regarded as structurally inaccessible, which would consequently prevent both polyHis-specific Western blotting and Ni-NTA-based IMAC purification. Under these conditions and also considering the low expression levels of the designated constructs, which would demand high temporal and material efforts to achieve sufficient biosynthesis and enrichment of HEK293-derived fusion proteins, the intended VASP-specific interaction study was finally abandoned. The focus of this work was consequently shifted towards analyzing the interactome of STIM1Ctail.

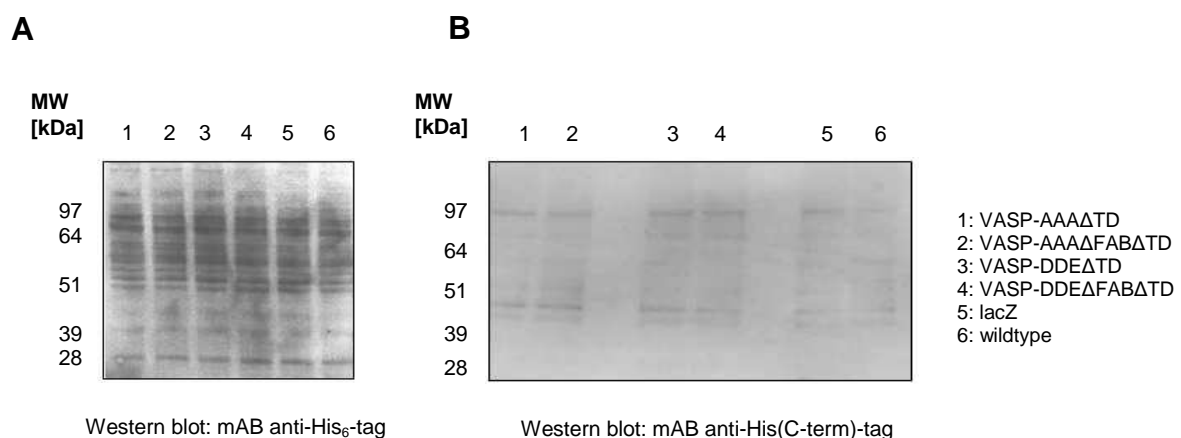


Figure 4.13: PolyHis-specific Western blotting of crude lysates of all four stable VASP-HEK293 cell lines in comparison to HEK-lacZ (positive control) and HEK-wt (negative control). Samples were separated by 1D-SDS-PAGE (4-12% Bis-Tris gels) and subsequently immunoblotted against the C-terminal His₆-tag using (A) the mAB anti-His₆-tag (Roche Diagnostics, 1:6,000) and (B) the mAB anti-His(C-term)-tag (Invitrogen GmbH, 1:5,000). In each case a sample amount of 50 µg was applied.

4.7 Generation of STIM1Ctail affinity column and platelet interactome screening

N-terminal coupling of purified recombinant STIM1Ctail protein (i.e. the total volume of all pooled STIM1Ctail SEC fractions, see 4.2) to the Affi-Gel 10 affinity matrix was performed as described in 3.9.4. Coupling efficiency was subsequently confirmed by 1D-SDS-PAGE of (a) the bead material prior and after incubation with STIM1Ctail; and (b) the column flow through in comparison to an aliquot of uncoupled pooled SEC fractions (data not shown).

Resting human platelets were isolated from healthy donors and lysed under native conditions (for details see 3.6.3 and 3.9.1), typically yielding protein concentrations of 5-7 mg/ mL. For each interaction experiment, platelet lysates of two different donors were then pooled and incubated with the STIM1Ctail affinity column (SC) overnight at 4°C. In parallel, to also evaluate the impact of unspecific protein binding to the affinity support, an equal volume of pooled platelet lysates was incubated with uncoupled Affi-Gel 10 matrix (i.e. control column, Ctrl). As outlined in 3.9.5, bound platelet proteins were finally eluted by applying a stepwise pH gradient from pH 6.0 to 2.0. The eluted fractions of both affinity columns were differentially analyzed by 1D-SDS-PAGE and subsequent silver staining (Figure 4.14). In addition, the column flow through as well as the first and the last wash fraction were also monitored. Accordingly, the bulk of platelet proteins passed the columns in the flow through fractions. Unspecific protein binding was efficiently reduced by washing with 10 CV PBS and by application of 3 CV glycine/ HCl pH 6.0 (i.e. the first elution step). The majority of specifically bound proteins were finally released from the affinity supports by addition of 3 CV glycine/ HCl pH 2.0, whereas eluting effects of glycine/ HCl pH 5.0 - pH 3.0 were relatively low. Comparing the pH 2.0 fractions of three independent biological replicates, a total of 18 differential protein bands were reproducibly detected in the SC vs the Ctrl samples (marked by numbered arrows in Figure 4.14). For identification of these putative STIM1Ctail interaction partners in resting human platelets, the respective protein bands were excised, tryptically digested and nano-LC-ESI-MS/MS analysis was performed on an LTQ XL and a Qtrap 4000 mass analyzer as described in 3.10.9 and 3.10.10.

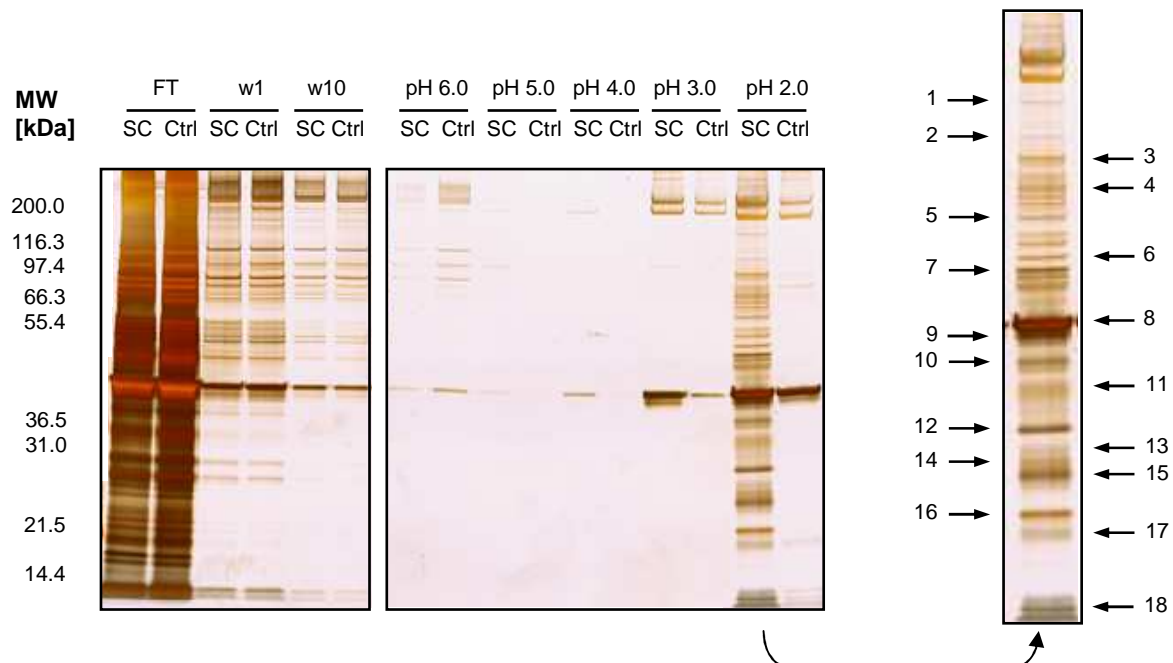


Figure 4.14: Interaction of native lysates of resting human platelets with the STIM1Ctail affinity column (SC) vs control column (Ctrl). Control by differential 1D-SDS-PAGE (10% Bis-Tris gels, silver staining). FT: column flow through (5 μ L); w1, w10: first and last wash fractions (20 μ L); pH 6.0 - pH 2.0: pooled glycine/ HCl elution fractions (20 μ L). Arrows indicate differential protein bands which were subsequently excised and analyzed by protein mass spectrometry.

4.8 Identification of differential proteins by nano-LC-ESI-MS/MS analysis

Data deriving from nano-LC-ESI-MS/MS analyses of all differential protein bands of SC vs Ctrl human platelet samples (i.e. three biological replicates) were searched against the UniProtKB/ Swiss-Prot human subset and validated as described in 3.10.10.3. Thereby, only protein identifications which had been verified by at least two independent corresponding peptides were accepted. As a result, of the 18 differential protein bands exemplarily depicted in Figure 4.14 a total of 14 were annotated adequately. Accordingly, a data summary of three independent MS/MS analyses delivered 93 individual proteins, with molecular masses stretching from approximately 270 to 11 kDa. A comprehensive overview of all protein identifications is provided in Table 4.1.

Based on detailed analyses via the UniProtKB/ Swiss-Prot knowledgebase, the majority of the 93 identified proteins - i.e. 55.9% - originated from the cytosol; another 15.1% were classified as being localized within or associated to cellular membranes (in particular the plasma membrane). Moreover, 7.5% of all identified proteins were

related to granules, vesicles or endosomes, and a total amount of 17.2% originated from diverse cellular organelles - such as the Golgi apparatus, the sarcoplasmic reticulum and, above all, mitochondria (12 individual proteins, i.e. 12.9%). The described subcellular distribution together with corresponding actual protein amounts are illustrated in Figure 4.15 A.

Table 4.1: Individual proteins identified in 14 of the 18 differential protein bands of SC vs Ctrl human platelet samples; summary of LTQ XL and Qtrap 4000 nano-LC-ESI-MS/MS data of three independent biological replicates. Hits are listed according to corresponding protein bands and with decreasing Mascot scores. MW: molecular weight [Da]; Acc.Nr.: UniProtKB/ Swiss-Prot accession number; MA: mass analyzer; PB: protein band in Figure 4.14.

#	Protein identifications	MW	Acc.Nr.	Score	MA	PB
1	Myosin heavy chain 9	226,532	P35579	12,169	LTQ	1
2	Talin 1	269,767	Q9Y490	1,078	LTQ	
3	Integrin alpha 2b	113,377	P08514	1,719	LTQ	2
4	Vinculin	123,799	P18206	984	LTQ	
5	Gelsolin	85,698	P06396	969	LTQ	3
6	Unc-112-related protein 2 (Kindlin 3)	75,953	Q86UX7	921	LTQ	5
7	Caldesmon, isoform 4	62,683	Q05682-4	648	Qtrap	
8	78 kDa glucose-regulated protein	72,333	P11021	632	Qtrap	
9	Very-long-chain specific acyl-CoA dehydrogenase	70,390	P49748	570	LTQ	
10	Syntaxin-binding protein 2	66,453	Q15833	235	LTQ	
11	Bridging integrator 2, isoform 1	61,874	Q9UBW5-1	179	Qtrap	
12	Platelet glycoprotein V, precursor	60,959	P40197	123	Qtrap	
13	ATP synthase subunit beta, precursor	56,560	P06576	1,482	LTQ	7
14	ATP synthase subunit gamma	32,996	P36542	1,095	Qtrap	
15	ATP synthase subunit b	28,909	P24539	920	Qtrap	
16	ATP5G1 protein	14,277	Q6FIH7	465	Qtrap	
17	ATP synthase subunit alpha, precursor	59,751	P25705	360	LTQ	
18	Integrin-linked protein kinase	51,419	Q13418	308	LTQ	
19	ATP5A1 protein	54,494	A8K092	264	Qtrap	
20	Pyruvate kinase isozymes M1/M2	57,937	P14618	150	LTQ	
21	Beta-actin	41,737	P60709	4,038	LTQ	8
22	Alpha-actin 1, skeletal muscle	42,051	P68133	2,077	LTQ	
23	Tropomodulin 3	39,595	Q9NYL9	229	Qtrap	
24	ACTA2 protein, fragment	36,807	Q13707	223	Qtrap	
25	DnaJ homolog subfamily B member 11, precursor	40,514	Q9UBS4	94	Qtrap	
26	DKFZp686D0972, hypothetical protein LOC345651	42,003	Q562R1	90	Qtrap	
27	Alpha-actin, cardiac muscle	42,019	P68032	2,077	LTQ	9
28	Gamma-actin	41,793	P63261	5,165	LTQ	10
29	Glyceraldehyde-3-phosphate dehydrogenase	36,053	P04406	503	LTQ	
30	Tropomyosin beta chain, isoform 2	32,990	P07951-2	292	Qtrap	
31	F-actin capping protein subunit alpha 1	32,923	P52907	266	LTQ	
32	Tropomyosin alpha 4 chain, isoform 2	32,723	P67936-2	197	Qtrap	
33	PDZ and LIM domain protein 1	36,072	O00151	122	Qtrap	
34	Ras suppressor protein 1	31,540	Q15404	691	LTQ	11
35	Tropomyosin alpha 1 chain, isoform 7	32,678	P09493-7	504	Qtrap	
36	Guanine nucleotide-binding protein subunit beta 1	37,377	P62873	375	LTQ	
37	Tropomyosin alpha 4 chain, isoform 1	28,522	P67936-1	248	Qtrap	
38	Guanine nucleotide-binding protein subunit beta 2	37,331	P62879	241	LTQ	
39	Prohibitin	29,804	P35232	217	Qtrap	
40	Tropomyosin alpha 3 chain, isoform 2	29,033	P06753-2	165	Qtrap	
41	F-actin capping protein subunit alpha 2	32,949	P47755	165	LTQ	
42	Tropomyosin alpha 3 chain, isoform 1	32,819	P06753	147	Qtrap	
43	PINCH 1	37,251	P48059	143	LTQ	
44	Clathrin light chain A, non-brain isoform	27,077	P09496-2	141	Qtrap	
45	1Q subcomponent-binding protein, precursor	31,362	Q07021	126	Qtrap	
46	Tubulin beta 1 chain	50,327	Q9H4B7	97	LTQ	

47	Tropomyosin alpha-1 chain	32,709	P09493	63	LTQ	
48	14-3-3 protein epsilon	29,174	P62258	770	LTQ	12
49	Keratin, type II cytoskeletal 1	66,039	P04264	745	Qtrap	
50	Ras-related protein Ral-B, precursor	23,409	P11234	683	LTQ	
51	14-3-3 protein zeta/delta	27,745	P63104	508	LTQ	
52	Keratin, type I cytoskeletal 9	62,064	P35527	489	Qtrap	
53	Ras-related protein Ral-A, precursor	23,567	P11233	450	LTQ	
54	Keratin, type I cytoskeletal 10	58,827	P13645	410	Qtrap	
55	14-3-3 protein eta	28,219	Q04917	311	LTQ	
56	Keratin, type I cytoskeletal 14	51,561	P02533	267	Qtrap	
57	GTP:AMP phosphotransferase	25,565	Q9UIJ7	128	Qtrap	
58	14-3-3 protein beta/alpha	28,082	P31946	80	LTQ	
59	14-3-3 protein sigma	27,774	P31947	70	LTQ	
60	Ras-related protein Rap-1B, precursor	20,825	P61224	1,320	LTQ	15
61	Ras-related protein Rap-1A, precursor	20,987	P62834	939	LTQ	
62	ATP synthase O subunit	23,277	P48047	260	LTQ	
63	Heat shock protein beta 1	22,783	P04792	252	Qtrap	
64	Ras-related protein Rab-8B	23,584	Q92930	216	LTQ	
65	Tumor protein D54, isoform 1	22,238	O43399-1	145	Qtrap	
66	Tumor protein D54, isoform 2	19,901	O43399-2	135	Qtrap	
67	NADH dehydrogenase iron-sulfur protein 3, precursor	30,242	O75489	120	Qtrap	
68	Ras-related protein Rab-8A	23,668	P61006	116	LTQ	
69	Myosin regulatory light chain 2, nonsarcomeric	19,794	P19105	1,829	LTQ	16
70	Myosin regulatory light chain 2, smooth muscle isoform	19,827	P24844	1,528	LTQ	
71	Myosin light chain 4	21,565	P12829	719	Qtrap	
72	Myosin regulatory light chain 12B	19,779	O14950	448	Qtrap	
73	ADP-ribosylation factor-like protein 8B	21,539	Q9NVJ2	284	LTQ	
74	ADP-ribosylation factor-like protein 8A	21,416	Q96BM9	240	LTQ	
75	Actin-related protein 2/3 complex subunit 4	19,667	P59998	202	LTQ	
76	Metalloproteinase inhibitor 3	24,145	P35625	200	LTQ	
77	Myosin regulatory light chain 3	19,794	Q53X45	142	Qtrap	
78	Ras-related protein Rab-1B	22,171	Q9H0U4	113	LTQ	
79	Transforming protein RhoA, precursor	21,768	P61586	490	LTQ	17
80	ADP-ribosylation factor 1	20,697	P84077	438	LTQ	
81	Calpain small subunit 1	28,316	P04632	415	LTQ	
82	Rho-related GTP-binding protein RhoB	22,123	P62745	313	LTQ	
83	Cofilin 1, non-muscle isoform	18,502	P23528	253	LTQ	
84	Ras-related C3 botulinum toxin substrate 1	21,450	P63000	248	LTQ	
85	ADP-ribosylation factor 5	20,530	P84085	211	LTQ	
86	ADP-ribosylation factor 4	20,511	P18085	188	LTQ	
87	Ras-related C3 botulinum toxin substrate 3	21,379	P60763	100	LTQ	
88	Myosin light polypeptide 6	16,930	P60660	1,169	LTQ	18
89	Myosin light polypeptide 6B	22,764	P14649	397	LTQ	
90	Peptidyl-prolyl cis-trans isomerase A	18,012	P62937	200	LTQ	
91	Platelet factor 4	10,845	P02776	173	LTQ	
92	Myosin light polypeptide 6, non-muscle isoform	18,037	G3V1V0	135	Qtrap	
93	Calmodulin	16,838	P62158	105	LTQ	

With regard to STIM1 acting in the context of platelet activation, adhesion, Ca²⁺-signaling and cytoskeleton reorganization, the identified proteins were further analyzed for functional features indicating participation in any of these issues (Figure 4.15 B). Accordingly, five proteins (i.e. 5.4%) were annotated as being involved in cell adhesion, another five in secretion processes. A total of 13 proteins (i.e. approximately 14.0 %) were implicated in intracellular signaling pathways. Strikingly, 34.4% of all identified proteins were related to cell shape dynamics, which included seven cytoskeleton and cytoskeleton adaptor proteins, and 25 proteins (i.e. 26.9%)

known to mediate cell shape remodelling. A more detailed analysis regarding the relevance of these data with respect to STIM1 function will be provided in 5.3.1.

To further validate these preliminary findings by alternative strategies, STIM1-specific IP and Co-IP experiments were subsequently performed on native lysates of resting platelets of both human and murine origin and samples were consequently analyzed for global and specific protein interactions.

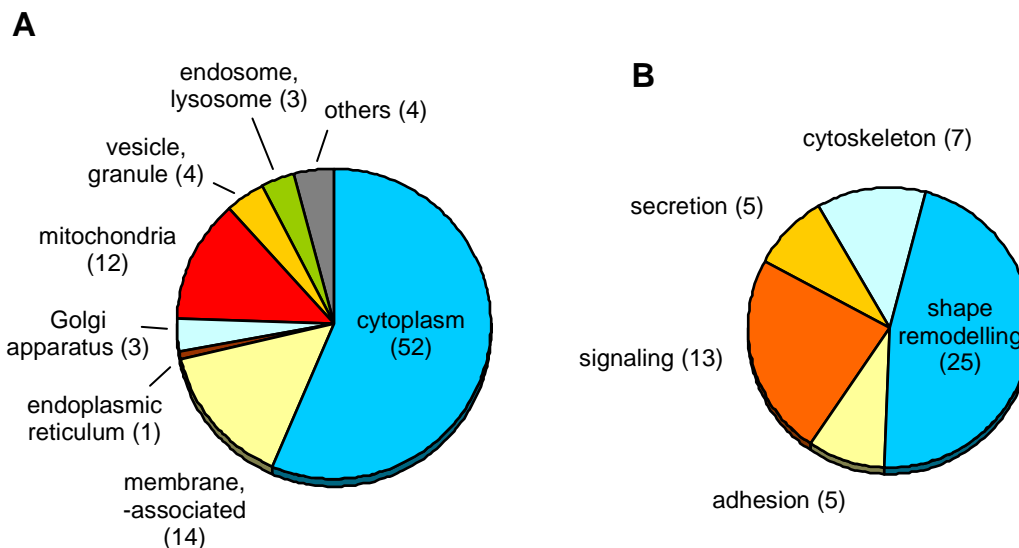


Figure 4.15: (A) Subcellular distribution of 93 proteins identified in 14 of the 18 differential protein bands of SC vs Ctrl human platelet samples. (B) Share of proteins being related to distinct features of platelet activation and/or STIM1 function. Data interpretation was based on the UniProtKB/ Swiss-Prot database (11/2009, human functional and subcellular localization entries). Total protein numbers are indicated in parentheses.

4.9 Interactome screening by STIM1-specific Co-IP in native platelet lysates

For an additional global interactome screening, STIM1-specific Co-IPs were performed on native resting platelet lysates of either human or murine wildtype ('STIM1^{+/+}') blood samples (as outlined in 3.10.7). As a negative control analogue STIM1-specific Co-IPs were performed on equally-treated platelet lysates of STIM1^{-/-} mice. Both mouse lines derived from C57Bl6-Sv129 (mixed background). The purified antibody-antigen complexes were subsequently separated by 1D-SDS-PAGE, silver-stained and differential proteins bands (i.e. in comparison to STIM1^{-/-} Co-IP samples, see Figure 4.16) were finally identified by protein mass spectrometry using a QStar Elite mass analyzer. Depending on the sample origin, the generated

spectra were searched either against the UniProtKB/ Swiss-Prot human or mouse subsets and validated as outlined in 3.10.10.3.

As a result for STIM1-specific Co-IP of human platelet lysates, all 16 differential protein bands depicted in Figure 4.16 could be annotated. Summarized data show a total of 40 individual proteins (Table 4.2), with molecular masses stretching from approximately 332 to 15 kDa.

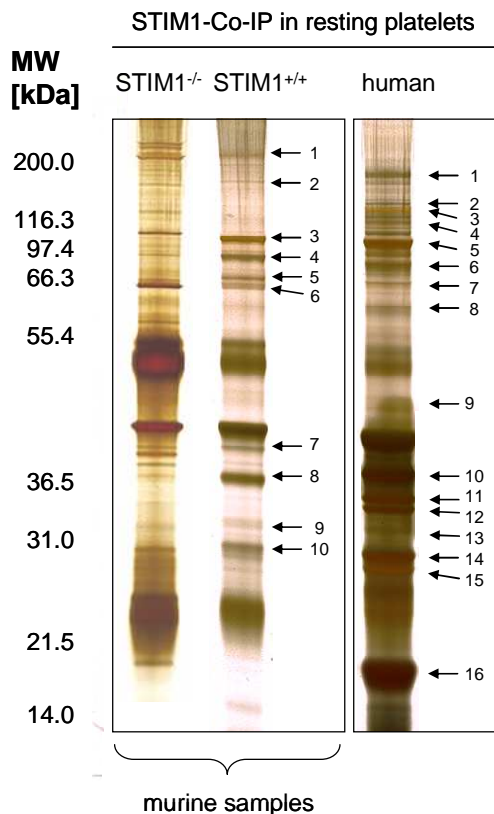


Figure 4.16: 1D-SDS-PAGE and subsequent silver staining of STIM1-specific Co-IP samples of native resting platelet lysates of both human and murine origin (STIM1^{+/+} and STIM1^{-/-}).

In each case a loading volume of 20 μ L was applied and separated on 10% Bis-Tris gels. Arrows indicate differential protein bands which were subsequently excised and analyzed by protein mass spectrometry. Samples were kindly provided by Dr. Attila Braun (Rudolf-Virchow-Center, Würzburg, Germany).

Table 4.2: Individual proteins identified in 16 differential protein bands of STIM1-specific Co-IP samples of native lysates of resting human platelets (summary of QStar Elite nano-LC-ESI-MS/MS data). Hits are listed according to corresponding protein bands and with decreasing Mascot scores. MW: molecular weight [Da]; Acc.Nr.: UniProtKB/ Swiss-Prot accession number; PB: protein band in Figure 4.16, lane 3.

#	Protein identifications	MW	Acc.Nr.	Score	PB
1	Desmoplakin	331,774	P15924	218	1
2	Junction plakoglobin	81,745	P14923	113	1
3	Talin 1	269,767	Q9Y490	1,171	2
4	Talin 2	271,613	Q9Y4G6	104	2
5	Myosin heavy chain 9	226,532	P35579	2,054	3
6	Emilin 1	106,667	Q9Y6C2	653	3
7	Multimerin 1	138,110	Q13201	553	3
8	Spectrin alpha chain	280,014	P02549	433	3
9	Platelet glycoprotein Ib alpha chain	68,955	P07359	130	3
10	Alpha-actinin 1	103,058	P12814	3,428	4
11	Alpha-actinin 4	104,854	O43707	1,768	4
12	Alpha-actinin 2	103,854	P35609	897	4

13	Integrin alpha 2b	113,377	P08514	1,211	5
14	Integrin beta 3	87,058	P05106	261	
15	Vinculin	123,799	P18206	184	
16	Integrin beta 1	88,415	P05556	137	
17	Gelsolin	85,698	P06396	442	6
18	Filamin A	280,739	P21333	402	
19	Platelet glycoprotein IV	53,053	P16671	320	
20	Myosin XVIIIa	233,115	Q92614	102	
21	Platelet glycoprotein V	60,959	P40197	445	7
22	78 kDa glucose-regulated protein	72,333	P11021	340	
23	Thrombospondin 1	129,383	P07996	186	8
24	Fibrinogen gamma chain	51,512	P02679	364	9
25	Fibrinogen alpha chain	94,973	P02671	167	
26	Beta-parvin	41,714	Q9HB11	65	10
27	PDZ and LIM domain protein 1	36,072	O00151	64	
28	Clusterin	52,495	P10909	222	11
29	Tropomyosin alpha 1 chain	32,709	P09493	651	12
30	Tubulin beta 1 chain	50,327	Q9H4B7	222	13
31	Tropomyosin alpha 4 chain	28,522	P67936	989	14
32	Tropomyosin beta chain	32,851	P07951	737	
33	Tropomyosin alpha 3 chain	32,819	P06753	452	
34	Ras suppressor protein 1	31,540	Q15404	88	
35	Putative tropomyosin alpha 3 chain-like protein	26,269	A6NL28	281	15
36	Myosin regulatory light polypeptide 9	19,827	P24844	1,278	16
37	Myosin regulatory light chain 2	19,794	P19105	1,276	
38	Myosin light polypeptide 6	16,930	P60660	244	
39	Leucine-rich repeat flightless-interacting protein 2	82,171	Q9Y608	103	
40	Fatty acid-binding protein 9	15,093	Q0Z7S8	95	

As illustrated in Figure 4.17 A, the majority of the 40 identified proteins were either localized in the cytoplasm (57.5%) or within (or associated to) cellular membranes (30.0%). The amount of proteins originating from other cellular compartments or organelles, however, was comparably low and thus negligible.

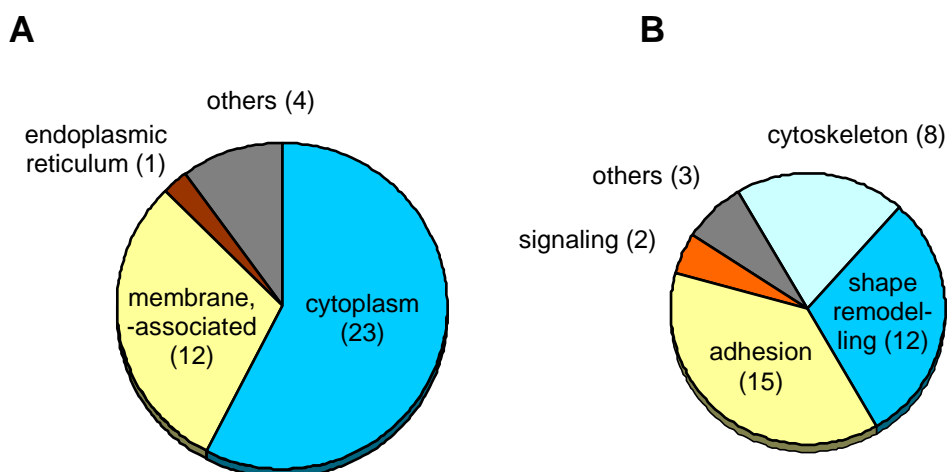


Figure 4.17: (A) Subcellular distribution of 40 proteins identified in STIM1-specific Co-IP samples of native lysates of resting human platelets. (B) Share of proteins being related to distinct features of platelet activation and/or STIM1 function. Data interpretation was based on the UniProtKB/ Swiss-Prot database (11/2009, human functional and subcellular localization entries). Total protein numbers are indicated in parentheses.

Functionally, the majority of identified proteins were classified as being related to cell adhesion (37.5%) or cellular shape maintenance and/ or remodelling (30.0%, see Figure 4.17 B). Upon additional inclusion of eight cytoskeleton proteins, the latter group of proteins being involved in cell shape-regulation even amounted to 50.0%. In contrast to the findings in 4.8, here only two of the identified proteins (i.e. 5.0%) were implicated in intracellular signaling pathways.

Parallel MS analyses of STIM1-specific Co-IP samples of native resting platelet lysates of STIM1^{+/+} mice also resulted in annotation of all ten differential protein bands displayed in Figure 4.16. Here, a total of 28 individual proteins were identified and are summarized in Table 4.3.

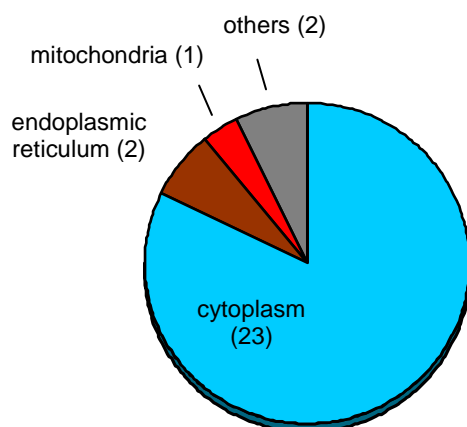
Table 4.3: Individual proteins identified in ten differential protein bands of STIM1-specific Co-IP samples of native resting platelet lysates of STIM1^{+/+} mice; summary of QStar Elite nano-LC-ESI-MS/MS data. Hits are listed according to corresponding protein bands and with decreasing Mascot scores. MW: molecular weight [Da]; Acc.Nr.: UniProtKB/ Swiss-Prot accession number; PB: protein band in Figure 4.16, lane 2.

#	Protein identifications	MW	Acc.Nr.	Score	PB
1	Spectrin alpha chain	279,865	P08032	1,001	1
2	Myosin light polypeptide 6	16,930	Q60605	896	
3	Spectrin beta chain	245,250	P15508	473	
4	Myosin light chain 4	21,159	P09541	369	
5	Myosin regulatory light chain 2-B	19,779	Q3THE2	314	
6	Myosin regulatory light polypeptide 9	19,854	Q9CQ19	228	
7	Myosin light chain 6B	22,749	Q8CI43	201	
8	Myosin light chain 3	22,422	P09542	129	
9	Uncharacterized protein KIAA1211	132,286	Q5PR69	106	2
10	Alpha-actinin 1	103,068	Q7TPR4	1,749	3
11	Alpha-actinin 4	104,977	P57780	1,425	
12	Alpha-actinin 2	103,653	Q9JI91	469	
13	Alpha-actinin 3	103,043	O88990	306	
14	Stromal interaction molecule 1	77,567	P70302	627	4
15	Ig mu chain C region secreted form	49,972	P01872	141	5
16	Stress-70 protein, mitochondrial	73,528	P38647	821	6
17	Heat shock cognate 71 kDa protein	70,871	P63017	614	
18	Heat shock-related 70 kDa protein 2	69,642	P17156	351	
19	78 kDa glucose-regulated protein	72,422	P20029	327	
20	Zyxin	60,546	Q62523	113	
21	Beta-actin	41,737	P60710	1,068	7
22	Tropomodulin 3	39,503	Q9JHJ0	349	
23	PDZ and LIM domain protein 1	35,774	O70400	1,000	8
24	Calponin 2	33,156	Q08093	67	9
25	Tropomyosin alpha 4 chain	28,468	Q6IRU2	434	10
26	Tropomyosin alpha 3 chain	32,863	P21107	204	
27	Tropomyosin alpha 1 chain	32,681	P58771	141	
28	Tropomyosin beta chain	32,837	P58774	113	

Molecular masses stretched from approximately 280 to 17 kDa. As in human STIM1-specific Co-IP samples, the majority of the identified proteins were localized in the cytoplasm (82.2%); however, this time there was no evidence for membrane- or

membrane-associated localization (Figure 4.18 A). The share of proteins derived from other cellular organelles or compartments was also negligible. Regarding protein function, only one protein was annotated as being involved in cell adhesion, another one in cell signaling (Figure 4.18 B). The majority of all identified murine proteins, namely 71.5%, were once again implicated in cell shape dynamics. This included 15 typical cytoskeleton and cytoskeleton adaptor proteins (i.e. 53.6%), and five proteins (i.e. 17.9%) known to mediate cell shape remodelling. For a more detailed analysis regarding the relevance of these data with respect to STIM1 function, please also refer to 5.3.1. Thus, as an intermediate result of all three global interactome screening approaches on native resting platelet lysates (4.8 and 4.9), STIM1 was reproducibly found in apparent interaction with diverse cytoskeleton components and cytoskeleton adaptor proteins, as well as with protein factors known to regulate cytoskeleton dynamics - and thus cell shape remodelling.

A



B

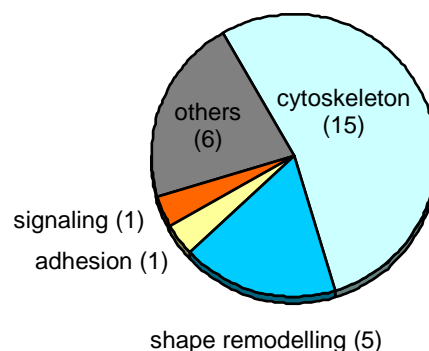


Figure 4.18: (A) Subcellular distribution of 28 proteins identified in STIM1-specific Co-IP samples of native lysates of resting STIM1^{+/+} mouse platelets. (B) Share of proteins being related to distinct features of platelet activation and/ or STIM1 function. Data interpretation was based on the UniProtKB/ Swiss-Prot database (11/2009, mouse functional and subcellular localization entries). Total protein numbers are indicated in parentheses.

4.10 Validation of specific STIM1-CLP36 interaction in resting murine platelets

As initially mentioned in 1.3.2, the question whether both the translocation of STIM1 dimers to the PM and subsequent STIM1-ORAI1 interaction depend on regulation of

further adaptor and/ or scaffolding factors still needs to be solved. For this purpose, the cytoskeleton- and shape-dynamics related protein datasets generated during this study were additionally searched for eligible candidates. Amongst the proteins identified during all three global interactome screening approaches on native resting platelet lysates (4.8 and 4.9), in particular one candidate - i.e. the cytoskeleton adaptor protein 'PDZ and LIM domain protein 1' (approximately 36 kDa, alternative names: CLP36, PDLIM1, CLIM1, Elfin) - proved to be promising as it was reproducibly detected in all three datasets (Table 4.1 #33, Table 4.2 #27, Table 4.3 #23; see also Figure 4.19).

MS/MS Fragmentation of **SAMPFTASPAPSTR**
Found in PDZ and LIM domain protein 1 (aa 123-136)

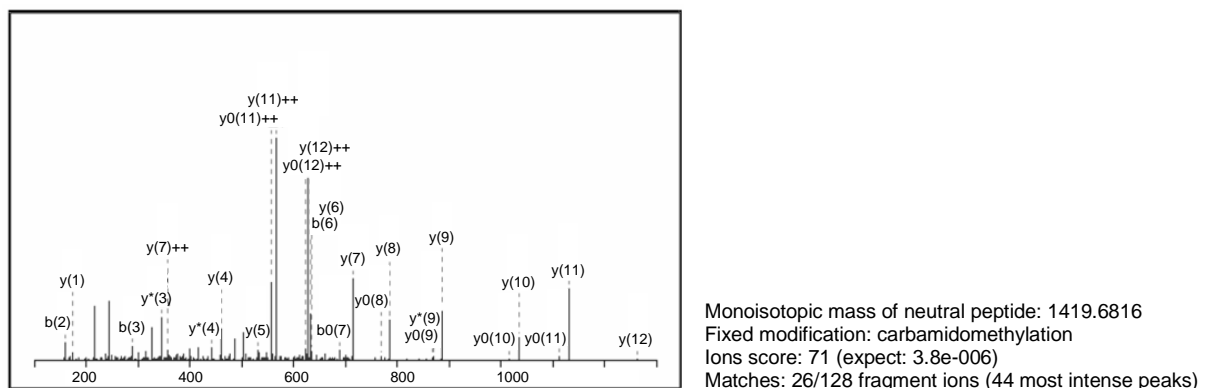


Figure 4.19: Identification of PDZ and LIM domain protein 1 by MS/MS analysis on a QStar Elite mass analyzer. Data derived from STIM1-specific Co-IP samples of native lysates of resting STIM1^{+/+} mouse platelets (see Figure 4.16, lane 2, PB 8; in-gel trypsinisation).

This theory was moreover backed by intensive literature research as well as by existence of adequate PDZ-binding motifs within the STIM1 aa-sequence (for further details please refer to 5.3.2). Hence, to validate the assumed interaction between STIM1 and CLP36, STIM1-specific Co-IP was performed on native lysates of resting platelets of STIM1^{+/+} mice as outlined in 3.10.7. The purified antibody-antigen complexes were subsequently separated by 1D-SDS-PAGE and immunoblotting was executed to validate simultaneous co-precipitation of CLP36 (Figure 4.20 B). As a specificity control of the used anti-STIM1 antibodies, a parallel STIM1-specific IP was also performed on resting platelets of STIM1^{+/+} and STIM1^{-/-} mice (both C57Bl6-Sv129, mixed background), followed by immunoblotting against the STIM1 protein (approximately 77.5 kDa; see Figure 4.20 A).

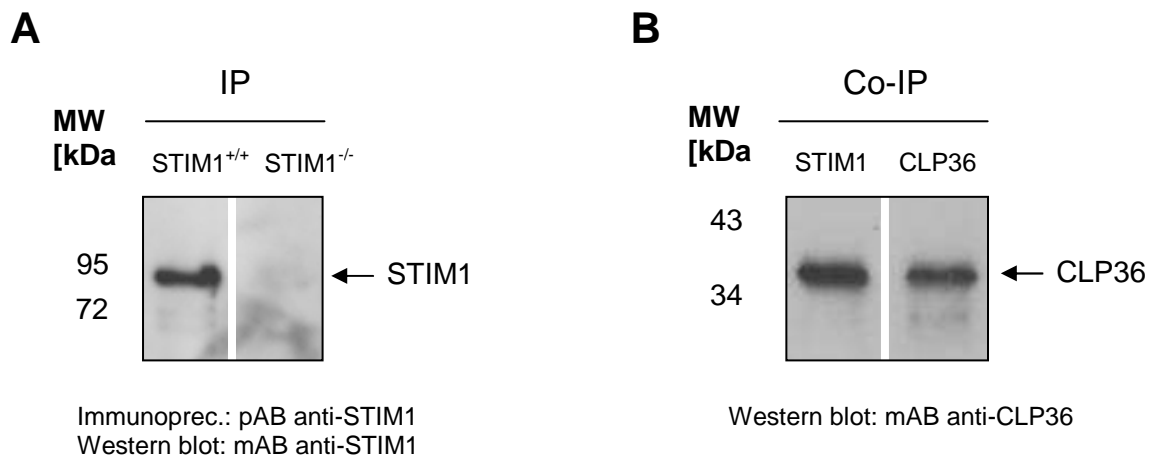


Figure 4.20: Analysis of STIM1-CLP36 interaction by Co-IP experiments. (A) STIM1-specific IP and -immunoblotting in resting platelets of STIM1^{+/+} and STIM1^{-/-} mice. (B) STIM1- and CLP36-specific IP and subsequent CLP36-specific immunoblotting in resting platelets of STIM1^{+/+} mice. Data were generated in cooperation with Dr. Attila Braun (Rudolf-Virchow-Center, Würzburg, Germany).

In addition, CLP36-specific IP and subsequent immunoblotting against CLP36 in purified platelet samples of STIM1^{+/+} mice served as a binding control for the monoclonal anti-CLP36 antibody (Figure 4.20 B). According to Figure 4.20, IP against STIM1 protein proved to be specific in resting platelet lysates of STIM1^{+/+} mice (presence of an 80 kDa STIM1 protein band in Figure 4.20 A) as evaluated in comparison to equally-treated STIM1^{-/-} samples, and moreover revealed concurrent co-precipitation of CLP36 when maintaining native conditions throughout the whole procedure (36 kDa protein band in Figure 4.20 B). Together with our previous observations (4.8 and 4.9), this finding thus provided further evidence for an *in vivo* interaction between STIM1 and CLP36 proteins in resting platelets.

4.11 GPIb-CLP36 interaction in resting platelets

As described in 5.3.1, the proteins identified in the course of this study can be organized in four functional complexes: (a) the signaling-related complex; (b) the actin-myosin complex; (c) the adhesion complex; and (d) the GPIb-IX-V subcomplex. Since the latter complex mediates the initial steps of platelet activation, namely platelet recruitment and rolling on the vessel surface, it was intriguing to examine whether there was any functional connection between GPIb-IX-V and STIM1 or CLP36, respectively (see also Table 4.1 #12 and Table 4.2 #9 and #21). For this

purpose, GPIb-specific Co-IPs, targeted either against the GPIb alpha or beta chain (i.e. GPIb α and GPIb β), were executed on native lysates of resting platelets of STIM1^{+/+} mice (wildtype C57Bl6-Sv129, mixed background). The resulting antibody-antigen complexes were subsequently separated by 1D-SDS-PAGE and immunoblotted for presence of co-precipitated CLP36. For additional verification, analogous counter-IPs were also performed against CLP36, and the generated samples were then immunoblotted against GPIb. The corresponding data are presented in Figure 4.21 A.

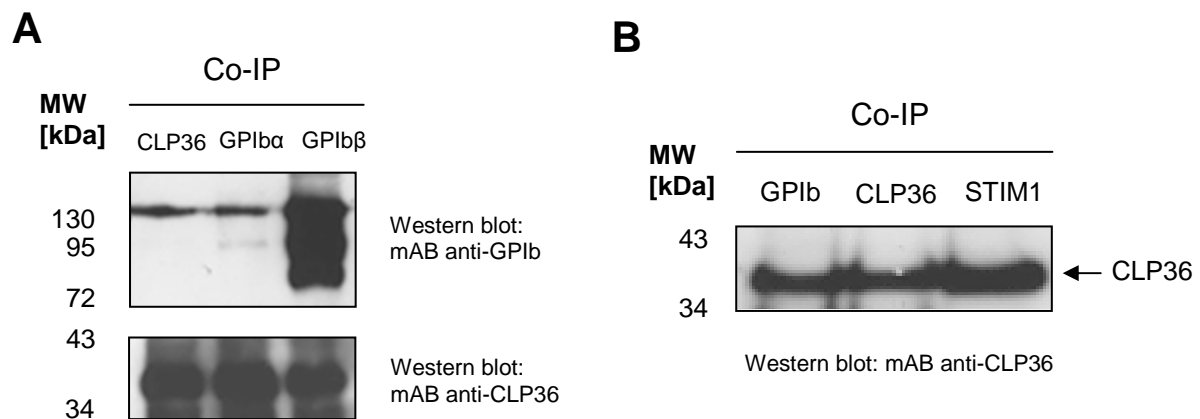


Figure 4.21: Analysis of GPIb-CLP36-STIM1 interaction in resting platelets of STIM1^{+/+} mice. (A) CLP36-, GPIb α - and GPIb β -specific Co-IPs and subsequent GPIb- and CLP36-specific immunoblotting. (B) GPIb-, CLP36- and STIM1-specific Co-IPs and subsequent CLP36-specific immunoblotting. Data were generated in cooperation with Dr. Attila Braun (Rudolf-Virchow-Center, Würzburg, Germany).

Accordingly, as verified by occurrence of an adequate 36 kDa protein band, CLP36 was detected in GPIb-specific Co-IPs and *vice versa* (i.e. 135 kDa GPIb α protein band in CLP36-specific Co-IP samples). Thus, an interaction between GPIb and CLP36 - either directly or indirectly via further adaptor proteins - appears as possible. In addition, repeated Co-IP experiments on native lysates of resting STIM1^{+/+} mouse platelets against (a) GPIb; (b) STIM1; and (c) CLP36 (as a specificity control for the monoclonal anti-CLP36 antibody), followed by CLP36-specific immunoblotting, furthermore outlined a potential CLP36-mediated structural linkage between GPIb and STIM1 (Figure 4.21 B).

4.12 Calpain effect on CLP36 stability

Since supporting studies by Dr. Attila Braun (Rudolf-Virchow-Center, Würzburg, Germany) indicated Ca^{2+} -dependent degradation of CLP36 by calpain endoproteases in activated $\text{STIM1}^{+/+}$ mouse platelets (wildtype C57Bl6-Sv129; for further details please refer to 5.3.4), this finding was validated by performing both *in silico* and *in vitro* calpain digestion assays of full-length human CLP36 protein.

In silico digestion was executed via the bioinformatics tools for calpain cleavage prediction provided on www.calpain.org (based on [202]). Here, the output data of all four prediction models (i.e. SVM-RBF kernel, SVM-linear kernel, PSSM and MKL) for processing of the human CLP36 aa-sequence were compared, with corresponding results being summarized in Table 4.4. Accordingly, of the total amount of 24 predicted calpain cleavage sites located in human CLP36, the most probable ones were at aa-positions H181, Q220 and V315 (independently determined by all four prediction algorithms). Two of these sites (i.e. H181 and Q220) were situated in between the CLP36 PDZ- and LIM-domain.

For *in vitro* calpain in-solution digestion based on Lakey et al. [201], 30 pmol of purified human CLP36 protein (purchased from Abnova) were incubated with 3 U calpain-1 and with 4.5 U calpain-2 as described in 3.10.8. Proteolytic peptides were subsequently analyzed on an LTQ-FT Ultra mass analyzer and the generated spectra were searched against the UniProtKB/ Swiss-Prot human subset with enzyme specificity being set to 'none' (see 3.10.10.3). All MS data were furthermore validated manually for fitting with the theoretically predicted calpain cleavage sites. To distinguish specific proteolytic peptides from unspecific ones as well as from peptide ions generated by spontaneous fragmentation of labile CLP36 sites, MS/MS spectra of 0.5 pmol human CLP36 protein without prior calpain treatment were recorded in an equal approach. The resulting data are summarized in Table 4.4 (in comparison to the *in silico* ones). For a detailed view please also refer to 7.5.

Of the 24 *in silico* predicted putative calpain cleavage sites in human CLP36, 16 were also unambiguously detected by this *in vitro* digestion approach. As in particular H181 was reproducibly identified by all *in silico* prediction models, as well as by the *in vitro* study, this site might be regarded as the most probable calpain target. Accordingly, calpain induction by increase of free intracellular Ca^{2+} (e.g. upon platelet activation) may mediate CLP36 shedding at H181 and thus separate the CLP36-PDZ- from the -LIM domain.

Table 4.4: *In silico* vs *in vitro* determined calpain cleavage sites in human CLP36 protein. (A) *In silico* sites were obtained via prediction models SVM-RBF kernel, SVM-linear kernel, PSSM and MKL. For each model the 10 best scores are displayed, with higher scores corresponding to higher cleavage probabilities. Amino acid cleavage positions identified by all four algorithms are shaded in blue. (B) *In vitro* data were generated by in-solution digestion of recombinant human CLP36 via calpain-1 and calpain-2 (based on Lakey et al. [201]) and subsequent analysis on an LTQ-FT Ultra mass analyzer. *In silico* predicted yet non-detected calpain cleavage sites, as well as unspecific fragmentation sites are shaded in grey, the most probable site is marked in red. The aa-sequence of full-length human CLP36 is provided below (based on the UniProtKB/ Swiss-Prot database, Acc.Nr. O00151). The CLP36 PDZ-domain is marked in green, the LIM-domain in yellow.

#	Cleavage position	<i>In silico</i> prediction models				<i>In vitro</i> detected cleavage position
		SVM-RBF kernel	SVM-linear kernel	PSSM	MKL	
1	Q9	0.14				Yes
2	F24	0.21	0.23			Yes
3	R32	0.12	0.12			No
4	V93		0.12			No
5	H115		0.12			Yes
6	S123	0.12				Yes
7	T128				0.36	Yes
8	T136	0.14	0.14		0.33	Yes
9	V139			0.80		No
10	T141			1.04	0.32	Yes
11	Q143			0.91		Yes
12	Y144	0.15	0.16			Yes
13	Y151				0.30	Yes, yet also unspecific
14	K166	0.12		1.75		Yes, yet also unspecific
15	H181	0.22	0.21	3.74	0.42	Yes
16	L217			1.84		Yes
17	Q220	0.13	0.12	3.98	0.32	Yes, yet also unspecific
18	R238			0.88		Yes
19	K241		0.13			Yes
20	K246				0.31	Yes
21	A248				0.32	No
22	R314			1.86		Yes
23	V315	0.14	0.13	2.02	0.38	No
24	T325				0.32	Yes

O00151|PDL1_Human PDZ and LIM domain protein 1 (CLP36); 329 aa

001 MTTQ**QIDLQG** **PGPWGFR**LVG **GKDFEQPLAI** **SRVTPGSKAA** **LANLCIGDVI**
051 **TAIDGENTS**N **MTHLEAQNRI** **KGCTDNLTLT** **V**ARSEHKVWS PLVTEEGKRH
101 PYKMNLASEP QEVLHIGSAH NRSAMPFTAS PASSTTARVI TNQYNNPAGL
151 YSSENISNFN NALESKTAAS GVEANSRPLD **H**AQPPSSLVI DKESEVYKML
201 QEKQELNEPP KQSTSFLVL**Q** EILESEEKGD PNKPSGFRSV KAPVTKVAAS
251 IGNAQKLPMC **DKCGTGIVGV** **FVKLRDRHRH** **PECYVCTDCG** **TNLKQKGHFF**
301 **VEDQIYCEKH** ARER**V**TPPEG YEVVTVFPK

As a consequence of these findings, a transgenic mouse line lacking the CLP36-LIM domain (i.e. 'CLP36^{ΔLIM}') was generated and analyzed regarding its morphological and functional platelet phenotype (including Ca²⁺-response). Here, all corresponding experiments were performed in cooperation with Dr. Attila Braun (Rudolf-Virchow-Center, Würzburg, Germany) and will be presented in section 5.3.5 of this work.

5 Discussion

5.1 Overview: Screening the VASP and STIM1 interactome in resting platelets

To specifically address the VASP and STIM1 interactome in resting platelets, a differential proteomics strategy was developed based on affinity-chromatography and subsequent protein identification by MS measurement (Figure 5.1).

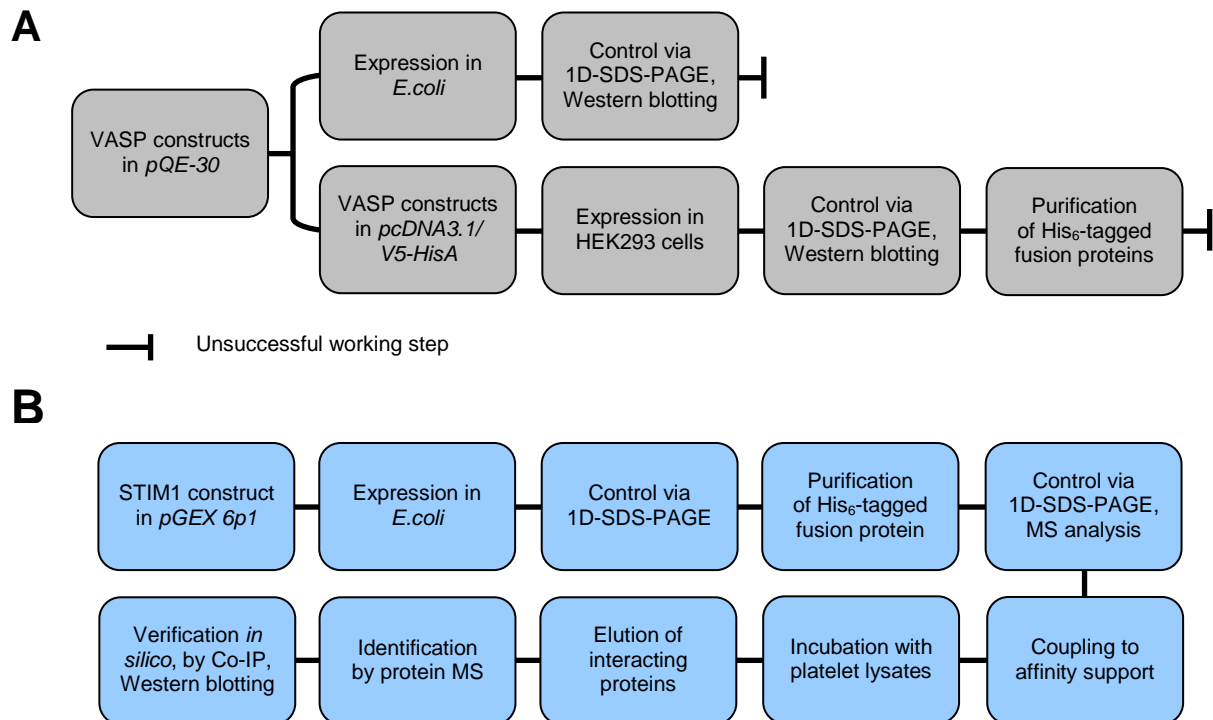


Figure 5.1: Workflow for platelet interactome screening via affinity chromatography based on recombinant (A) VASP proteins (1) in *pQE-30* vector: VASP-AAA, VASP-DDE; (2) in *pcDNA3.1/V5-HisA* vector: VASP-AAA Δ TD, VASP-DDE Δ TD, VASP-AAA Δ FAB Δ TD and VASP-DDE Δ FAB Δ TD (B) STIM1 protein: STIM1Ctail, in *pGEX 6p1* vector.

Inspired by studies of Benz et al. [199], affinity-tagged fusion proteins of phosphomimetic mutants of human VASP (VASP-AAA and -DDE) and of the cytoplasmic portion of human STIM1 (STIM1Ctail) were overexpressed in *E.coli* Rosetta, consequently purified and finally immobilized on an affinity support to thus generate the required affinity matrices. In this context, recombinant protein expression was controlled by 1D-SDS-PAGE of bacterial lysates and subsequent Coomassie staining, as well as by Western blotting or by MS analysis.

However, as indicated by these controls, the expression levels of VASP fusion proteins were not sufficient for the intended purpose. Therefore, the VASP DNA-

constructs were further modified (i.e. VASP-AAA/ -DDE Δ TD and VASP-AAA/ -DDE Δ FAB Δ TD) and cloned into the eukaryotic expression vector *pcDNA3.1/V5-HisA* for subsequent stable transfection into HEK293 cells (for details see 5.2.2). Following this strategy, heterologous expression of all four VASP constructs was finally achieved. Nevertheless, whereas subsequent IMAC purification via the introduced C-terminal His₆-tags verifiably isolated recombinant STIM1Ctail protein, this technique did not succeed in case of the generated VASP fusion proteins. This was probably due to both low protein expression levels and structural inaccessibility of the constructs' His₆-affinity tag. As a consequence, the intended VASP-specific interaction study was finally abandoned and the focus of this work was shifted towards an analysis of the STIM1 interactome in resting platelets.

During platelet purification, particular care was taken to preserve resting platelet conditions and thus prevent unintended activation (see 3.6.3 and 3.9.1). Moreover, to maintain protein folding structures even during cell lysis, platelet material was treated under mild conditions, e.g. by applying non-ionic detergents in the lysis buffer. The resulting native platelet lysates were then incubated with the generated STIM1-specific affinity support. Upon elution, samples were separated by 1D-SDS-PAGE and differential protein bands were finally analyzed by nano-LC-ESI-MS/MS. By this approach, a total of 93 individual proteins were identified. In parallel, STIM1-specific Co-IP experiments both in human and in murine native platelet lysates, followed by MS analysis, resulted in identification of another 68 proteins. This also included an additional amount of 36 proteins which had not been detected by the initial affinity-column based approach. One promising candidate, the 'PDZ and LIM domain protein 1' (or 'CLP36'), was finally chosen for a more detailed verification.

5.2 Analysis of the VASP interactome in platelets

5.2.1 Expression of human VASP fusion proteins in *E.coli*

In 2008, Benz et al. presented a differential proteomics approach to identify the phospho-interactome of VASP in human endothelial cells [199]. Accordingly, using N-terminally His₆-tagged human VASP-DNA in pQE-30 as a template (based on [203]), the VASP phosphorylation sites S157, S239 and T278 were exchanged (a) with alanines (S157A, S239A, T278A) to mimic a constitutively non-phosphorylated state; or (b) with acidic amino acids (S157D, S239D, T278E) to mimic constitutive VASP phosphorylation. Prokaryotic plasmid expression in *E.coli* B strain BL21

resulted in fusion proteins of 45 kDa (His₆-VASP-S157A, S239A, T278A; i.e. 'VASP-AAA') or 50 kDa (His₆-VASP-S157D, S239D, T278E; i.e. 'VASP-DDE'). These were subsequently purified as described by Bachmann et al. [59] and covalently coupled to an Affi-Gel 10 support. In parallel, the cytosolic protein fraction of endothelial EA.hy926 cells was prepared as described in [204] and then applied to the generated VASP-affinity columns. Bound proteins were finally eluted and analyzed by 2D-PAGE and protein mass spectrometry via MALDI-TOF-PMF. Of the eleven detected proteins which revealed specific interaction with VASP-AAA and not with VASP-DDE, α II-spectrin was further verified by Co-IP, GST pull-down assays and confocal immunofluorescence microscopy. Deriving from these studies, the authors identified α II-spectrin as a novel VASP interaction partner and consequently proposed a new mechanism for actin cytoskeleton formation and perijunctional filament assembly during cell-cell adhesion. In this context, the spectrin-VASP interaction was moreover reported as being down-regulated upon PKA-mediated phosphorylation of the VASP S157 residue [199, 205].

Based on this previous study, we here intended application of a similar approach to enable efficient screening of the phospho-specific VASP interactome in human platelets. For this purpose, adequate affinity-tagged phospho-mimetic VASP-AAA and -DDE constructs were kindly provided by Prof. Dr. Thomas Renné (Department of Molecular Medicine and Surgery, Karolinska Institute, Stockholm, Sweden). However, even though prokaryotic plasmid expression was performed as outlined by Benz et al. [199], biosynthesis of sufficient protein amounts turned out to be challenging in our hands. This could have been due to codon bias problems during heterologous expression of human VASP-DNA sequences in *E.coli* BL21. Generally, the 'codon bias' describes the phenomenon that the frequency of occurrence of different synonymous codons in coding DNA varies in between species. This species-dependent 'preference' of certain codons is reflected by the respective intracellular pool of tRNAs - and thus directly impacts mRNA translation. At presence of atypical codons, as given during heterologous expression of eukaryotic gene material in prokaryotic systems, recombinant protein synthesis may consequently be decelerated, interrupted (leading to truncated protein fragments), or totally inhibited. For *E.coli* B strains, such rare codons are represented by AGG, AGA, AUA, CUA, CCC and GGA, which thus negatively affects synthesis of R-, I-, L-, P- and G-rich aa-sequences (see Table 5.1).

Table 5.1: Frequency of occurrence of selected codons (per 1,000 bp of coding DNA) in *E.coli* B vs *Homo sapiens*. Values were based on the codon usage database on <http://www.kazusa.or.jp/codon>. In addition, the amount of these codons within the human VASP nt-sequence is also provided.

Codon	Encoded amino acid	Frequency of occurrence per 1,000 bp		# in human VASP nt-seq.
		<i>E.coli</i> B	<i>Homo sapiens</i>	
AGG	R	2.1	12.0	6
AGA	R	2.4	12.2	3
AUA	I	5.0	7.5	1
CUA	L	3.4	7.2	2
CCC	P	2.4	19.8	26
GGA	G	8.2	16.5	10

Since the human VASP nt-sequence contains several of these codons - particularly 26 CCC and 10 GGA that encode for the central proline- and glycine-rich regions (see Table 5.1) - prokaryotic synthesis of human VASP-AAA and -DDE fusion proteins may be affected here. This would explain the observed low expression levels in *E.coli* BL21 as well as the presence of multiple additional protein bands in an MW-range of 40 to 50 kDa upon 1D-SDS-PAGE of bacterial culture samples (see 4.1). Accordingly, the latter ones probably indicate truncated versions of the intended fusion proteins caused by an interrupted biosynthesis. Due to these limitations, VASP protein expression was consequently also examined in *E.coli* Rosetta and *E.coli* BL21-CodonPlus-RP, since these strains provide additional tRNAs for the indicated codons [206]. However, neither this approach nor further modification of the expression conditions (e.g. by varying incubation temperatures or by using high-level expression media such as Superbroth medium and Overnight Express Instant TB Medium) contributed to a subsequently improved fusion protein synthesis.

5.2.2 Expression of human VASP fusion proteins in HEK293

Benz et al. finally circumvented the described codon bias problem by supplementing their bacterial growth medium with additional amounts of the limiting tRNAs and by lowering the incubation temperature to 12°C ([199], unpublished data). However, due to further limitations inherent to the strategy applied by Benz et al., which *per se* demanded additional modification of the applied VASP constructs (see below), we decided to completely change to a human-derived model system. For this purpose, the HEK293 cell line was chosen for eukaryotic expression of the intended VASP fusion proteins. Being easy to transfect and maintain under cell culture conditions, HEK293 (i.e. immortalized human embryonic kidney cells) are commonly widely applied both as a eukaryotic model organism to study protein effects *in vitro*, and as

an efficient cellular producer strain for synthesis of transgenic proteins, as well as of adenoviral and retroviral vectors.

As a prerequisite for generation of recombinant VASP proteins in HEK293 cells, the original VASP-AAA- and -DDE DNA-constructs were (a) specifically modified via deletion of the C-terminal TD-domain to prevent hetero-oligomerization with endogenous, HEK-derived VASP proteins (i.e. 'VASP-AAA/ -DDE Δ TD'); and (b) cloned from the prokaryotic *pQE-30* plasmid into the eukaryotic expression vector *pcDNA3.1/V5-HisA*. This vector confers both a V5- and a His₆-tag to the C-terminal end of the resulting fusion protein. Moreover, as mentioned in the beginning, an issue which had not been considered by Benz et al. when performing their VASP-specific interactome screening approach [199] was the risk of co-purifying unspecific cytoskeleton-associated proteins due to the high affinity of VASP bait material to actin filaments [59-61, 207]. During differential MS analyses these unspecific components can consequently not be distinguished from 'true' VASP interaction partners, hence increasing the rate of false positive identifications. In addition, since cytoskeleton and cytoskeleton-associated proteins are commonly highly abundant in biological samples, respective contamination would probably mask the presence of lower abundant yet VASP-specific interacting candidates, which furthermore limits subsequent MS analyses and thus the potential of this approach. Hence, to address these issues, two additional VASP-constructs were developed, displaying deletion of the VASP TD- and -FAB-domains (i.e. 'VASP-AAA/ -DDE Δ FAB Δ TD', see Figure 5.2). For evaluation and verification of both transfection efficiency and recombinant protein expression, a fifth HEK293 cell line stably expressing the *pcDNA3.1/V5-HisA lacZ* vector construct was finally also established as a positive control.

However, even though all generated stable HEK293 cell lines reproducibly expressed the intended fusion proteins (as monitored by β -gal staining and tag-specific Western blotting), subsequent IMAC purification targeted against the C-terminal His₆-tag still failed. This could have been due to insufficient protein expression levels as evidenced by the absence of specifically enriched protein bands in Coomassie-stained 1D-SDS control gels of crude recombinant HEK293 cell lysates. Improving expression conditions and increasing the cellular amounts applied during purification did also not contribute to enhanced protein yields.

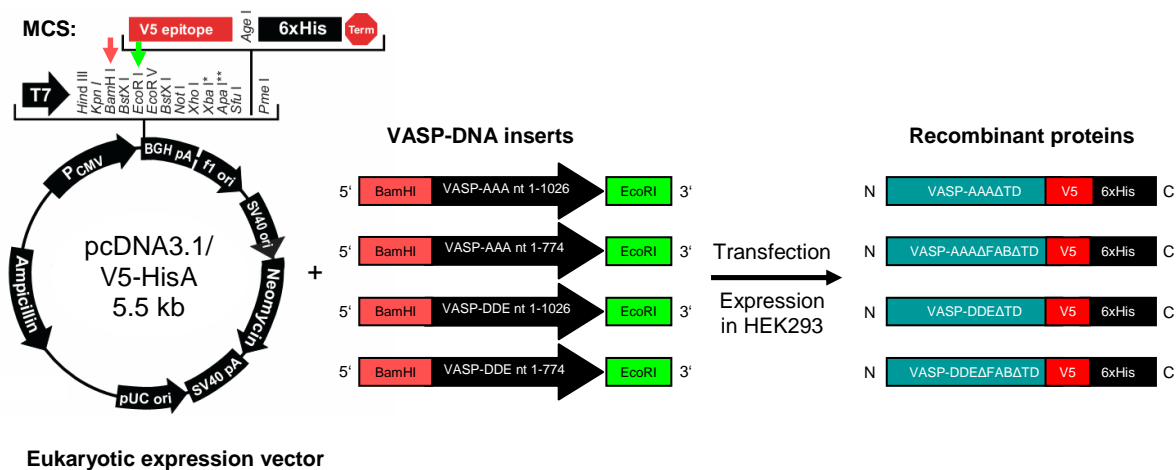


Figure 5.2: Strategy for eukaryotic expression of truncated, affinity-tagged VASP proteins VASP-AAAΔTD, VASP-AAAΔFABΔTD, VASP-DDEΔTD and VASP-DDEΔFABΔTD in HEK293 cells.

Apart from low expression levels, negative impact of primary and higher-order protein structures of the expressed VASP constructs on the indicated workflow might also be discussed, particularly with regard to efficiency of the IMAC-based protein enrichment. As an example, the C-terminal His₆-tag of the VASP fusion proteins might be structurally inaccessible, an issue which had also been addressed within the manufacturer's instructions of the Qiagen Ni-NTA Spin Kit. Consistent with this theory, though performing multiple Western blotting experiments with various His-tag-specific primary antibodies, the C-terminal His₆-tag could not be detected in any of the stable HEK293 cell lines. This was particularly unexpected as adequate expression of all fusion proteins could reproducibly be monitored by similar Western blotting targeted against the constructs' C-terminal V5-tag, which is located just upstream of the His₆-tag (see 4.5 and 4.6). Since unintended His-tag deletion could moreover be excluded by full-length DNA-sequencing, the most probable explanation of this observation might thus be given by the initially mentioned structural inaccessibility of the VASP fusion proteins' C-terminal His₆-tag. However, in contrast to this theory, the C-terminal His₆-tag could also not be detected within HEK-lacZ positive controls where limiting structural effects of adjacent aa-sequences could *per se* be excluded. As indicated by both β-gal staining and V5-specific Western blotting (see 4.5), this finding was also not due to inadequate protein expression levels or inappropriate Western blotting conditions. Therefore insufficient affinity and/ or specificity of the applied His-tag-specific primary antibodies also have to be considered in this context. As an example, this issue has previously been reported by

Debeljak et al. [208] who observed striking variability when testing four different antibodies targeted against C-terminal His₆-tags.

Taken together, the difficulties in purifying human VASP-derived proteins from stably-transfected HEK293 cells under native conditions might have been caused by multiple reasons: This may include low protein expression levels as well as presumably limiting effects of primary and higher-order protein structures on the applied IMAC-based enrichment techniques.

5.2.3 Concluding remarks on the VASP-specific interactome study

Heterologous expression of affinity-tagged phospho-mimetic VASP fusion proteins failed both in the used prokaryotic and eukaryotic model systems. Protein synthesis in *E.coli* was most probably inhibited as a consequence of the codon bias problem inherent to prokaryotic vs eukaryotic expression. In this context, particularly the VASP central proline- and glycine-rich domains might have contributed to severe deceleration of translation, finally resulting in reduced yields of target protein which, upon purification, were not sufficient for subsequent generation of VASP-specific affinity columns. Regarding stably-transfected eukaryotic HEK293 cells the problem was comparable: Though adequate protein expression was validated by V5-specific Western blotting, only low recombinant protein levels could be detected, consequently resulting in insufficient protein enrichment. In addition, IMAC-based protein purification might have been further limited by partial or total structural inaccessibility of the constructs' C-terminal His₆-tag, which was consistent with our finding of generated fusion proteins being undetectable by His₆-specific Western blotting. In future attempts, this challenge might be faced by moving the His₆-tag to the opposite end of the protein. However, since our interactome screening approach was targeted against free and unaltered N-terminal VASP domains, such a strategy was not advisable here. Therefore, under the given conditions, the intended VASP-specific interactome study was stopped and the focus of this work was shifted towards an analysis of the STIM1 interactome.

Nevertheless, the generated stable cell lines might still be useful to address the phospho-specific VASP interactome of the eukaryotic HEK293 model system in alternate approaches. Since the respective VASP fusion proteins contain both His₆- and V5-tags, V5-specific Co-IP experiments could be performed on native HEK293 cell lysates and co-precipitated putative VASP interaction partners could

subsequently be analyzed by differential SDS-PAGE and protein MS. The data deriving from such an approach might also be relevant with regard to the VASP interactome of platelets and consequently enable targeted studies here as well.

Another strategy to address the phospho-specific VASP interactome of platelets is provided by classical Co-IPs against endogenous platelet VASP. In this context, VASP phosphorylation can for instance be induced by addition of specific PKA agonists (such as the AC activator forskolin), which, depending on the applied concentration, would mediate phosphorylation first of VASP S157, followed by S239 and finally T278. However, when performing such an approach, it is challenging to control and discriminate single and multiple VASP phosphorylation events, and to adequately deduce the accompanying effects on the related phospho-site specific interactomes. Moreover, due to the high affinity of VASP to cytoskeleton actin filaments, it has to be considered that the detected putative VASP-interaction partners could still originate from co-purified actin-bound yet VASP-unrelated proteins.

Finally, to enable a more stringent control of VASP phosphorylation patterns when performing VASP-specific interactome studies, an alternative strategy could be applied: Native platelet lysates could be analyzed in an affinity chromatography approach based on resin-bound synthetic peptides which specifically contain only one of the three characteristic VASP phosphorylation sites in either phosphorylated or non-phosphorylated form. Since these sites are located in close proximity of well-defined VASP domains (i.e. the recruiting poly-Pro-site, as well as the GAB- and the FAB-region; [61]), one disadvantage of this approach might be that withdrawal of S157, S239 and T278 from their functional surroundings may also result in a loss of biological relevance of the delivered data.

5.3 Analysis of the STIM1 interactome in platelets

5.3.1 Remarks on the identified STIM1 interactome

The resulting total amount of 161 proteins detected throughout the STIM1-related study (see 4.8 and 4.9) still contained several redundant isoforms, as well as proteins not distinctively related to platelets, including typical organelle-specific and metabolic ones. Upon removal of these components, the number of identifications was finally reduced to 87. In this context, candidates which had been annotated as 'precursors' (based on the UniProtKB/ Swiss-Prot entries) were treated similar to 'mature' ones.

Of these remaining 87 individual proteins, 23 were repeatedly discovered by at least two independent approaches - i.e. (a) the STIM1Ctail affinity column strategy, or STIM1-specific Co-IP either in (b) human; or (c) mouse platelet lysates - including a total of seven which were even detected by all three performed analyses (see Figure 5.3 and Table 5.2).

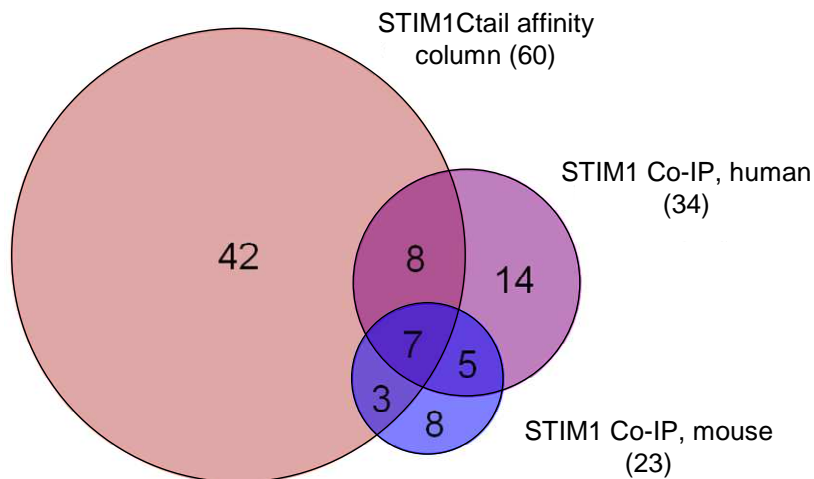


Figure 5.3: Relative display and intersectional regions of platelet-related proteins identified by all STIM1-specific interactome studies performed in this work. The total number of proteins detected in each approach is provided in parenthesis.

Apart from Ras suppressor protein-1, which reportedly plays a role in Ras signal transduction pathways, these multiply detected proteins were closely related to diverse cytoskeletal functions. Myosin, tubulin and β -actin (i.e. cytoplasmic actin) are typical cytoskeleton proteins; tropomyosin is implicated in actin filament stabilization [209, 210]. Gelsolin and tropomodulin are both involved in actin-cytoskeleton modelling: Ca^{2+} -regulated gelsolin binds to the barbed ends of actin filaments, where it promotes actin-monomer-to-filament assembly (i.e. 'nucleation') and prevents monomer exchange (i.e. 'capping function') [211]. Tropomodulin, on the other hand, inhibits both elongation and depolymerization at the pointed ends of actin-filaments, thus stabilizing short proto-filaments which particularly define membrane skeleton geometry [212].

Table 5.2: List of proteins repeatedly identified during all STIM1-specific interactome studies. SC: STIM1Ctail affinity column approach; hIP: STIM1-specific Co-IP in human platelets; mIP: STIM1-specific Co-IP in platelets of STIM1^{+/+} mice. Positive identifications are marked by an 'X'.

#	Protein identifications	SC	hIP	mIP
1	Alpha-actinin 1		X	X
2	Alpha-actinin 2		X	X
3	Alpha-actinin 4		X	X
4	Beta-actin	X		X
5	Gelsolin	X	X	
6	Integrin alpha 2b	X	X	
7	Myosin heavy chain 9	X	X	
8	Myosin light chain 4	X		X
9	Myosin light polypeptide 6	X	X	X
10	Myosin regulatory light chain 2	X	X	X
11	Myosin regulatory light polypeptide 9		X	X
12	PDZ and LIM domain protein 1	X	X	X
13	Platelet glycoprotein V	X	X	
14	Ras suppressor protein 1	X	X	
15	Spectrin alpha chain		X	X
16	Talin 1	X	X	
17	Tropomodulin 3	X		X
18	Tropomyosin alpha 1 chain	X	X	X
19	Tropomyosin alpha 3 chain	X	X	X
20	Tropomyosin alpha 4 chain	X	X	X
21	Tropomyosin beta chain	X	X	X
22	Tubulin beta 1 chain	X	X	
23	Vinculin	X	X	

Other identified proteins are related to cytoskeleton attachment: α -actinins crosslink F-actin filaments and mediate actin anchoring to various intracellular and membrane structures [213]. PDZ and LIM domain protein 1 (alternative names: CLP36, PDLIM1, CLIM1, Elfin) acts as a protein-to-cytoskeleton adaptor [213, 214], spectrin maintains plasma membrane integrity and regulates Ca²⁺-dependent cytoskeleton movement at membrane regions (e.g. during secretion) [215], and at cell-substratum contacts talin-1 connects the actin cytoskeleton to the plasma membrane [216, 217]. In this context, a notable number of proteins were also directly related to cell adhesion and movement. One such example is provided by vinculin, an F-actin-binding protein implicated in maintenance of cell morphology, as well as cell-to-matrix adhesion and locomotion [51, 69-71, 218]. Moreover, it regulates the expression of E-cadherin, i.e. a Ca²⁺-dependent cell adhesion protein at the cell surface. Finally, with glycoprotein V (GPV) and integrin α_{IIb} , typical platelet-derived adhesive membrane proteins were discovered: In detail, the GPIb-IX-V complex component GPV functions in the context of vWF-dependent platelet adhesion to the blood vessel wall [219, 220]. Upon subsequent platelet activation, integrin α_{IIb} , as part of the integrin $\alpha_{IIb}\beta_3$ fibrinogen receptor, mediates platelet-platelet interaction - and thus thrombus formation [221, 222].

Deriving from these preliminary findings, almost all non-redundant, platelet-related proteins identified in the course of this study were organized in four functional complexes: (a) the actin-myosin complex; (b) the adhesion complex, which also included the (c) GPIb-IX-V subcomplex; and (d) the signaling-related complex (compare Table 5.3).

Table 5.3: Functional grouping of non-redundant, platelet-related proteins identified during all performed STIM1-specific interactome screenings. Evaluations were based on functional annotations provided by the UniProtKB/ Swiss-Prot database.

Actin-myosin complex	Adhesion complex	Signaling-related complex
ACTA2 protein	Alpha-actinin 1	Calmodulin
Actin-related protein 2/3 complex SU 4	Alpha-actinin 2	Guanine nucleotide-bind. prot. SU beta 1
Alpha-actin	Alpha-actinin 3	Guanine nucleotide-bind. prot. SU beta 2
Alpha-actinin 1	Alpha-actinin 4	Leucine-rich rep. flightless-interact. prot. 2
Alpha-actinin 2	Beta-parvin	14-3-3 protein alpha/ beta
Alpha-actinin 3	Filamin A	14-3-3 protein delta/ zeta
Alpha-actinin 4	Integrin alpha 2b	14-3-3 protein epsilon
Beta-actin	Integrin beta 1	14-3-3 protein eta
Caldesmon	Integrin beta 3	14-3-3 protein sigma
Calponin 2	Integrin-linked protein kinase	Ras-related C3 botulinum toxin subst. 1
Cofilin 1	Kindlin 3	Ras-related C3 botulinum toxin subst. 3
F-actin capping protein SU alpha 1	Multimerin 1	Ras-related protein Rab-1B
F-actin capping protein SU alpha 2	PDZ and LIM domain protein 1	Ras-related protein Rab-8A
Filamin A	PINCH1	Ras-related protein Rab-8B
Gamma-actin	Platelet glycoprotein IV	Ras-related protein Ral-A
Gelsolin	Spectrin alpha chain	Ras-related protein Ral-B
Myosin XVIIIa	Spectrin beta chain	Ras-related protein Rap-1A
Myosin heavy chain 9	Talin 1	Ras-related protein Rap-1B
Myosin light chain 3	Talin 2	Ras suppressor protein 1
Myosin light chain 4	Thrombospondin 1	Rho-related GTP-binding protein RhoB
Myosin light chain 6B	Vinculin	Transforming protein RhoA
Myosin light polypeptide 6	Zyxin	
Myosin regulatory light chain 2		
Myosin regulatory light chain 3		
Myosin regulatory light chain 12B		
Myosin regulatory light polypeptide 9		
PDZ and LIM domain protein 1		
Tropomodulin 3		
Tropomyosin alpha chain		
Tropomyosin alpha 1 chain		
Tropomyosin alpha 3 chain		
Tropomyosin alpha 4 chain		
Tropomyosin beta chain		
	GPIb-IX-V subcomplex	
	Filamin A	
	PDZ and LIM domain protein 1	
	Platelet glycoprotein Ib alpha chain	
	Platelet glycoprotein V	
	Spectrin alpha chain	
	Spectrin beta chain	

The 'signaling-related complex' mainly contained typical components of the Ras-, Rho- and 14-3-3 signaling pathway. As these protein factors are altogether involved in a huge variety of intracellular regulatory processes and are thus probably not specifically related to the STIM1 function, they were only of minor interest in the context of this work.

The 'actin-myosin complex', on the other hand, predominantly consisted of cytoskeleton proteins of the actin family, as well as of myosin and tropomyosin. In addition, it comprised filament crosslinking components, such as α -actinin or caldesmon, and proteins mediating cytoskeleton polymerization (e.g. the Arp-2/3

complex), branching (filamin A), capping, or shape remodelling (cofilin-1, calponin-2) [67, 210, 213, 219] . Since some of the members initially organized in the actin-myosin complex - i.e. α -actinins, filamin A and cytoskeleton adaptor protein CLP36 - are also related to stabilization of adherens-type junctions by anchoring cytoskeleton filaments and associated proteins to the plasma membrane, these candidates were moreover also included in the so-called 'adhesion complex'.

Generally, this third functional complex summarized a total of 22 proteins involved in cell-cell or cell-substratum interaction, particularly in the context of platelet adhesion. As an example, upon activation of kindlin-3, which is present in the F-actin surrounding ring structure of podosomes in hematopoietic cells, the integrin receptor subunits β_1 and β_3 regulate platelet-to-endothelial cell adhesion [85, 222, 223]. This is mediated via binding to a wide array of ligands, such as collagen, laminin, cytotactin, vitronectin, thrombospondin, vWF or VCAM1. In addition, integrin β_3 , as part of the already-mentioned integrin $\alpha_{IIb}\beta_3$ fibrinogen receptor, interacts with fibronectin and soluble fibrinogen during platelet-platelet interaction [221, 222]. In activated platelets, the integrin β_3 subunits of integrin $\alpha_{IIb}\beta_3$ or $\alpha_V\beta_3$ receptors are also implicated in downregulation of thrombin generation by binding to multimerin-1, i.e. an extracellular matrix protein which stabilizes platelet factor V. Another component closely connected to regulation of integrin inside-out signaling is the integrin-linked protein kinase (ILK) which, together with integrin signaling effector PINCH-1 and cytoskeleton-associated β -parvin, forms the so-called IPP focal adhesion complex [224, 225]. Finally, intracellular linkage of integrin to the actin cytoskeleton is mediated by talins, in particular by adhesion plaque protein talin-2 [216, 217]. Apart from integrins, further detected cell adhesion-related molecules were platelet membrane glycoprotein IV (GPIV; interacts with collagen, thrombospondin and oxidized LDL, [226]), and zyxin which binds to α -actinin and targets Ena/ VASP family members to regions of focal adhesion [51, 69-71].

In addition, with platelet glycoprotein Ib alpha chain (GPIb α) and platelet glycoprotein V (GPV) two subunits of the vWF-binding GPIb-IX-V receptor complex were identified. Since this platelet membrane complex, known to support the initial step of platelet rolling on the exposed subendothelial surface of injured blood vessels, generally co-localizes with filamin A (via direct GPIb α interaction) and spectrin, and since CLP36 has been reported to be closely associated to these two proteins [213],

all these components were consequently summarized in a fourth functional complex - i.e. the adhesional 'GPIIb-IX-V subcomplex'.

Interestingly, apart from the signaling-related complex, filamin A and CLP36 proved to be associated to all described functional complexes. Moreover, as the latter one was also amongst those proteins which were reproducibly detected in all performed STIM1-specific interactome screening approaches this putative STIM1 interaction candidate was finally selected and further examined in more detail. This included evaluation of the specificity of interaction (e.g. via targeted Co-IP experiments), as well as functional analysis with regard to its implication in STIM1-mediated platelet effects.

5.3.2 STIM1 interaction with PDZ and LIM domain protein family member CLP36

Classification of the 'PDZ and LIM domain protein family' (PDLIM) is based on structural similarities: Accordingly, each family member contains at least one PDZ domain (i.e. 'postsynaptic density 95, discs large and zonula occludens-1') and at least one LIM domain (i.e. 'Lin-11, Isl-1 and Mec-3') [227]. These two frequent protein-protein interaction motifs are related to multiple biological processes, such as regulation of actin structure and dynamics, or integrin-dependent adhesion and signaling [228-232]. In this context, they also function in organization of postsynaptic density and neuronal pathfinding, as well as in regulation of membrane protein activity and trafficking.

In detail, the PDZ domain consists of 80-100 aa residues, including a highly conserved GLGF sequence [233], and has been reported to bind to short C-terminal as well as internal PDZ binding motifs found in a variety of interaction partners [234]. The LIM domain (approximately 60 aa), on the other hand, is a conserved zinc-binding, cysteine-rich motif consisting of two tandemly repeated zinc-fingers and containing the consensus sequence $CX_2CX_{16-23}HX_2CX_2CX_2CX_{16-21}CX_2(C/H/D)$ [235]. Though LIM domains have been detected in various proteins and are involved in multiple cellular functions, no distinct LIM domain binding motif has yet been identified. However, in some proteins LIM domains have been observed to form dimers with other LIM domains and are moreover frequently involved in linking proteins to specific protein kinases (e.g. Src, Clik, or PKC; [236-238]) and phosphatases [213, 239]. Since discovery of the first PDZ-LIM domain protein, enigma, in 1994 [240], ten PDLIM proteins have been identified in mammals so far,

and are organized in four subfamilies (Figure 5.4 A): (a) actinin-associated LIM proteins (ALP); (b) enigma and enigma-homologue proteins (ENH); (c) LIM domain kinases (LIMK1, LIMK2); and (d) LIM domain only protein-7 (LMO7) [241, 242].

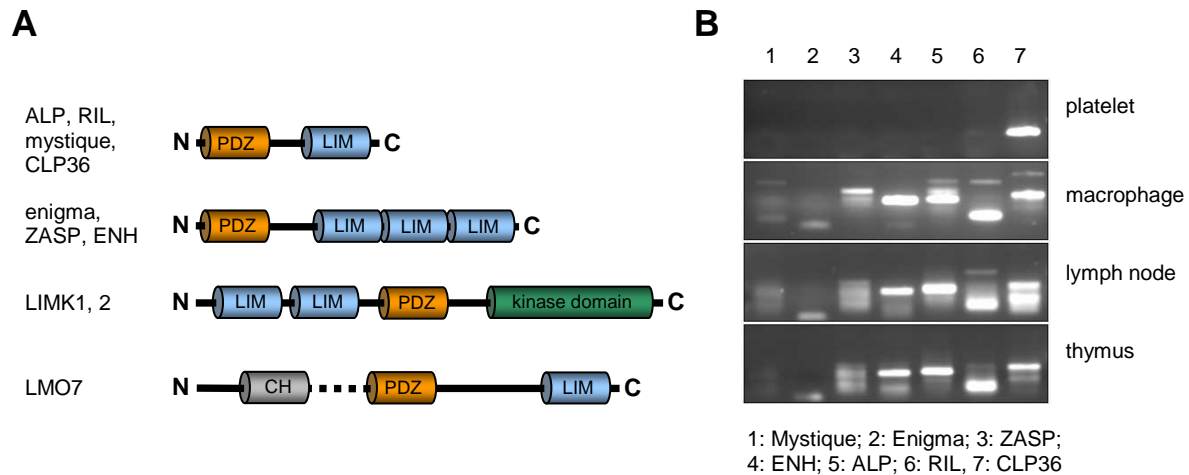


Figure 5.4: The PDLIM protein family. (A) Structural organization of ALP-, enigma-, LIMK- and LMO7-PDLIM subfamilies. (B) PDLIM protein specific mRNA expression profiles of murine blood cells (platelets, macrophages) and lymphatic tissue (lymph nodes, thymus). This RT-PCR study was exclusively targeted against members of the PDLIM ALP- and enigma-subfamilies (i.e. mystique, ALP, RIL, CLP36 and enigma, ZASP, ENH) and was performed by Dr. Attila Braun (Rudolf-Virchow-Center, Würzburg, Germany).

Together with mystique (PDLIM2, SLIM), ALP (PDLIM3), and RIL (PDLIM4), the 36 kDa protein CLP36 belongs to the PDLIM ALP-subfamily. It thus contains one N-terminal PDZ domain and, following a short linker region, one C-terminal LIM domain [227]. Previous studies of Kotaka et al. indicated CLP36 co-localization with α -actinin- 2 at myocardial Z-lines [243]. Later, in 2000, Bauer et al. also reported CLP36 association with α -actinin-1 in resting platelets and moreover observed translocation of this protein complex to regions of newly generated actin filaments upon platelet activation [213]. These data are consistent with our own observations: As revealed by RT-PCR studies on the expression profile of several PDLIM family members in murine blood cells and lymphatic tissue, CLP36 appears to be the sole member of the PDLIM ALP- and enigma-subfamilies which is expressed in platelets (Figure 5.4 B). Thus, the platelet effects reported by Bauer et al. are distinctively related to CLP36 and not biased by overlapping activities of other PDLIM proteins.

According to Vallenius et al., the described interaction of CLP36 with non-muscle α -actinin isoforms (i.e. α -actinin-1, but also α -actinin-4) is executed via the CLP36 PDZ domain and involved in actin stress fiber-mediated processes, such as regulation of cell shape, polarity, migration and cytokinesis in non-muscle cells [214]. However, in contrast to this finding, deriving from yeast 2-hybrid experiments Bauer et al. concluded that the observed association between CLP36 and α -actinin-1 is rather due to binding of the short CLP36 intervening region to the spectrin-like repeats 2 and 3 of α -actinin-1 - and hence not dependent on the CLP36 PDZ and LIM domains [213]. Thus, the true impact of CLP36 related protein interactions and subsequent effects are still far from being fully understood.

To validate the association of STIM1 and CLP36 indicated by our studies, the full-length aa-sequence of human STIM1 was analyzed for putative PDZ binding sites by applying the Expasy-Prosit database search tool for protein domains, families and functional sites (<http://prosite.expasy.org>). As displayed in Figure 5.5 A, nine such PDZ binding sites were identified, with the first two - i.e. STIM1 aa 344-347 (PEAL) and aa 402-405 (LDDV) - being moreover located in close proximity to the annotated STIM1-ORAI1 binding site (STIM1 aa 384-389, KKKRNT). This *in silico* evidence for an apparent interaction between STIM1 and the CLP36 PDZ domain was also verified *in vivo*, since STIM1-specific Co-IP experiments on native lysates of resting platelets resulted in concomitant co-precipitation of CLP36 in STIM1^{+/+} mice, whereas this effect was totally absent in equally-treated samples of STIM1^{-/-} animals (see 4.10). Thus, at least in resting platelets, an interaction of STIM1 and CLP36 appears to be most likely. Interestingly, when subsequently performing multiple sequence alignments of human, mouse, rat, *Xenopus laevis*, *Fugu* and *Drosophila melanogaster* STIM1 proteins (via the Blastp sequence alignment tool provided on <http://blast.ncbi.nlm.nih.gov>), the first two *in silico* predicted PDZ binding sites moreover proved to be highly conserved amongst species, in particular mammalian ones (Figure 5.5 B). This strongly indicates their implication in distinct biological processes. In this context, CLP36 binding to one of these two PDZ binding motifs might mask the ORAI1 binding site of STIM1. As premature STIM1-ORAI1 complex formation would consequently be prevented, the proposed CLP36-STIM1 interaction might consequently have a stabilizing effect on platelet resting conditions. However, this theory requires further validation by supplementary studies, which would also include specific identification of the involved STIM1 PDZ binding site.

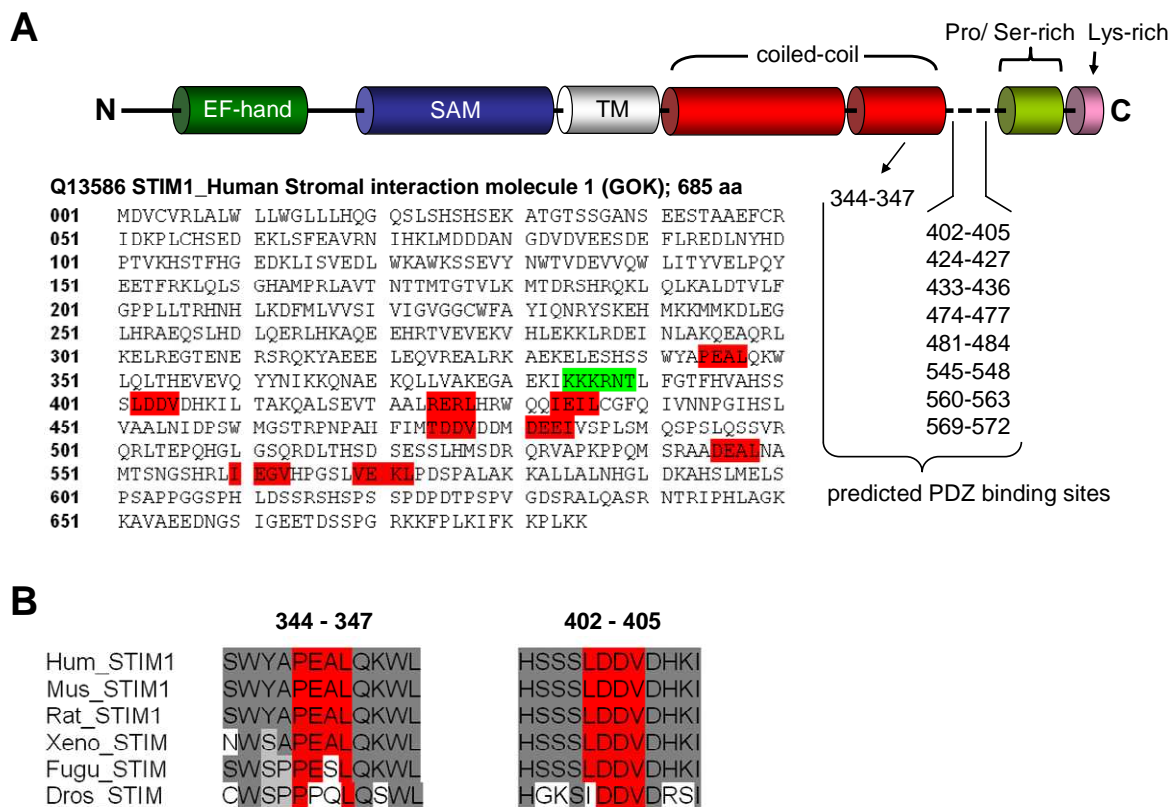


Figure 5.5: PDZ binding sites in human STIM1 protein as annotated by the ExPASy-Prosite database search tool. (A) Nine putative PDZ binding sites (marked in red) were identified in the human STIM1 full length aa-sequence. The first two sites, STIM1 aa 344-347 (PEAL) and aa 402-405 (LDDV), are situated adjacent to the STIM1-ORAI1 binding site (marked in green). (B) Sequence alignments of the first two PDZ binding sites (marked in red) of human, mouse, rat, *Xenopus laevis*, *Fugu* and *Drosophila melanogaster* STIM1 proteins.

5.3.3 GPIb-CLP36 interaction

As outlined in 5.3.1, based on database and literature research functional association of CLP36 to the adhesional GPIb-IX-V subcomplex appeared to be plausible. Indeed, GPIb-specific Co-IPs targeted against both receptor subunits GPIb α and GPIb β in native resting platelets lysates of STIM1^{+/+} mice (i.e. C57Bl6-Sv129 mixed background, wildtype) reproducibly resulted in co-precipitation of CLP36 - and *vice versa* (see 4.11). Thus, an association between GPIb and CLP36 was also indicated *in vivo*; however, whether this interaction occurs directly or by interaction with further adaptor proteins still needs to be determined.

Generally, the GPIb-IX-V receptor complex consists of four transmembrane subunits: GPIb α , covalently linked to GPIb β via disulfide-bridges, and non-covalently attached GPIX and GPV [219, 220]. Moreover, the GPIb α cytoplasmic domains (i.e. aa 557-575) interact with the C-terminal region of actin-binding filamin A, which was also identified in our own STIM1-specific interactome screening approaches [244, 245]. This association was reported as crucial for platelet adhesion to vWF, for stabilizing platelet shape and integrity under resting conditions, as well as for regulating signal transduction during platelet activation [246, 247]. In 2006, Nakamura et al. unravelled the crystal structure of the GPIb α -filamin A complex and localized the GPIb α binding site at filamin A domain 17 [219]. Based on these findings and on previously published data concerning the GPIb-IX-V receptor composition [248], the entire protein complex composed of GPIb-IX-V, filamin A and F-actin was finally assembled as depicted in Figure 5.6. In addition, as published by Bauer et al. [213], α -actinin-mediated crosslinking of F-actin filaments, as well as CLP36 interaction with both F-actin and α -actinin were also included in this schematic drawing.

In detail, filamin A - which forms homodimers via its C-terminal domains - anchors the cell surface receptor complex GPIb-IX-V to the F-actin cytoskeleton. This association is mediated by (a) interaction between the cytoplasmic part of GPIb α and filamin A domain 17; and (b) conserved actin-binding domains located at the filamin A N-termini and typically contain two CH-domains. F-actin filament crosslinking is mediated by symmetric antiparallel α -actinin dimers. These are rod-shaped 100 kDa proteins with (a) an N-terminal globular head harbouring the 2-CH-actin-binding domain; and (b) a C-terminal tail containing two Ca²⁺-binding EF-hand motifs [249-252]. The latter domains have been related to α -actinin targeting to integrin β -subunits and focal adhesion sites. As reported by Bauer et al., at least for α -actinin-1 this function appears to be modulated by CLP36, which commonly co-localizes with this particular α -actinin isoform. Accordingly, upon interaction of the CLP36 short linker sequence with α -actinin spectrin-like repeats 2 and 3, binding of α -actinin-1 to integrin subunits and adhesional plaques is inhibited. This also explains the absence of CLP36 at focal adhesions in activated platelets [213]. Instead, the CLP36- α -actinin-1 complex is retained on actin filaments and stress fibers, where it executes its actin bundling activity [250]. As a consequence, the observed co-precipitation of CLP36 in GPIb-specific Co-IP experiments is probably due to its firm

association with the α -actinin-F-actin complex (or with F-actin alone). Hence the GPIb-CLP36 interaction presumably has to be regarded as an indirect one.

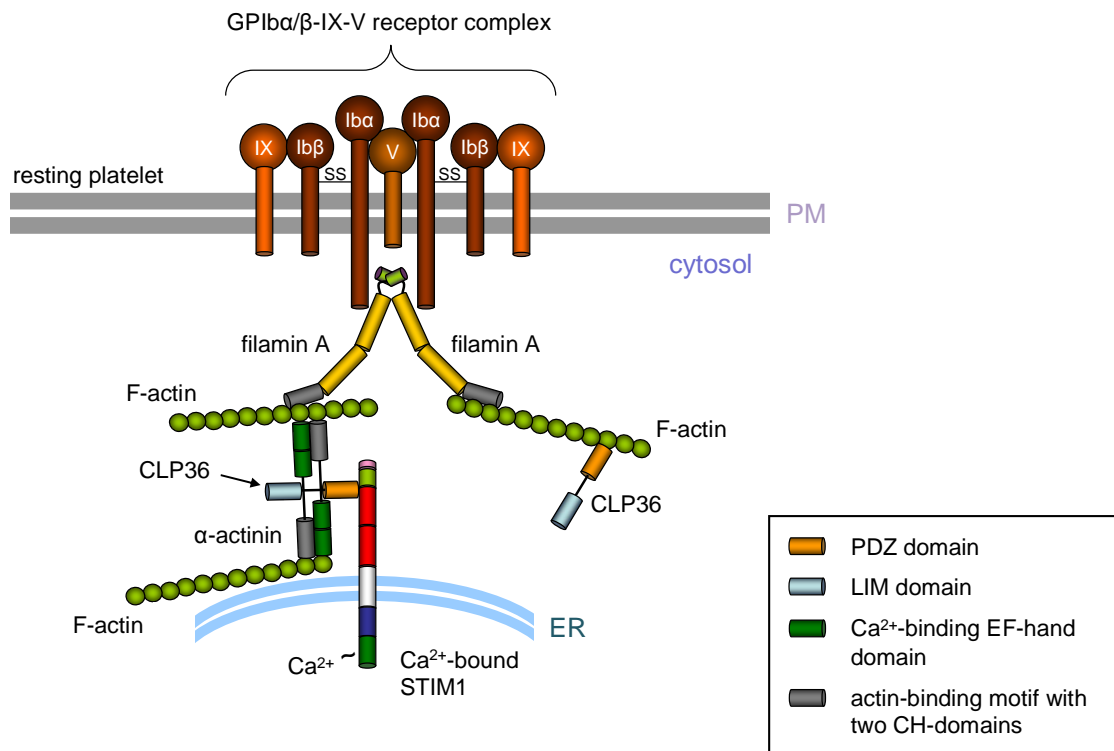


Figure 5.6: Scheme of the GPIb-IX-V receptor complex in association with dimerized filamin A and F-actin filaments (based on [219]). Included are CLP36 interactions with F-actin and F-actin-coupled α -actinin as reported by Bauer et al. for resting platelets [213]. Moreover, binding of the CLP36 PDZ domain to ER-localized STIM1 monomers, as derived from our own studies, is depicted below.

Moreover, under the described conditions the PDZ and LIM domains of α -actinin-bound CLP36 are free to link further proteins - for instance related to cell signaling, as well as to regulation of cell shape and integrity - to the F-actin filaments. In this context, as illustrated in Figure 5.6, CLP36 may also function as an adaptor that anchors the cytoplasmic tail of ER-localized STIM1 to the cytoskeleton. This binding may have a stabilizing effect on the platelets' resting state, thus preventing uncontrolled intravascular activation since homotypic oligomerization of STIM1 monomers and subsequent formation of ER-PM junctions are consequently avoided - until platelet activity is finally induced by the interaction of GPIb-IX-V with subendothelial vWF.

However, it has to be mentioned that although CLP36 was specifically found in association with GPIb and - in a separate approach - with STIM1 (both indicated by our Co-IP studies), this does not necessarily prove CLP36-mediated interrelation between these two components. On the contrary, CLP36 is implicated in so many cellular processes that these two findings might also be completely independent. Thus, for further confirmation of this theory, more enhanced functional assays will have to be performed.

5.3.4 Ca²⁺-dependent degradation of CLP36 by calpain

Based on the finding of an association between CLP36 and Ca²⁺-sensing STIM1, the question was posed how CLP36 may be affected by STIM1-related fluctuation of intracellular calcium levels. For this purpose, Braun et al. investigated the impact of artificially induced SOCE on CLP36 stability in purified platelets of STIM1^{+/+} mice (i.e. C57Bl6-Sv129 mixed background, wildtype). In detail, by adding the Ca²⁺-ionophore ionomycin in presence of 1 mM extracellular calcium, Ca²⁺-influx increased via direct stimulation of store-operated cation entry across the biological membranes (SOCE) [253]. Interestingly, as depicted in Figure 5.7 A (left), subsequent Western blotting revealed distinct degradation of CLP36 over time, whereas protein levels of GPIb and tubulin (loading control) remained relatively unaltered. Moreover, since this effect on CLP36 levels was not observable when platelets were equally treated in absence of extracellular calcium (under these conditions, ionomycin-induced Ca²⁺-fluxes were solely due to calcium store depletion), it was clearly a consequence of SOCE-mediated [Ca²⁺]_i increase (Figure 5.7 B, left).

Thus having an obvious evidence for Ca²⁺-dependent protein degradation, the next step was to investigate a potential implication of calpain activity. Generally, calpains are Ca²⁺-dependent cysteine proteases [254-256] and functionally closely related to cytoskeleton reorganization, cell motility - and also hemostasis [257, 258]. There are two classes of ubiquitously expressed calpains: calpain-1 (μ -calpain), which only requires micromolar Ca²⁺-concentrations for full activity, and calpain-2 (m-calpain), which demands presence of higher (i.e. millimolar) calcium levels [254]. In activated mouse platelets, calpain has been shown to mediate proteolytic processing of various targets, such as talin, filamin and other proteins related to cytoskeleton integrity, contractility or integrin signaling (e.g. integrin $\alpha_{IIb}\beta_3$) [257, 259]. Thereby, according to Azam et al., calpain-1 accounts for 80% of the total platelet calpain

activity and is particularly relevant during Ca^{2+} -dependent late platelet response [254].

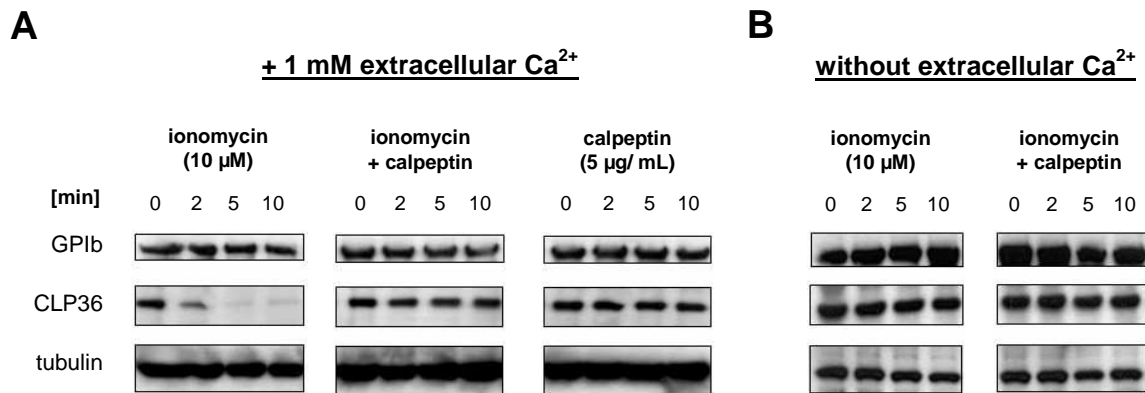


Figure 5.7: SOCE-dependent degradation of CLP36 by calpain. Platelets of $\text{STIM1}^{+/+}$ mice ($n=2$) were treated with calcium ionophore ionomycin and/ or specific calpain inhibitor calpeptin (A) in presence or (B) in absence of extracellular calcium. Time-dependent protein levels of GPIb, CLP36 and tubulin (loading control) were subsequently determined via specific Western blotting. Data were kindly provided by Dr. Attila Braun (Rudolf-Virchow-Center, Würzburg, Germany).

Based on this knowledge, Braun et al. repeated their experiments in presence of the specific calpain inhibitor calpeptin. As a result, upon ionomycin addition, pre-treatment with calpeptin efficiently prevented the previously observed SOCE-induced degradation of CLP36 in platelets of $\text{STIM1}^{+/+}$ mice (Figure 5.7 A, middle). Hence, it may be concluded that SOCE-induced $[\text{Ca}^{2+}]_i$ increase upon platelet activation also induces platelet calpain (i.e. presumably calpain-1) which consequently mediates Ca^{2+} -dependent limited proteolysis of various target proteins - including CLP36. This theory was further backed both by *in silico* prediction of calpain cleavage sites in the CLP36 aa-sequence, as well as by *in vitro* calpain digestion assays of recombinant human CLP36 protein (see 4.12): Accordingly, of the 24 calpain cutting sites predicted *in silico* for CLP36, 19 were also identified by the MS-based *in vitro* digestion assay. However, since three of these sites were also detected in undigested samples and may thus as well result from unspecific spontaneous fragmentation, the total amount of putative calpain cleavage sites of CLP36 was reduced to 16. One of these candidates, i.e. CLP36 H181, was reproducibly identified by all four *in silico* prediction models, as well as by the *in vitro*

calpain digestion assay, and hence represents the most promising calpain cleavage site located in human CLP36.

Deriving from these findings, calpain, as induced by SOCE-mediated increase of intracellular Ca^{2+} -levels (e.g. upon platelet activation), may mediate proteolytic cleavage of CLP36 at aa-position H181 (or other sites) and consequently disconnect the CLP36 PDZ from the LIM domain. This parting of the CLP36 short linker sequence may also negatively affect its previously described interaction with the spectrin-like repeats 2 and 3 of α -actinin-1. As a consequence, CLP36 would dissociate from α -actinin-1, hence leaving its F-actin bound state. Assuming an association of CLP36 and STIM1 via the CLP36 PDZ domain in resting platelets (as depicted in Figure 5.6), Ca^{2+} -unloaded STIM1 monomers would subsequently be released from their cytoskeleton-anchored resting state and finally be able to dimerize and translocate to the ORAI1 complex at regions of ER-PM junctions.

5.3.5 Negative regulation of GPVI signaling by CLP36

Since CLP36 turned out to be the sole expressed PDLIM family member in murine platelets (see Figure 5.4 B), its loss of function cannot be compensated by other PDLIM proteins. Thus, disruption of the *Clp36* gene provides a promising tool to further characterize the proteins physiological role *in vivo*, particularly with regard to platelet activation and subsequent Ca^{2+} -signaling. In this context, there is plenty of data available indicating implication of the CLP36 PDZ domain in multiple protein-protein interactions (see 5.3.2). Moreover, the related PDZ binding sites are well defined. In contrast, the functional impact of the CLP36 LIM domain still needs to be further specified. For this purpose, Braun et al. generated a transgenic mouse line (C57Bl6-Sv129 mixed background) where the CLP36 LIM domain has been deleted by inserting a Geo-gene-trap cassette (containing a downstream transcriptional termination sequence) in the intronic region between exon 5 and 6 of the *Clp36* locus - and hence upstream of the LIM domain encoding region. As a consequence, CLP36 transcription is terminated prematurely at the inserted site, hence resulting in expression of the chimeric $\text{CLP36}^{\Delta\text{LIM}}$ - β -GEO fusion protein instead of full-length CLP36. In the following, mice homozygously expressing this truncated version of CLP36 are referred to as ' $\text{Clp36}^{\Delta\text{LIM}}$ ' mice.

Platelets of $\text{Clp36}^{\Delta\text{LIM}}$ mice were subsequently analyzed morphologically and functionally. Accordingly, upon comparison to wildtype samples (i.e. C57Bl6-Sv129

mixed background), Clp36^{ΔLIM} platelets did not reveal any specific morphological differences: Platelet spreading as well as F-actin and stress fiber formation were normal, and so was the subcellular distribution of the truncated protein. Also blood platelet counts, mean platelet volume and platelet life span were unaffected. Thus, the CLP36 LIM domain was apparently not involved in platelet production, structural integrity and actin cytoskeleton remodelling. However, when Clp36^{ΔLIM} platelet activation was functionally tested in presence of different agonists, an enhanced response to GPVI agonists (e.g. collagen or C-reactive protein CRP) has been observed *in vitro*, which resulted in increased degranulation, integrin $\alpha_{IIb}\beta_3$ activation and aggregation. In this context, it is important to note that this unexpected effect was not due to a *per se* pre-activated state of Clp36^{ΔLIM} platelets since there was no evidence for spontaneous aggregation. Moreover, GPVI-independent platelet activation, e.g. via induction of GPCR signaling by thrombin, TxA₂ or ADP (see 1.1.3) proved to be unaltered in comparison to wildtype samples. Thus, the detected prothrombotic Clp36^{ΔLIM} phenotype can specifically be related to an amplified GPVI signaling cascade.

GPVI is an Ig-like platelet collagen receptor and crucial for platelet activation upon contact with the subendothelial matrix [260]. It is non-covalently attached to the signal-transducing Fc receptor gamma chain (FcR γ), which harbours a so-called 'immunoreceptor tyrosine-based activation motif' (ITAM) [261]. Collagen binding to GPVI induces FcR γ tyrosine phosphorylation by the Src family kinases Fyn and Lyn [262, 263]; ITAM phosphorylation, on the other hand, links the Syk kinase to the GPVI-FcR γ receptor complex. This results in a series of tyrosine phosphorylation events, followed by recruitment of adaptor proteins and subsequent induction of effector proteins such as PI3K and PLC γ 2 [264]. As a consequence, PLC γ 2-mediated hydrolysis of PIP₂ into IP₃ and DAG (see also 1.1.3) culminates in (a) IP₃-induced Ca²⁺-store release, consequently leading to SOCE; and (b) further increase of Ca²⁺-influx due to DAG-mediated activation of platelet 'transient receptor potential cation channels' (e.g. TRPC6) [265, 266]. This sudden enhancement of [Ca²⁺]_i subsequently promotes Ca²⁺-dependent downstream signaling pathways, finally leading to thrombus formation.

In accordance with this model, upon GPVI activation by CRP application, Braun et al. noticed increased Ca²⁺-store depletion (in absence of extracellular Ca²⁺), as well as an elevated SOCE (in presence of extracellular Ca²⁺) in Clp36^{ΔLIM} platelets (Figure

5.8). Thereby, the induced Ca^{2+} -fluxes exceeded those of equally treated wildtype samples, which provides further evidence that the observed prothrombotic $\text{Clp36}^{\Delta\text{LIM}}$ phenotype is related to an enhanced GPVI-ITAM signaling.

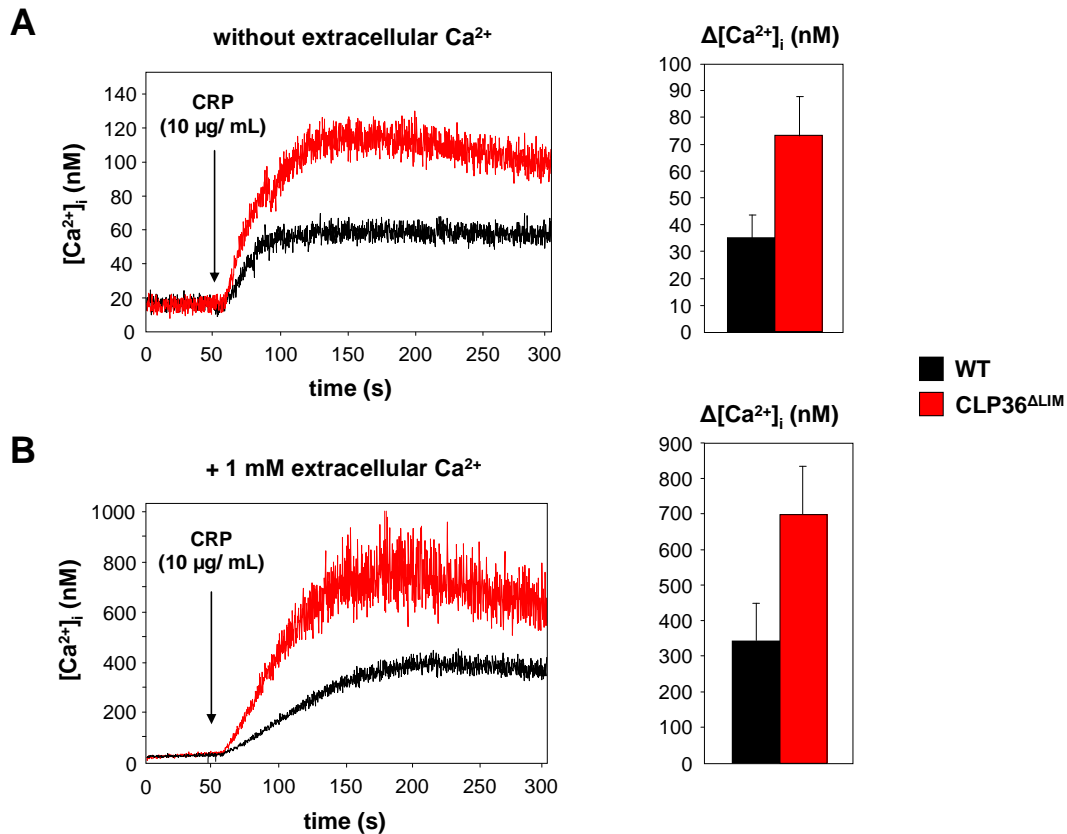


Figure 5.8: CRP-induced Ca^{2+} -signaling in $\text{Clp36}^{\Delta\text{LIM}}$ vs wildtype (wt) platelets. Time-dependent fluorimetric Ca^{2+} -measurements were performed upon addition of 10 $\mu\text{g}/\text{mL}$ CRP in (A) absence of extracellular Ca^{2+} ($n=4$); or (B) presence of 1 mM extracellular Ca^{2+} ($n=6$). Store release was significantly increased in $\text{Clp36}^{\Delta\text{LIM}}$ vs wt samples (A), which consequently also resulted in an elevated SOCE in response to CRP (B). Data were kindly provided by Dr. Attila Braun (Rudolf-Virchow-Center, Würzburg, Germany).

However, when DTS Ca^{2+} -stores were artificially depleted by addition of the non-competitive SERCA inhibitor thapsigargin, the consequent Ca^{2+} -flux of $\text{Clp36}^{\Delta\text{LIM}}$ platelets was similar to the one measured in wildtype samples. This indicates that CLP36 may not directly function in the process of Ca^{2+} -store release or SOCE complex assembly. Instead, it is more likely to act as an endogenous negative regulator of GPVI-ITAM signaling, presumably by CLP36 LIM domain-dependent cytoskeleton retention of some of the involved protein kinases (see also 5.3.2). This theory was further backed by the finding that both tyrosine phosphorylation of

multiple proteins related to the GPVI signaling cascade and PLC γ 2 activity, as determined by IP $_3$ -measurements, were markedly elevated in CRP-activated Clp36 Δ LIM vs wildtype platelets. All described data related to the analysis of GPVI-ITAM signaling in Clp36 Δ LIM mice are currently under submission [267].

5.3.6 Concluding remarks on the STIM1-specific interactome study

Having intensively analyzed the interactome of the cytosolic part of STIM1 in resting human and mouse platelets, a total of 87 non-redundant, platelet-related proteins were identified which displayed association with this Ca $^{2+}$ -sensing molecule. These components could be organized in four functional complexes: (a) the actin-myosin complex; (b) the adhesion complex, including the (c) GPIb-IX-V subcomplex; and (d) the signaling-related complex. One of the most promising candidates in this context, the 'PDZ and LIM domain protein 1' (CLP36), was finally chosen for a more detailed verification.

Deriving from cooperative studies with Dr. Attila Braun (Rudolf-Virchow-Center, Würzburg, Germany), CLP36 was consequently identified as a putative negative regulator of platelet activity, with possible implication in both STIM1- as well as GPVI-mediated effects. Accordingly, under resting platelet conditions, α -actinin-bound CLP36, via its PDZ domain, presumably anchors the STIM1 cytosolic region to the F-actin cytoskeleton. Assuming that both homotypic oligomerization of STIM1 and its subsequent translocation to sites of ER-PM junctions is consequently prevented, the proposed CLP36-STIM1 interaction may contribute to avoid uncontrolled intravascular platelet activation. Our data also indicate implication of the GPIb-IX-V receptor complex in this context; however, this finding might also be due to CLP36/STIM1-independent linking of GPIb subunits to F-actin filaments (as e.g. mediated by GPIb-bound filamin A). Thus it needs to be further examined. Moreover, as revealed by *in silico* site predictions, two of the putative PDZ binding sites of STIM1 (i.e. STIM1 aa 344-347 and aa 402-405) are located in close proximity to the annotated STIM1-ORAI1 binding site (STIM1 aa 384-389). Thus, binding of CLP36 to either of these motifs might also have a masking effect on this latter site and hence inhibit premature STIM1-ORAI1 interaction. However, for further verification of these preliminary findings, the functional impact of the described interactions needs to be specified in more detail. As an example, deletion of the CLP36 PDZ domain and/ or

of the assumed PDZ binding sites of STIM1 may provide feasible tools to characterize the true nature of interaction in future *in vitro* and *in vivo* studies.

Apart from the discussed functional association between CLP36 and STIM1, analyses of Clp36^{ΔLIM} mice furthermore revealed that loss of the CLP36 LIM domain directly affected GPVI-ITAM signaling: Accordingly, in comparison to wildtype samples, an elevated PLC γ 2-activity has been observed in platelets of Clp36^{ΔLIM} mice in response to CRP, with consequently enhanced Ca²⁺-store depletion and Ca²⁺-influx (data currently under submission, [267]). As indicated by Braun et al., this effect was presumably due to an increased recruitment of protein kinases related to the GPVI-ITAM signaling pathway in Clp36^{ΔLIM} samples, whereas in wildtype samples, upon interaction with the LIM domain of α -actinin-bound full-length CLP36, the same components would be maintained in a cytoskeleton-associated, fixed state. However, to fully understand the mechanism of how CLP36 regulates GPVI-ITAM signaling, the identity of these kinases still needs to be resolved.

In addition, calpain-dependent degradation of CLP36 was also observed as a consequence of SOCE in wildtype platelets. Hence it is striking to assume that this Ca²⁺-dependent protease, which mediates limited proteolysis of multiple key factors related to platelet activation (see 5.3.4), might also be implicated in this process as well. This is particularly true as multiple putative calpain cleavage sites were identified within the CLP36 aa-sequence, with the most probable one, H181, being located within the CLP36 short linker region. Accordingly, following platelet stimulation with e.g. GPVI agonists, the subsequent moderate [Ca²⁺]_i increase, which results from store depletion, TRPC6 activation and early SOCE, may activate platelet calpain and hence promote proteolytic degradation of F-actin-localized CLP36. As a consequence, cytoskeleton-retained protein kinases (via the CLP36 LIM domain), as well as F-actin-anchored STIM1 monomers (via the CLP36 PDZ domain) would finally be released from their immobilized state, hence contributing to a further enhancement of both GPVI-ITAM signaling and SOCE-mediated Ca²⁺-influx.

Taken together, this recent study, which originally focused on identifying novel STIM1 interaction partners in resting platelets, indicates a multifaceted role of the cytoskeleton adaptor protein CLP36 during prevention of intravascular occlusive thrombus formation. In this context, CLP36 appears to function as an important negative regulator of both STIM1- and GPVI-mediated effects particularly taking place during late platelet response (i.e. platelet degranulation and aggregation).

Thus, the tendency of intravascular platelet activation and hence the risk of manifestation of acute ischemic diseases (e.g. stroke or myocardial infarction) might, in addition to further factors, be directly related to the endogenous CLP36 activity. Therefore, further research on this promising protein candidate may help in the ongoing task of unravelling the physiological mechanisms regulating prevention of uncontrolled intravascular platelet activation, and might thus improve our understanding of cardiovascular pathologies.

6 Literature

- [1] Despopoulos, A., Silbernagl, S. (2008) Color Atlas of Physiology. 6th edn. Thieme, Stuttgart, 88ff.
- [2] Hartwig, J, Italiano, J., Jr. (2003) The birth of the platelet. *J Thromb Haemost* 1, 1580-1586.
- [3] Deutsch, V. R., Torner, A. (2006) Megakaryocyte development and platelet production. *Brit J Haem* 134, 453-466.
- [4] Ruggeri, M. Z. (2002) Platelets in atherothrombosis. *Nat. Med.* 8, 1227-1234.
- [5] Zellner, M., Winkler, W., Hayden, H., Diestinger, M., et al. (2005) Quantitative validation of different protein precipitation methods in proteome analysis of blood platelets. *Electrophoresis* 26, 2481-2489.
- [6] Despopoulos, A., Silbernagl, S. (2008) Color Atlas of Physiology. 6th edn. Thieme, Stuttgart, 102ff.
- [7] Diacovo, T. G., Catalina, M. D., Siegelman, M. H., von Andrian, U. H. (1998) Circulating activated platelets reconstitute lymphocyte homing and immunity in L-selectin-deficient mice. *J Exp Med* 187, 197-204.
- [8] Nannizzi-Alaimo, L., Alves, V. L., Phillips, D. R. (2003) Inhibitory effects of glycoprotein IIb/IIIa antagonists and aspirin on the release of soluble CD40 ligand during platelet stimulation. *Circulation* 107, 1123-1128.
- [9] Welt, F. G., Rogers, S. D., Zhang, X., Ehlers, R., et al. (2004) GP IIb/IIIa inhibition with eptifibatide lowers levels of soluble CD40L and RANTES after percutaneous coronary intervention. *Catheter Cardiovasc Interv* 61, 185-189.
- [10] Celotti, F., Colciago, A., Negri-Cesi, P., Pravettoni, A., et al. (2006) Effect of platelet-rich plasma on migration and proliferation of SaOS-2 osteoblasts: role of platelet-derived growth factor and transforming growth factor- β . *Wound Repair Regen* 14, 195-202.
- [11] O'Connell, S.M., Impeduglia, T., Hessler, K., Wang, X.J., et al. (2008) Autologous platelet-rich fibrin matrix as cell therapy in the healing of chronic lower-extremity ulcers. *Wound Repair Regen* 16, 749-756.
- [12] Siess, W., Grünberg, B., Luber, K., Vauti, F., et al. (1992) Platelet signal transduction mechanisms induced by eicosanoids. *Eicosanoids* 5, 13-15.
- [13] Jain, R. K., Duda, D. G., Clark, J. W., Loeffler, J. S. (2006) Lessons from phase III clinical trials on anti-VEGF therapy for cancer. *Nat Clin Pract Oncol* 3, 24-40.
- [14] Vroiling, L., Yuana, Y., Schuurhuis, G.J., van Hinsbergh, V. W., et al. (2007) VEGFR2 expressing circulating (progenitor) cell populations in volunteers and cancer patients. *Thromb Haemost* 98, 440-450.
- [15] Maynard, D. M., Heijnen, H. F., Horne, M. K., White, J. G., et al. (2007) Proteomic analysis of platelet alpha-granules using mass spectrometry. *J Thromb Haemost* 5, 1945-1955.
- [16] McNicol, A., Israels, S. J. (1999) Platelet dense granules: structure, function and implications for haemostasis. *Thromb. Res.* 95, 1-18.

- [17] Kenney, D. M., Linck, R. W. (1985) The cytoskeleton of unstimulated blood platelets: structure and composition of the isolated marginal microtubular band. *J Cell Sci* 78, 1-22.
- [18] Fox, J. E., Boyles, J. K., Berndt, M. C., Steffen, P. K., et al. (1988) Identification of a membrane skeleton in platelets. *J Cell Biol* 106, 1525-1538.
- [19] Boyles, J., Fox, J. E., Phillips, D. R., Stenberg, P. E. (1985) Organization of the cytoskeleton in resting, discoid platelets: preservation of actin filaments by a modified fixation that prevents osmium damage. *J Cell Biol* 101, 1463-1472.
- [20] Schwarz, U. R., Walter, U., Eigenthaler, M. (2001) Taming platelets with cyclic nucleotides. *Biochem Pharmacol* 62, 1153-1161.
- [21] Offermanns, S. (2000) The role of heterotrimeric G proteins in platelet activation. *Biol Chem* 381, 389-396.
- [22] Philipose, S., Konya, V., Sreckovic, I., Marsche, G., et al. (2010) The prostaglandin E2 receptor EP4 is expressed by human platelets and potently inhibits platelet aggregation and thrombus formation. *Arterioscler Thromb Vasc Biol* 30,2416-2423.
- [23] Geiger, J., Nolte, C., Butt, E., Sage, S. O., et al. (1992) Role of cGMP and cGMP-dependent protein kinase in nitrovasodilator inhibition of agonist-evoked calcium elevation in human platelets. *Proc Natl Acad Sci USA* 89, 1031-1035.
- [24] Soderling, S. H., Beavo, J. A. (2000) Regulation of cAMP and cGMP signaling: new phosphodiesterases and new functions. *Curr Opin Cell Biol* 12, 174-179.
- [25] Gambaryan, S., Geiger, J., Schwarz, U. R., Butt, E., et al. (2004) Potent inhibition of human platelets by cGMP analogs independent of cGMP-dependent protein kinase. *Blood* 103, 2593-2600.
- [26] Fox, J. E., Berndt, M. C. (1989) Cyclic AMP-dependent phosphorylation of glycoprotein Ib inhibits collagen-induced polymerization of actin in platelets. *J Biol Chem* 264, 9520-9526.
- [27] Hettasch, J. M., Sellers, J. R. (1991) Caldesmon phosphorylation in intact human platelets by cAMP-dependent protein kinase and protein kinase C. *J Biol Chem* 266, 11876-11881.
- [28] Butt, E., Walter, U. (1996) Cyclic nucleotides: measurement and function. In: *Platelets: A practical approach*. Edited by Watson, S. University Press, Oxford, 259-278.
- [29] Surks, H. K. (2007) cGMP-dependent protein kinase I and smooth muscle relaxation: a tale of two isoforms. *Circulation research* 101, 1078-1080.
- [30] Fredrickson, B. J., Dong, J. F., McIntire, L. V., Lopez, J. A. (1998) Shear-dependent rolling on von Willebrand factor of mammalian cells expressing the platelet glycoprotein Ib-IX-V complex. *Blood* 92, 3684-3693.
- [31] Nieswandt, B., Brakebusch, C., Bergmeier, W., Schulte, V., et al. (2001) Glycoprotein VI but not alpha2beta1 integrin is essential for platelet interaction with collagen. *EMBO J* 20, 2120-2130.
- [32] Saelman, E. U., Nieuwenhuis, H. K., Hese, K. M., de Groot, P. G., et al. (1994) Platelet adhesion to collagen types I through VIII under conditions of stasis and flow is mediated by GPIa/IIa (alpha 2 beta 1-integrin). *Blood* 83, 1244-1250.

- [33] Tsuji, M., Ezumi, Y., Arai, M., Takayama, H. (1997) A novel association of Fc receptor gamma-chain with glycoprotein VI and their co-expression as a collagen receptor in human platelets. *J Biol Chem* 272, 23528-23531.
- [34] Watson, S. P., Gibbins, J. (1998) Collagen receptor signalling in platelets: extending the role of the ITAM. *Immunol Today* 19, 260-264.
- [35] Roberts, W., Michno, A., Aburima, A., Naseem, K. M. (2009) Nitric oxide inhibits von Willebrand factor-mediated platelet adhesion and spreading through regulation of integrin alpha(IIb)beta(3) and myosin light chain. *J Thromb Haemost* 7, 2106-2115.
- [36] Shattil, S. J., Brass, L. F. (1987) Induction of the fibrinogen receptor on human platelets by intracellular mediators. *J Biol Chem* 262, 992-1000.
- [37] Lian, L., Wang, Y., Draznin, J., Eslin, D., et al. (2005) The relative role of PLCbeta and PI3Kgamma in platelet activation. *Blood* 106, 110-117.
- [38] Gohla, A., Offermanns, S., Wilkie, T. M., Schultz, G. (1999) Differential involvement of Galpha12 and Galpha13 in receptor-mediated stress fiber formation. *J Biol Chem* 274, 17901-17907.
- [39] Klages, B., Brandt, U., Simon, M. I., Schultz, G., et al. (1999) Activation of G12/G13 results in shape change and Rho/Rho-kinase-mediated myosin light chain phosphorylation in mouse platelets. *J Cell Biol* 144, 745-754.
- [40] Shattil, S. J. (1999) Signaling through platelet integrin alpha IIb beta 3: inside-out, outside-in, and sideways. *Thromb Haemost* 82, 318-325.
- [41] Prevost, N., Woulfe, D., Tanaka, T., Brass, L. F. (2002) Interactions between Eph kinases and ephrins provide a mechanism to support platelet aggregation once cell-to-cell contact has occurred. *Proc Natl Acad Sci USA* 99, 9219-9224.
- [42] Angelillo-Scherrer, A., de Frutos, P., Aparicio, C., Melis, E., et al. (2001) Deficiency or inhibition of Gas6 causes platelet dysfunction and protects mice against thrombosis. *Nat Med* 7, 215-221.
- [43] Nachmias, V. T., Yoshida, K. I. (1988) The cytoskeleton of the blood platelet: a dynamic structure. *Adv Cell Biol* 2, 181-211.
- [44] Stossel, T. P. (1993) On the crawling of animal cells. *Science* 260, 1086-1094.
- [45] Kang, F., Purich, D. L., Southwick, F. S. (1999) Profilin promotes barbed-end actin filament assembly without lowering the critical concentration. *J Biol Chem* 274, 36963-36972.
- [46] Pollard, T. D., Borisy, G. G. (2003) Cellular motility driven by assembly and disassembly of actin filaments. *Cell* 112, 453-465.
- [47] dos Remedios, C. G., Chhabra, D., Kekic, M., Dedova, I. V., et al. (2003) Actin binding proteins: regulation of cytoskeletal microfilaments. *Physiol Rev* 83, 433-473.
- [48] Witke, W. (2004) The role of profilin complexes in cell motility and other cellular processes. *Trends Cell Biol* 14, 461-469.
- [49] Yarmola, E. G., Bubb, M. R. (2006) Profilin: emerging concepts and lingering misconceptions. *Trends Biochem Sci* 31, 197-205.
- [50] Krause, M., Bear, J. E., Loureiro, J. J., Gertler, F. B. (2002) The Ena/VASP enigma. *J Cell Sci* 115, 4721-4726.

- [51] Reinhard, M., Jarchau, T., Reinhard, K., Walter U. (1999) VASP. In: Guidebook to the cytoskeletal and motor proteins. Edited by Kreis, T., Vale, R. University Press, Oxford, 168-171.
- [52] Gertler, F. B., Niebuhr, K., Reinhard, M., Wehland, J., et al. (1996) Mena, a relative of VASP and *Drosophila Enabled*, is implicated in the control of microfilament dynamics. *Cell* 87, 227-239.
- [53] Reinhard, M., Jouvenal, K., Tripier, D., Walter, U. (1995) Identification, purification, and characterization of a zyxin-related protein that binds the focal adhesion and microfilament protein VASP (vasodilator-stimulated phosphoprotein). *Proc Natl Acad Sci USA* 92, 7956-7960.
- [54] Butt, E., Abel, K., Krieger, M., Palm, D., et al. (1994) cAMP- and cGMP-dependent protein kinase phosphorylation sites of the focal adhesion vasodilator-stimulated phosphoprotein (VASP) in vitro and in intact human platelets. *J Biol Chem* 269, 14509-14517.
- [55] Aszodi, A., Pfeifer, A., Ahmad, M., Glauner, M., et al. (1999) The vasodilator-stimulated phosphoprotein (VASP) is involved in cGMP- and cAMP-mediated inhibition of agonist-induced platelet aggregation, but is dispensable for smooth muscle function. *EMBO J* 18, 37-48.
- [56] Hauser, W., Knobloch, K. P., Eigenthaler, M., Gambaryan, S., et al. (1999) Megakaryocyte hyperplasia and enhanced agonist-induced platelet activation in vasodilator-stimulated phosphoprotein knockout mice. *Proc Natl Acad Sci USA* 96, 8120-8125.
- [57] Kwiatkowski, A. V., Gertler, F. B., Loureiro, J. J. (2003) Function and regulation of Ena/VASP proteins. *Trends Cell Biol* 13, 386-392.
- [58] Ball, L. J., Kühne, R., Hoffmann, B., Häfner, A., et al. (2000) Dual epitope recognition by the VASP EVH1 domain modulates polyproline ligand specificity and binding affinity. *EMBO J* 19, 4903-4914.
- [59] Bachmann, C., Fischer, L., Walter, U., Reinhard, M. (1999) The EVH2 domain of the vasodilator stimulated phosphoprotein mediates tetramerization, F-actin binding, and actin bundle formation. *J Biol Chem* 274, 23549-23557.
- [60] Ahern-Djamali, S. M., Comer, A. R., Bachmann, C., Kastenmeier, A. S., et al. (1998) Mutations in *Drosophila enabled* and rescue by human vasodilator-stimulated phosphoprotein (VASP) indicate important functional roles for Ena/VASP homology domain 1 (EVH1) and EVH2 domains. *Mol Biol Cell* 9, 2157-2171.
- [61] Ferron, F., Rebowski, G., Lee, S. H., Dominguez, R. (2007) Structural basis for the recruitment of profilin-actin complexes during filament elongation by Ena/VASP. *EMBO J* 26, 4597-4606.
- [62] Ermekova, K. S., Zambrano, N., Linn, H., Minopoli, G., et al. (1997) The WW domain of neural protein FE65 interacts with proline-rich motifs in Mena, the mammalian homolog of *Drosophila enabled*. *J Biol Chem* 272, 32869-32877.
- [63] Bear, J. E., Krause, M., Gertler, F. B. (2001) Regulating cellular actin assembly. *Curr Opin Cell Biol*, 13, 158-166.
- [64] Mahoney, N. M., Rozwarski, D. A., Fedorov, E., Fedorov, A. A., et al. (1999) Profilin binds proline-rich ligands in two distinct amide backbone orientations. *Nat Struct Biol* 6, 666-671.
- [65] Chereau, D., Dominguez, R. (2006) Understanding the role of the G-actin-binding domain of Ena/VASP in actin assembly. *J Struct Biol* 155, 195-201.

- [66] Bear, J. E., Svitkina, T. M., Krause, M., Schafer, D. A., et al. (2002) Antagonism between Ena/VASP proteins and actin filament capping regulates fibroblast motility. *Cell* 109, 509-521.
- [67] Skoble, J., Auerbuch, V., Goley, E. D., Welch, M. D., et al. (2001) Pivotal role of VASP in Arp2/3 complex-mediated actin nucleation, actin branch-formation, and *Listeria monocytogenes* motility. *J Cell Biol* 155, 89-100.
- [68] Barzik, M., Kotova, T. I., Higgs, H. N., Hazelwood, L., et al. (2005) Ena/VASP proteins enhance actin polymerization in the presence of barbed end capping proteins. *J Biol Chem* 280, 28653-28662.
- [69] Reinhard, M., Jouvenal, K., Tripier, D., Walter, U. (1995) Identification, purification, and characterization of a zyxin-related protein that binds the focal adhesion and microfilament protein VASP (vasodilator-stimulated phosphoprotein). *Proc Natl Acad Sci USA* 92, 7956-7960.
- [70] Brindle, N. P., Holt, M. R., Davies, J. E., Price, C. J., et al. (1996) The focal-adhesion vasodilator-stimulated phosphoprotein (VASP) binds to the proline-rich domain in vinculin. *Biochem J* 318,753–757.
- [71] Krause, M., Dent, E. W., Bear, J. E., Loureiro, J. J., et al. (2003) Ena/VASP proteins: regulators of the actin cytoskeleton and cell migration. *Annu Rev Cell Dev Biol* 19, 541-564.
- [72] Harbeck, B., Hüttelmaier, S., Schluter, K., Jockusch, B. M., et al. (2000) Phosphorylation of the vasodilator-stimulated phosphoprotein regulates its interaction with actin. *J Biol Chem* 275, 30817-30825.
- [73] Blume, C., Benz, P. M., Walter, U., Ha, J., et al. (2007) AMP-activated protein kinase impairs endothelial actin cytoskeleton assembly by phosphorylating vasodilator-stimulated phosphoprotein. *J Biol Chem* 282, 4601-4612.
- [74] Howe, A. K., Hogan, B. P., Juliano, R. L. (2002) Regulation of vasodilator-stimulated phosphoprotein phosphorylation and interaction with Abl by protein kinase A and cell adhesion. *J Biol Chem* 277, 38121-38126.
- [75] Halbrügge, M., Friedrich, C., Eigenthaler, M., Schanzenbacher, P., et al. (1990) Stoichiometric and reversible phosphorylation of a 46-kDa protein in human platelets in response to cGMP- and cAMP-elevating vasodilators. *J Biol Chem* 265, 3088-3093.
- [76] Zahedi, R. P., Lewandrowski, U., Wiesner, J., Wortelkamp, S., et al. (2008) Phosphoproteome of resting human platelets. *J Proteome Res* 7, 526-534.
- [77] Rink, T. J., Sage, S. O. (1990) Calcium signaling in human platelets. *Annu Rev Physiol* 52, 431-449.
- [78] Hathaway, D. R., Adelstein, R. S. (1979) Human platelet myosin light chain kinase requires the calcium-binding protein calmodulin for activity. *Proc Natl Acad Sci USA* 76, 1653-1657.
- [79] Shattil, S. J., Brass, L. F. (1987) Induction of the fibrinogen receptor on human platelets by intracellular mediators. *J Biol Chem* 262, 992-1000.
- [80] Brune, B., Ullrich, V. (1991) Different calcium pools in human platelets and their role in thromboxane A₂ formation. *J Biol Chem*, 266, 19232-19237.

- [81] Cavallini, L., Coassin, M., Alexandre, A. (1995) Two classes of agonist-sensitive calcium stores in platelets, as identified by their differential sensitivity to 2,5-di-(tert-butyl)-1,4-benzohydroquinone and thapsigargin. *Biochem J* 2, 449-52.
- [82] Papp, B., Enyedi, A., Kovacs, T., Sarkadi, B., et al. (1991) Demonstration of two forms of calcium pumps by thapsigargin inhibition and radio-immuno blotting in platelet membrane vesicles. *J Biol Chem*, 266, 14593-14596.
- [83] Enouf, J., Bredoux, R., Papp, B., Djaffar, I., et al. (1992) Human platelets express the SERCA2-b isoform of Ca (2+)-transport ATPase. *Biochem J* 1, 135-140.
- [84] El-Daher, S. S., Patel, Y., Siddiqua, A., Hassock, S., et al. (2000) Distinct localization and function of (1, 4, 5) IP (3) receptor subtypes and the (1, 3, 4, 5) IP (4) receptor GAP1 (IP4BP) in highly purified human platelet membranes. *Blood* 95, 3412-3422.
- [85] Varga-Szabo, D., Braun, A., Nieswandt, B. (2009) Calcium signaling in platelets. *J Thromb Haemost*, 7, 1057-1066.
- [86] Sage, S. O., Yamoah, E. H., Heemskerk, J. W. (2000) The roles of P(2X1) and P(2TAC) receptors in ADP-evoked calcium signalling in human platelets. *Cell Calcium* 28, 119-126.
- [87] Hassock, S. R., Zhu, M. X., Trost, C., Flockerzi, V., et al. (2002) Expression and role of TRPC proteins in human platelets: evidence that TRPC6 forms the store independent calcium entry channel. *Blood* 100, 2801-2811.
- [88] Muik, M., Frischauf, I., Derler, I., Fahrner, M., et al. (2008) Dynamic coupling of the putative coiled-coil domain of ORAI1 with STIM1 mediates ORAI1 channel activation. *J Biol Chem* 283, 8014-8022.
- [89] Prakriya, M., Lewis, R. S. (2003) CRAC channels: activation, permeation, and the search for a molecular identity. *Cell Calcium* 33, 311-21.
- [90] Roos, J., DiGregorio, P. J., Yeromin, A. V., Ohlsen, K., et al. (2005) STIM1, an essential and conserved component of store-operated Ca²⁺ channel function. *J Cell Biol* 169, 435-445.
- [91] Liou, J., Kim, M. L., Heo, W. D., Jones, J. T., et al. (2005) STIM is a Ca²⁺ sensor essential for Ca²⁺ store-depletion-triggered Ca²⁺ influx. *Curr Biol* 15, 1235-1241.
- [92] Zhang, S. L., Yu, Y., Roos, J., Kozak, J. A., et al. (2005) STIM1 is a Ca²⁺ sensor that activates CRAC channels and migrates from the Ca²⁺ store to the plasma membrane. *Nature* 437, 902-905.
- [93] Feske, S., Gwack, Y., Prakriya, M., Srikanth, S., et al. (2006) A mutation in Orai1 causes immune deficiency by abrogating CRAC channel function. *Nature* 441, 179-185.
- [94] Prakriya, M., Feske, S., Gwack, Y., Srikanth, S., et al. (2006) Orai1 is an essential pore subunit of the CRAC channel. *Nature* 443, 230-233.
- [95] Stathopoulos, P. B., Mitsuhiro, I. (2010) Partial unfolding and oligomerization of stromal interaction molecules as an initiation mechanism of store operated calcium entry. *Biochem Cell Biol* 88, 175-183.
- [96] Bergmeier, W., Stefanini, L. (2009) Novel molecules in calcium signaling in platelets. *J Thromb Haemost* 7, 187-190.

- [97] Grosse, J., Braun, A., Varga-Szabo, D., Beyersdorf, N., et al. (2007) An EF hand mutation in Stim1 causes premature platelet activation and bleeding in mice. *J Clin Invest* 117, 3540-3550.
- [98] Stathopoulos, P. B., Zheng, L., Li, G. Y., Plevin, M. J., et al. (2008) Structural and mechanistic insights into STIM1-mediated initiation of store-operated calcium entry. *Cell* 135, 110-122.
- [99] Cai, X., Cookson, M. (2007) Molecular evolution and functional divergence of the Ca²⁺ sensor protein in store-operated Ca²⁺ entry: stromal interaction molecule. *PLoS One* 2, e609.
- [100] Tolhurst, G., Carter, R. N., Amisten, S., Holdich, J. P., et al. (2008) Expression profiling and electrophysiological studies suggest a major role for Orai1 in the store-operated Ca²⁺ influx pathway of platelets and megakaryocytes. *Platelets* 19, 308-313.
- [101] Braun, A., Varga-Szabo, D., Kleinschnitz, C., Pleines, I., et al. (2009) Orai1 (CRACM1) is the platelet SOC channel and essential for pathological thrombus formation. *Blood* 113, 2056-2063.
- [102] Lis, A., Peinelt, C., Beck, A., Parvez, S., et al. (2007) CRACM1, CRACM2, and CRACM3 are store-operated Ca²⁺ channels with distinct functional properties. *Curr Biol* 17, 794-800.
- [103] Roberts-Thomson, S. J., Peters, A. A., Grice, D. M., Monteith, G. P. (2010) ORAI-mediated calcium entry: Mechanism and roles, diseases and pharmacology. *Pharmacology & Therapeutics* 127, 121-130.
- [104] Ji, W., Xu, P., Li, Z., Lu, J., et al. (2008) Functional stoichiometry of the unitary calcium-release-activated calcium channel. *Proc Natl Acad Sci USA* 105, 13668-13673.
- [105] Penna, A., Demuro, A., Yeromin, A. V., Zhang, S. L., et al. (2008) The CRAC channel consists of a tetramer formed by Stim-induced dimerization of Orai dimers. *Nature* 456, 116-120.
- [106] Maruyama, Y., Ogura, T., Mio, K., Kato, K., et al. (2009) Tetrameric Orai1 is a teardrop-shaped molecule with a long, tapered cytoplasmic domain. *J Biol Chem* 284, 13676-13685.
- [107] Wu, M. M., Buchanan, J., Luik, R. M., Lewis, R. S. (2006) Ca²⁺ store depletion causes STIM1 to accumulate in ER regions closely associated with the plasma membrane. *J Cell Biol* 174, 803-813.
- [108] Xu, P., Lu, J., Li, Z., Yu, X., et al. (2006) Aggregation of STIM1 underneath the plasma membrane induces clustering of Orai1. *Biochem Biophys Res Commun* 350, 969-976.
- [109] Várnai, P., Tóth, B., Tóth, D. J., Hunyady, L., et al. (2007) Visualization and manipulation of plasma membrane-endoplasmic reticulum contact sites indicates the presence of additional molecular components within the STIM1-Orai1 complex. *J Biol Chem* 282, 29678-29690.
- [110] Muik, M., Fahrner, M., Derler, I., Schindl, R., et al. (2009) A cytosolic homomerization and a modulatory domain within STIM1 C terminus determine coupling to ORAI1 channels. *J Biol Chem* 284, 8421-8426.
- [111] Park, C. Y., Hoover, P. J., Mullins, F. M., Bachhawat, P., et al. (2009) STIM1 clusters and activates CRAC channels via direct binding of a cytosolic domain to Orai1. *Cell* 136, 876-890.
- [112] Markham, K., Bai, Y., Schmitt-Ulms, G. (2007) Co-immunoprecipitations revisited: an update on experimental concepts and their implementation for sensitive interactome investigations of endogenous proteins. *Anal Bioanal Chem* 389, 461-473.
- [113] Kaboord, B., Perr, M. (2008) Isolation of proteins and protein complexes by immunoprecipitation. *Methods Mol Biol* 424, 349-364.

- [114] Miernyk, J. A., Thelen, J. J. (2008) Biochemical approaches for discovering protein-protein interactions. *Plant J* 53, 597-609.
- [115] Nisnevitch, M., Firer, M. A. (2001) The solid phase in affinity chromatography: strategies for antibody attachment. *J Biochem Biophys Methods* 49, 467-480.
- [116] Turková, J. (1999) Oriented immobilization of biologically active proteins as a tool for revealing protein interactions and function. *J Chromatogr B Biomed Sci Appl* 722, 11-31.
- [117] Sisson, T. H., Castor, C. W. (1990) An improved method for immobilizing IgG antibodies on protein A-agarose. *J Immunol Methods* 127, 215-220.
- [118] Ford, C. F., Suominen, I., Glatz, C. E. (1991) Fusion tails for the recovery and purification of recombinant proteins. *Protein Expr Purif* 2, 95-107.
- [119] Waugh, D. S. (2005) Making the most of affinity tags. *Trends Biotechnol* 23, 316-320.
- [120] Arnau, J., Lauritzen, C., Petersen, G. E., Pedersen, J. (2006) Current strategies for the use of affinity tags and tag removal for the purification of recombinant proteins. *Protein Expr Purif* 48, 1-13.
- [121] Lee, W. C., Lee, K. H. (2004) Applications of affinity chromatography in proteomics. *Anal Biochem* 324, 1-10.
- [122] Azarkan, M., Huet, J., Baeyens-Volant, D., Looze, Y., et al. (2007) Affinity chromatography: a useful tool in proteomics studies. *J Chromatogr B Analyt Technol Biomed Life Sci* 849, 81-90.
- [123] Muronetz, V. I., Sholukh, M., Korpela, T. (2001) Use of protein-protein interactions in affinity chromatography. *J Biochem Biophys Methods* 49, 29-47.
- [124] Kellogg, D. R., Moazed, D. (2002) Protein- and immunoaffinity purification of multiprotein complexes. *Methods Enzymol* 351, 172-83.
- [125] Terpe, K. (2003) Overview of tag protein fusions: from molecular and biochemical fundamentals to commercial systems. *Appl Microbiol Biotechnol*, 60, 523-533.
- [126] Harper, S., Speicher, D. W. (2011) Purification of proteins fused to glutathione S-transferase. *Methods Mol Biol* 681, 259-280.
- [127] Xu, X., Song, Y., Li, Y., Chang, J., et al. (2010) The tandem affinity purification method: an efficient system for protein complex purification and protein interaction identification. *Protein Expr Purif* 72, 149-156.
- [128] Gaberc-Porekar, V., Menart, V. (2001) Perspectives of immobilized-metal affinity chromatography. *J Biochem Biophys Methods* 49, 335-360.
- [129] Block, H., Maertens, B., Spiestersbach, A., Brinker, N., et al. (2009) Immobilized-metal affinity chromatography (IMAC): a review. *Methods Enzymol*, 463, 439-473.
- [130] Brymora, A., Valova, V. A, Robinson, P. J. (2004) Protein-protein interactions identified by pull-down experiments and mass spectrometry. *Curr Protoc Cell Biol* 17.5.
- [131] Guan, H., Kiss-Toth, E. (2008) Advanced technologies for studies on protein interactomes. *Adv Biochem Eng Biotechnol* 110, 1-24.
- [132] Mori, S., Barth, H. G. (1999) Size exclusion chromatography. 1st edn. Springer Verlag, Berlin, 4ff.

- [133] Lottspeich, F., Engels, J. W. (2006) *Bioanalytik*. 2nd edn. Spektrum Akademischer Verlag, Elsevier GmbH, München, 231ff.
- [134] Graves, P. R., Haystead, T. A. (2002) Molecular biologist's guide to proteomics. *Microbiol Mol Biol Rev* 66, 39-63.
- [135] Perkins, D. N., Pappin, D. J., Creasy, D. M., Cottrell, J. S. (1999) Probability-based protein identification by searching sequence databases using mass spectrometry data. *Electrophoresis* 20, 3551-3567.
- [136] Martens, L., van Damme, P., van Damme, J., Staes, A., et al. (2005) The human platelet proteome mapped by peptide-centric proteomics: a functional protein profile. *Proteomics* 5, 3193-3204.
- [137] Schütte, H., Kula, M. R. (1990) Pilot- and process-scale techniques for cell disruption. *Biotechnol Appl Biochem* 12, 599-620.
- [138] Benov, L., Al-Ibraheem, J. (2002) Disrupting *Escherichia coli*: a comparison of methods. *J Biochem Mol Biol* 35, 428-431.
- [139] Vedyappan, G., Bikandi, J., Braley, R., Chaffin, W. L. (2000) Cell surface proteins of *Candida albicans*: preparation of extracts and improved detection of proteins. *Electrophoresis* 21, 956-961.
- [140] Naglak, T. J., Hettwer, D. J., Wang, H. Y. (1990) Chemical permeabilization of cells for intracellular product release. *Bioprocess Technol* 9, 177-205.
- [141] Falconer, R. J., O'Neill, B. K., Middelberg, A. P. (1998) Chemical treatment of *Escherichia coli*. II. Direct extraction of recombinant protein from cytoplasmic inclusion bodies in intact cells. *Biotechnol Bioeng* 57, 381-386.
- [142] Linke, D. (2009) Detergents: an overview. *Methods Enzymol* 463, 603-617.
- [143] Shapiro, A. L., Vinuela, E., Maizel, J.V. jr. (1967) Molecular weight estimation of polypeptide chains by electrophoresis in SDS-polyacrylamide gels. *Biochem Biophys Res Commun* 28, 815-820.
- [144] Rabilloud, T. (1999) Solubilization of proteins in 2-D electrophoresis. *Methods Mol Biol* 112, 9-19.
- [145] O'Farrell, P.H. (1975) High resolution two-dimensional electrophoresis of proteins. *J Biol Chem* 250, 4007-4021.
- [146] Görg, A., Weiss, W., Dunn, M. J. (2004) Current two-dimensional electrophoresis technology for proteomics. *Proteomics* 4, 3665-3685.
- [147] Steinberg, T. H. (2009) Protein gel staining methods: an introduction and overview. *Methods Enzymol* 463, 541-563.
- [148] Barrett, A. J., Rawlings, N. D. (1995) Families and clans of serine peptidases. *Arch Biochem Biophys* 318, 247-250.
- [149] Olsen, J. V., Ong, S. E., Mann, M. (2004) Trypsin cleaves exclusively C-terminal to arginine and lysine residues. *Mol Cell Proteomics* 3, 608-614.
- [150] Cleland, W. W. (1964) Dithiothreitol, a new protective reagent for SH groups. *Biochemistry* 3, 480-482.

- [151] Voet D., Voet J.G. (2004) *Biochemistry*. 3rd. edn. John Wiley and Sons Inc., Hoboken, 133.
- [152] Mitulovic, G., Mechtler, K. (2006) HPLC techniques for proteomics analysis - a short overview of latest developments. *Brief Funct Genomic Proteomic* 5, 49-60.
- [153] Peng, J., Gygi, S. P. (2001) Proteomics: the move to mixtures. *J Mass Spectrom* 36, 1083-1091.
- [154] Lottspeich, F., Engels, J. W. (2006) *Bioanalytik*. 2nd edn. Spektrum Akademischer Verlag, Elsevier GmbH, München, 217.
- [155] Voet D., Voet J.G. (2004) *Biochemistry*. 3rd. edn. John Wiley and Sons Inc., Hoboken, 134.
- [156] Lottspeich, F., Engels, J. W. (2006) *Bioanalytik*. 2nd edn. Spektrum Akademischer Verlag, Elsevier GmbH, München, 223 ff.
- [157] Gruber, K. A., Stein, S., Brink, L., Radhakrishnan, A., et al. (1976) Fluorometric assay of vasopressin and oxytocin: a general approach to the assay of peptides in tissues. *Proc Natl Acad Sci USA* 73, 1314-1318.
- [158] von Hagen, J. (2008) *Proteomics sample preparation*. 1st edn. Wiley-VCH Verlag GmbH & Co KGaA, Weinheim, 56.
- [159] Wolters, D. A., Washburn, M. P., Yates, J. R. 3rd (2001) An automated multidimensional protein identification technology for shotgun proteomics. *Anal Chem* 73, 5683-5690.
- [160] Fournier, M. L., Gilmore, J. M., Martin-Brown, S. A., Washburn, M. P. (2007) Multidimensional separation-based shotgun proteomics. *Chem Rev* 107, 3654-3686.
- [161] Banks, J. F. Jr., Quinn, J. P., Whitehouse, C. M. (1994) LC/ESI-MS determination of proteins using conventional liquid chromatography and ultrasonically assisted electrospray. *Anal Chem* 66, 3688-3695.
- [162] Robertson, D. H., Hurst, J. L., Bolgar, M. S., Gaskell, S. J., et al. (1997) Molecular heterogeneity of urinary proteins in wild house mouse populations. *Rapid Commun Mass Spectrom* 11, 786-790.
- [163] Karas, M., Hillenkamp, F. (1988) Laser desorption ionization of proteins with molecular masses exceeding 10,000 daltons. *Anal Chem* 60, 2299-2301
- [164] Beavis, R. C., Chait, B. T. (1996) Matrix-assisted laser desorption ionization mass-spectrometry of proteins. *Methods Enzymol* 270, 519-551.
- [165] Sickmann, A., Mreyen, M., Meyer, H. E. (2003) Mass spectrometry – a key technology in proteome research. *Adv Biochem Eng Biotechnol* 83, 141-176.
- [166] Marshall, A. G., Hendrickson, C. L. (2002) Fourier transform ion cyclotron resonance detection: principles and experimental configurations. *Int J Mass Spectrom* 215, 59.
- [167] Scigelova, M., Makarov, A. (2006) Orbitrap mass analyzer - overview and applications in proteomics. *Proteomics* 6, 16-21.
- [168] Makarov, A., Denisov, E., Lange, O., Horning, S. (2006) Dynamic range of mass accuracy in LTQ Orbitrap hybrid mass spectrometer. *J Am Soc Mass Spectrom* 17, 977-982.
- [169] Makarov, A., Denisov, E., Kholomeev, A., Balschun, W., et al. (2006) Performance evaluation of a hybrid linear ion trap/orbitrap mass spectrometer. *Anal Chem* 78, 2113-2120.
- [170] Matsuura, S., Umebayashi, S., Okuyama, C., Oba, K., et al. (1985) Characteristics of the newly developed MCP and its assembly. *IEEE Trans* 32, 350.

- [171] Dubois, F., Knochenmuss, R., Zenobi, R., Brunelle, A., et al. (1999) A comparison between ion-to-photon and microchannel plate detectors. *Rapid Commun Mass Spectrom* 13, 786-791.
- [172] Fenn, J. B., Mann, M., Meng, C. K., Wong, S. F., et al. (1989) Electrospray ionization for mass spectrometry of large biomolecules. *Science* 246, 64-71.
- [173] Siethoff, C., Lohaus, C., Meyer H. E. (1999) *Microcharacterization of proteins*. 2nd edn. VCH-Wiley Verlagsgesellschaft, Weinheim, 245-273.
- [174] Dole, M., Mack, L. L., Hines, R. L., Mobley, R. C., et al. (1968) Molecular beams of macroions. *J Chem Phys* 49, 2240-2249.
- [175] Schmelzeisen-Redeker, G., Bütfering, L., Röllgen, F. W. (1989) Desolvation of ions and molecules in thermospray mass spectrometry. *Int J Mass Spectrom Ion Processes* 90, 139-150.
- [176] Iribarne, J. V, Thomson, B. A. (1976) On the evaporation of small ions from charged droplets. *J Phys Chem* 64, 2287-2293.
- [177] Smith, R. D., Loo, J. A., Edmonds, C. G., Barinaga, C. J., et al. (1990) New developments in biochemical mass spectrometry: electrospray ionization. *Anal Chem* 62, 882-899.
- [178] Schaefer, H., Chervet, J. P., Bunse, C., Joppich, C., et al. (2004) A peptide preconcentration approach for nano-high-performance liquid chromatography to diminish memory effects. *Proteomics* 4, 2541-2544.
- [179] Niessen, W. M., Tinke, A. (1995) Liquid chromatography-mass spectrometry. General principles and instrumentation. *J Chromatography* 703, 37-57.
- [180] Lottspeich, F., Engels, J. W. (2006) *Bioanalytik*. 2nd edn. Spektrum Akademischer Verlag, Elsevier GmbH, München, 357 ff.
- [181] de Hoffmann, E. (1996) Tandem mass spectrometry: A primer. *J Mass Spectrom* 31, 129-137.
- [182] Siethoff, C., Lohaus, C., Meyer H. E. (1999) *Microcharacterization of proteins*. 2nd edn. VCH-Wiley Verlagsgesellschaft, Weinheim, 252.
- [183] Stafford, G. C., Kelley, P. E., Syka, J. E. P., Reynolds, W. E., et al. (1984) Recent improvements in and analytical applications of advanced ion trap technology. *Int J Mass Spectrom* 60, 85-98.
- [184] Lottspeich, F., Engels, J. W. (2006) *Bioanalytik*. 2nd edn. Spektrum Akademischer Verlag, Elsevier GmbH, München, 361.
- [185] Douglas, D. J., Frank, A. J., Mao, D. (2005) Linear ion traps in mass spectrometry. *Mass Spectrom Rev* 24, 1-29.
- [186] Schwartz, J. C., Senko, M. W., Syka, J. E. P. (2002) A two-dimensional quadrupole ion trap mass spectrometer. *J Am Soc Mass Spectrom* 13, 659-669.
- [187] Roepsdorff, P., Fohlmann, J. (1984) Proposal for common nomenclature for sequence ions in mass spectra of peptides. *Biomed Mass Spectrom* 11, 601.
- [188] Biemann, K. (1992) Mass spectrometry of peptides and proteins. *Annu Rev Biochem* 61, 977-1010.
- [189] Steen, H., Mann, M. (2004) The ABC's (and XYZ's) of peptide sequencing. *Nat Rev Mol Cell Biol* 5, 699-711.

- [190] Eng, J. K., McCormack, A. L., Yates, J. R. 3rd. (1994) An approach to correlate tandem mass spectral data of peptides with amino acid sequences in a protein database. *J Am Soc Mass Spectrom* 5, 976-989.
- [191] Geer, L. Y., Markey, S. P., Kowalak, J. A., Wagner, L., et al. (2004) Open mass spectrometry search algorithm. *J Proteome Res* 3, 958-964.
- [192] Kapp, E., Schütz, F. (2007) Overview of tandem mass spectrometry (MS/MS) database search algorithms. *Curr Protoc Protein Sci* 49, 25.2.1-25.2.19.
- [193] Craig, R., Beavis, R. C. (2004) TANDEM: Matching proteins with tandem mass spectra. *Bioinformatics* 20, 1466-1467.
- [194] Sadygov, R. G., Cociorva, D., Yates, J. R. 3rd (2004) Large-scale database searching using tandem mass spectra: looking up the answer in the back of the book. *Nat Methods* 1, 195-202.
- [195] Cagney, G., Amiri, S., Premawaradena, T., Lindo, M., et al. (2003) In silico proteome analysis to facilitate proteomics experiments using mass spectrometry. *Proteome Sci* 13, 5.
- [196] Stephan, C., Reidegeld, K. A., Hamacher, M., van Hall, A., et al. (2006) Automated reprocessing pipeline for searching heterogeneous mass spectrometric data of the HUPO Brain Proteome Project pilot phase. *Proteomics* 6, 5015-5029.
- [197] Elias, J. E., Haas, W., Faherty, B. K., Gygi, S. P. (2005) Comparative evaluation of mass spectrometry platforms used in large-scale proteomics investigations. *Nat Methods* 2, 667-675.
- [198] Elias, J. E., Gygi, S. P. (2007) Target-decoy search strategy for increased confidence in large-scale protein identifications by mass spectrometry. *Nat Methods* 4, 207-214.
- [199] Benz, P. M., Blume, C., Moebius, J., Oschatz, C., et al. (2008) Cytoskeleton assembly at endothelial cell-cell contacts is regulated by alpha II-spectrin-VASP complexes. *J Cell Biol* 180, 205-219.
- [200] Blum, H., Beier, H., Gross, H. J. (1987) Improved silver staining of plant proteins, RNA and DNA in polyacrylamide gels. *Electrophoresis* 8, 93-99.
- [201] Lakey, A., Labeit, S., Gautel, M., Ferguson, C., et al. (1993) Kettin, a large modular protein in the Z-disc of insect muscles. *EMBO J* 12, 2863-2871.
- [202] DuVerle, D. A., Ono, Y., Sorimachi, H., Mamitsuka, H. (2011) Calpain cleavage prediction using multiple kernel learning. *PLoS One* 6, e19035, 1-9.
- [203] Haffner, C., Jarchau, T., Reinhard, M., Hoppe, J., et al. (1995) Molecular cloning, structural analysis and functional expression of the proline-rich focal adhesion and microfilament-associated protein VASP. *EMBO J* 14, 19-27.
- [204] Herwald, H., Dedio, J., Kellner, R., Loos, M., et al. (1996) Isolation and characterization of the kininogen-binding protein p33 from endothelial cells. Identity with the gC1q receptor. *J Biol Chem* 271, 13040-13047.
- [205] Benz, P. M., Feller, S. M., Sickmann, A., Walter, U., et al. (2008) Prostaglandin-induced VASP phosphorylation controls alpha II-spectrin breakdown in apoptotic cells. *Int Immunopharmacol* 8, 319-324.
- [206] Novy, R., Drott, D., Yaeger, K., Mierendorf, R. (2001) Overcoming the codon bias of E.coli for enhanced protein expression. *InNovations* 12, 1-3.

- [207] Phizicky, E. M., Fields, S. (1995) Protein-protein interactions: methods for detection and analysis. *Microbiol Rev* 59, 94-123.
- [208] Debeljak, N., Feldman, L., Davis, K. L., Komel, R., et al. (2006) Variability in the immunodetection of His-tagged recombinant proteins. *Anal Biochem* 359, 216-223.
- [209] Lehman, W., Hatch, V., Korman, V., Rosol M., et al. (2000) Tropomyosin and actin isoforms modulate the localization of tropomyosin strands on actin filaments. *J Mol Biol* 302, 593-606.
- [210] Ono, S., Ono K. (2002) Tropomyosin inhibits ADF/cofilin-dependent actin filament dynamics. *J Cell Biol* 156, 1065-1076.
- [211] Sun, H. Q., Yamamoto, M., Mejillano, M., Yin, H. L. (1999) Gelsolin, a multifunctional actin regulatory protein. *J Biol Chem* 274, 33179-33182.
- [212] Weber, A., Pennise, C. R., Babcock, G. G., Fowler, V. M. (1994) Tropomodulin caps the pointed ends of actin filaments. *J Cell Biol* 127, 1627-1635.
- [213] Bauer, K., Kratzer, M., Otte, M., de Quintana, K. L., et al. (2000) Human CLP36, a PDZ-domain and LIM-domain protein, binds to alpha-actinin-1 and associates with actin filaments and stress fibers in activated platelets and endothelial cells. *Blood* 96, 4236-4245.
- [214] Vallenius, T., Luukko, K., Makela, T. P. (2000) CLP-36 PDZ-LIM protein associates with nonmuscle alpha-actinin-1 and alpha-actinin-4. *J Biol Chem* 275, 11100-11105.
- [215] Chakrabarti, A., Kelkar, D. A., Chattopadhyay, A. (2006) Spectrin organization and dynamics: new insights. *Biosci Rep* 26, 369-386.
- [216] Burn, P., Kupfer, A., Singer, S. J. (1988) Dynamic membrane-cytoskeletal interactions: specific association of integrin and talin arises in vivo after phorbol ester treatment of peripheral blood lymphocytes. *Proc Natl Acad Sci USA* 85, 497-501.
- [217] Escolar, G., Diaz-Ricart, M., White, J. G. (1995) Talin does not associate exclusively with alpha 2b beta 3 integrin in activated human platelets. *J Lab Clin Med* 125, 597-607.
- [218] Peng, X., Nelson, E. S., Maiers, J. L., DeMali, K. A. (2011) New insights into vinculin function and regulation. *Int Rev Cell Mol Biol* 287, 191-231.
- [219] Nakamura, F., Pudas, R., Heikkinen, O., Permi, P., et al. (2006) The structure of the GPIIb-filamin A complex. *Blood* 107, 1925-1932.
- [220] Andrews, R. K., López, J. A., Berndt, M. C. (1997) Molecular mechanisms of platelet adhesion and activation. *Int J Biochem Cell Biol* 29, 91-105.
- [221] Calvete, J. J. (1995) On the structure and function of platelet integrin alpha IIb beta 3, the fibrinogen receptor. *Proc Soc Exp Biol Med* 208, 346-360.
- [222] Shattil, S. J. (1999) Signaling through platelet integrin alpha IIb beta 3: inside-out, outside-in, and sideways. *Thromb Haemost* 82, 318-325.
- [223] Lefort, C. T., Rossaint, J., Moser, M., Petrich, B. G., et al. (2012) Distinct roles for talin-1 and kindlin-3 in LFA-1 extension and affinity regulation. *Blood*, Epub ahead of print.
- [224] Wu, C. (2004) The PINCH-ILK-parvin complexes: assembly, functions and regulation. *Biochim Biophys Acta* 1692, 55-62.
- [225] Wickström, S. A., Lange, A., Montanez, E., Fässler, R. (2010) The ILK/PINCH/parvin complex: the kinase is dead, long live the pseudokinase! *EMBO J* 29, 281-291.

- [226] Huang, M. M., Bolen, J. B., Barnwell, J. W., Shattil, S. J., et al. (1991) Membrane glycoprotein IV (CD36) is physically associated with the Fyn, Lyn, and Yes protein-tyrosine kinases in human platelets. *Proc Natl Acad Sci USA* 88, 7844-7848.
- [227] Zheng, M., Cheng, H., Banerjee, I., Chen, J. (2010) ALP/Enigma PDZ-LIM domain proteins in the heart. *J Mol Cell Biol* 2, 96-102.
- [228] Harris, B. Z., Lim, W. A. (2001) Mechanism and role of PDZ domains in signaling complex assembly. *J Cell Sci* 114, 3219-3231.
- [229] Long, J. F., Tochio, H., Wang, P., Fan, J. S., et al. (2003) Supramodular structure and synergistic target binding of the N-terminal tandem PDZ domains of PSD-95. *J Mol Biol* 327, 203-214.
- [230] Jani, K., Schock, F. (2007) Zasp is required for the assembly of functional integrin adhesion sites. *J Cell Biol* 179, 1583-1597.
- [231] Kadrmas, J. L., Beckerle, M. C. (2004) The LIM domain: from the cytoskeleton to the nucleus. *Nat Rev Mol Cell Biol* 5, 920-931.
- [232] Schaffar, G., Taniguchi, J., Brodbeck, T., Meyer, A. H., et al. (2008) LIM-only protein 4 interacts directly with the repulsive guidance molecule A receptor Neogenin. *J Neurochem* 107, 418-431.
- [233] Ponting, C. P., Phillips, C. (1995) DHR domains in syntrophins, neuronal NO synthases and other intracellular proteins. *Trends Biochem Sci* 20, 102-103.
- [234] Jemth, P., Gianni, S. (2007) PDZ domains: folding and binding. *Biochemistry* 46, 8701-8708.
- [235] Gill, G. N. (1995) The enigma of LIM domains. *Structure* 3, 1285-1289.
- [236] Zhang, Y., Tu, Y., Zhao, J., Chen, K., et al. (2009) Reversion-induced LIM interaction with Src reveals a novel Src inactivation cycle. *J Cell Biol* 184, 785-792.
- [237] Vallenius, T., Makela, T. P. (2002) Clik1: a novel kinase targeted to actin stress fibers by the CLP-36 PDZ-LIM protein. *J Cell Sci* 115, 2067-2073.
- [238] Kuroda, S., Tokunaga, C., Kiyohara, Y., Higuchi, O., et al. (1996) Protein-protein interaction of zinc finger LIM domains with protein kinase C. *J Biol Chem* 271, 31029-31032.
- [239] Cuppen, E., Gerrits, H., Pepers, B., Wieringa, B., et al. (1998) PDZ motifs in PTP-BL and RIL bind to internal protein segments in the LIM domain protein RIL. *Mol Biol Cell* 9, 671-683.
- [240] Wu, R.Y., Gill, G. N. (1994) LIM domain recognition of a tyrosine-containing tight turn. *J Biol Chem* 269, 25085-25090.
- [241] Xia, H., Winokur, S. T., Kuo, W. L., Altherr, M. R., et al. (1997). Actinin associated LIM protein: identification of a domain interaction between PDZ and spectrin-like repeat motifs. *J Cell Biol* 139, 507-515.
- [242] Te Velthuis, A. J., Bagowski, C. P. (2007) PDZ and LIM domain-encoding genes: molecular interactions and their role in development. *Scientific World Journal* 7, 1470-1492.
- [243] Kotaka, M., Ngai, S. M., Carcia-Barcelo, M., Tsui, S. K. W., et al. (1999) Characterization of the human 36-kDa carboxyl terminal LIM domain protein (hCLIM1). *J Cell Biochem* 72, 279-285.
- [244] Meyer, S. C., Zuerbig, S., Cunningham, C. C., Hartwig, J. H., et al. (1997) Identification of the region in actin-binding protein that binds to the cytoplasmic domain of glycoprotein IB alpha. *J Biol Chem* 272, 2914-2919.

- [245] Feng, S., Reséndiz, J. C., Lu, X., Kroll, M. H. (2003) Filamin A binding to the cytoplasmic tail of glycoprotein Ib alpha regulates von Willebrand factor-induced platelet activation. *Blood* 102, 2122-2129.
- [246] Williamson, D., Pikovski, I., Cranmer, S. L., Mangin, P., et al. (2002) Interaction between platelet glycoprotein Ib alpha and filamin-1 is essential for glycoprotein Ib/ IX receptor anchorage at high shear. *J Biol Chem* 277, 2151-2159.
- [247] Yap, C. L., Hughan, S. C., Cranmer, S. L., Nesbitt, W. S., et al. (2000) Synergistic adhesive interactions and signaling mechanisms operating between platelet glycoprotein Ib/ IX and integrin alpha IIb beta 3: studies in human platelets and transfected Chinese hamster ovary cells. *J Biol Chem* 275, 41377-41388.
- [248] Solum, N. O., Clemetson, K. J. (2005) The discovery and characterization of platelet GPIb. *J Thromb Haemost* 3, 1125-1132.
- [249] Podlubnaya, Z. A., Tskhovrebova, L. A., Zaalishsvili, M. M., Stefanenko, G. A. (1975) Electronmicroscopic study of alpha-actinin. *J Mol Biol* 92, 357-359.
- [250] Djinovic-Carugo, K., Young, P., Gaute I. M., Saraste, M. (1999) Structure of the alpha-actinin rod: molecular basis for cross-linking of actin filaments. *Cell* 98, 537-546.
- [251] Mimura, N., Asano, A. (1986) Isolation and characterization of a conserved actin-binding domain from rat hepatic actinogelin, rat skeletal muscle, and chicken gizzard alpha-actinins. *J Biol Chem* 261, 10680-10687.
- [252] Otey, C. A., Pavalko, F. M., Burrige, K. (1990) An interaction between alpha-actinin and the beta 1 integrin subunit in vitro. *J Cell Biol* 111, 721-729.
- [253] Morgan, A. J., Jacob, R. (1994) Ionomycin enhances Ca²⁺ influx by stimulating store-regulated cation entry and not by a direct action at the plasma membrane. *Biochem J* 300, 665-672.
- [254] Azam, M., Andrabi, S. S., Sahr, K. E., Kamath, L., et al. (2001) Disruption of the mouse mu-calpain gene reveals an essential role in platelet function. *Mol Cell Biol*. 21, 2213-20.
- [255] Croall, D. E., DeMartino, G. N. (1991) Calcium-activated neutral protease (calpain) system: structure, function, and regulation. *Physiol Rev* 71, 813-847.
- [256] Suzuki, K., Sorimachi, H., Yoshizawa, T., Kinbara, K., et al. (1995) Calpain: novel family members, activation, and physiologic function. *Biol Chem Hoppe Seyler* 376, 523-529.
- [257] Croce, K., Flaumenhaft, R., Rivers, M., Furie, B., et al. (1999) Inhibition of calpain blocks platelet secretion, aggregation, and spreading. *J Biol Chem* 274,36321-36327.
- [258] Potter, D. A., Tirnauer, J. S., Janssen, R., Croall, D. E., et al. (1998) Calpain regulates actin remodeling during cell spreading. *J Cell Biol* 141, 647-662.
- [259] Hayashi, M., Suzuki, H., Kawashima, S., Saido, T. C., et al. (1999) The behavior of calpain-generated N- and C-terminal fragments of talin in integrin-mediated signaling pathways. *Arch Biochem Biophys* 371, 133-141.
- [260] Nieswandt, B., Watson, S. P. (2003) Platelet-collagen interaction: is GPVI the central receptor? *Blood* 102, 449-461.

- [261] Tsuji, M., Ezumi, Y., Arai, M., Takayama, H. (1997) A novel association of Fc receptor gamma-chain with glycoprotein VI and their co-expression as a collagen receptor in human platelets. *J Biol Chem* 272, 23528-23531.
- [262] Gibbins, J. M., Okuma, M., Farndale, R., Barnes, M., et al. (1997) Glycoprotein VI is the collagen receptor in platelets which underlies tyrosine phosphorylation of the Fc receptor gamma-chain. *FEBS Lett* 413, 255-259.
- [263] Suzuki-Inoue, K., Tulasne, D., Shen, Y., Bori-Sanz, T., et al. (2002) Association of Fyn and Lyn with the proline-rich domain of glycoprotein VI regulates intracellular signaling. *J Biol Chem* 277, 21561-21566.
- [264] Watson, S. P., Auger, J. M., McCarty, O. J., Pearce, A. C. (2005) GPVI and integrin alpha IIb beta 3 signaling in platelets. *J Thromb Haemost* 3, 1752-1762.
- [265] Hassock, S. R., Zhu, M. X., Trost, C., Flockerzi, V., et al. (2002) Expression and role of TRPC proteins in human platelets: evidence that TRPC6 forms the store-independent calcium entry channel. *Blood* 100, 2801-2811.
- [266] Ramanathan, G., Gupta, S., Thielmann, I., Pleines, I., et al. (2011) Defective diacylglycerol-induced Ca²⁺ entry but normal agonist-induced activation responses in TRPC6-deficient mouse platelets. *J Thromb Haemost*, doi: 10.1111/j.1538-7836.2011.04596.x.
- [267] Gupta, S., Braun, A., Morowski, M., Premisler, T., et al. (2012) CLP36 is a negative regulator of GPVI signaling in platelets. *Circulation Research*, currently under submission.

7 Appendix

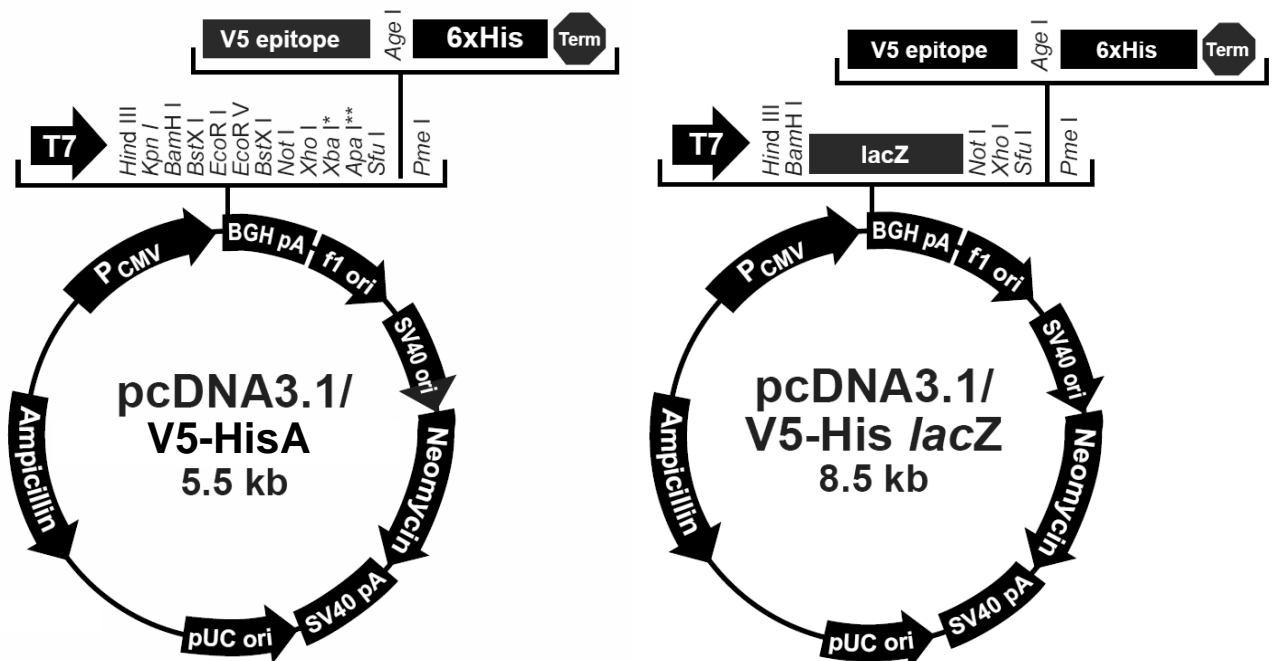
7.1 Vector maps

7.1.1 pcDNA3.1/V5-HisA and lacZ

MCS:

	T7 promoter/priming site				<i>Hind</i> III		<i>Kpn</i> I		<i>Bam</i> H I									
861	ATTAATACGA	CTCACTATAG	GGAGACCCAA	GCTGGCTAGT	TAA	GCT	TGG	TAC	CGA	GCT	CGG							
						Ala	Trp	Tyr	Arg	Ala	Arg							
			<i>Bst</i> X I*	<i>Eco</i> R I		<i>Eco</i> R V		<i>Bst</i> X I*		<i>Not</i> I								
922	ATC	CAC	TAG	TCC	AGT	GTG	GTG	GAA	TTC	TGC	AGA	TAT	CCA	GCA	CAG	TGG	CGG	CCG
	Ile	His	***	Ser	Ser	Val	Val	Glu	Phe	Cys	Arg	Tyr	Pro	Ala	Gln	Trp	Arg	Pro
	<i>Xho</i> I		<i>Xba</i> I		<i>Apa</i> I	<i>Sfu</i> I							V5 epitope					
976	CTC	GAG	TCT	AGA	GGG	CCC	TTC	GAA	GGT	AAG	CCT	ATC	CCT	AAC	CCT	CTC	CTC	GGT
	Leu	Glu	Ser	Arg	Gly	Pro	Phe	Glu	Gly	Lys	Pro	Ile	Pro	Asn	Pro	Leu	Leu	Gly
				<i>Age</i> I		Polyhistidine tag							<i>Pme</i> I					
1030	CTC	GAT	TCT	ACG	CGT	ACC	GGT	CAT	CAT	CAC	CAT	CAC	CAT	TGA	GTTTAAACCC			
	Leu	Asp	Ser	Thr	Arg	Thr	Gly	His	His	His	His	His	His	***				
				BGH Reverse priming site														
1083	GCTGATCAGC	CTCGACTGTG	CCTTCTAGTT	GCCAGCCAT														

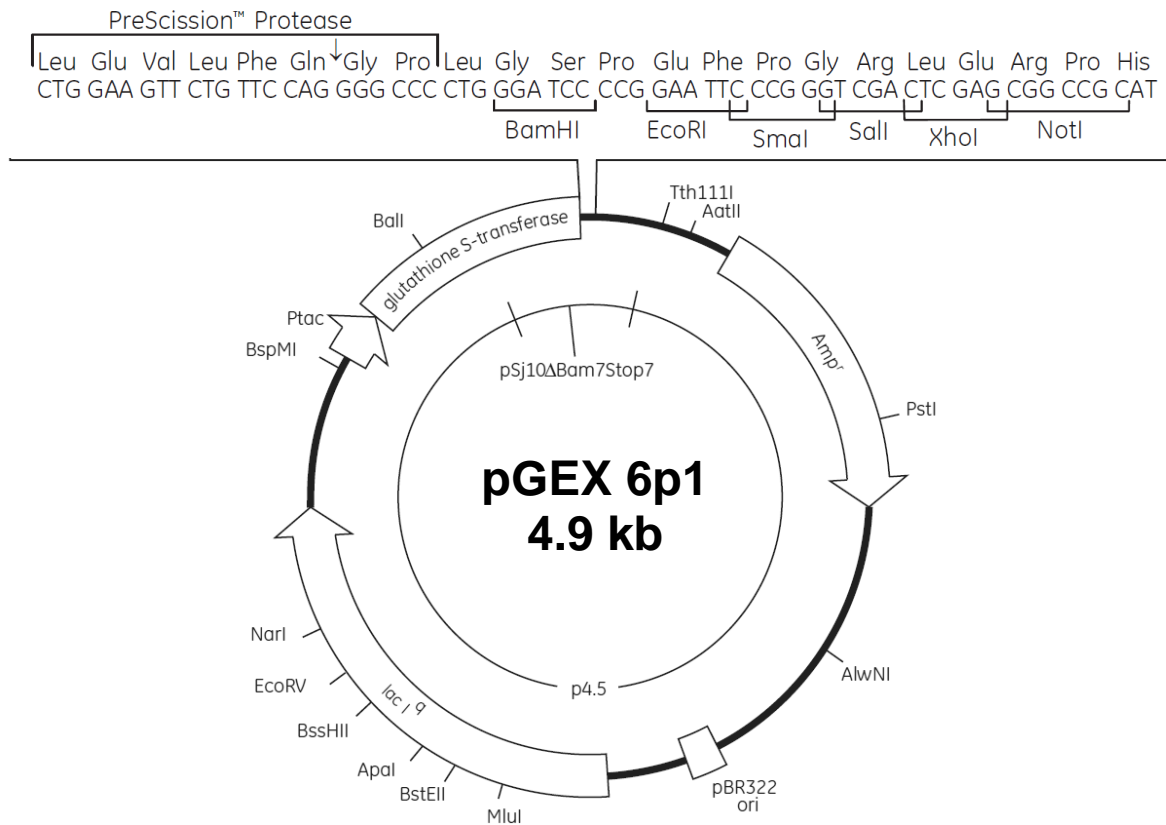
*Note that there are two *Bst*X I sites in the polylinker.



based on the Invitrogen user manuals

7.1.2 pGEX 6p1

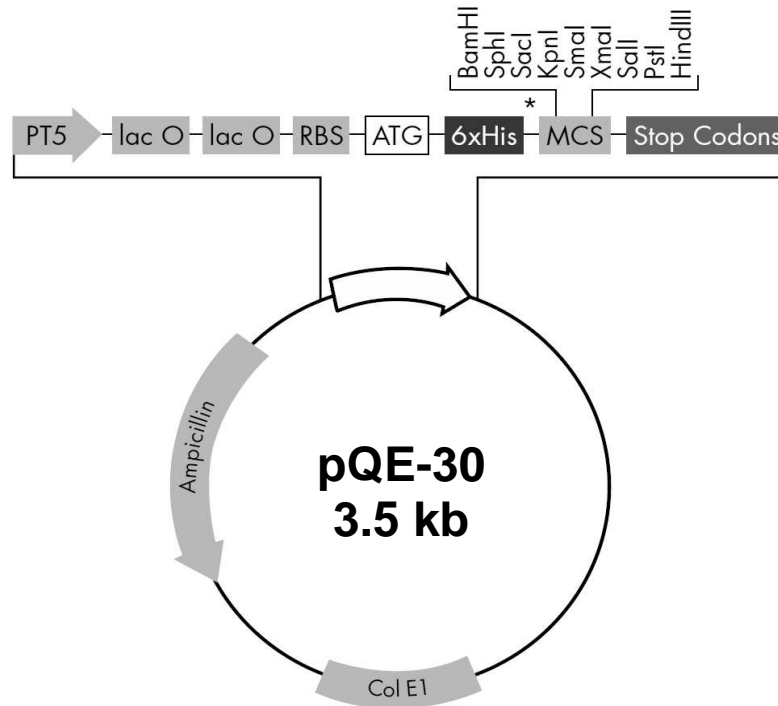
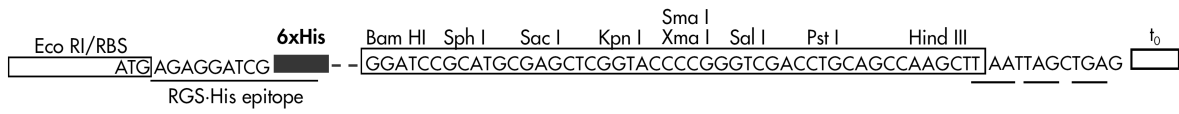
MCS:



based on the GE Healthcare user manuals

7.1.3 pQE-30

MCS:



based on the Qiagen user manuals

7.2 Applied full-length nt-sequences

7.2.1 *Homo sapiens* vasodilator-stimulated phosphoprotein (VASP), mRNA

NCBI reference sequence: NM_003370.3

Length 2298 nt. The coding sequence is marked in yellow.

```

1  tgtgggtgcg gggagtgga ttttggaaacg aaatgtaacg aagagaagta cagtagtaag
61  agtaaacactg tagccgccac cggcaagggg tgcgcgctgg ggagcggacg ctgcatcccc
121  tttctgctgc aggaacctct catcagaccg cctgagggaa gggcgcccg gagacccgcc
181  cggccccggt ccacattctc cccaggaagc cggactctat gggcggggac cctgggggag
241  cctgagccga gcccggagcc agccccgaac ccctgaacct ccagccaggg gcgccccggg
301  agcagccagc ccgtgggcga gccgcccgcc cgccgagcag ccatgagcga gacggtcatc
361  tgttccagcc gggccactgt gatgctttat gatgatggca acaagcgatg gctccctgct
421  ggcacgggtc cccaggcctt cagccgcgctc cagatctacc acaaccccac ggccaattcc
481  tttcgcgtcg tgggcggaa gatgcagccc gaccagcagg tggtcatcaa ctgtgccatc
541  gtccggggtg tcaagtataa ccaggccacc cccaacttcc atcagtggcg cgacgctcgc
601  caggtctggg gcctcaactt cggcagcaag gaggatgcgg cccagtttgc cgccggcatg
661  gccagtgcgc tagaggcgtt ggaaggaggt gggccccctc cacccccagc acttcccacc
721  tggtcggtcc cgaacggccc ctccccggag gaggtggagc agcagaaaag gcagcagccc
781  ggcccgtcgg agcacataga gcgccgggtc tccaatgcag gaggcccacc tgtccccccc
841  gctgggggtc cacccccacc accaggacct ccccctctc caggtcccc cccaccccc
901  ggtttgcccc cttcgggggt cccagctgca gcgcacggag cagggggagg accaccccct
961  gcacccccctc tcccggcagc acagggccct ggtggtgggg gagctggggc cccaggcctg
1021 gccgcagcta ttgctggagc caaactcagg aaagtgcagc agcaggagga ggcctcaggg
1081 gggcccacag cccccaaagc tgagagtgg cgaagcggag gtgggggact catggaagag
1141 atgaacgcca tgctggccc gagaaggaaa gccacgcaag ttggggagaa aacccccaa
1201 gatgaatctg ccaatcagga ggagccagag gccagagtcc cggcccagag tgaatctgtg
1261 cggagaccct gggagaagaa cagcacaacc ttgccaaag tgaagtctgc ttcttcgggtg
1321 accacttccg agacccaacc ctgcacgccc agctccagt attactcgga cctacagagg
1381 gtgaaacag agcttctgga agaggtgaag aaggaattgc agaaagtgaa agaggaaatc
1441 attgaagcct tcgtccagga gctgaggaag cggggttctc cctgaccaca gggaccaga
1501 agaccgcctt ctcctttccg cacaccggc ctgtcaccct gctttccctg cctctacttg
1561 acttggaaat ggctgaagac tacacaggaa tgcatcgctc ccactcccc tcccacttgg
1621 aaaactccaa gggggtgtgg cttccctgct cacaccaca ctggctgctg attggctggg
1681 gaggcccccg cccttttctc cctttggctc ttccccctc ccatccccct ggggccggtc
1741 cctctgctgg ggatgcacca atgaaccca caggaagggg gaaggaaagga gggaatttca
1801 cattcccttg ttctagatct actttaacgc ttaatgcctt caaagtcttg gtttttttaa
1861 gaaaaaaaa tatatatata tttgggtttt gggggaaaag ggaaattttt ttttctcttt
1921 ggttttgata aaatgggatg tgggagtttt taaagtctat agccctgggc ttgccccatt
1981 tggggcagct atthaagggg aggggatgtc tcaccgggct gggggtgaga tatccccca
2041 cccaggggac tccccttccc tctggctcct tccccttttc tatgaggaaa taagatgctg
2101 taactttttg gaacctcagt tttttgattt tttatttggg taggttttgg ggtccaggcc
2161 atttttttta ccccttggag gaaataagat gagggagaaa ggagaagggg aggaaacttc
2221 tcccctccca ccttcacctt tagcttcttg aaaatgggccc cctgcagaat aaatctgcca
2281 gtttttataa aaaaaaaa

```

7.2.2 *Homo sapiens* stromal interaction molecule 1 (STIM1), mRNA

NCBI reference sequence: NM_003156.3

Length 4062 nt. The coding sequence is marked in yellow.

```

1  ctggacctgg gcaccgccag ccgcctgggc acgggactgg gcggggggcgc tgacctcggc
61  ctaggaggcc caggatcccg gagacgcccg gcacctcagg accctgcggg tcgcacgcc
121  tccccagctt ctgctgctcg ccgctcttcg gcagggcgag gtcaggtgcc cccttctcgc
181  ctctcttctc ttctcttctc ttctctctcc acttctgtgc ccgcgagagc tccggccgcc
241  cccttccgca ggggtgtagt aatctgcgga gctgacagca gccccgcagc caccctgcc
301  gaagtctccg gaagcggcac gagctcaggg cgccgcagcc ccggcgagcc cactgttggg
361  cctgaggagc cagccctcct cccgcacca aacttggagc acttgacctt tggctgttg
421  agggggcagg ctgcggggtg gctggacagc tgcggagccc cgagggcatc ttgcctggag

```

481 accgtcggct gcactcccgg gctcctggct ttgcctctgg gatcccgagg tgtccacatc
 541 agacgcatgt tgactgagac ctagagtcac ggatgtatgc gtccgtcttg cctgtggct
 601 cctctgggga ctccctctgc accagggcca gagcctcagc catagtcaaca gtgagaaggc
 661 gacaggaacc agctcggggg ccaactctga ggagtccact gcagcagagt tttgccgaat
 721 tgacaagccc ctgtgtcaca gtgaggatga gaaactcagc ttcgaggcag tccgtaacat
 781 ccacaaactg atggacgatg atgccaatgg tgatgtggat gtggaagaaa gtgatgagtt
 841 cctgagggaa gacctcaatt accatgacct aacagtgaaa cacagcacct tccatgggtga
 901 ggataagctc atcagcgtgg aggacctgtg gaaggcatgg aagtcacag aagtatacaa
 961 ttggaccgtg gatgaggtgg tacagtggct gatcacatat gtggagctgc ctcagtatga
 1021 ggagaccttc cggagctgc agctcagtg ccacgcatg ccaaggctgg ctgtcaccaa
 1081 caccacctg acagggactg tgctgaagat gacagaccg agtcacgagc agaagctgca
 1141 gctgaaggct ctggatacag tgctctttgg gcctcctctc ttgactcgcc ataatacact
 1201 caaggacttc atgctggtgg tgtctatcgt tattggtgtg ggcggctgct ggtttgccta
 1261 tatccagaac cgttactcca aggagcacat gaagaagatg atgaaggact tggaggggtt
 1321 acaccgagct gagcagagtc tgcacacact tcaggaaaagg ctgcacaagg cccaggagga
 1381 gcaccgcaca gtggaggtgg agaaggtcca tctggaaaag aagctgcgag atgagatcaa
 1441 ccttgctaag caggaagccc agcggctgaa ggagctgcgg gagggtactg agaatgagcg
 1501 gagccgcca aaatatgctg aggaggagtt ggagcaggtt cgggaggcct tgaggaaagc
 1561 agagaaggag ctagaatctc acagctcatg gtatgctcca gaggcccttc agaagtggct
 1621 gcagctgaca catgaggtgg aggtgcaata ttacaacatc aagaagcaaa atgctgagaa
 1681 gcagctgctg gtggccaagg agggggctga gaagataaaa aagaagagaa acacactctt
 1741 tggcaccttc cacgtggccc acagctcttc cctggatgat gtagatcata aaattctaac
 1801 agctaagcaa gcaactgagc aggtgacagc agcattgcgg gagcgcctgc accgctggca
 1861 acagatcgag atcctctgtg gcttccagat tgtcaacaac cctggcatcc actcactggt
 1921 ggctgccttc aacatagacc ccagctggat gggcagtaga cgcccccaacc ctgctcactt
 1981 catcatgact gacgacgtgg atgacatgga tgaggagatt gtgtctcctt tgtccatgca
 2041 gtcccctagc ctgcagagca gtgttcggca gcgcctgacg gagccacagc atggcctggg
 2101 atctcagagg gatttgacct attccgattc ggagtcctcc ctccacatga gtgaccgcca
 2161 gcgtgtggcc cccaaacctc ctcagatgag ccgtgctgca gacgagctc tcaatgccat
 2221 gacttccaat ggcagccacc ggctgatcga gggggctccac ccagggtctc tggtgagaaa
 2281 actgctgac agccctgccc tggccaagaa ggcattactg gcgctgaacc atgggctgga
 2341 caaggcccac agcctgatgg agctgagccc ctccagccca cctgggtggct ctccacattt
 2401 ggattcttcc cgttctcaca gccccagctc cccagaccca gacacaccat ctccagttgg
 2461 ggacagccga gccctgcaag ccagccgaaa cacacgcatt cccacactgg ctggcaagaa
 2521 ggctgtggct gaggaggata atggctctat tggcgaggaa acagactcca gccagggccg
 2581 gaagaagttt cccctcaaaa tctttaagaa gcctcttaag aagtaggcag gatggggtgg
 2641 cagtaaaggg acagcttgct ctccctggg tgttctgtct ctccctccct ccttctctc
 2701 aagataactg gcccacagag tggggcatgg gaagggtgg tccaggggtc tgggactgt
 2761 acatacctgc cccctcatcc ttgggtcctt cattattatt tattaactga ccaccatggc
 2821 ctgctgccc tgccctcgtc ccaaccatgg gctgctgctg tcaactccctc tccacttcag
 2881 tgcatgtctt agttgctggt cctcagctc ccagctccac ctctggggtt cagcttctgt
 2941 ctctgctgct ccagttttga ggtttggttt ctgtttctg tctctgtctt tcgggctcct
 3001 cctcccacc actcccacac tccocctagc agttgcaggg aagataggac gagtagcttc
 3061 tgacatgtgt gcctcagatc tgttccacc cactcacagt ggttctgttt gctccagact
 3121 ggggctaggg cctaactttt gaagtttgtt ctttgggtatt gatgtgggtc agaaggagcc
 3181 tcatcctaata ctactcagg cctccagggg tccatggggg agtgaaacca attctcagag
 3241 aacaaccac cagagacttt taaagagagg ccaggcttgg gaatgggttg ggagaggcat
 3301 ctgttcattg gagcatgagt ggatgccaga actgtaggtt ataaggcagt cactttttct
 3361 ctctactccc acccacacct gcctccctct taccctgct cccccacact gcaggaggat
 3421 ttgtctctaa gagggtgctg cccaaagctc cccaagcatc aatactccta gggctcagga
 3481 caagtggctc ccctggccag gagagccaca gccatgatac agggctctta tggagccctg
 3541 gagttggttg gcaaggatgc tgtcattttt tgaacaaaa gacaaacagg ttaaaaggaa
 3601 aaaaagtaat ctgaatttcc caagtgccta cgctgcatat tcccctgtt agatcccatt
 3661 tcatgttac tttgtagct tggccagagg ctcaaaaagg acacaaccag tttggggaag
 3721 ggggtggctaa ggaagatggt ataggtgaag gcggctgtgt gaccactttc cccaccctt
 3781 cccaccctct agacaactct ctcccttacc tgtttttgct atggctgtaa aggtattttt
 3841 cctctgcccc actccctgcc atacctttat cctgggatcc tattttgggc ctggggtggg
 3901 tatacctggg gctggtctta ggaggtgct aggtgcaga ctgccttcta ctccctggac
 3961 accctcaaat ggggttttct gtgttatttc ataaaattct ttgaagtcca ataaagcatg
 4021 taggagattt taaccactaa aaaaaaaaaa aaaaaaaaaa aa

7.2.3 *Homo sapiens* PDZ and LIM domain 1 (PDLIM1), mRNA

NCBI reference sequence: NM_020992.2

Length 1462 nt. The coding sequence is marked in yellow.

```

1  gcccgcgccc cgccgctctt tctccgacag ctgccggggg tgccctgcaa gctgttccgc
61  gcgtcctgcc cgtctgtccc cgggggtcgt cgcccgccac agccgcgcca tgaccaccca
121  gcagatagac ctccagggcc cggggccgtg gggcttccgc ctctgtggcg gcaaggactt
181  cgagcagcct ctccgccattt cccgggtcac tcttgggaagc aaggcggctc tagctaattt
241  atgtattgga gatgtaatca cagccattga tggggaaaat actagcaata tgacacactt
301  ggaagctcag aacagaatca aaggctgcac agacaacttg actctcactg tagccagatc
361  tgaacataaa gtctgggtctc ctctggtgac ggaggaaggg aagcgtcadc catacaagat
421  gaatttagcc tctgaacccc aggaggctct gcacatagga agcgcccaca accgaagtgc
481  catgcccttt accgcctcgc ctgcctccag cactactgcc agggctcatc caaaccagta
541  caacaaccca gctggcctct actcttctga aaatatctcc aacttcaaca atgccctgga
601  gtcaaagact gctgccagcg ggggtggaggc gaacagcaga cccttagacc atgctcagcc
661  tccaagcagc cttgtcatcg acaagaatc tgaagtttac aagatgcttc aggagaaaca
721  ggagttgaat gagccccgca aacagtcac gtcttctctg gttttgcagg aaatcctgga
781  gtctgaagaa aaaggggatc ccaacaagcc ctccaggattc agaagtgtta aagctcctgt
841  cactaaagtg gctgcgtcga ttggaaatgc tcagaagtgg cctatgtgtg acaaatgtgg
901  cactgggatt gttggtgtgt ttgtgaagct gcgggaccgt caccgccacc ctgagtgtta
961  tgtgtgcact gactgtggca ccaacctgaa acagaagggc catttctttg tggaggatca
1021  aatctactgt gagaagcatg cccgggagcg agtcacacca cctgaggggt atgaagtggg
1081  cactgtgttc cccaagtga ccagcagatc tgaccactgt tctccagcag gcctctgctg
1141  cagctttttc tctcagtgtt ctggcctctc cctctcttga aagttctctg cttactttgg
1201  ttttccctct gcttgtaaaa cattgagtcc cctccctgcc ttggttaatt gactcacacc
1261  agctgtgcca tgcccgcctt tacaattaaa ggaaaactgt tttgttcagt gtcaccttgt
1321  cagcaacact gtgtcccttc gccccaccgt tcttctctgc tgcatttggg catcagccaa
1381  atttgaaccc aatcaaatat aacgtgtctg acactgattt tgtttttact caataaatgt
1441  atagactaca aaaaaaaaaa aa

```

7.2.4 *Mus musculus* stromal interaction molecule 1 (Stim1), mRNA

NCBI reference sequence: NM_009287.4

Length 3609 nt. The coding sequence is marked in yellow.

```

1  cccgggacctg gcccgctgcgc gtccgcctgc tgcaccgggg caccaggagc cgcagaggta
61  cgggaccggc cgggggagct gacctcggcc taggagtctt aggatcccgg agacatccgt
121  gtctgtctgg gcctgtagggt cgcacgcccga agccctagct gctgaggctc accgctgttt
181  ctccggggcga ggtcaggtgc cccccttctc tctctctctc tctccctccc ccacctcagt
241  gcggggcggga gattctgccc gcctcctccc gcaggggtgc agcaggctgc ggagctgaca
301  gcggccccgc agccaccctg ctcaaaactc ccggaagcag atagagctca ggcgcgcccc
361  gcagccccgg cggacctaca gttggaccgg agactccgat ccttctgcgt ccaaacttgg
421  ggcacttgac ctctgccttat cggaggagggt aagcccgcag gtggctggac agctgcggcg
481  ccgcgagggc atcttgcttt ggaaccgtcg gctgcactcc ctgactctgg gatttgcttc
541  tgggatccaa aggtgtctac agcaggcgca tgttgactga gacctaccgt catggatgtg
601  tgcgcccgtc ttgccctgtg gcttcttttg gggctccttc tgcacaggg ccagagtctc
661  agccatagtc acagtgaaaa gaatacagga gctagctccg gggcgacttc tgaagagtct
721  accgaagcag agttttgccg aattgacaag cccctgtgcc acagtgagga tgagaagctc
781  agctttgagg ccgtccgaaa catccataag ctgatggatg acgatgccaa tggatgatgt
841  gatgtggaag aaagtgatga gttcctaagg gaagacctca attacatga cccaacagtg
901  aaacatagca ccttccatgg tgaggataag cttatcagcg tggaggacct gtggaaggcg
961  tggaaagtcat cagaagtgta caactggact gtggatgagg tgatacagtg gctcattacg
1021  tatgtggagc tgccacagta tgaggaaacc ttccggaagt tgcagcttac tggccacgcc
1081  atgccaaggc tagcagtaac caacaccacc atgacagggc ctgtactgaa gatgacagat
1141  cggagccaca ggcagaagct gcagctgaag gccctggaca cagtgtctgt tggcctcctc
1201  ctcttgactc ggcataatca cctgaaggac ttcattgctg tggatgtctt cgttatgggt
1261  tgggttgact gctgttttgc ctatatccag aaccgttact ctaaggagca catgaagaaa
1321  atgatgaagg atctggaagg gttacaccgg gctgagcaga gtctgcatga ccttcaggaa
1381  aggctgcaca agggccagga ggagcaccga actgtggaag tagagaaggt ccacctggag

```

```

1441 aagaagctgc gagatgagat caaccttgcc aagcaggaag ctcagcggct gaaggagctg
1501 agggagggta ctgagaatga gaggagccgt caaaaatatg ctgaggaaga gctggagcag
1561 gttcgggagg ccttgaggaa agcagagaag gagctggaat cacacagctc atggtatgct
1621 cctgaggccc tgcagaagtg gctgcagctg acccatgagg tggaggtgca gtactacaac
1681 atcaagaagc aaaatgcaga gaggcagctg ctgggtggcca aggagggggc tgagaaaaata
1741 aaaaagaaga gaaacacgct ttttggtaac ttccatgtgg cccacagctc ttccctggat
1801 gatgtggatc ataaaaatcct aactgctaag caagctctga gtgaggtgac agcggcactg
1861 agggagcggc tgcaccgggtg gcagcagatc gagatcctct gcggtttcca gattgtcaat
1921 aaccccgcca tccactcctt ggtggctgct ctcaacatcg accccagctg gatgggcagc
1981 acccgcccta accccgcccc ctccatcatg actgacgatg tggatgacat ggatgaggag
2041 attgtctcgc ccttgtccat gcagtcccc agcctgcaga gcagtgtccg gcagcgcctg
2101 acggagccac agcttggcct gggatctcag agggatttga cccattccga ttcggagtcc
2161 tccctccaca tgagtgaccg ccagcgtgtg gcccccaagc ctctcagat gggcctgtct
2221 gcagatgaag ctctcaatgc catgccttcc aatggcagcc atcggctgat tgagggggctc
2281 catccaggat ctctgggtgga gaaactgcct gacagccctg ctctggccaa gaagacattt
2341 atggcgttga accatggcct agacaaggcc cacagcctga tggagctgaa cccctcagtc
2401 ccacctggtg gctccccact tttggattct tcccattctc ttagccccag ttcccagac
2461 ccagacacgc catctccagt tggggacaac cgagctctgc agggtagccg aaacacacga
2521 attccccact tggctggcaa gaaggcaatg gctgaggagg ataatggttc cattggtgag
2581 gagacagact ccagtccagg caggaagaag tttcctctca aaatttttaa gaagcctctt
2641 aagaagtagg cagactaggg tggtagtggt gagacagcct gtccttccct ggtcttctctg
2701 ccttcacctc ccttccttcc tttgcaatat ctggctccta gagtggggca cagaggggct
2761 ggcccaaggg cctgggcact gtacatatct gccctgctca tccttggctc ttcatcatta
2821 tttattaact gaccaccatg gcctgcctgt cgggaaaccc ttccacccat gggctgctgc
2881 tgtcacatct tctccacttc agtgcattgt ttagttgctc ttccctcagt tcccactcca
2941 cttttggggt ccagcttctg tctctgctgt cccagttttg aggtttgggt tttgtttctg
3001 tctctgctt tcaggctcct ctctcccatt actccccaac gatcctagca gttgtgggga
3061 agataggagg agtaacttct gacacctgta cctcagatct gttcatccta ctcacagcca
3121 ttctgcctac cccagactgg gccacggctc tgatctctgg ggtttgttct atggaagtgt
3181 ggtagactgg agggaaacct atcctggagc tcctttggat ctccagggct ccatcagggg
3241 agtggaaacca actcccaggg aacaagtcac cagagtttta aagagagacc aggcttgtga
3301 ttgatgggag agacttctcc cagttggagg atgagtagat gccaaaagctg tgggctgtaa
3361 ggcagttgcc atttctctct tgccctgcc acacctgcct tcctcttacc tctgctcccc
3421 tatattgcag gagtgtatct cttaaagagg gctgcctga agctccccat cagcatcagc
3481 actactgggg ctcagggcaa ctggctcccc tggctatggg agccacagtc atgacacagg
3541 gctcttgtgg agccctgggc aaggatgta tatttgaacc aaaagacaaa cagttttaaa
3601 ataaaaaaaa

```

7.2.5 *Mus musculus* PDZ and LIM domain 1 (elfin) (Pdlim1), mRNA

NCBI reference sequence: NM_016861.4

Length 1524 nt. The coding sequence is marked in yellow.

```

1 ggggctgcag cgacgcggcc ggggcggatc tgtccccgcc ctcgctcgcg accccgcccc
61 tcccaggatc tcccaactcc cgccgcgcgc tctttctccg acagctgctc cgggagcccc
121 gcgcgcctg cagttctgtg ccttgcctgt ctgtcccttc cgattgtgcc tagcgatgac
181 caccacagcag attgttctcc agggcccggg tccttgggggt ttccgcctcg tgggcggcaa
241 ggacttcgaa caacctctcg ccatttcccg ggtcactccc ggaagcaagg ctgctatagc
301 gaatttatgt attggagatt taatcacagc catcgatggg gaagatacca gcagcatgac
361 acacttggaa gctcagaaca aatcaaggg ctgcgcagac aacatgacgc tcacagtatc
421 caggcttgaa cagaagattt ggtctcctct agtgaccgag gaggggaaac gtcaccccta
481 caagatgaat ttagcgtcgg aaccccaaga agtcctgcac ataggaagtg cccacaaccg
541 aagtgccatg ccatttaact cctcacctgc tcccagcacc cgggtcatca caaacagta
601 caacagccca actggcctct actcatccga aaacatctct aacttcaaca atgctgtgga
661 gtcgaagacc tcagccagtg gggaggaggc gaacagcagg cccgtggttc agcctcatcc
721 ctccggcagc cttatcattg acaaggactc tgaagtttac aagatgcttc aggagaagca
781 agaattaaac gagcccccca aacagtccac atccttctct gttctgcagg agatcctgga
841 gtcagatggg aaaggggatc ccaacaagcc atcaggattt agaagtgta aagctccagt
901 caccaaagtg gctgcatctg ttggaaatgc tcagaagctg cccatctgtg acaaatgtgg
961 aactggtatt gttggtgtgt ttgtgaagct gagggatcac catcgcacc ctgaaatgcta

```

```

1021 tgtgtgcacc gactgtggca tcaacctgaa acagaagggc catttctttg tagaggatca
1081 gatctactgt gaaaagcatg cccgggagcg ggtcactccg cctgagggct acgatgtggt
1141 cacagtgttc cgcgagtgat ggagaggacc tgccctgtct actgccctcc agccagcctg
1201 ctgcacctgg ttctcggaat attctggctc tctcctccct gacagtctctg tgcttactta
1261 gtgtagtca tgcgcaataa acattggggt tcgtctgggc tgactgactc ccaactggcag
1321 ggtgacatct gcttttatat tattgggaga tggttttgtc cctgtccctt caccacacc
1381 tcaatgcacc ttcttcaact ggagtcttct ctgctgcaaa tggacattgg tccattggaa
1441 ctaagccaaa tgtagtatct ctgatgttac ttggttttac ttaataaatt tagactttaa
1501 agcaaaaaaa aaaaaaaaaa aaaa

```

7.3 Applied full-length aa-sequences

7.3.1 *Homo sapiens* vasodilator-stimulated phosphoprotein (VASP), protein

UniProtKB/ Swiss-Prot Acc.Nr.: P50552. Length 380 aa; MW 39,830 Da

```

10      20      30      40      50      60
MSETVICSSR ATVMLYDDGN KRWLPAGTGP QAFSRVQIYH NPTANSFRV V GRKMQPDQQV
70      80      90      100     110     120
VINCAIVRGV KYNQATPNFH QWRDARQVWG LNFGSKEDAA QFAAGMASAL EALEGGGPPP
130     140     150     160     170     180
PPALPTWSVP NGPSPEEVEQ QKRQOPGPSE HIERRVSNAG GPPAPPAGGP PPPPGPPPPP
190     200     210     220     230     240
GPPPPPGLPP SGVPAAAHGA GGGPPPAPPL PAAQPGGGG AGAPGLAAAI AGAKLRKVS K
250     260     270     280     290     300
QEEASGGPTA PKAESGRSGG GGLMEEMNAM LARRRKATQV GEKTPKDESA NQEEPEARVP
310     320     330     340     350     360
AQSESVRRPW EKNSTTLPRM KSSSSVTTSE TQPCTPSSSD YSDLQRVKQE LLEE VKKELQ
370     380
KVKEEII EAF VQELRKR GSP

```

7.3.2 *Homo sapiens* stromal interaction molecule 1 (STIM1), protein

UniProtKB/ Swiss-Prot Acc.Nr.: Q13586. Length 685 aa; MW 77,423 Da

```

10      20      30      40      50      60
MDVCVRLALW LLWGLLLHQG QLSHSHSEK ATGTSSGANS EESTAAEF CR IDKPLCHSED
70      80      90      100     110     120
EKLSFEAVRN IHKLMDD DAN GDVDVEESDE FLREDLNYHD PTVKHSTFHG EDKLISVEDL
130     140     150     160     170     180
WKAWKSSEVY NWTVDEVVQW LITYVELPQY EETFRKLQLS GHAMPRLAVT NTTMTGTVLK
190     200     210     220     230     240
MTDRSHRQKL QLKALDTVLF GPPLLTRHNH LKDFMLV VSI VIGVGGCWFA YIQNRYSKEH
250     260     270     280     290     300
MKMMKDLEG LHRAEQSLHD LQERLHKAQE EHRTVEVEKV HLEKKLRDEI NLAQQAQRL

```

```

    310          320          330          340          350          360
KELREGTENE RSRQKYAE EEE LEQVREALRK AEKELESHSS WYAPEALQKW LQLTHEVEVQ
    370          380          390          400          410          420
YYNIKKQNAE KQLLVAKEGA EKIKKKRNTL FGTFFVAHSS SLDDVDHKIL TAKQALSEVT
    430          440          450          460          470          480
AALRERLHRW QQIEILCGFQ IVNNPGIHSL VAALNIDPSW MGSTRPNPAH FIMTDDVDDM
    490          500          510          520          530          540
DEEIVSPLSM QSPSLQSSVR QRLTEPQHGL GSQRDLTHSD SESSLHMSDR QRVAPKPPQM
    550          560          570          580          590          600
SRAADEALNA MTSNGSHRLI EGVHPGSLVE KLPDSPALAK KALLALNHGL DKAHSLMELS
    610          620          630          640          650          660
PSAPPGGSPH LDSSRSHSPS SPDPDTPSPV GDSRALQASR NTRIPHLAGK KAVAEEDNGS
    670          680
IGEETDSSPG RKKFPLKIFK KPLKK

```

7.3.3 *Homo sapiens* PDZ and LIM domain 1 (PDLIM1), protein

UniProtKB/ Swiss-Prot Acc.Nr.: O00151. Length 329 aa; MW 36,072 Da

```

    10          20          30          40          50          60
MTTQQIDLQG PGPWGFRLVG GKDFEQPLAI SRVTPGSKAA LANLCIGDVI TAIDGENTS N
    70          80          90          100         110         120
MTHLEAQNRI KGCTDNLTLT VARSEHKVWS PLVTEEGKRH PYKMNLASEP QEVLHIGSAH
   130         140         150         160         170         180
NRSAMPFTAS PASSTTARVI TNQYNNPAGL YSSENISNFN NALESKTAAS GVEANSRPLD
   190         200         210         220         230         240
HAQPPSSLVI DKESEVYKML QEKQELNEPP KQSTSFLVLQ EILESEEKGD PNKPSGFRSV
   250         260         270         280         290         300
KAPVTKVAAS IGNAQKLPMC DKCGTGIVGV FVKLRDRHRH PECYVCTDCG TNLKQKGHFF
   310         320
VEDQIYCEKH ARERVTPPEG YEVVTVFPK

```


7.3.4 *Mus musculus* stromal interaction molecule 1 (Stim1), protein

UniProtKB/ Swiss-Prot Acc.Nr.: P70302. Length 685 aa; MW 77,567 Da

```

      10      20      30      40      50      60
MDVCARLALW LLWGLLLHQG QLSLSHSHSEK NTGASSGATS EESTEAEFCR IDKPLCHSED
      70      80      90     100     110     120
EKLSFEAVRN IHKLMDDDDAN GDVDVEESDE FLREDLNYHD PTVKHSTFHG EDKLISVEDL
     130     140     150     160     170     180
WKAWKSSEVY NWTVDEVIQW LITYVELPQY EETFRKLQLT GHAMPRLAVT NTTMTGTVLK
     190     200     210     220     230     240
MTDRSHRQKL QLKALDTVLF GPPLLTRHNH LKDFMLVVSI VIGVGGCWFA YIQNRYSKEH
     250     260     270     280     290     300
MKKMMKDLEG LHRAEQSLHD LQERLHKAQE EHRTVEVEKV HLEKKLRDEI NLAKQEAQRL
     310     320     330     340     350     360
KELREGTENE RSRQKYAEEE LEQVREALRK AEKELESHSS WYAPEALQKW LQLTHEVEVQ
     370     380     390     400     410     420
YYNIKKQNAE RQLLVAKEGA EKIKKKRNTL FGTFHVAHSS SLDDVDHKIL TAKQALSEVT
     430     440     450     460     470     480
AALRERLHRW QQIEILCGFQ IVNPNGIHSL VAALNIDPSW MGSTRPNPAH FIMTDDVDDM
     490     500     510     520     530     540
DEEIVSPLSM QSPSLQSSVR QRLTEPQLGL GSQRDLTHSD SESSLHMSTR QRVAPKPPQM
     550     560     570     580     590     600
GRAADEALNA MPSNGSHRLI EGVHPGSLVE KLPDSPALAK KTFMALNHGL DKAHSLMELN
     610     620     630     640     650     660
PSVPPGGSPL LDSSHSLSPS SPDPDTPSPV GDNRALQGSR NTRIPHLAGK KAMAEEDNGS
     670     680
IGEETDSSPG RKKFPLKIFK KPLKK

```

7.3.5 *Mus musculus* PDZ and LIM domain 1 (elfin) (Pdim1), protein

UniProtKB/ Swiss-Prot Acc.Nr.: O70400. Length 327 aa; MW 35,774 Da

```

      10      20      30      40      50      60
MTTQQIVLQG PGPWGFRLVG GKDFEQPLAI SRVTPGSKAA IANLCIGDLI TAIDGEDTSS
      70      80      90     100     110     120
MTHLEAQNKI KGCADNMTLT VSRSEQKIWS PLVTEEGKRH PYKMNLASEP QEVLHIGSAH
     130     140     150     160     170     180
NRSAMPFTAS PAPSTRVITN QYNSPTGLYS SENISNFNNA VESKTSASGE EANSRPVVQP
     190     200     210     220     230     240
HPSGSLIIDK DSEVYKMLQE KQELNEPPKQ STSFLVLQEI LESDGKGDPN KPSGFRSVKA

```

```

      250          260          270          280          290          300
PVTKVAASVG NAQKLPICDK CGTGIVGVFV KLRDHHRHPE CYVCTDCGIN LKQKGHFFVE
      310          320
DQIYCEKHAR ERVTPPEGYD VVTVFRE

```

7.4 Sequencing data

Full-length sequencing of VASP-deletion constructs in *pcDNA3.1/V5-HisA* vector was provided by GATC Biotech (Konstanz, Germany). Sequencing primers were T7-Fwd and BGH-Rev; the delivered nucleotide sequences were analyzed via the GATC Viewer software.

Legend:

VASP-starting sequence:	ATGAGCGAGA
VASP Δ TD-ending:	TACTCG
VASP Δ FAB Δ TD-ending:	GGTCGAAGC
V5-tag:	GGTAAGCCTATCCCTAACCTCTCCTCGGTCTCGATTCTACG
His ₆ -tag:	CATCATCATCATCATTGA (His codons: 'CAT' or 'CAC')
BamHI-restriction site:	GGATCC
EcoRI-restriction site:	GAATTC

7.4.1 Sequencing of VASP-AAA Δ TD (in *pcDNA3.1/V5-HisA*)

VASP-AAA Δ TD, T7-Fwd-sequence:

```

CGAGCTCGGATCCATGAGCGAGACGGTCATCTGTTCCAGCCGGGCCACTGTGATGCTTTATGATGATGGCA
ACAAGCGATGGCTCCCTGCTGGCACGGGTCCCCAGGCCTTCAGCCGCGTCCAGATCTACCACAACCCCACG
GCCAATTCCTTTTCGCGTCGTGGGCCGGAAGATGCAGCCCGACCAGCAGGTGGTCATCAACTGTGCCATCGT
CCGGGGTGTCAAGTATAACCAGGCCACCCCAACTTCCATCAGTGGCGCGACGCTCGCCAGGTCTGGGGC
CTCAACTTCGGCAGCAAGGAGGATGCGGGCCAGTTTGGCCCGGCATGGCCAGTGCCCTAGAGGCGTTGG
AAGGAGGTGGGCCCCCTCCACCCCGAGCACTTCCCACCTGGTCCGTCCCGAACCGGCCCTCCCGGAGGA
GGTGGAGCAGCAGAAAAGGCAGCAGCCCGCCCGTCCGGAGCACATAGAGCGCCGGGTCCGCAATGCAGG
AGGCCACCTGCTCCCCCGCTGGGGGTCCACCCCAACCAGGACCTCCCCCTCCTCCAGGTCCCCC
CCACCCCGAGGTTGCCCCCTTCGGGGGTCCCAGCTGCAGCGCACGGAGCAGGGGGAGGACCACCCCT
G

```

VASP-AAA Δ TD, BGH-Rev-sequence (complementary):

```

CACCCCTGCACCCCTCTCCCGGCAGCACAGGGCCCTGGTGGTGGGGGAGCTGGGGCCCCAGGCCTGG
CCGCAGCTATTGCTGGAGCCAAACTCAGGAAAGTCGCGAAGCAGGAGGAGGCCTCAGGGGGGCCACAGC
CCCCAAAGCTGAGAGTGGTCAAGCGGAGGTGGGGACTCATGGAAGAGATGAACGCCATGCTGGCCCGG
AGAAGGAAAGCTGCGCAAGTTGGGGAGAAAACCCCAAGGATGAATCTGCCAATCAGGAGGAGCCAGAGG
CCAGAGTCCCGGCCAGAGTGAATCTGTGCGGAGACCCTGGGAGAAGAACAGCACAACCTTGCCAAGGAT
GAAGTCGTCTTCTCGGTGACCACTTCCGAGACCCAACCCTGCACGCCAGCTCCAGTGATTACTCGGAATT
CTGCAGATATCCAGCACAGTGGCGGCCGCTCGAGTCTAGAGGGCCCTTCGAAAGGTAAGCCTATCCCTAAC
CTCTCCTCGGTCTCGATTCTACGCGTACCGGTATCATCACCATCACCATTGA

```

VASP-AAAΔTD, sequence alignment with human VASP:

Query: human VASP
 Subject 1: VASP-AAAΔTD, T7-Fwd-sequence
 Length: 619 nt
 Score = 1109 bits (600), Expect = 0.0, Identities = 604/606 (99%), Gaps = 0/606 (0%)

```

QUERY 1   ATGAGCGAGACGGTCATCTGTTCCAGCCGGGCCACTGTGATGCTTTATGATGATGGCAAC 60
          |||
SBJCT 14   ATGAGCGAGACGGTCATCTGTTCCAGCCGGGCCACTGTGATGCTTTATGATGATGGCAAC 73

QUERY 61   AAGCGATGGCTCCCTGCTGGCACGGGTCCCCAGGCCTTCAGCCGCGTCCAGATCTACCAC 120
          |||
SBJCT 74   AAGCGATGGCTCCCTGCTGGCACGGGTCCCCAGGCCTTCAGCCGCGTCCAGATCTACCAC 133

QUERY 121  AACCCACGGCCAATTCCTTTCGCGTCGTGGGCCGGAAGATGCAGCCCGACCAGCAGGTG 180
          |||
SBJCT 134  AACCCACGGCCAATTCCTTTCGCGTCGTGGGCCGGAAGATGCAGCCCGACCAGCAGGTG 193

QUERY 181  GTCATCAACTGTGCCATCGTCCGGGGTGTCAAGTATAACCAGGCCACCCCAACTTCCAT 240
          |||
SBJCT 194  GTCATCAACTGTGCCATCGTCCGGGGTGTCAAGTATAACCAGGCCACCCCAACTTCCAT 253

QUERY 241  CAGTGGCGCGACGCTCGCCAGGTCTGGGGCCTCAACTTCGGCAGCAAGGAGGATGCGGCC 300
          |||
SBJCT 254  CAGTGGCGCGACGCTCGCCAGGTCTGGGGCCTCAACTTCGGCAGCAAGGAGGATGCGGCC 313

QUERY 301  CAGTTTGCCGCGGCATGGCCAGTGCCTAGAGGCGTTGGAAGGAGGTGGGCCCCCTCCA 360
          |||
SBJCT 314  CAGTTTGCCGCGGCATGGCCAGTGCCTAGAGGCGTTGGAAGGAGGTGGGCCCCCTCCA 373

QUERY 361  CCCCAGCACTTCCACCTGGTTCGGTCCCGAACGGCCCTCCCCGGAGGAGGTGGAGCAG 420
          |||
SBJCT 374  CCCCAGCACTTCCACCTGGTTCGGTCCCGAACGGCCCTCCCCGGAGGAGGTGGAGCAG 433

QUERY 421  CAGAAAAGGCAGCAGCCCGGCCCGTTCGGAGCACATAGAGCGCCGGGTCATGCAGGA 480
          |||
SBJCT 434  CAGAAAAGGCAGCAGCCCGGCCCGTTCGGAGCACATAGAGCGCCGGGTCATGCAGGA 493
          S157A (nt 469-471)

QUERY 481  GGCCACCTGCTCCCCCGCTGGGGGTCCACCCACCACCAGGACCTCCCCCTCCTCCA 540
          |||
SBJCT 494  GGCCACCTGCTCCCCCGCTGGGGGTCCACCCACCACCAGGACCTCCCCCTCCTCCA 553

QUERY 541  GGTCCCCCCCCACCCAGGTTTGGCCCCCTTCGGGGTCCAGCTGCAGCGCACGGAGCA 600
          |||
SBJCT 554  GGTCCCCCCCCACCCAGGTTTGGCCCCCTTCGGGGTCCAGCTGCAGCGCACGGAGCA 613

QUERY 601  GGGGA 606
          |||
SBJCT 614  GGGGA 619
  
```

Query: human VASP
 Subject 2: VASP-AAAΔTD, BGH-Rev-sequence
 Length: 528 nt
 Score = 750 bits (406), Expect = 0.0, Identities = 416/419 (99%), Gaps = 2/419 (0%)

```

QUERY 611  CACCCCTGCACCCCTCTCCCGCAGCACAGGGCCCTGGTGGTGGGGGAGCTGGGGCCC 670
          |||
SBJCT 1     CACCCCTGCACCCCTCTCCCGCAGCACAGGGCCCTGGTGGTGGGGGAGCTGGGGCCC 60

QUERY 671  CAGGCCTGGCCGACGCTATTGCTGGAGCCAACTCAGGAAAGTCAGC-AAGCAGGAGGAG 729
          |||
SBJCT 61   CAGGCCTGGCCGACGCTATTGCTGGAGCCAACTCAGGAAAGTC-SCCAAGCAGGAGGAG 119
          S239A (nt 715-717)
  
```

```

QUERY 730 GCCTCAGGGGGGCCACAGCCCCAAAGCTGAGAGTGGTTCGAAGCGGAGGTGGGGGACTC 789
          |||
SBJCT 120 GCCTCAGGGGGGCCACAGCCCCAAAGCTGAGAGTGGTTCGAAGCGGAGGTGGGGGACTC 179

QUERY 790 ATGGAAGAGATGAACGCCATGCTGGCCCGGAGAAGGAAAGCCACC CAAGTTGGGGAGAAA 849
          |||
SBJCT 180 ATGGAAGAGATGAACGCCATGCTGGCCCGGAGAAGGAAAGCCGCC CAAGTTGGGGAGAAA 239
          |||
          T278A (nt 832-834)

QUERY 850 ACCCCCAAGGATGAATCTGCCAATCAGGAGGAGCCAGAGGCCAGAGTCCCGGCCAGAGT 909
          |||
SBJCT 240 ACCCCCAAGGATGAATCTGCCAATCAGGAGGAGCCAGAGGCCAGAGTCCCGGCCAGAGT 299

QUERY 910 GAATCTGTGCGGAGACCCTGGGAGAAGAACAGCACAACTTGCCAAGGATGAAGTCGTCT 969
          |||
SBJCT 300 GAATCTGTGCGGAGACCCTGGGAGAAGAACAGCACAACTTGCCAAGGATGAAGTCGTCT 359

QUERY 970 TCTTCGGTGACCACTTCCGAGACCCAACCCTGCACGCCAGCTCCAGTGATTACTCGGA 1028
          |||
SBJCT 360 TCTTCGGTGACCACTTCCGAGACCCAACCCTGCACGCCAGCTCCAGTGATTACTCGGA 418
          |||

```

7.4.2 Sequencing of VASP-AAAΔFABΔTD (in pcDNA3.1/V5-HisA)

VASP-AAAΔFABΔTD, T7-Fwd-sequence:

```

CTTGGTACCGAGCTCGGATCCATGAGCGAGACGGTTCATCTGTTCCAGCCGGGCCACTGTGATGCTTTATGAT
GATGGCAACAAGCGATGGCTCCCTGCTGGCACGGGTCCCCAGGCCCTCAGCCGCGTCCAGATCTACCACAA
CCCCACGGCCAATTCCTTTTCGCGTCTGTTGGCCCGGAAGATGCAGCCCGACCAGCAGGTGGTTCATCAACTGTG
CCATCGTCCGGGGTGTCAAGTATAACCAGGCCACCCCCAACTTCCATCAGTGGCGCGACGCTCGCCAGGTC
TGGGGCCTCAACTTCGGCAGCAAGGAGGATGCGGCCAGTTTGCCGCGGCATGGCCAGTGCCCTAGAGG
CGTTGGAAGGAGGTGGGCCCCCTCCACCCCCAGCACTTCCACCTGGTCCGTCGTCGGAACGGCCCCCTCCCC
GGAGGAGGTGGAGCAGCAGAAAAGGCAGCAGCCCGGCCCGTCCGAGCACATAGAGCGCCGGGTCCGCGAA
TGCAGGAGGCCACCTGCTCCCCCGCTGGGGGTCCACCCCCACCAGGACCTCCCCCTCCTCCAGGT
CCCCCCCCACCCCCAGGTTTGCCTCCCTTCGGGGTCCAGCTGCAGCGCACGGAGCAGGGGGAGGACCA
CCCCCTGCACCCCCCTCCTCCGCGCAGCACAGGGCCCTGGTGGTGGGGGAGCTGGGGCCCCAGGCCTGGCC
GCACTATTGCTGGAGCCAACTCAGGAAAA

```

VASP-AAAΔFABΔTD, BGH-Rev-sequence (complementary):

```

CAGGTCCCCCCCCACCCCCAGGTTTGCCTCCCTTCGGGGGTCCCAGCTGCAGCGCACGGAGCAGGGGGAG
GACCACCCCTGCACCCCTCTCCCGGCAGCACAGGGCCCTGGTGGTGGGGGAGCTGGGGCCCCAGGCC
TGGCCGACAGCTATTGCTGGAGCCAACTCAGGAAAGTCGCGAAGCAGGAGGAGGCCTCAGGGGGGCCAC
AGCCCCAAAGCTGAGAGTGGTTCGAAGCGAATTCGCAGATATCCAGCACAGTGGCGGCCGCTCGAGTCTA
GAGGGCCCTTCGAAAGGTAAGCCTATCCCTAACCCCTCTCCTCGGTCTCGATTCTACGCGTACCGGT
ACCATCACCATTGA

```

VASP-AAAΔFABΔTD, sequence alignment with human VASP:

Query: human VASP
 Subject 1: VASP-AAAΔFABΔTD, T7-Fwd-sequence
 Length: 732 nt
 Score = 1295 bits (701), Expect = 0.0, Identities = 709/711 (99%), Gaps = 1/711 (0%)

```

QUERY 1 ATGAGCGAGACGGTTCATCTGTTCCAGCCGGGCCACTGTGATGCTTTATGATGATGGCAAC 60
          |||
SBJCT 22 ATGAGCGAGACGGTTCATCTGTTCCAGCCGGGCCACTGTGATGCTTTATGATGATGGCAAC 81

QUERY 61 AAGCGATGGCTCCCTGCTGGCACGGGTCCCCAGGCCTTCAGCCGCGTCCAGATCTACCAC 120
          |||
SBJCT 82 AAGCGATGGCTCCCTGCTGGCACGGGTCCCCAGGCCTTCAGCCGCGTCCAGATCTACCAC 141
          |||

```

```

QUERY 121 AACCCACGGCCAATTCCTTTTCGCGTCGTGGGCCGGAAGATGCAGCCCGACCAGCAGGTG 180
      |||
SBJCT 142 AACCCACGGCCAATTCCTTTTCGCGTCGTGGGCCGGAAGATGCAGCCCGACCAGCAGGTG 201

QUERY 181 GTCATCAACTGTGCCATCGTCCGGGGTGTCAAGTATAACCAGGCCACCCCAACTTCCAT 240
      |||
SBJCT 202 GTCATCAACTGTGCCATCGTCCGGGGTGTCAAGTATAACCAGGCCACCCCAACTTCCAT 261

QUERY 241 CAGTGGCGCGACGCTCGCCAGGTCTGGGGCCTCAACTTCGGCAGCAAGGAGGATGCGGCC 300
      |||
SBJCT 262 CAGTGGCGCGACGCTCGCCAGGTCTGGGGCCTCAACTTCGGCAGCAAGGAGGATGCGGCC 321

QUERY 301 CAGTTTGC CGCCGGCATGGCCAGTGCCTTAGAGGCGTTGGAAGGAGGTGGGCCCCCTCCA 360
      |||
SBJCT 322 CAGTTTGC CGCCGGCATGGCCAGTGCCTTAGAGGCGTTGGAAGGAGGTGGGCCCCCTCCA 381

QUERY 361 CCCCCAGCACTTCCACCTGGTTCGGTCCCGAACGGCCCTCCCCGAGGAGGTGGAGCAG 420
      |||
SBJCT 382 CCCCCAGCACTTCCACCTGGTTCGGTCCCGAACGGCCCTCCCCGAGGAGGTGGAGCAG 441

QUERY 421 CAGAAAAGGCAGCAGCCCGGCCGTCGGAGCACATAGAGCGCCGGGTC TCC AATGCAGGA 480
      |||
SBJCT 442 CAGAAAAGGCAGCAGCCCGGCCGTCGGAGCACATAGAGCGCCGGGTC GCG AATGCAGGA 501
      S157A (nt 469-471)

QUERY 481 GGCCACCTGCTCCCCCGCTGGGGGTCCACCCACCACCAGGACCTCCCCCTCCTCCA 540
      |||
SBJCT 502 GGCCACCTGCTCCCCCGCTGGGGGTCCACCCACCACCAGGACCTCCCCCTCCTCCA 561

QUERY 541 GGTCCCCCCCCACCCAGTTTGGCCCTTCGGGGTCCAGCTGCAGCGCACGGAGCA 600
      |||
SBJCT 562 GGTCCCCCCCCACCCAGTTTGGCCCTTCGGGGTCCAGCTGCAGCGCACGGAGCA 621

QUERY 601 GGGGAGGACCACCCCTGCACCCCTCTCCCGGCAGCACAGGGCCCTGGTGGTGGGGGA 660
      |||
SBJCT 622 GGGGAGGACCACCCCTGCACCCCTCTCCCGGCAGCACAGGGCCCTGGTGGTGGGGGA 681

QUERY 661 GCTGGGGCCCCAGGCCTGGCCGCACTATTGCTGGAGCCAAACTCAGGAAA 711
      |||
SBJCT 682 GCTGGGGCCCCAGGCCTGGCCGCACTATTGCTGGAGCCAAACTCAGGAAA 731

```

Query: human VASP
Subject 2: VASP-AAAD Δ FAB Δ TD, BGH-Rev-sequence
Length: 361 nt
Score = 427 bits (231), Expect = 7e-124, Identities = 236/238 (99%), Gaps = 2/238 (0%)

```

QUERY 539 CAGGTCCCCCCCCACCCAGGTTTGGCCCTTCGGGGTCCAGCTGCAGCGCACGGAG 598
      |||
SBJCT 1 CAGGTCCCCCCCCACCCAGGTTTGGCCCTTCGGGGTCCAGCTGCAGCGCACGGAG 60

QUERY 599 CAGGGGAGGACCACCCCTGCACCCCTCTCCCGGCAGCACAGGGCCCTGGTGGTGGGG 658
      |||
SBJCT 61 CAGGGGAGGACCACCCCTGCACCCCTCTCCCGGCAGCACAGGGCCCTGGTGGTGGGG 120

QUERY 659 GAGCTGGGGCCCCAGGCCTGGCCGCACTATTGCTGGAGCCAAACTCAGGAAAGTC AGC - 717
      |||
SBJCT 121 GAGCTGGGGCCCCAGGCCTGGCCGCACTATTGCTGGAGCCAAACTCAGGAAAGTC - GCG 179
      S239A (nt 715-717)

QUERY 718 AAGCAGGAGGAGGCTCAGGGGGGCCACAGCCCCAAAGCTGAGAGTGGTTCGAAGCG 775
      |||
SBJCT 180 AAGCAGGAGGAGGCTCAGGGGGGCCACAGCCCCAAAGCTGAGAGTGGTTCGAAGCG 237

```



```

QUERY 421 CAGAAAAGGCAGCAGCCCGGCCCGTCGGAGCACATAGAGCGCCGGGTCTCCAATGCAGGA 480
          |||
SBJCT 442 CAGAAAAGGCAGCAGCCCGGCCCGTCGGAGCACATAGAGCGCCGGGTCGACAATGCAGGA 501
          |||
          S157D (nt 469-471)

QUERY 481 GGCCACCTGCTCCCCCGCTGGGGGTCCACCCCCACCACCAGGACCTCCCCCTCCTCCA 540
          |||
SBJCT 502 GGCCACCTGCTCCCCCGCTGGGGGTCCACCCCCACCACCAGGACCTCCCCCTCCTCCA 561

QUERY 541 GGTCCCCCCCCACCCCAGGTTTGCCCCCTTCGGGGGTCCAGCTGCAGCGCACGGAGCA 600
          |||
SBJCT 562 GGTCCCCCCCCACCCCAGGTTTGCCCCCTTCGGGGGTCCAGCTGCAGCGCACGGAGCA 621

QUERY 601 GGGGAGGACCACCCCTGCACCCCTCTCCCGGCAGCACAGGGCCCTGGTGGTGGGGGA 660
          |||
SBJCT 622 GGGGAGGACCACCCCTGCACCCCTCTCCCGGCAGCACAGGGCCCTGGTGGTGGGGGA 681

QUERY 661 GCTGGGGCCCCAGGCCTGGCCGCAGCTATTGCTGGAGCCAAACTCAGGAAAGTC-AGCAA 719
          |||
SBJCT 682 GCTGGGGCCCCAGGCCTGGCCGCAGCTATTGCTGGAGCCAAACTCAGGAAAGTCGA-CAA 740
          |||
          S239D (nt 715-717)

QUERY 720 GCAGGAGGAGCCTCAGGGGGGCCACAGCCCCAAAGCTGAGAGTGGTGAAGCGGAGG 779
          |||
SBJCT 741 GCAGGAGGAGCCTCAGGGGGGCCACAGCCCCAAAGCTGAGAGTGGTGAAGCGGAGG 800

QUERY 780 TGGGGACTCATGGAAGAGATGAACGCCATGCTGGCCCGGAGAAGGAAAGCC-ACGCAAG 838
          |||
SBJCT 801 TGGGGACTCATGGAAGAGATGAACGCCATGCTGGCCCGGAGAAGGAAAGCCGA-CAA 859
          |||
          T278E (nt 832-834)

QUERY 839 TTGGGGAGAAAACCCCAAGGATGAATCTGCCAATCAGGAGGAGCCAGAGG 889
          |||
SBJCT 860 TTGGGGAGAAAACCCCAAGGATGAATCTGCCAATCAGGAGGAGCCAGAGG 910

```

Query: human VASP
Subject 2: VASP-DDEΔTD, BGH-Rev-sequence
Length: 620 nt
Score = 896 bits (485), Expect = 0.0, Identities = 495/499 (99%), Gaps = 4/499 (0%)

```

QUERY 532 CCTCTCCAGGTCACCCCAAGGTTTGCCCCCTTCGGGGGTCCAGCTGCAGCG 591
          |||
SBJCT 1 CCTCTCCAGGTCACCCCAAGGTTTGCCCCCTTCGGGGGTCCAGCTGCAGCG 60

QUERY 592 CACGGAGCAGGGGAGGACCACCCCTGCACCCCTCTCCCGGCAGCACAGGGCCCTGGT 651
          |||
SBJCT 61 CACGGAGCAGGGGAGGACCACCCCTGCACCCCTCTCCCGGCAGCACAGGGCCCTGGT 120

QUERY 652 GGTGGGGGAGCTGGGGCCCCAGGCCTGGCCGCAGCTATTGCTGGAGCCAAACTCAGGAAA 711
          |||
SBJCT 121 GGTGGGGGAGCTGGGGCCCCAGGCCTGGCCGCAGCTATTGCTGGAGCCAAACTCAGGAAA 180

QUERY 712 GTC-AGCAAGCAGGAGGAGGCCTCAGGGGGGCCACAGCCCCAAAGCTGAGAGTGGTCCG 770
          |||
SBJCT 181 GTCGA-CAAAGCAGGAGGAGGCCTCAGGGGGGCCACAGCCCCAAAGCTGAGAGTGGTCCG 239
          |||
          S239D (nt 715-717)

QUERY 771 AAGCGGAGGTGGGGACTCATGGAAGAGATGAACGCCATGCTGGCCCGGAGAAGGAAAGC 830
          |||
SBJCT 240 AAGCGGAGGTGGGGACTCATGGAAGAGATGAACGCCATGCTGGCCCGGAGAAGGAAAGC 299

QUERY 831 C-ACGCAAGTTGGGGAGAAAACCCCAAGGATGAATCTGCCAATCAGGAGGAGCCAGAGG 889
          |||
SBJCT 300 CGA-GCAAGTTGGGGAGAAAACCCCAAGGATGAATCTGCCAATCAGGAGGAGCCAGAGG 358
          |||
          T278E (nt 832-834)

```

```

QUERY  890  CCAGAGTCCCGGCCAGAGTGAATCTGTGCGGAGACCCTGGGAGAAGAACAGCACAACT  949
          |||
SBJCT   359  CCAGAGTCCCGGCCAGAGTGAATCTGTGCGGAGACCCTGGGAGAAGAACAGCACAACT  418

QUERY  950  TGCCAAGGATGAAGTCGTCTTCTTCGGTGACCACTTCCGAGACCCAAACCCTGCACGCCA  1009
          |||
SBJCT   419  TGCCAAGGATGAAGTCGTCTTCTTCGGTGACCACTTCCGAGACCCAAACCCTGCACGCCA  478

QUERY  1010  GCTCCAGTGATTACTCGGA  1028
          |||
SBJCT   479  GCTCCAGTGATTACTCGGA  497

```

7.4.4 Sequencing of VASP-DDE Δ FAB Δ TD (in *pcDNA3.1/V5-HisA*)

VASP-DDE Δ FAB Δ TD, T7-Fwd-sequence:

```

CTTGGTACCGAGCTCGGATCCATGAGCGAGACGGTCATCTGTTCCAGCCGGGCCACTGTGATGCTTTATGAT
GATGGCAACAAGCGATGGCTCCCTGCTGGCACGGGTCCCCAGGCCTTCAGCCCGTCCAGATCTACCACAA
CCCCACGGCCAATTCTTTTCGCGTCTGTTGGCCGGAAGATGCAGCCCGACCAGCAGGTGGTCATCAACTGTG
CCATCGTCCGGGGTGTCAAGTATAACCAGGCCACCCCAACTTCCATCAGTGGCGCGACGCTCGCCAGGTC
TGGGGCCTCAACTTCGGCAGCAAGGAGGATGCGGCCAGTTTCCCGCCGGCATGGCCAGTGCCTTAGAGG
CGTTGGAAGGAGGTGGGCCCCCTCCACCCCAAGCACTTCCACCTGGTCCGGAACGGCCCTCCCC
GGAGGAGGTGGAGCAGCAGAAAAGGCAGCAGCCGGCCCGTCCGAGCACATAGAGCGCCGGGTGCACAA
TGCAGGAGGCCACCTGCTCCCCCGCTGGGGTCCACCCCAACCAGGACCTCCCCCTCCTCCAGGT
TCCCCCAACCCCAAGTTTGGCCCTTCGGGGTCCACCCCAACCAGGACCTCCCCCTCCTCCAGGT
ACCCCTGCACCCCTCTCCCGCAGCACAGGGCCCTGGTGGTGGGGGAGCTGGGGCCCAAGGCCTGGC
CGCAGCTATTGCTGAAGCCAACTCAGGAAAGTCGACAAGCAGGAGGAGGCCTCAGGGGGCCACAGCC
CCCAAAGCTGAGAGTGGTGAAGCGAATTCTGCAGATATCCAGCACAGTGGCGCCGCTCGAGTCTAGAGG
GCCCTTCGAAAGTAAGCCTATCCCTAACCCCTCTCCTCGGTCTCGATTCTACGCGTACCGGTATCATCACCA
TCACCATTAAGTTTAAACCCGCTGATCAGCCTCGACTGTGCCTTCTAGTTGCCAGCCATCTGTTGTTGCCCC
TCCCCCGTGC

```

VASP-DDE Δ FAB Δ TD, BGH-Rev-sequence (complementary):

```

GCGGAACTTCCCCCTCCTCCAGGTCCCCCCCCACCCCAAGGTTGCCCCCTTCGGGGTCCCAGCTGCAG
CGCACGGAGCAGGGGGAGGACCACCCCTGCACCCCTCTCCCGCAGCACAGGGCCCTGGTGGTGGGG
GAGCTGGGGCCCAAGCCTGGCCGAGCTATTGCTGAAGCCAACTCAGGAAAGTCGACAAGCAGGAGGA
GGCTCAGGGGGCCACAGCCCCAAAGCTGAGAGTGGTGAAGCGAATTCTGCAGATATCCAGCACAG
TGGCGCCGCTCGAGTCTAGAGGGCCCTTCGAAAGTAAGCCTATCCCTAACCCCTCTCCTCGGTCTCGATTCT
ACGCGTACCGGTATCATCACCATCACCATTGA

```

VASP-DDE Δ FAB Δ TD, sequence alignment with human VASP:

```

Query:          human VASP
Subject 1:      VASP-DDE $\Delta$ FAB $\Delta$ TD, T7-Fwd-sequence
Length:         998 nt
Score = 1399 bits (757), Expect = 0.0, Identities = 773/777 (99%), Gaps = 3/777 (0%)

```

```

QUERY  1  ATGAGCGAGACGGTCATCTGTTCCAGCCGGGCCACTGTGATGCTTTATGATGATGGCAAC  60
          |||
SBJCT  22  ATGAGCGAGACGGTCATCTGTTCCAGCCGGGCCACTGTGATGCTTTATGATGATGGCAAC  81

QUERY  61  AAGCGATGGCTCCCTGCTGGCACGGGTCCCCAGGCCTTCAGCCCGTCCAGATCTACCAC  120
          |||
SBJCT  82  AAGCGATGGCTCCCTGCTGGCACGGGTCCCCAGGCCTTCAGCCCGTCCAGATCTACCAC  141

QUERY  121  AACCCACGGCCAATTCCTTTTCGCGTCTGTTGGCCGGAAGATGCAGCCCGACCAGCAGGTG  180
          |||
SBJCT  142  AACCCACGGCCAATTCCTTTTCGCGTCTGTTGGCCGGAAGATGCAGCCCGACCAGCAGGTG  201

QUERY  181  GTCATCAACTGTGCCATCGTCCGGGGTGTCAAGTATAACCAGGCCACCCCAACTTCCAT  240
          |||
SBJCT  202  GTCATCAACTGTGCCATCGTCCGGGGTGTCAAGTATAACCAGGCCACCCCAACTTCCAT  261

```



```

QUERY 241 CAGTGGCGCGACGCTCGCCAGGTCTGGGGCCTCAACTTCGGCAGCAAGGAGGATGCGGCC 300
          |||
SBJCT 262 CAGTGGCGCGACGCTCGCCAGGTCTGGGGCCTCAACTTCGGCAGCAAGGAGGATGCGGCC 321

QUERY 301 CAGTTTGC CGCCGGCATGGCCAGTGCCTTAGAGGC GTTGAAGGAGGTGGGCCCCCTCCA 360
          |||
SBJCT 322 CAGTTTGC CGCCGGCATGGCCAGTGCCTTAGAGGC GTTGAAGGAGGTGGGCCCCCTCCA 381

QUERY 361 CCCCCAGCACTTCCACCTGGTCGGTCCCGAACGGCCCCCTCCCCGGAGGAGGTGGAGCAG 420
          |||
SBJCT 382 CCCCCAGCACTTCCACCTGGTCGGTCCCGAACGGCCCCCTCCCCGGAGGAGGTGGAGCAG 441

QUERY 421 CAGAAAAGGCAGCAGCCCGGCCGTCGGAGCACATAGAGCGCCGGGTC TCCAAATGCAGGA 480
          |||
SBJCT 442 CAGAAAAGGCAGCAGCCCGGCCGTCGGAGCACATAGAGCGCCGGGTC GACAAATGCAGGA 501
          |||
          S157D nt 469-471)

QUERY 481 GGCCCACTGCTCCCCCGCTGGGGGTCCACCCACCACCAGGACCTCCCCCTCTCCA 540
          |||
SBJCT 502 GGCCCACTGCTCCCCCGCTGGGGGTCCACCCACCACCAGGACCTCCCCCTCTCCA 561

QUERY 541 GGTCCCCCCCCACCCCAAGTTTGGCCCCCTTCGGGGGTCCAGCTGCAGCGCACGGAGCA 600
          |||
SBJCT 562 GGTCCCCCCCCACCCCAAGTTTGGCCCCCTTCGGGGGTCCAGCTGCAGCGCACGGAGCA 621

QUERY 601 GGGGGAGGACCACCCCTGCACCCCTCTCCCGGCAGCACAGGGCCCTGGTGGTGGGGG 659
          |||
SBJCT 622 GGGGGAGGACCACCCCTGCACCCCTCTCCCGGCAGCACAGGGCCCTGGTGGTGGGGG 681

QUERY 660 AGCTGGGGCCCCAGGCTGGCCGAGCTATTGCTGGAGCCAAACTCAGGAAAGTC- AGCA 718
          |||
SBJCT 682 AGCTGGGGCCCCAGGCTGGCCGAGCTATTGCTGGAGCCAAACTCAGGAAAGTC GA-CA 740
          |||
          S239D (nt 715-717)

QUERY 719 AGCAGGAGGAGGCCTCAGGGGGGCCACAGCCCCAAAGCTGAGAGT GGTCGAAGCG 775
          |||
SBJCT 741 AGCAGGAGGAGGCCTCAGGGGGGCCACAGCCCCAAAGCTGAGAGT GGTCGAAGCG 797
          |||

```

Query: human VASP
 Subject 2: VASP-DDEΔFABΔTD, BGH-Rev -sequence
 Length: 384 nt
 Score = 442 bits (239), Expect = 3e-128, Identities = 247/249 (98%), Gaps = 2/249 (0%)

```

QUERY 528 TCCCCCTCCTCCAGGTCCCCCCCCACCCCAAGTTTGGCCCCCTTCGGGGGTCCAGCTGC 587
          |||
SBJCT 9 TCCCCCTCCTCCAGGTCCCCCCCCACCCCAAGTTTGGCCCCCTTCGGGGGTCCAGCTGC 68

QUERY 588 AGCGCACGGAGCAGGGGGAGGACCACCCCTGCACCCCTCTCCCGGCAGCACAGGGCCC 647
          |||
SBJCT 69 AGCGCACGGAGCAGGGGGAGGACCACCCCTGCACCCCTCTCCCGGCAGCACAGGGCCC 128

QUERY 648 TGGTGGTGGGGGAGCTGGGGCCCCAGGCCTGGCCGAGCTATTGCTGGAGCCAAACTCAG 707
          |||
SBJCT 129 TGGTGGTGGGGGAGCTGGGGCCCCAGGCCTGGCCGAGCTATTGCTGGAGCCAAACTCAG 188

QUERY 708 GAAAGTC- AGCAAAGCAGGAGGAGGCCTCAGGGGGGCCACAGCCCCAAAGCTGAGAGT G 766
          |||
SBJCT 189 GAAAGTC GA-CAAAGCAGGAGGAGGCCTCAGGGGGGCCACAGCCCCAAAGCTGAGAGT G 247
          |||
          S239D (nt 715-717)

QUERY 767 GTCGAAGCG 775
          |||
SBJCT 248 GTCGAAGCG 256
          |||

```

7.5 Table 7.1: Data of the *in vitro* calpain in-solution digestion assay

In silico vs *in vitro* determined calpain cleavage sites in human CLP36 protein. *In vitro* data were generated by in-solution digestion of recombinant human CLP36 via calpain-1 and calpain-2 (based on Lakey et al. [201]) and subsequent analysis on an LTQ-FT Ultra mass analyzer. MS data were searched for adjacent fragments fitting on either side of the indicated cleavage positions. In each case, the three fragments with the highest ion scores are displayed. *In silico* predicted yet non-detected calpain cleavage sites, as well as unspecific fragmentation sites are shaded in grey.

#	<i>in silico</i> predicted site	adjacent <i>in vitro</i> fragments as detected by LTQ-FT Ultra MS analysis	ion score	aa start-end
1	Q9	Q.GPGPWGFRLVGGKDF.E	48	010-024
		Q.GPGPWGFRLV.G	55	010-019
		Q.GPGPWGFRLVGGKDF.E	55	010-024
2	F24	F.EQPLAISRVTPGSK.A	39	025-038
		F.EQPLAISRVTPGSK.A	53	025-038
		F.EQPLAISRVTPGSK.A	59	025-038
		Q.GPGPWGFRLVGGKDF.E	41	010-024
		Q.GPGPWGFRLVGGKDF.E	48	010-024
		Q.GPGPWGFRLVGGKDF.E	55	010-024
3	R32	No		
4	V93	No		
5	H115	A.SEPQEV LH.I	38	108-115
		A.SEPQEV LH.I	47	108-115
6	S123	E.PQEV LHIGSAHNRS.A	67	110-123
		A.SEPQEV LHIGSAHNRS.A	89	108-123
		A.SEPQEV LHIGSAHNRS.A	106	108-123
		S.AMPFTASPASSTT.A	77	124-136
		S.AMPFTASPASSTTARVIT.N	85	124-141
		S.AMPFTASPASSTTARVITNQY.N	93	124-144
7	T128	T.ASPASSTTARVITN.Q	52	129-142
		T.ASPASSTTARVITNQY.N	92	129-144
		T.ASPASSTTARVITNQY.N	96	129-144
8	T136	H.NRSAMPFTASPASSTT.A	70	121-136
		H.NRSAMPFTASPASSTT.A	72	121-136
		S.AMPFTASPASSTT.A	77	124-136
		T.ARVITNQYNNPAGLYSSE.N	92	137-154
		T.ARVITNQYNNPAGLYSSE.N	98	137-154
		T.ARVITNQYNNPAGLYSSENISNFNNALE.S	104	137-164
9	V139	No		
10	T141	A.SPASSTTARVIT.N	62	130-141
		A.SPASSTTARVIT.N	70	130-141
		S.AMPFTASPASSTTARVIT.N	85	124-141
		T.NQYNNPAGLYSSENISNFNN.A	97	142-161
		T.NQYNNPAGLYSSENISNF.N	97	142-159
		T.NQYNNPAGLYSSENISNF.N	100	142-160
11	Q143	F.TASPASSTTARVITNQ.Y	78	128-143
		A.SPASSTTARVITNQ.Y	99	130-143
		A.SPASSTTARVITNQ.Y	107	130-143
12	Y144	S.AMPFTASPASSTTARVITNQY.N	93	124-144
		T.ASPASSTTARVITNQY.N	96	129-144
		F.TASPASSTTARVITNQY.N	98	128-144
		Y.NNPAGLYSSENISNFNNAL.E	129	145-163
		Y.NNPAGLYSSENISNFNNALE.S	132	145-164
		Y.NNPAGLYSSENISNFNNA.L	137	145-162
13	Y151	Yes, yet also unspecific		
14	K166	Yes, yet also unspecific		
15	H181	K.TAASGVEANSRPLDH.A	74	167-181
		K.TAASGVEANSRPLDH.A	79	167-181
		K.TAASGVEANSRPLDH.A	96	167-181
		H.AQPPSSLVIDKESSEVY.K	64	182-197

		H.AQPPSSLVIDKESEVYK.M	74	182-198
		H.AQPPSSLVIDKESEVYK.M	78	182-198
16	L217	L.NEPPKQSTSFL.V	41	207-217
17	Q220	Yes, yet also unspecific		
18	R238	Q.EILESEEEKGDPNKPSGFR.S	47	221-238
		Q.EILESEEEKGDPNKPSGFR.S	54	221-238
		Q.EILESEEEKGDPNKPSGFR.S	58	221-238
19	K241	K.APVTKVAASIGNA.Q	70	242-254
		K.APVTKVAASIGNA.A	71	242-253
		K.APVTKVAASIGNA.A	76	242-253
20	K246	R.SVKAPVTK.V	44	239-246
		K.VAASIGNAQK.L	63	247-256
		K.VAASIGNAQ.K	66	247-255
		K.VAASIGNAQ.K	69	247-255
21	A248	No		
22	R314	R.VTPPEGYEVVTVFPK.-	75	315-329
		R.VTPPEGYEVVTVFPK.-	83	315-329
		R.VTPPEGYEVVTVFPK.-	93	315-329
23	V315	No		
24	T325	A.RERVTPPEGYEVVT.V	42	312-325
		R.VTPPEGYEVVT.V	42	315-325
		R.VTPPEGYEVVT.V	65	315-325

7.6 Persönliche Daten

7.6.1 Lebenslauf

Name: Thomas Premisler
Anschrift: Stadelmannstrasse 45
63739 Aschaffenburg

Geburtsdatum: 02.07.1979

Geburtsort: Dresden

Nationalität: Deutsch

Familienstand: verheiratet

Schulausbildung:

09/1986 - 08/1992 Grundschule, 64. Oberschule Dresden-Laubegast

09/1992 - 12/1992 Gymnasium, 94. Oberschule Dresden

01/1993 - 06/1999 Gymnasium, Steigerwald Landschulheim Wiesentheid
Abschluss Abitur

Studium:

10/2000 - 07/2001 Diplomstudiengang Biologie, Universität Würzburg

10/2001 - 07/2004 Bachelorstudiengang Biomedizin, Universität Würzburg
Abschluss Bachelor of Science

10/2004 - 04/2006 Masterstudiengang Biomedizin, Universität Würzburg
Abschluss Master of Science

06/2006 - 01/2007 Promotionsstudium, Universität Würzburg,
Institut für Klinische Neurobiologie (AG Prof. Dr. Sendtner)
Abbruch 2007, Wechsel ans Rudolf-Virchow-Zentrum

02/2007 - 11/2008 Promotionsstudium, Universität Würzburg,
Rudolf-Virchow-Zentrum (DFG-Forschungszentrum für Experimentelle
Biomedizin), AG Proteinmassenspektrometrie und funktionelle
Proteomik (Prof. Dr. Albert Sickmann)

12/2008 - 05/2011 Fortführung und Beendigung des Promotionsstudiums an der TU
Dortmund nach Übersiedlung der Arbeitsgruppe ins Leibniz-Institut für
Analytische Wissenschaften - ISAS - e.V., Dortmund

seit 06/2011 Postdoc-Stelle in der Universität Würzburg, Physiologisches Institut I,
AG Kardiovaskuläre Physiologie (Prof. Dr. Michaela Kuhn)

7.6.2 Veröffentlichungen

1. Wiesner, J., Premisler, T., Sickmann A. (2008) Application of electron transfer dissociation (ETD) for the analysis of posttranslational modifications. *Proteomics* 8, 4466-4483.
2. Premisler, T., Zahedi, R. P., Lewandrowski, U., Sickmann, A. (2009) Recent advances in yeast organelle and membrane proteomics. *Proteomics* 9, 4731-4743.
3. Burkhart, J. M., Premisler, T., Sickmann, A. (2011) Quality control of nano-LC-MS systems using stable isotope-coded peptides. *Proteomics* 11, 1049-1057.
4. Premisler, T., Lewandrowski, U., Sickmann, A., Zahedi, R. P. (2011) Phosphoproteome analysis of the platelet plasma membrane. *Methods Mol Biol* 728, 279-290.
5. Premisler, T., Lewandrowski, U., Zahedi, R. P., Sickmann, A. (2011) Subcellular analysis of the platelet proteome. *Current Proteomics* 8, 181-192.
6. Gupta, S., Braun, A., Morowski, M., Premisler, T., et al. (2012) CLP36 is a negative regulator of GPVI signaling in platelets. *Circulation Research*, currently under submission.

7.6.3 Vorträge

1. "Phosphorylation-specific interaction and regulation of VASP". 22nd European Platelet Meeting, Halle-Wittenberg, Deutschland, 11.-13.10. 2007.
2. "Phosphorylation-specific interaction and regulation of the vasodilator-stimulated phosphoprotein". BMBF QuantPro Verbundtreffen, München, Deutschland, 09.-10.12.2007.
3. "Phosphorylation-specific interaction and regulation of VASP in platelets". BMBF QuantPro Verbundtreffen, Würzburg, Deutschland, 21.-23.04.2008.

7.6.4 Posterpräsentationen

1. "Regulation and interaction of VASP - a proteomic approach". Joint Symposium of the SFB612, SFB688 and GRK1089, Düsseldorf-Kaiserswerth, Deutschland, 30.09.-02.10.2007.
2. "Phosphorylation-specific interaction and regulation of vasodilator-stimulated phosphoprotein". 7th HUPO World Congress Amsterdam, Niederlande, 17.-20.08.2008.
3. "Phosphorylation-specific interaction and regulation of vasodilator-stimulated phosphoprotein in endothelial cells". Proteomic Forum Berlin, Deutschland, 29.03.-02.04.2009.

8 Danksagung

Mein besonderer Dank gilt Prof. Dr. Albert Sickmann für die Möglichkeit der Promotion anhand einer solch herausforderungsvollen Themenstellung, sowie für die stetige Unterstützung, die hilfreichen Diskussionen und vor allem die reichhaltigen Möglichkeiten bei der Realisierung dieser Arbeit.

Herrn Prof. Dr. Jan Hengstler danke ich nicht nur für die freundliche Übernahme des Zweitgutachtens, sondern auch für seine sofortige Bereitschaft, uns im Zuge der Übersiedlungsphase unserer Arbeitsgruppe von Würzburg nach Dortmund übergangsweise seine S1-Räumlichkeiten am Leibniz-Institut für Arbeitsforschung zur Verfügung zu stellen.

Weiterhin möchte ich Vorab all den Professoren danken, die sich als Prüfer dieser Arbeit im Rahmen des Promotionskolloquiums an der TU Dortmund zur Verfügung stellen werden.

Herrn Prof. Dr. Thomas Renné (Department für Molekulare Medizin und Chirurgie, Karolinska Institut, Stockholm, Schweden) danke ich für die Möglichkeit zur Bearbeitung des VASP-Projektes und die damit einhergehenden fruchtbaren Diskussionen. Gleiches gilt in selbem Maße für Herrn Prof. Dr. Ulrich Walter (Institut für Klinische Biochemie und Pathobiochemie, Zentrum für Innere Medizin, Würzburg). Ich möchte mich auch bei den Mitgliedern ihrer Arbeitsgruppen bedanken, die mir während der Zeit, in der ich in ihren Räumlichkeiten tätig war, stets mit Rat und Tat zur Seite standen. Hervorzuheben sind in diesem Zusammenhang Dr. Sabine Herterich und Dr. Thomas Jarchau.

Herrn Prof. Dr. Bernhard Nieswandt (Rudolf-Virchow-Zentrum, Würzburg) danke ich für die Möglichkeit zur Bearbeitung des STIM1-Projektes. Insbesondere danke ich Dr. Attila Braun für die vielen Gespräche und Denkanstöße bei der Beurteilung der STIM1-MS-Daten, sowie für die vielfältigen Zuarbeiten, wie etwa Co-IP Experimente und Calciummessungen in murinem Thrombozytenmaterial, die immens halfen, diese Arbeit abzurunden. Desweiteren waren aus besagter Arbeitsgruppe auch Dr. Irina Pleines und Shuchi Gupta mit im STIM1-Projekt involviert - auch ihnen sei daher an dieser Stelle aufs herzlichste gedankt. Gleiches gilt für alle anderen

Mitarbeiter des Rudolf-Virchow-Zentrums der Universität Würzburg für die stets unkomplizierte und kooperative Zusammenarbeit. Besonderer Dank geht dabei an Sylvia Luckner für ihre Hilfe am ÄKTA FPLC System.

Allen Sickmännern und -frauen sowohl aus Würzburg, als auch aus Dortmund möchte ich für das herausragende und inspirierende Arbeitsklima danken. Besonders zu erwähnen sind hierbei Dr. René P. Zahedi und vor allem mein Betreuer Dr. Urs Lewandrowski. Seine geduldige Art, mir immer wieder aufs Neue die Welt der Proteinanalytik im Allgemeinen und die der Massenspektrometrie im Speziellen zu erklären, sowie sein stets offenes Ohr für alle meine Fragen halfen mir ungemein, die Höhen und Tiefen einer Promotion einigermaßen unbeschadet zu überstehen. Die Schnelligkeit, mit der er dieses Manuskript korrekturgelesen hatte, hat mich zudem nachhaltig beeindruckt. Extra angemerkt seien an dieser Stelle außerdem noch die gute Zusammenarbeit mit Julia M. Burkhart während der Anfangszeit des VASP-Projektes und die willkommenen Ablenkungen mit und durch Beate Eyrich und Florian Beck.

Ich danke für die finanzielle Unterstützung dieser Arbeit: Einmal seitens der Deutschen Forschungsgemeinschaft im Rahmen des SFB688, zum anderen seitens des BMBF Verbundprojektes QuantPro.

Zu guter Letzt möchte ich natürlich auch meiner Familie danken, allen voran meinen Eltern und Schwiegereltern, die mich kontinuierlich über all die Jahre unterstützt haben und mir stets eine große Hilfe waren. Ein ganz besonderes Dankeschön geht an meine Frau Claudia. Ohne ihre liebevolle Unterstützung, ihren motivierenden Zuspruch in Tiefphasen und ihre unendliche Geduld und Toleranz bei allen räumlich-zeitlichen Einschränkungen, die die Promotionsphase mit sich brachte, wäre diese Arbeit nicht möglich gewesen. Claudia, diese Dissertation ist Dir gewidmet!

9 Eidesstattliche Erklärung

Ich versichere, dass ich die hier vorliegende Dissertation

„Mass Spectrometry-Based Interaction Study of the STIM1 and VASP Proteins
(Massenspektrometrie-basierte Interaktionsstudie der Proteine STIM1 und VASP)“

selbständig und ohne unerlaubte Hilfe angefertigt, und mich dabei keiner anderen als der von mir ausdrücklich bezeichneten Quellen und Hilfsmittel bedient habe.

Ich erkläre außerdem, dass diese Dissertation weder in gleicher noch in abgewandelter Form bereits in einem anderen Prüfungsverfahren vorgelegen hat.

Aschaffenburg, den 18.06.2012

(Thomas Premsler)